*Author:*
**Ward, Alexander**

*Title:*
**Investigating the NF-KappaB and Nrf2/Keap1 pathways in venous endothelial cells under acute shear stress**
*Implications for vein graft failure*

# INVESTIGATING THE NF-κB AND NRF2/KEAP1 PATHWAYS IN VENOUS ENDOTHELIAL CELLS UNDER ACUTE SHEAR STRESS: IMPLICATIONS FOR VEIN GRAFT FAILURE

**ALEXANDER OWEN WARD**

A dissertation submitted to the University of Bristol in accordance with the requirements of the degree of Doctor of Philosophy in the Department of Translational Health Sciences, Bristol Medical School, 69 St Michael's Hill, Bristol, BS2 8DZ

June 2018

43,066 words

## ABSTRACT

The long saphenous vein (LSV) is commonly used as a conduit in coronary artery bypass grafting (CABG); however, long term patency remains limited by the development of intimal hyperplasia and superimposed atherosclerosis. Upon engraftment of the LSV, there is a necessity to accommodate a vastly increased flow rate and wall shear stress, the effect of which, remains poorly defined. Venous endothelial cell (vEC) activation induced by vein harvest and the acutely altered shear stress rates (or acute high shear stress (AHSS) at 12dyn/cm$^2$) is thought to be pivotal for development of later-stage pathologies, but little is known about the signalling pathways involved. In this thesis, the involvement of two transcription factors, NF-κB and Nrf2, in vEC activation were assessed in the context of AHSS.

Firstly, NF-κB was activated in the LSV endothelium and HUVECs, in response to AHSS. This was further supported by the detection of AHSS-induced NF-κB target inflammatory genes including MCP-1, which was reduced with NF-κB inhibition prior to the onset of AHSS. Additionally, AHSS enhanced monocyte adhesion to the endothelium, *in vitro* and *ex vivo,* and reduced endothelial cell-cell contacts, both of which were reversed with NF-κB inhibition prior to the onset of AHSS. The second aim was to promote cellular defence prior to the onset of AHSS, through activation of the Nrf2-Keap1 antioxidant regulatory system. In response to AHSS *in vitro*, there was an Nrf2 target gene transcriptional response; however, not induced by increased Nrf2 translocation, but rather, increased dissociation from and nuclear export of Keap1. When Nrf2 was pre-activated, however, far from preventing the pro-inflammatory response to AHSS, the inflammatory response of venous ECs was increased. This contradictory finding appears to be mediated in part by the dysregulation of Keap1 under AHSS, suggesting that this cellular defence system is not a suitable target in the treatment acute vein graft inflammation.

Pharmacological modulation of vein graft patency has proven to be exceedingly difficult, with the identification of suitable targets providing the primary hurdle, due to the complex disease aetiology and multicellular pathology. This thesis, provides evidence that inhibition of acute EC activation and inflammation as a result of AHSS may represent an exciting and unexplored strategy for improving vein graft outcome, with the NF-κB transcription factor emerging as a potential target for localised inhibition prior to grafting.

## DEDICATIONS AND ACKNOWLEDGEMENTS

First and foremost, I would like to express huge gratitude to both of my supervisors, Professor Sarah George and Mr Mustafa Zakkar. Your support for both myself and the project have been unwavering since day one and I am honoured to have worked under your combined supervision for the past three years. I have benefitted hugely from both of your supervisions, which were very complementary to one another and really taught me a vast amount, both scientifically and pastorally. Both of you have pushed when I needed to be pushed, but also given me freedom to develop my own ideas and, most of all, mentored me to become a better and more dedicated researcher. I really cannot thank you both enough for this.

In addition to this, I would like to thank Professor Saadeh Suleiman, for without whom I would not be here. You believed in me before starting in Bristol and have helped me immeasurably and for this I will be forever grateful. I would like to further thank Professors Gianni Angelini and Massimo Caputo, for your continued support and funding for myself and the project, as well as your hugely appreciated encouragement during the past 3 years. A final thank you here to Dr Guido Buonincontri, Dr Steve Sawiak and Professors James Bourne and Chris Petkov for helping me onto this path.

Of my colleagues, for putting up with my untidy bench and training me in many new experimental techniques, I would like to thank Kerry (for numerous Chilli Daddy's too!), Steve S, Steve W, Jason, Graciela, Helen, Rosaria, Beth and Cress. To the surgeons, Gustavo, Bruno and Roberto, for a non-stop supply of saphenous veins. To many other friends in the lab, Michele, Maddie, David, Eva and many more, who have made these a wonderful 3 years in Bristol and shared and helped in the experience.

A special thank you to Marie, for putting up with my invasion of her life and flat, you have helped make me a better person both at home and work. Another huge thank you to Burns, Dave and Boo for helping me through tougher times and, of course, for many fun-filled Fridays. Also, huge thanks to Jamie McC and Tariq for your friendship and help these past years.

Finally, an immeasurable thank you to my parents (and sisters!) for their unswerving support and belief in me, having been there whenever I needed them and for everything they have done to get me here. Thank you all…

## AUTHOR'S DECLARATION

I declare that the work in this thesis was carried out in accordance with the requirements of the University's *Regulations and Code of Practice for Research Degree Programmes* and that it has not been submitted for any other academic award. Except where indicated by specific reference in the text, the work is the candidate's own work. Work done in collaboration with, or with the assistance of, others, is indicated as such. Any views expressed in this thesis are those of the author.

SIGNED: …… DATE: ……

## PLAGIARISM DECLARATION

I declare that some of the text used in this thesis has been taken from the published review, 'A.O.Ward et al., *Activation and inflammation of the venous endothelium in vein graft disease,* Atherosclerosis, Oct 2017, pp266-274', and that the text utilised was written by myself.

SIGNED BY FIRST AUTHOR: …… DATE: ……

SIGNED BY SENIOR AUTHOR: …….. DATE: ……

# TABLE OF CONTENTS


LIST OF FIGURES XVII

LIST OF TABLES XXIII

LIST OF SUPPLEMENTARY VIDEOS XXV

LIST OF ABBREVIATIONS XXVII

1. INTRODUCTION 1

**1.1 ISCHAEMIC HEART DISEASE AND MANAGEMENT 2**

**1.2 SAPHENOUS VEIN GRAFT FAILURE 4**

1.2.1 Temporal pathogenesis of VGF 4

1.2.2 Haemodynamic contribution to VGF 7

1.2.3 Pathology of intimal hyperplasia and accelerated atherosclerois 8

1.2.4 CABG conduit comparison 11

1.2.5 Current strategies to improve SVG patency and EC integrity 14

**1.3 VASCULAR INFLAMMATION AND THE ENDOTHELIUM 18**

1.3.2 Nuclear factor kappa B signalling pathway 21

**1.4 ANTIOXIDANT RESPONSE AND SIGNALLING 23**

1.4.1 Transcriptional control and redox balance 25

1.4.2 Nrf2/Keap1 signalling pathway 27

**1.5 INTERACTIONS BETWEEN THE NRF2/KEAP1 AND NF-κB PATHWAYS 30**

1.5.1 Direct interactions 31

1.5.2. Indirect interactions 32

**1.6 SHEAR STRESS AND THE ENDOTHELIUM 33**

1.6.1 Transduction of mechanical forces in the vasculature 33

1.6.2 Prolonged laminar shear stress and protective signalling 34

1.6.3 Chronic inflammation and abnormal haemodynamics 37

1.6.4 Acute exposure to high shear stress and inflammatory activation 38

**1.7 RATIONALE FOR THIS THESIS 42**

1.7.1 Hypotheses 42

1.7.2 Experimental approach 43

**2. MATERIALS AND METHODS 45**

**2.1 MATERIALS 46**

2.1.1 Reagents used in tissue and cell culture 46

2.1.2 Immunochemical reagents 47

2.1.3 Adenoviruses 50

**2.2 CULTURE OF HUVECS 51**

2.2.1 Cell Passage 51

2.2.2 Cryopreservation and resuscitation 51

2.2.3 Cell counting 52

**2.3 CULTURE OF THP-1 CELLS 52**

2.3.1 Cell subculture 52

**2.4 OVEREXPRESSION OF NRF2, KEAP1, NF-κB AND IκBα 53**

2.4.1 Ectopic overexpression of WT- IκBα, WT-Nrf2 and DN-Nrf2 in HUVECs 53

**2.5 SHEAR STRESS INDUCTION IN PARALLEL PLATE FLOW CHAMBER 53**

2.5.1 Cell Culture 53

2.5.2 Shear stress 54

**2.6 *IN VITRO* REAL-TIME MONOCYTE ADHESION ASSAY 56**

**2.7 *EX VIVO* HUMAN LONG SAPHENOUS VEIN PERFUSION MODEL 58**

2.7.2 *En face* preparation 60

2.7.3 Intimal RNA extraction 61

2.7.4 *Ex vivo* monocyte adhesion 61

2.7.5 Validation of automated THP-1 cell enumeration 62

**2.8 IMMUNOCYTOCHEMISTRY 63**

2.8.1 Dual immunocytochemistry for MCP-1/IκBα AND VE-Cadherin 63

2.8.2 Immunocytochemistry analysis 64

2.8.3 Validation of automated MCP-1 and IκBα intensity analysis 66

2.8.4 Validation of automated VE-cadherin cell-cell contact analysis 68

**2.9 IMMUNOFLUORESCENCE ON TISSUE SAMPLES 70**

2.9.1 LSV dual *en face* NF-κB/MCP-1 and vWF immunofluorescence 70

2.9.2 Imaris *en face* immunofluorescence analysis FOR nuclear NF-κB 71

2.9.3 Validation of Imaris 3D analysis process 72

2.9.4 Validation of MCP-1 *en face* immunofluorescence 76

**2.10 MOLECULAR BIOLOGY 78**

2.10.1 RNA extraction 78

2.10.2 RNA purification and quantification 78
2.10.3 Quantitative RT-PCR (RT-qPCR) 79
2.10.4 Primer Design and sequences 81

**2.11 WESTERN BLOTTING 83**

2.11.1 SDS Protein extraction 83
2.11.2 Nuclear and cytosolic protein fractionation 83
2.11.3 Protein Assay 83
2.11.4 Polyacrylamide Gel Electrophoresis (PAGE) 84
2.11.5 Protein transfer and protein detection 84
2.11.6 Densitometry 85

**2.12 NF-κB ACTIVITY ASSAY 85**

**2.13 STATISTICAL ANALYSIS 86**

**3. NF-κB ACTIVATION IN VENOUS ENDOTHELIUM IN RESPONSE TO ACUTE HIGH SHEAR STRESS 87**

**3.1 INTRODUCTION 88**

**3.2 RESULTS 90**

3.2.1 EC pro-inflammatory response to acute shear stress *in vitro* 90
3.2.2 Pro-inflammatory response of *ex vivo* LSV ECs to acute shear stress 94
3.2.3 NF-κB response to AHSS - *in vitro* 98
3.2.4 NF-κB response to AHSS in the LSV endothelium - *ex vivo* 102
3.2.5 NF-κB inhibtion and vEC response to AHSS – *in vitro* 104
3.2.6 NF-κB inhibtion and vEC response to AHSS – *ex vivo* 116

3.2.7 NF-κB inhibtion and vEC phenotypic response to TNF-α and AHSS 118

**3.3 DISCUSSION 130**

**4. NRF2/KEAP1 RESPONSE TO ACUTE HIGH SHEAR STRESS IN VENOUS ENDOTHELIAL CELLS 145**

**4.1 INTRODUCTION 147**

**4.2 RESULTS 151**

4.2.1 Nrf2/Keap1 response to AHSS 151

4.2.2 Pharmacological activation of Nrf2 and the endothelial response to AHSS 156

4.2.3 Effect of adenoviral-mediated overexpression of Nrf2 on the endothelial response to AHSS 162

4.2.4 Effect of inhibition of Nrf2 on the endothelial response to AHSS 168

**4.3 DISCUSSION 173**

**5. GENERAL DISCUSSION 184**

**5.1 INTRODUCTORY SUMMARY 185**

**5.2 HYPOTHESES, AIMS AND IMPLEMENTATION 186**

**5.3 NF-κB PATHWAY INVOLVEMENT IN VEC ACTIVATION 187**

**5.4 NRF2 PATHWAY INVOLVEMENT IN VEC ACTIVATION 189**

**5.5 FUTURE WORK 193**

5.5.1 NF-κB and vein graft failure 193

5.5.2 Nrf2 and the AHSS response 193

5.5.3 NF-κB and Nrf2: potential crosstalk 194

**5.6 CONCLUSION 194**

**6. APPENDIX 198**

**7. REFERENCES 206**

## LIST OF FIGURES


1. INTRODUCTION 1

1.1 ISCHAEMIC HEART DISEASE AND MANAGEMENT 2

FIGURE 1.1. Interventional treatment strategies for IHD 3

1.2 SAPHENOUS VEIN GRAFT FAILURE 4

FIGURE 1.2. Early and late stage vein graft failure 6

FIGURE 1.3. Mechanism of late-stage VGF 10

FIGURE 1.4. Structural differences between large arteries and veins 12

1.3 VASCULAR INFLAMMATION AND THE ENDOTHELIUM 18

FIGURE 1.5. Endothelial cell acute inflammatory responses 19

FIGURE 1.6. NF-κB classical pathway 23

1.4 ANTIOXIDANT RESPONSE AND SIGNALLING 23

FIGURE 1.7. Keap1/Nrf2 pathway under basal and oxidative stress conditions 30

1.5 SHEAR STRESS AND THE ENDOTHELIUM 33

FIGURE 1.8. Mechanical forces in the vasculature 33

FIGURE 1.9. Protective signalling in the quiescent endothelium 36

1.6 RATIONALE FOR THIS THESIS 42

2. MATERIALS AND METHODS 45

2.5 SHEAR STRESS INDUCTION IN PARALLEL PLATE FLOW CHAMBER 53

FIGURE 2.1. Schematic diagram of the parallel plate flow chamber 55

FIGURE 2.2. Parallel plate flow chamber model 56

**2.6 *IN VITRO* REAL-TIME MONOCYTE ADHESION ASSAY 56**

**FIGURE 2.3. Bioflux 200, 48-well plate and integrated system 58**

**2.7 *EX VIVO* HUMAN LONG SAPHENOUS VEIN PERFUSION MODEL 58**

**FIGURE 2.4. *Ex Vivo* perfusion system 59**

**FIGURE 2.5. *En face* preparation of LSV 60**

**FIGURE 2.6. CellProfiler output from adhered monocyte counts 62**

**2.8 IMMUNOCYTOCHEMISTRY 63**

**FIGURE 2.7. Outputs from CellProfiler MCP-1/IκBα analysis 66**

**FIGURE 2.8. Outputs from CellProfiler VE-Cadherin analysis 69**

**2.9 IMMUNOFLUORESCENCE ON TISSUE SAMPLES 70**

**FIGURE 2.9. Validation of Imaris 3D endothelial cell analysis process 75**

**FIGURE 2.10. FIJI-based analysis of MCP-1 en face immunofluorescence 77**

**3. NF-κB ACTIVATION IN VENOUS ENDOTHELIUM IN RESPONSE TO ACUTE HIGH SHEAR STRESS 87**

**3.1 INTRODUCTION 88**

**3.2 RESULTS 90**

**FIGURE 3.2. ALSS did not induce pro-inflammatory mRNA profiles in HUVECs 91**

**FIGURE 3.3. MCP-1 levels were increased in response to AHSS 93**

**FIGURE 3.4. MCP-1 transcript levels were increased in LSV ECs within vein segments under AHSS, ex vivo 95**

**FIGURE 3.5. AHSS exposure increased levels of MCP-1 in the LSV endothelium 97**

**FIGURE 3.6. AHSS activated NF-κB classical pathway 99**

FIGURE 3.7. AHSS promoted transcriptional activation of NF-κB 101

FIGURE 3.8. AHSS induced NF-κB translocation in LSV ECs 102

FIGURE 3.9. BAY11-7085 prevented TNF-α induced gene response 105

FIGURE 3.10. NF-κB inhibition attenuated the pro-inflammatory mRNA response under conditions of AHSS 107

FIGURE 3.11. Overexpression of IκBα was achieved optimally with the highest dose of WT-IκBα adenovirus 109

FIGURE 3.12. Overexpression of IκBα prevented some pro-inflammatory gene responses under AHSS 111

FIGURE 3.13. IκBα overexpression reduced MCP-1 under AHSS 112

FIGURE 3.14. IκBα overexpression increased levels of IκBα under AHSS 114

FIGURE 3.15. BAY11-7085 pre-treatment prevented increases in AHSS-driven MCP-1 production in LSV ECs 116

FIGURE 3.16. BAY11-7085 protected against TNF-α induced cell-cell contact 119

FIGURE 3.17. IκBα overexpression reduced AHSS induced disruption of endothelial barrier 120

FIGURE 3.18. AHSS, not IκBα overexpression, altered endothelial shape under flow 125

FIGURE 3.19. BAY11-7085 pre-treatment reduced AHSS-induced monocyte adhesion 127

FIGURE 3.20. BAY11-7085 retarded AHSS-induced monocyte adhesion to the LSV endothelium 129

3.3 DISCUSSION 130

FIGURE 3.21. EC involvement of the NF-κB classical pathway under acute shear stress 143

4. NRF2/KEAP1 RESPONSE TO ACUTE HIGH SHEAR STRESS IN VENOUS ENDOTHELIAL CELLS 145

4.1 INTRODUCTION 147

4.2 RESULTS 151

FIGURE 4.1. AHSS upregulated mRNA levels of HO-1 and GCLM, but not NQO-1. 151

FIGURE 4.2. AHSS increased HO-1 protein levels at both 4 and 6 hours 152

FIGURE 4.3. AHSS triggers the nuclear export of Nrf2 and Keap1 155

FIGURE 4.4. Sulforaphane induced Nrf2 translocation at the maximal dosage. 157

FIGURE 4.5. SFN pre-treatment increased levels of HO-1 and GCLM, which remained enhanced with AHSS exposure. 159

FIGURE 4.6. SFN pre-treatment did not consistently reduce pro-inflammatory levels as a result of AHSS 161

FIGURE 4.7. Validation of adenoviral-mediated overexpression of WT-Nrf2 163

FIGURE 4.8. Overexpression of Nrf2 increased HO-1 mRNA levels both in static and flow conditions 165

FIGURE 4.9. Dose-dependent effect of Nrf2 overexpression of Nrf2 on inflammatory mRNA expression 167

FIGURE 4.10. Adenoviral-overexpression of DN-Nrf2 reduced endogenous Nrf2 168

FIGURE 4.11. DN-Nrf2 overexpression reduced antioxidant levels in ECs subjected to AHSS 171

FIGURE 4.12. DN-Nrf2 overexpression did not affect levels of pro-inflammatory genes 172

**4.3 DISCUSSION 173**

**FIGURE 4.13. EC involvement of the Nrf2/Keap1 pathway under acute shear stress 183**

**5. GENERAL DISCUSSION 184**

**5.6 CONCLUSION 194**

**FIGURE 5.1. Mechanistic summary figure 196**

## LIST OF TABLES


2. MATERIALS AND METHODS 45

TABLE 2.1. Details of primary antibodies 48

TABLE 2.2. Details of secondary antibodies 49

TABLE 2.3. Details of cell/nuclear stains and mounting medium 49

TABLE 2.4. Locations of companies where immunochemical reagents were purchased 49

TABLE 2.5. Modules used in CellProfiler-based immunocytochemistry analysis 65

TABLE 2.6. Process of Imaris 3D *en face* immunofluorescence analysis 71

TABLE 2.7. RT-qPCR program conditions 80

TABLE 2.7. List of primer sequences 82

## LIST OF SUPPLEMENTARY FIGURES AND VIDEOS


6. APPENDIX 198

**SUPPLEMENTARY FIGURE 1. IgG CONTROL IMAGES FOR IMMUNOCYTOCHEMISTRY 198**

**SUPPLEMENTARY FIGURE 2. IgG CONTROL IMAGES FOR MCP-1 *EN FACE* IMMUNOFLUORESCENCE 199**

**SUPPLEMENTARY FIGURE 3. IgG CONTROL IMAGES FOR NF-κB *EN FACE* IMMUNOFLUORESCENCE 200**

**SUPPLEMENTARY VIDEO 1. Z-STACK OF MCP-1 *EN FACE* IMMUNOFLUORESENCE 201**

**SUPPLEMENTARY VIDEO 2. Z-STACK OF MCP-1 *EN FACE* IMMUNOFLUORESENCE WITH MCP-1 SEGMENTATION OVERLAID 202**

**SUPPLEMENTARY VIDEO 3. Z-STACK OF NF-κB *EN FACE* IMMUNOFLUORESENCE 203**

**SUPPLEMENTARY VIDEO 4. REAL-TIME MONOCYTE ADHESION TO vECs *IN VITRO* 204**

## LIST OF ABBREVIATIONS

| | |
|---|---|
| **A** | |
| aEC | Arterial endothelial cell |
| AFI | Arbitrary fluorescence intensity |
| AHSS | Acute high shear stress |
| ALSS | Acute low shear stress |
| ANOVA | Analysis of Variance |
| Ap-1 | Activating protein 1 |
| ApoE | Apoliporotein E |
| ARE | Antioxidant response element |
| ASK1 | Apoptosis signal-regulating kinase 1 |
| ATF2 | Activating transcription factor 2 |
| **B** | |
| BCA | Bicinchoninic acid |
| Bcl2 | B-Cell lymphoma 2 |
| BMK1 | Big mitogen activated protein kinase 1 (also known as ERK5) |
| BSA | Bovine Serum Albumin |
| **C** | |
| CABG | Coronary artery bypass graft |
| CBP | Creb binding protein |
| CCR2 | C-C chemokine receptor 2 |
| CCL5 | C-C chemokine ligand 5 |
| CD40 | Cluster of differentiation 40 |
| cGMP | Cyclic guanosine monophosphate |
| CO | Carbon monoxide |
| COPD | Chronic obstructive pulmonary disease |
| c-Src | Proto-oncogene tyrosine-protein kinase Src |
| Cul3 | Cullin 3 |
| **D** | |
| DMSO | Dimethyl sulphoxide |
| DNA | Deoxyribonucleic acid |
| DPBS | Dulbecco's phosphate buffered saline |
| DUSP | Dual specificity phosphatase |

**E**

| | |
|---|---|
| EC | Endothelial cell |
| ECBM | Endothelial cell basal medium |
| ECGM | Endothelial cell growth medium |
| ECM | Extracellular matrix |
| EDTA | Ethylenediaminetetraacetic acid |
| EEL | External elastic lamina |
| ELISA | Enzyme linked immunosorbent assay |
| eNOS | Endothelial nitric oxide synthase |
| EPC | Endothelial progenitor cell |
| EphB4 | Ephrin type-B receptor 4 |
| ERK1/2 | Extracellular signal-regulated kinase 1/2 |
| ERK5 | Extracellular signal-regulated kinase 5 |

**F**

| | |
|---|---|
| FAK | Focal adhesion kinase |

**G**

| | |
|---|---|
| GAPDH | Glyceraldehyde 3-Phosphate dehydrogenase |
| GCLC | Glutamate cysteine ligase, catalytic subunit |
| GCLM | Glutamate cysteine ligase, modifier subunit |
| GFP | Green fluorescent protein |
| GPCR | G-protein coupled receptor |
| GPx | Glutathione peroxidase |
| GSH | Glutathione |
| GTPase | Guanosine triphosphate hydrolase |

**H**

| | |
|---|---|
| $H_2O_2$ | Hydrogen peroxide |
| HEK293 | Human embryonic kindey 293 cell line |
| HO-1 | Heme-oxygenase 1 |
| HPLC | High performance liquid chromatography |
| HRP | Horseradish peroxidase |
| HUVEC | Human umbilical venous endothelial cell |

**I**

| | |
|---|---|
| ICAM-1 | Intercellular adhesion molecule 1 |

| | |
|---|---|
| ICC | Immunocytochemistry |
| IEL | Internal elastic lamina |
| IF | Immunofluorescence |
| IgG | Immunoglobulin G |
| IH | Intimal hyperplasia |
| IHD | Ischaemic heart disease |
| IKKα | IκB Kinase complex subunit alpha |
| IKKβ | IκB Kinase complex subunit beta |
| IL | Interleukin |
| IMA | Internal Mammary artery |
| IκBα | Nuclear factor of kappa light polypeptide gene enhancer in B-cells inhibitor, alpha |
| **J** | |
| JNK | c-Jun N-terminal kinases |
| **K** | |
| Keap1 | Kelch-like ECH-associated protein 1 |
| KLF2 | Lung Kruppel-like factor 2 |
| **L** | |
| LAD | Left anterior descending coronary artery |
| LDL | Low-density lipoprotein |
| LIMA | Left internal mammary artery |
| LSS | Laminar shear stress |
| LSV | Long saphenous vein |
| LTβR | Lymphotoxin beta receptor |
| **M** | |
| MAP3K | Mitogen activated protein kinase kinase kinase |
| MAPK | Mitogen activated protein kinase |
| MCP-1 | Monocyte chemotactic protein 1 |
| MEF2 | Myocyte enhancer factor 2 |
| MEK | Mitogen activated protein kinase kinase (MKK) |
| MEKK3 | mitogen-activated protein kinase kinase kinase 3 |
| Mins | Minutes |
| MKP-1 | Mitogen activated protein kinase phosphatase 1 |
| MMP | Matrix metalloproteinase |

| | |
|---|---|
| mRNA | Messenger ribonucleic acid |
| MSK1 | Mitogen- and stress-activated protein kinase |
| **N** | |
| NADPH | Nicotinamide adenine dinucleotide phosphate |
| NEH | Nrf2-ECH homology domain |
| NFκB | Nuclear factor of kappa light polypeptide gene enhancer in B-cells |
| NIK | NFκB inducing kinase |
| NLRP3 | NACHT, LRR & PYD domain containing protein 3 |
| NO | Nitric oxide |
| NOX | NADPH Oxidase |
| NQO1 | NADPH Quinone dehydrogenase 1 |
| Nrf2 | Nuclear factor erythroid 2 related factor 2 |
| **O** | |
| $O_2^{\bullet-}$ | Superoxide |
| ODN | Oligodeoxynucleotide |
| $ONOO^-$ | Peroxynitrite |
| OSS | Oscillatory shear stress |
| **P** | |
| PAGE | Polyacrylamide gel electrophoresis |
| PAK | p21 activated kinase |
| PBST | Phosphate buffered saline with Tween 20 |
| PCI | Percutaneous coronary intervention |
| PDGF | Platelet derived growth factor |
| PECAM-1 | Platelet-endothelial cellular adhesion molecule 1 |
| pfu | Plaque forming units |
| PGI2 | Prostacyclin |
| PI3K | Phosphoinositide 3 kinase |
| PKA | Protein kinase A |
| PKC | Protein kinase C |
| PVAT | Perivascular adipose tissue |
| **R** | |
| Rac1 | Ras-related C3 botulinum toxin substrate 1, |
| rAd | Recombinant Adenovirus |
| RANTES | Regulated on activation, normal T-Cell expressed and secreted |

| | |
|---|---|
| Rbx1 | Ring box 1 |
| RHD | Rel homology domain |
| RHO | Ras homologue pathway |
| RhoA | Ras homologue gene family, member A |
| RIP1 | Receptor interacting protein 1 |
| RNS | Reactive nitrogen species |
| ROS | Reactive oxygen species |
| RT | Room temperature |
| RT-qPCR | Reverse transcription quantitative polymerase chain reaction |
| **S** | |
| SAPK | Stress activated protein kinase |
| SDS | Sodium dodecyl sulphate |
| SEM | Standard error of mean |
| SEMA3F | Semaphorin 3F |
| Ser | Serine |
| SFN | Sulforaphane |
| SOD | Superoxide dismutase |
| SVG | Saphenous vein graft |
| **T** | |
| TAD | Transcription activation domain |
| TAK1 | Transforming growth factor beta-activated kinase 1 |
| TGF-β | Transforming growth factor beta |
| TIMP | Tissue inhibitor of metalloproteinase |
| TLR4 | Toll-like receptor 4 |
| TNFR | Tumour necrosis factor receptor |
| TNF-α | Tumour necrosis factor alpha |
| tPA | Tissue plasminogen activator |
| TRADD | Tumour necrosis factor receptor associated death domain |
| TRAF2/5 | Tumour necrosis factor receptor associated factor 2/5 |
| **V** | |
| VCAM-1 | Vascular cell adhesion molecule |
| vEC | Venous endothelial cell |
| VE-Cad | Vascular endothelial cell cadherin |

| | |
|---|---|
| VEGFA | Vascular endothelial growth factor A |
| VEGFR2 | Vascular endothelial growth factor receptor 2 |
| VSMC | Vascular smooth muscle cell |
| **W** | |
| WB | Western blot |
| Wks | Weeks |
| WT | Wild type |
| **Y** | |
| Yrs | Years |

# 1. INTRODUCTION

## 1.1 ISCHAEMIC HEART DISEASE AND MANAGEMENT

Ischaemic heart disease (IHD) remains the leading cause of morbidity and mortality in the Western world (Mozaffarian *et al.*, 2015). It occurs as a result of mismatch in oxygen supply and demand, usually due to atherosclerosis in one or more of the coronary arteries leading to significant stenosis in the coronary circulation. With an epidemiological transition occurring globally, developing, low to middle income countries are also facing dramatically increasing rates of death from IHD accounting for up to 28% of mortality in these regions (Gaziano *et al.*, 2010). Disease prevalence is exacerbated by extrinsic and intrinsic factors. Extrinsic risk factors include smoking, socioeconomic status and a diet high in saturated fat. By their very nature, extrinsic risk factors are relatively easily modified, and their effects are preventable. Whereby, the cessation of smoking or improvement of diet offer huge benefits in reducing cardiovascular-associated diseases. Intrinsically, IHD is worsened by certain genetic predispositions and hyperlipidaemia, which also contribute significantly to the progressive pathology of atherosclerosis and correlate strongly with increased morbidity (Davignon *et al.*, 1988; Barter *et al.*, 2007). With its' current and burgeoning burden across the world, it is essential that treatments for IHD are advanced through improved understanding of molecular aetiology of both pharmacological and interventional strategies.

Management of IHD can be problematic, given the differing severities of stenosis and speeds of progression; however, management approaches fall into two categories. The first of these is non-invasive management. This can involve alterations to extrinsic risk factors, including modified diet and cessation of smoking, or use of pharmacological agents aimed at moderating thrombotic events, blood pressure regulation and lipid accumulation. Alternatively, IHD can be managed through invasive means, either catheter based (invasive cardiology) or surgical, which both function to re-vascularise cardiac tissue distal to the site of stenosis, thus re-balancing the mismatch in oxygen supply and demand (Hansson Hansson, 2005). Percutaneous coronary

interventions (PCI), such as balloon angioplasty and stenting (FIGURE 1.1.A. and B., respectively), aim to unblock the coronary stenosis. Whereas, coronary artery bypass graft (CABG) surgery (FIGURE 1.1.C.) diverts blood flow from the aorta to the obstructed coronary artery, distal to the site of blockage, with the use of an autologous, non-diseased vessel, most commonly the long saphenous vein (LSV) and internal mammary artery (IMA). CABG remains the gold standard intervention in many patients in the presence of complex coronary disease, diabetes and poor ventricular function (Alderman *et al.*, 1997; Eagle *et al.*, 2004; Serruys *et al.*, 2009; Mohr *et al.*, 2013).

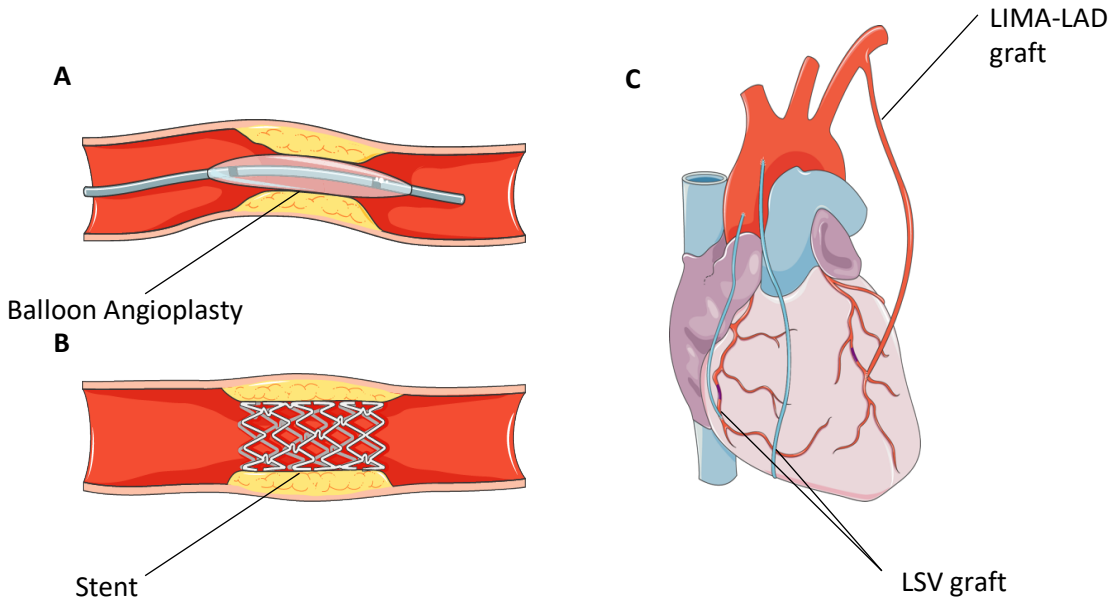


**FIGURE 1.1. Interventional treatment strategies for IHD**

Diagrammatic representation of interventional approaches for the treatment of IHD. This figure was created using images from the Servier medical art library (smart.servier.com).

A. Catheter and balloon angioplasty
B. Catheter and bare metal stent
C. CABG with a single LIMA-LAD graft and two LSV grafts

## 1.2 SAPHENOUS VEIN GRAFT FAILURE

The LSV is the most commonly used conduit for CABG in patients with multi-vessel coronary artery disease (CAD) because it is easy and quick to harvest, and it can provide enough length to bypass multiple diseased coronaries (Eagle *et al.*, 2004; Serruys *et al.*, 2009; Wan *et al.*, 2012). The left internal mammary artery (LIMA) to left anterior descending coronary artery (LAD) (FIGURE 1.1.A.) is the graft of choice for patients receiving a single graft or two neighbouring grafts (as a Y or sequential graft) due to its higher long-term patency of approximately 85-95% after 10 years, compared with 50-60% patency in LSV grafts, as well as the improved long-term survival benefit (Lytle *et al.*, 1985; Sabik, 2011; Garatti *et al.*, 2014). The use of LIMA, however, is mainly restricted by its length. In contrast, for patients with multi-vessel CAD, at least one or more LSV grafts will still be used and, despite increases in the usage of multiple arterial grafts, the LSV remains a highly important conduit in CABG (Goldman *et al.*, 2011; Garatti *et al.*, 2014). The use of LSV is not without limitations, however. Its longevity continues to be complicated by the development of vascular inflammation, intimal hyperplasia (IH) and superimposed accelerated atherosclerosis leading to compromised graft efficacy and ultimately, vein graft failure (VGF) (Newby *et al.*, 2000).

### 1.2.1 TEMPORAL PATHOGENESIS OF VGF

VGF can be separated into two distinct temporal categories; firstly, early graft failure defined as occurring within one month to one-year post-implantation and which arises in 3-15% of venous grafts (FIGURE 1.2.). This early graft failure is due to occlusive thrombotic events and is most commonly due to technical mismanagement of surgery. It is considered that the use of high pressure distension, as an attempt to avoid venospasm prior to implantation, and the removal of the vasa vasorum during vessel harvest, which induces tissue ischaemia and a loss of innervation deep into the medial layer of the vessel, are major contributors to early graft failure (Rousou *et al.*, 2009; Dashwood *et al.*, 2013). Both venospasm and stripping of the pedicle of the

LSV lead to decreases in the vessel distensibility, and reductions in oxygen supply to both intimal and medial layers. These in turn induce EC and VSMC dysfunction, respectively, which contribute significantly to thrombotic events (Souza *et al.*, 2002). Both of these practices also cause focal disruption to the endothelial monolayer, triggering fibrin deposition and, in turn, platelet and erythrocyte aggregation to the surface of the vein graft wall. Once aggregated to the site of injury, platelets become activated, secreting thrombospondin, fibrinogen and β-thromboglobulin, amongst numerous other clotting factors, contributing largely to early thrombotic events in SVGs (Dobrin *et al.*, 1992; Verrier *et al.*, 1996; Wan *et al*., 2012). In addition to the platelet-driven clotting factor secretion, venous conduits also possess innately reduced antithrombotic abilities as compared with arterial equivalents (Cox *et al.*, 1991; Motwani *et al.*, 1998). The advent of both low-pressure distension, for vein preparation, and the 'no-touch' technique, for graft harvest and implantation, can reduce the possibility of thrombotic events early in the life of the graft, in addition to greatly extending long-term patency (Angelini *et al.*, 1990; Dashwood *et al.*, 2013; De Souza *et al.*, 2017).

Pharmacological interventions targeting thromboses are also widely used for the prevention of early graft failure. Commonly, this includes treatment with anti-platelet agent, aspirin, which drastically reduces the risk of thrombosis when initiated early, following CABG (Stein *et al.*, 2004). Additionally, aspirin may be used in conjunction with clopidogrel as part of a dual anti-platelet therapy; not only has this dual therapy been shown to be effective at increasing early graft patency rates, but it also halves 30-day mortality when compared with aspirin alone (Deo *et al.*, 2013). Another advantage of clopidogrel treatment is its ability to reduce VSMC proliferation, an important contributor to late VGF (Deo *et al*., 2013). Late stage graft failure is characterised initially by endothelial dysfunction, followed by the progressive development of intimal hyperplasia and superimposed atherosclerosis, which leads to graft occlusion after rupture of atherosclerotic plaques and thrombosis. Vein graft occlusion due to late stage VGF

occurs in approximately 50-60% of vein grafts within 10 years (FIGURE 1.2.) (Harskamp *et al.*, 2013). As such, the remainder of Section 1.2. will focus on the events leading to late stage VGF.

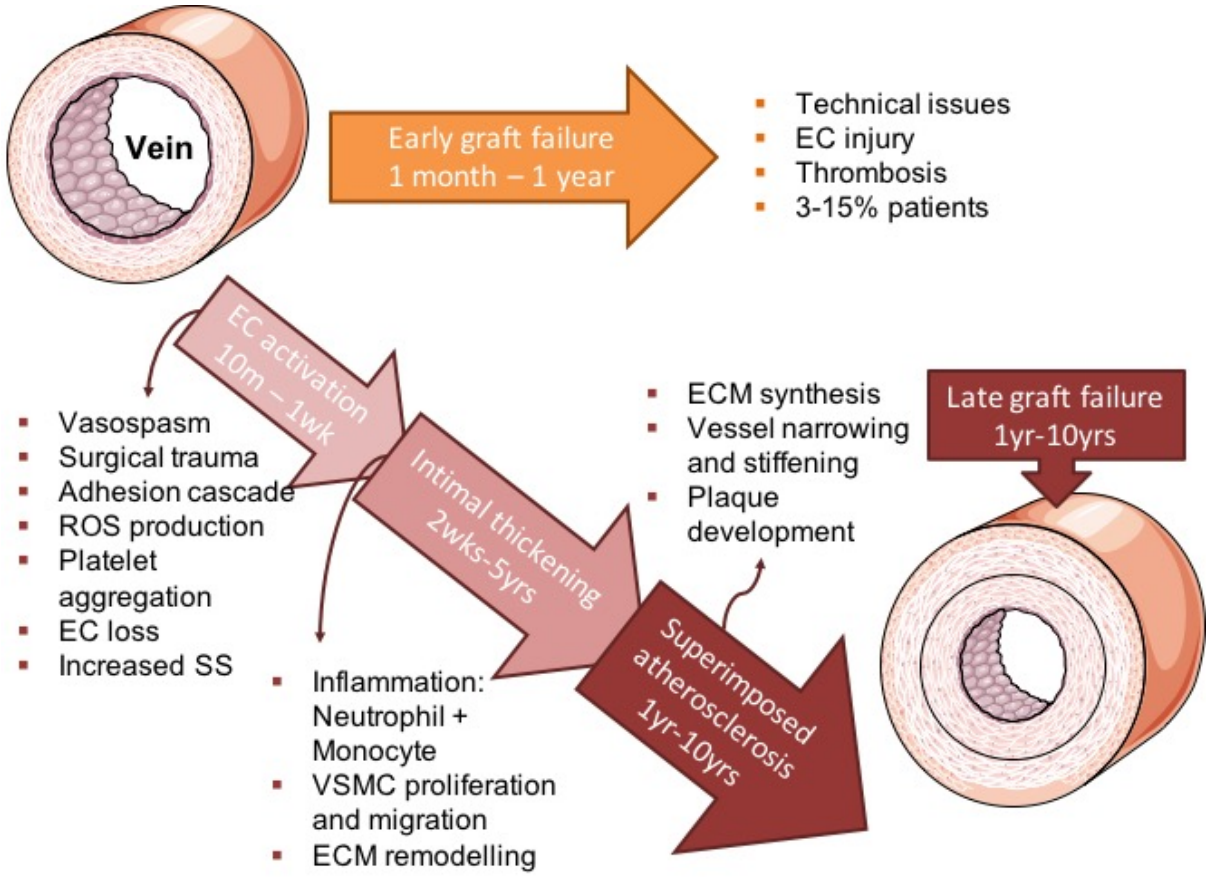


**FIGURE 1.2. Early and late stage vein graft failure**

Vein graft failure (VGF) occurs early or late after implantation. Early VGF occurs within one month to one year after surgery as a result of thrombosis, mainly caused by technical issues with surgery. Late stage VGF is a slower process characterised by early EC injury and activation, which precedes IH development, superimposed atherosclerosis and, ultimately, occlusion of the lumen.

EC: endothelial cell; ROS: reactive oxygen species; ECM: extracellular matrix; VSMC: vascular smooth muscle cell; SS: shear stress; 10m: 10 minutes; 2wks: 2 weeks; 1 yr: 1 year. This figure was partly created with the Servier medical art library (smart.servier.com).

### 1.2.2 HAEMODYNAMIC CONTRIBUTION TO VGF

Endothelial Cells (ECs) play a pivotal role in regulating vascular homeostasis, with the quiescent endothelium protecting the vascular tree through the promotion of an anti-coagulant and anti-inflammatory environment, as well as regulating lipoprotein permeability (Chiu *et al.*, 2011). The role of ECs in the development of VGF, however, remains relatively poorly understood; previous studies have suggested that ECs may not be important as they are lost following surgery (Komori *et al.*, 2002; Xu *et al.*, 2003; Torsney *et al.*, 2004; Isaji *et al.*, 2017). Most of these studies, however, observed late time points, from between 24 hours to 1 week after implantation, and did not address the immediate changes in ECs (i.e. <24 hours). Moreover, it has not been determined whether EC denudation and loss are purely due to vessel manipulation and biomechanical changes occurring during harvest and immediately after implantation; or are driven by EC activation and apoptosis in response to acute changes in unconditioned ECs following graft implantation. Endothelial loss as a result of grafting is thought to further exacerbate processes involved in early IH pathogenesis, such as platelet aggregation, inflammatory cell infiltration and mitogenesis (Owens, 2010; Osgood *et al.*, 2014). Circulating endothelial progenitor cells are known to limit the duration of such processes, via the restoration of the endothelial monolayer from roughly one week after vessel implantation (Xu *et al.*, 2003; Zampetaki *et al.*, 2008). This re-endothelialisation is vitally important to re-establishing the homeostatic function of the endothelium. However, in the interval between implantation and endothelial restoration, the path to pathogenesis has already begun, perhaps irreversibly.

It is widely accepted that harvesting and implantation of the LSV impacts on EC integrity to some degree, despite continued attempts to better preserve the endothelium through minimising manipulation (Hwang *et al.*, 2012; Harskamp *et al.*, 2013; Sen *et al.*, 2013). However, many of these studies into EC integrity in the LSV fail to address the degree of dysfunction in the

preserved endothelium. In fact, studies using an *ex vivo* perfusion model of LSV, demonstrated that venous ECs are preserved, but activated, in response to graft preparation (Kwei *et al.*, 2004; Osgood *et al.*, 2014). These findings are corroborated by the demonstration that acute exposure of LSV to high shear stress is associated with minimum denudation and significant pro-inflammatory response in venous ECs (Zakkar *et al.*, 2011). There remain radical and unavoidable changes to the environment of the saphenous vein after implantation that are inherent in the procedure. Immediately after implantation of the LSV into arterial circulation, the vessel is exposed to a much higher rate of blood flow, resulting in significant increased longitudinal wall shear stress (from 0.5-4 dyn/cm$^2$ to 12-30 dyn/cm$^2$) (Dobrin *et al.*, 1989). These changes result in the vein graft acutely experiencing new haemodynamic forces considerably greater than it is able to accommodate (Chiu *et al*., 2011). This arterial environmental transformation contributes significantly to the acute inflammatory response known to be associated with endothelial dysfunction and the development of intimal hyperplasia (IH), though the exact mechanism remains unclear (Lytle *et al.*, 1985; Amano *et al.*, 1991; Motwani *et al.*, 1998; Sarjeant *et al.*, 2002; Harskamp *et al.*, 2013). In addition to the involvement of arterial haemodynamics in the development of IH, the configuration of the vessel and the graft-artery anastomosis also influences focal development of IH (Ghista *et al.*, 2013). Similar to the focal nature of plaque distribution at bifurcations in atherosclerosis, disturbed flow patterns at sites of graft anastomosis induce vascular injury, which, in turn, triggers inflammatory cascades, IH pathogenesis and accelerated atherosclerotic lesions (Keynton *et al.*, 2001; Ghista *et al.*, 2013).

### 1.2.3 PATHOLOGY OF INTIMAL HYPERPLASIA AND ACCELERATED ATHEROSCLEROIS

IH is the result of chronic structural changes occurring in vein grafts due to abnormal migration and proliferation of vascular smooth muscle cells (VSMCs) accompanied by an increase in extracellular matrix (ECM) degradation and deposition (Bryan *et al.*, 1994; Sarjeant *et al.*, 2002; Mitra *et al.*, 2006). Within a normal 'healthy' vessel, interactions between ECs and VSMCs, and

between VSMCs and ECM, sustain a quiescent phenotype in VSMCs (West *et al.*, 2001). Despite the LSV graft generally being considered as 'non-diseased', this cell-cell or cell-matrix interaction has already gone awry, and many veins possess a degree of intimal thickening and fibrosis even before implantation (Thiene *et al.*, 1980).

Following initial endothelial injury, and subsequent EC dysfunction, however, the balance of physiological intimal thickening is tipped in the direction of pathogenesis. Aggregated platelets adhered to the graft wall secrete mitogenic and inflammatory factors affecting VSMCs and ECs alike, including platelet derived growth factor (PDGF), transforming growth factor β (TGF-β) and interleukin 1 (IL-1) (de Vries *et al.*, 2016). Redox balance is also extremely important in the maintenance of normal functionality in the vascular wall. The bioavailability of endothelium derived relaxing factors, nitric oxide (NO) and prostaglandin (PGI2), is fundamental to the maintenance of vascular tone, as well as to the regulation of EC quiescence and VSMC proliferation, migration and contractility (FIGURE 1.9.) (West *et al.*, 2001). The dysregulation of NO balance has profound effects on the vascular wall, particularly in the context of the vein graft. Whereby the tipping of this balance towards reduced NO availability and increased ROS production, in particular, superoxide ($O2^{\bullet-}$) generation, partly through eNOS uncoupling by combined actions of NADPH oxidase (NOX) and arginase enzymes, significantly potentiates IH pathogenesis (West *et al*., 2001; Guzik *et al.*, 2005; Forstermann, 2008; Siragusa *et al.*, 2016). Increased superoxide generation functions to scavenge NO (together forming peroxynitrite (ONOO-)) and directly regulate VSMC proliferation, which begins the development of a highly atherogenic environment, initiated by endothelial dysfunction (Zakkar *et al.*, 2015). These factors together help contribute to the phenotypic switching in VSMCs, from a contractile to synthetic state, and the initiation of migration of VSMCs into the intima and their proliferation (FIGURE 1.3.) (Uchida *et al.*, 1996; Newby *et al.*, 2000; Mitra *et al.*, 2006; Owens *et al.*, 2015).

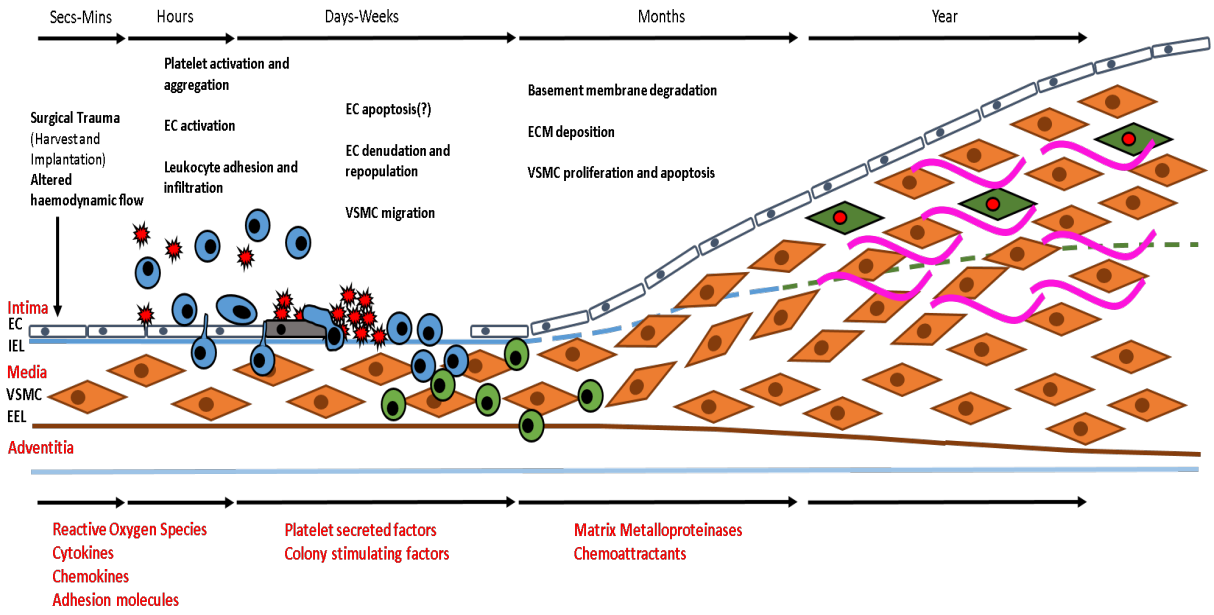


**FIGURE 1.3. Mechanism of late-stage VGF**

Temporal development of late stage vein graft failure beginning from surgical trauma and altered haemodynamics, ultimately leading to intimal thickening and vascular remodelling through the combined actions of multiple vascular cell types and extracellular matrix interactions. EC: endothelial cell; ECM: extracellular matrix; VSMC: vascular smooth muscle cell; IEL: internal elastic lamina; EEL: external elastic lamina.

VSMC migration is not only driven by the presence of chemo-attractants and matrix metalloproteinase (MMP) proteolytic action, but also requires the additional remodelling of the cytoskeleton and contacts with the ECM (Newby, 2005). MMPs play a fundamental role in VGF due to their wide-ranging capabilities in degradation of ECM components. The ability of MMPs to regulate degradation of the ECM of the basement membrane, as well as cell-cell contacts (cadherins) between VSMCs, also provides VSMCs with the capacity to de-differentiate from a contractile to synthetic VSMC, migrate into the intima and, once there, proliferate (FIGURE 1.3.) (Newby, 2005; Rzucidlo *et al.*, 2007). Between 2 and 4 weeks after surgery, intimal thickening is apparent, owing to the accumulation of VSMCs and extensive collagen and proteoglycan

deposition, which leads to the inward enlarging of the intimal layer (FIGURE 1.3.) (Owens, 2010). The multitude of elements contributing to IH occurring between one month and one year after bypass, result in widespread remodelling throughout the SVG. Within one year, the thickened, fibrotic, stiffer vessel becomes the ideal environment for the formation of atherosclerotic lesions (Walts *et al.*, 1987; Motwani *et al.*, 1998; Owens *et al.*, 2015). Atherogenic-type lesions predominate in the SVG after the first year; though they do not develop quite as they do in the arterial system. Lesions, although more pronounced at sites of anastomosis, are much more diffuse throughout the length of the vessel as compared with the focally distributed atherosclerotic plaques commonly found in the coronary vasculature (Ratliff *et al.*, 1989; Yahagi *et al.*, 2016). Besides the obvious differences in speed of progression and lesion localisation, SVG atheromas still share many features with coronary atheromas, such as the presence of both VSMC- and macrophage-derived foam cell populations, presence of a thin fibrous cap and intra-plaque haemorrhage (Yahagi *et al*., 2016). SVG lesion development predisposes the graft to constant risk of plaque rupture and relapse of symptoms of coronary atherosclerosis, including acute myocardial infarction. With the huge complexity of the processes ultimately leading to late-stage VGF, and the dangers that this poses to patients, there is a drastic need for improved understanding of the molecular nature of all stages of the pathology.

### 1.2.4 CABG CONDUIT COMPARISON

LSV and IMA differ vastly in structure and functional capability. Structurally, the IMA is a very elastic artery with a medial layer formed of distinct sheets of interspersed wave-like collagen and VSMCs arranged circumferentially with very little variability (Canham *et al.*, 1997). Interestingly, the IMA shares a great deal of structural homology with the LAD, with the primary differences being that the LAD possesses a smaller VSMC medial area and more elastin (Prim *et al*., 2016). Whereas the LSV is considerably more varied in size and structure, with a much narrower medial layer composed primarily of collagen, fenestrated elastic laminae, less elastin

and fewer VSMCs (FIGURE 1.4.) (Canham *et al.*, 1997). Thus, the LSV suffers from compliance mismatch under higher physiological pressures, when implanted into the arterial circulation. This results in the vessel being less able to passively expand to accommodate the higher-pressure due to its inherently thinner, less dense medial layer and its highly aligned collagen structure (Ghista *et al.*, 2013).

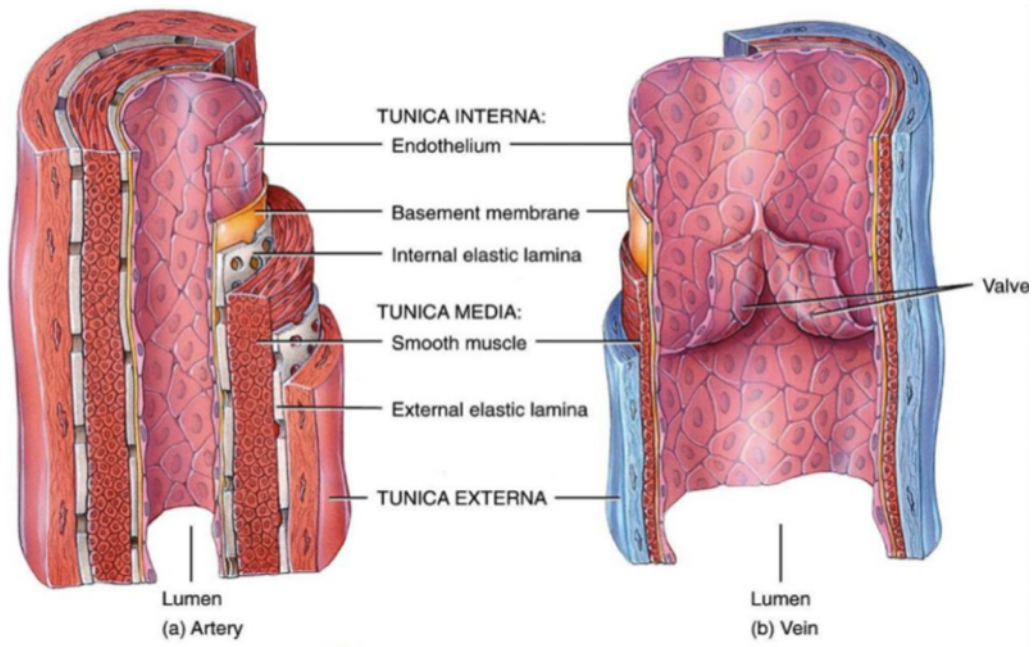


**FIGURE 1.4. Structural differences between large arteries and veins**

The walls of large arteries and veins are structurally different. The arterial wall is considerably thicker than the venous wall, with a larger density of elastic fibre and VSMCs within the medial layer, allowing the vessel to accommodate much higher pressures. In contrast, both the medial and adventitial layers of veins are less densely populated, compared to arteries. ECs within the intima are also vastly different between these two branches of the vasculature, with arterial ECs more elongated and aligned with the direction of flow, compared to shorter, rounder, non-aligned venous ECs. Figure taken from www.anatomylibrary.us

Structural differences between the arterial and venous vasculature have been understood since the 17th century; however, the structurally discrete features of the endothelium in these two tissues was not appreciated until the mid-20th century (Weibel *et al.*, 1964; Florey, 1966). In development, arterial and venous vascular beds emanate from molecularly distinct foundations, and differences in ephrin B2/EphB4, Vascular endothelial growth factor A (VEGF-A) and Notch signalling pathways, amongst several others, define vessel identity even before initiation of circulatory flow (Aitsebaomo *et al.*, 2008). These very early features of the developing vasculature indicate the predetermined nature of the arteriovenous endothelium. However, due to the extremely heterogeneous and structurally diverse tissue locations of the endothelium throughout the body, its composition and structure is tissue dependent and heavily influenced by extrinsic factors.

Within mature healthy blood vessels, the endothelium is typically continuous and non-fenestrated, with each cell within the monolayer being attached through intercellular tight or adherens junctions (Aird, 2007). Arterial ECs (aECs) exhibit many more tight junctions per cell than venous ECs (vECs), owing to the considerably higher pressure within the arterial system (Dejana, 2004). Greater tight junction distribution in aECs functions to prevent para-cellular transport, thus reducing endothelial permeability to solutes and lipids (Bazzoni *et al.*, 2004). Moreover, different haemodynamic patterns between the arterial and venous tree result in aEC alignment with the direction of flow, as such, they become elongated and flattened, whereas vECs do not align with flow and are morphologically shorter and wider (Aird, 2007). Interestingly, such morphological features can be reversible both *in vivo* and *in vitro* suggesting that EC phenotypes maintain a degree of plasticity (Flaherty *et al.*, 1972). This adaptability is particularly evident *in vitro*, with the loss and gain of numerous expressed genes characteristic of EC type (or location) once cells have been passaged, clearly showing the impact of cellular microenvironment on EC phenotype (Lacorre *et al.*, 2004). When comparing the impact of altered haemodynamics (mainly shear stress), Zakkar *et al*. observed that vECs respond to acute

changes in shear stress by inducing a pro-inflammatory profile mediated by the activation of MAPK signalling pathways, while aECs remained resistant to such stimuli through action of atheroprotective signalling pathways (Zakkar *et al.*, 2008) (FIGURES 1.5 and 1.9.). This differential response is in part related to the fact that aECs react to shear stress by upregulating anti-inflammatory mediators such as MAP kinase phosphatase 1 (MKP-1), Nrf2 and KLF2; whereas this response appears to be innately reduced in vECs (Dekker *et al.*, 2006; Zakkar *et al.*, 2008; Zakkar *et al.*, 2009).

It has also been suggested, however, that it is not only environmental influences that determine mature EC fate, but that epigenetic modifications also function to more rigidly and locally define the role of the endothelium (Chi *et al.*, 2003). In a study by Deng *et al*., human coronary aECs in culture showed greater increases in adhesion-, proliferation- and apoptosis-related genes when stimulated with oxidised LDL than ECs from human LSV (Deng *et al.*, 2006). This phenotypic intransience *in vitro* can help in our understanding of inherent susceptibility to atherosclerosis in aECs, as compared with vECs; and, perhaps also in the early response of vECs to conditions of the arterial environment after CABG surgery. Heterogeneity in the endothelium, due to its vascular origin, is an integral property of the cell type, allowing it to be governed by both its surrounding environment and pre-determined cell fate. However, this same heterogeneity makes understanding vascular disorders, and subsequent therapeutic targeting of the endothelium, increasingly complex.

### 1.2.5 CURRENT STRATEGIES TO IMPROVE SVG PATENCY AND EC INTEGRITY

Owing to the finite lifespan of vein grafts, the likelihood that patients may have to have follow-up procedures or receive a form of prophylaxis is relatively high. However, to date, despite the wealth of studies investigating graft maintenance, no effective treatment exists for the extension of SVG patency (Wan *et al*., 2012). Despite the obvious benefits to prolongation of patency on patient's lives, if left untreated, vein graft failure can further contribute to the

recurrence of angina or development of myocardial infarction (MI). Intraoperative measures, such as the 'no-touch' technique, whereby, during harvest of the LSV, the perivascular fat surrounding the vessel is preserved, have been found to ameliorate thrombotic events related to early graft failure; however, their effect later in the life of the graft still remains unclear (Souza *et al.*, 2002). Of particular growing interest, is the potential benefit of perivascular adipose tissue (PVAT) preservation on the pathophysiology of the vein graft. PVAT has long been overlooked in vascular biology, far from being simply an energy source, PVAT releases and receives a number of functional substances known to influence vessel behaviour, affecting functions as diverse as relaxation to inflammation (Szasz *et al.*, 2012). It is well recognised that the use of the 'no-touch' technique results in greater preservation of the endothelium following harvest; however, what is less well documented is the function that remaining PVAT has in maintaining VSMC quiescence and contraction (Dashwood *et al.*, 2013; Fernandez-Alfonso *et al.*, 2017). The refinement of LSV surgical harvest and preparation techniques has enabled a reduction in conduit damage prior to implantation; however, pharmacological advances do not appear to be progressing at the same speed, or with anything like similar results (Souza *et al*., 2002; Alexander *et al.*, 2005; Alexander *et al.*, 2005; Taggart *et al.*, 2015).

Another perioperative intervention effectual in both animal and human models is the use of external sheaths around the graft, first described in 1963 (Parsonnet *et al.*, 1963). Use of an external, porous stent surrounding the saphenous vein in a porcine model of arteriovenous bypass grafting resulted in significant reductions in intimal thickening (Angelini *et al.*, 1996; Izzat *et al.*, 1996; Jeremy *et al.*, 2004). Two primary features of the sheath are: porosity, to allow for angiogenic growth of microvessels in order to keep the newly forming 'neoadventitia' oxygenated (in essence, the regrowth of the absent vasa vasorum) (George et al., 2001); and non-restrictiveness, permitting the formation of a matrix between the vessel and sheath for outgrowth of microvessels (Jeremy *et al.*, 2007). External sheaths have also been shown to prevent effects associated with the distension of the graft under arterial pressure and resultant

regions of disturbed flow appear to be corrected in a porcine model of vein grafting (Jeremy *et al*., 2007). This finding was validated in the first successful in-man trial of external stenting, whereby stented vessels showed decreased deformation of the lumen and overall vessel structure, as well as a significant reduction in IH development with one-year post-implantation (Taggart *et al.*, 2015). However, opposing results were seen the Extent trial, in which the external Dacron stent was utilised in CABG patients; disappointingly all stented vessels thrombosed within 19 months after surgery and the trial was stopped, perhaps due to the rigidity of the stent (Murphy *et al.*, 2007). Despite the reasonably promising nature of external stenting seen in preclinical and small clinical studies, the development of a suitable material fulfilling a multitude of desired specifications remains the challenge faced by clinicians, chemists and biologists.

Developments of pharmacologic interventions for the treatment of VGF continue to endeavour in pursuit of a suitable therapeutic target for both cellular specificity and efficacy. Secondary prevention of the symptoms of late VGF pharmacologically provides equally demanding questions relating to treatment strategy. Addressing maintenance of EC functionality after surgical trauma is of paramount importance, peri-operatively, for SVGs; this requires preservation of endothelial coverage, as well as preservation of the vasomotor actions of ECs (Woodward *et al.*, 2016). Recent developments have led to the renewed interest in the pleiotropic effects of statins for preservation of EC function, due to their role in the conservation of redox balance in the endothelium and vascular wall (Margaritis *et al.*, 2014). In addition to the widely understood lipid-lowering effects of statins, it has been reported that they are able to prevent activation of pro-oxidant systems whilst boosting cellular defence mechanisms (Cannon *et al.*, 2004; Kulik *et al.*, 2008; Kulik *et al.*, 2011; Curl *et al.*, 2016). Pre-treatment of CABG patients with Atorvastatin improved redox balance in patients after surgery, as well as in an *ex vivo* SVG model, shown by reduced plasma levels of monodialdehyde, a marker of oxidative stress, and inhibition of oxidant enzyme, nicotinamide adenine dinucleotide phosphate (NADPH) oxidase (NOX) activity, respectively (Antoniades *et al.*, 2010). Antoniades

and colleagues further showed that Atorvastatin ameliorates vascular redox state through eNOS coupling in the presence of its co-factor, Tetrahydrobiopterin (BH4), ultimately leading to reduced vascular superoxide ($O_2^{\bullet}$) production and improved vessel function (Antoniades *et al.*, 2011). Additional agents targeting NADPH oxidase and NO generation which have shown some promise in pre-clinical studies, include nitroaspirins, NO donors, eicosanoids, phosphodiesterase inhibitors (e.g. sildenafil) and corticosteroids, such as dexamethasone (Muzaffar *et al.*, 2005; Zakkar *et al.*, 2011). Finally, it is well understood that aspirin has a profound impact on reduction of early graft failure by prevention of thrombotic events due to its antiplatelet activity. However, aspirin alone, or in combination with clopidogrel, does not yet appear to significantly impact upon longer-term graft patency (Harskamp *et al.*, 2013).

In addition to more well-established treatments, the potential for gene therapy in VGF offers an interesting therapeutic direction. Intraoperatively, the saphenous vein is easily accessible, allowing *in situ* delivery of gene therapies directly to the tissue (Harskamp *et al.*, 2013; George *et al.*, 2011). Many pre-clinical trials of gene therapy show promise in these controlled settings, with very diverse targets including MMPs, tissue inhibitor of MMPs (TIMPs), MCP-1 and eNOS (George *et al.*, 1998; George *et al.*, 2000; West *et al.,* 2001; Turner *et al.*, 2005; Akowuah *et al.*, 2005; Schepers *et al.*, 2006; George *et al*., 2011). However, to date, only one randomised controlled trial has assessed gene therapy; the PREVENT-IV study (Alexander *et al.*, 2005). The trial involved the use of a decoy oligonucleotide, edifoligide, which binds to the transcription factor, E2F, known to have a role in the initiation of IH (Giangrande Giangrande *et al.*, 2007). Edifoligide appeared to have no benefit in preventing VGF at between 12 and 18 months post-surgery and the trial failed at stage IV (Alexander *et al.*, 2005).

If late VGF is diagnosed, and the opportunity for pharmacological management has passed, medical or surgical interventions will be employed; however, the risks associated with revascularisation are significant. Such management would involve either a repeat CABG surgery

or percutaneous interventions depending on patient characteristics and occlusion status (Harskamp *et al*., 2013). Cases of in-stent restenosis and recurrent VGF after multiple CABG surgeries or PCI are common. Despite showing reasonable revascularisation rates, repeat surgeries are associated with high morbidity rates and return of symptoms, including MI and angina, are frequent (Harskamp *et al.*, 2013). The obvious successes seen with CABG surgery are unquestionable, nevertheless, late vein graft failure, despite many surgical and preclinical advances, remains a significant and, as yet, pharmacologically untreated clinical challenge.

## 1.3 VASCULAR INFLAMMATION AND THE ENDOTHELIUM

Vascular inflammation is a complex response to acute and chronic harmful stimuli involving all aspects of the vascular wall including the endothelium and ECM as well as circulating immune system cells (neutrophils, monocytes and lymphocytes) (Sprague *et al*., 2009). Activators of the inflammatory response are numerous and include circulating cytokines, platelet products, reactive oxygen species (ROS), reactive nitrogen species (RNS), angiotensin II and biomechanical factors (Sprague *et al.*, 2009). Once activated, ECs initiate complex networks of adhesion molecules, cytokines and recruitment of inflammatory cells, which act to disseminate physiological changes within the endothelium and the vascular wall through interactions with VSMCs and ECM (Szmitko *et al.*, 2003). Vasospasm, surgical trauma and hypoxia during harvesting of the LSV typically result in EC activation (Bryan *et al.*, 1994; Motwani *et al.*, 1998). The induction of pro-inflammatory signalling pathways and EC activation, which can be partly ameliorated by the utilization of minimum or 'no touch' techniques during the harvest process (Dries *et al.*, 1992; Souza *et al.*, 1999; Cornelissen *et al.*, 2004). ECs are further activated by the sudden exposure to new mechanical forces in the arterial circulation, including distension and increased shear stress (Gosling *et al.*, 1999; Golledge *et al.*, 2000).

EC activation results in the triggering of the adhesion cascade characterised by the rapid expression of chemokines, such as monocyte chemotactic protein 1 (MCP-1)) and the expression of adhesion molecules, including those of the selectin family (E-selectin and P-selectin) and the cellular adhesion molecule family, intercellular adhesion molecule 1 (ICAM1), platelet endothelial cell adhesion molecule 1 (PECAM1) and vascular cell adhesion molecule 1 (VCAM1) (Berk *et al.*, 2001; Bonetti *et al.*, 2003,). Initial activation of the endothelium rapidly leads to leukocyte recruitment, which is in part mediated through changes in calcium ($Ca^{2+}$) homeostasis and the Ras homologue (RHO) pathway (FIGURE 1.5.A) (Birch *et al.*, 1994; Dixit *et al.*, 2012). Activation of the RHO pathway, through ligand binding to G-protein coupled receptors (GPCRs), causes loosening of tight junctions between ECs and activates GTPases; whereas, increases in intracellular $Ca^{2+}$ facilitates the movement of P-selectin to the luminal surface (Pober *et al.*, 2007). Together, these rapid actions of GPCRs and $Ca^{2+}$ help to facilitate leukocyte trans-endothelial migration (Ley *et al.*, 2007). However, the actions of transduction through RHO and $Ca^{2+}$ are transient and GPCRs quickly become desensitised (approximately 10 minutes post-stimulus), this phase of acute inflammation is commonly known as type I (FIGURE 1.5.A.) (Gainetdinov *et al.*, 2004).

---

**FIGURE 1.5. Endothelial cell acute inflammatory responses**

The endothelium is the first point of contact for systemic sources of inflammation; as such, its response is hugely important in propagation of inflammatory stimuli through the vessel wall and beyond. (A) Upon insult of acute high shear stress, *in vitro*, vECs activate the Rho-GTPase pathway which affects downstream effectors and the cytoskeleton. Within the first 10 minutes of acute high flow there is also an increase in intracellular calcium leading to movement of P-selectin to the luminal surface. Together these actions constitute type I (acute) inflammation. (B) Following this, there is activation of a more prolonged (type II) inflammatory response, which results in the activation of MAPK-mediated and NF-$\kappa$B pro-inflammatory pathways; resulting in expression of adhesion molecules, cytokines, chemokines and increases in intracellular ROS. The interplay between ECs and VSMCs acutely under shear stress remains unclear with the extent of intercellular communication a relatively unexplored area.

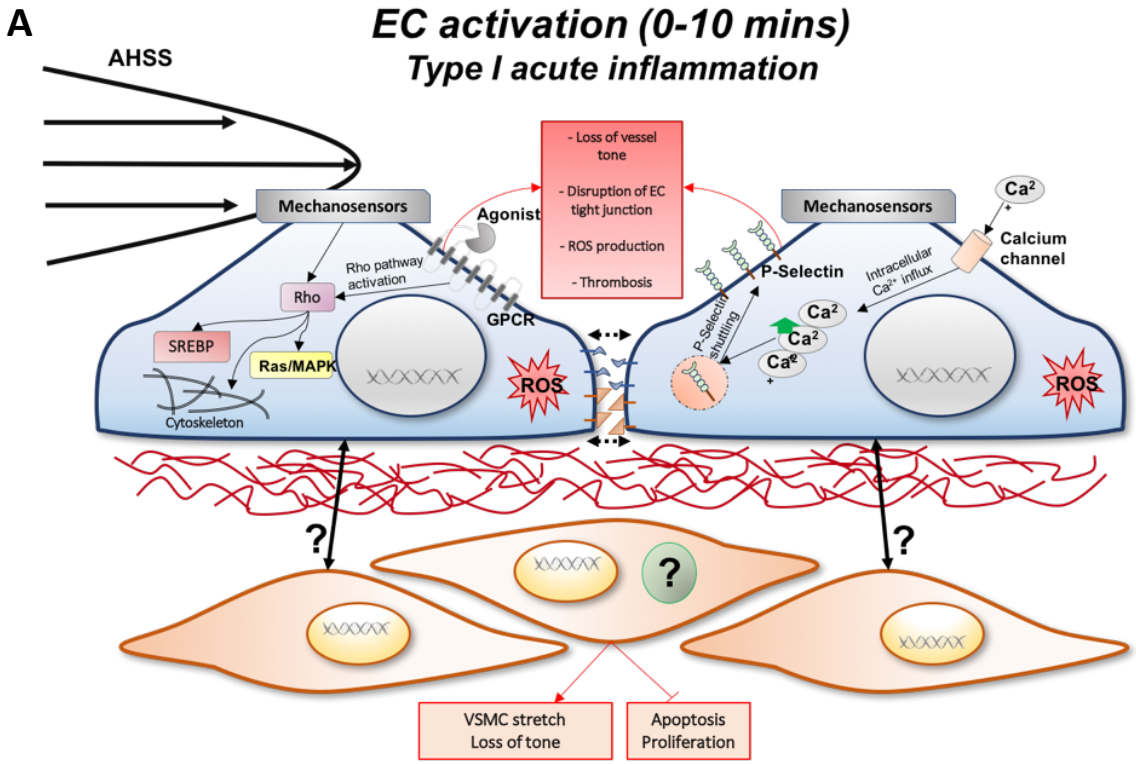
A
EC activation (0-10 mins)
Type I acute inflammation
AHSS
Mechanosensors
Agonist
- Loss of vessel tone
- Disruption of EC tight junction
- ROS production
- Thrombosis
Rho pathway activation
Rho
SREBP
Ras/MAPK
Cytoskeleton
GPCR
ROS
P-Selectin
P-Selectin shuttling
Ca2
Calcium channel
Intracellular Ca2+ influx
?
VSMC stretch
Loss of tone
Apoptosis
Proliferation

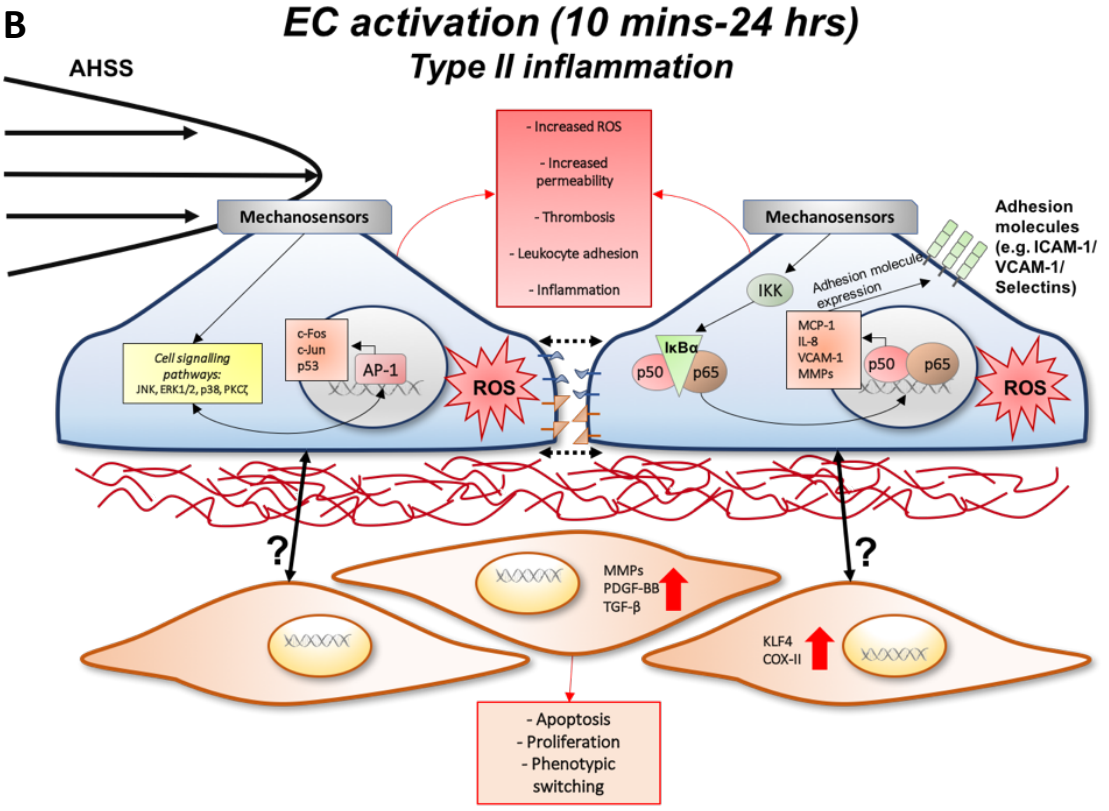
B
EC activation (10 mins-24 hrs)
Type II inflammation
AHSS
Mechanosensors
- Increased ROS
- Increased permeability
- Thrombosis
- Leukocyte adhesion
- Inflammation
Adhesion molecules (e.g. ICAM-1/ VCAM-1/ Selectins)
Adhesion molecules expression
IKK
IκBα
p50
p65
MCP-1
IL-8
VCAM-1
MMPs
Cell signalling pathways:
JNK, ERK1/2, p38, PKCζ
c-Fos
c-Jun
p53
AP-1
ROS
?
MMPs
PDGF-BB
TGF-β
KLF4
COX-II
- Apoptosis
- Proliferation
- Phenotypic switching

Prolonged, or type II, inflammatory activation of ECs requires the sustained action of physiologic stress- or cytokine-mediated signalling through the involvement of mitogen activated protein kinases (MAPKs) and pro-inflammatory transcription factors such as nuclear factor kappa B (NF-$\kappa$B) and activating protein 1 (AP-1) (Baeuerle *et al.*, 1994; Ahmad *et al.*, 1998; Dong *et al.*, 2002; Van der Heiden *et al.*, 2010). Typically, NF-$\kappa$B and MAPK mediated inflammatory responses involve the comparable, but not exclusive, expression of many genes associated with the adhesion cascade, cytokines, chemokines and MMPs in a time-dependent and evolving manner between 10 minutes and 24 hours after activation (FIGURE 1.5.B.) (Munro *et al.*, 1989; Tak *et al.*, 2001). Having such integral roles in the propagation of inflammatory responses makes these pathways exciting therapeutic targets for the treatment of vein graft inflammation, as well as many other vascular pathologies involving inflammation.

### 1.3.2 NUCLEAR FACTOR KAPPA B SIGNALLING PATHWAY

Since its discovery almost three decades ago, NF-$\kappa$B has become one of the most prominently studied cell signalling pathways due to its ability to modulate a multitude of cell behaviours (Sen *et al.*, 1986; Napetschnig *et al.*, 2013). NF-$\kappa$B transcription factors are a family of several distinct members (p50, p52, Rel-A (p65), Rel-B and c-Rel) which function as homo- or hetero-dimers in the regulation of gene transcription (Lawrence, 2009). The pathway can be activated by a range of stimuli from cytokines, including tumour necrosis factor alpha (TNF-$\alpha$) and interleukin 1 (IL-1), to physiologic stresses, such as ultraviolet light damage (Ghosh *et al.*, 1998). These activators induce two separate branches of the pathway, classical and alternative, which regulate very diverse cellular responses including proliferation, differentiation and the immune response.

Following receptor ligation of TNF-$\alpha$ with TNF receptor (TNFR) in the classical pathway (FIGURE 1.6), there is a recruitment of adaptor protein complexes involving TNF-receptor associated death domain (TRADD), serine/threonine kinase receptor interacting protein 1 (RIP1) and TNF

receptor associated factor (TRAF2/5) (Bradley, 2008). In turn, this receptor-adaptor complex further recruits MAPKs, MEKK3 and TAK1, which phosphorylate and thereby activate the IκB kinase (IKK) complex, consisting of IKK-α, IKK-β and NIK (Karin *et al.*, 2000). Once activated, the IKK complex phosphorylates IκBα, inducing its dissociation from NF-κB and subsequent ubiquitination and degradation (FIGURE 1.6.) (Karin *et al.*, 2000). This allows the release of NF-κB, p50/p65 heterodimer, into the cytosol and facilitates nuclear translocation (Baeuerle *et al.*, 1994). Members of the IκB family, when complexed with NF-κB, are able to maintain the localisation (and inactivity) of the NF-κB/IκBα complex through balancing the constant shuttling between the nucleus and the cytosol (Johnson *et al.*, 1999). In order to maintain the movement balance between the cellular compartments, IκBα masks one of two NFκB nuclear localisation sequences and itself has an exposed nuclear export sequence (Li *et al.*, 2002). Interestingly, IκBα is one of multiple genes whose transcription is regulated by NF-κB, as part of its transient activation and negative regulatory feedback system; the protein itself contains a nuclear localisation sequence allowing the displacement of NF-κB from bound DNA (Verma *et al.*, 1995). In addition to IκBα, negative regulation of the NF-κB pathway involves the transcription of ubiquitin modifying enzymes, A20 and Cezanne (Enesa *et al.*, 2008; Zakkar *et al.*, 2015). Both enzymes function exclusively on the TNF-receptor mediated classical NF-κB signalling pathway to limit further activation upstream to IκBα dissociation at the level of adaptor protein, RIP1, recruitment (Wertz *et al.*, 2004; Enesa *et al.*, 2008).

By contrast, the alternative pathway employs the RelB/p52 NF-κB heterodimer, and, for its activation, the constitutive processing of the p52 precursor and RelB inhibitor, p100, by an IKK-α homodimer is required (Hayden *et al.*, 2008). Upstream activation of this non-classical branch of the pathway is also achieved by different ligand-receptor complexes, including LTβR and CD40 (Sun, 2011). The two branches of NFκB regulate distinct sets of genes which account for the huge variation of biological responses mediated through both arms of this complex signalling pathway.

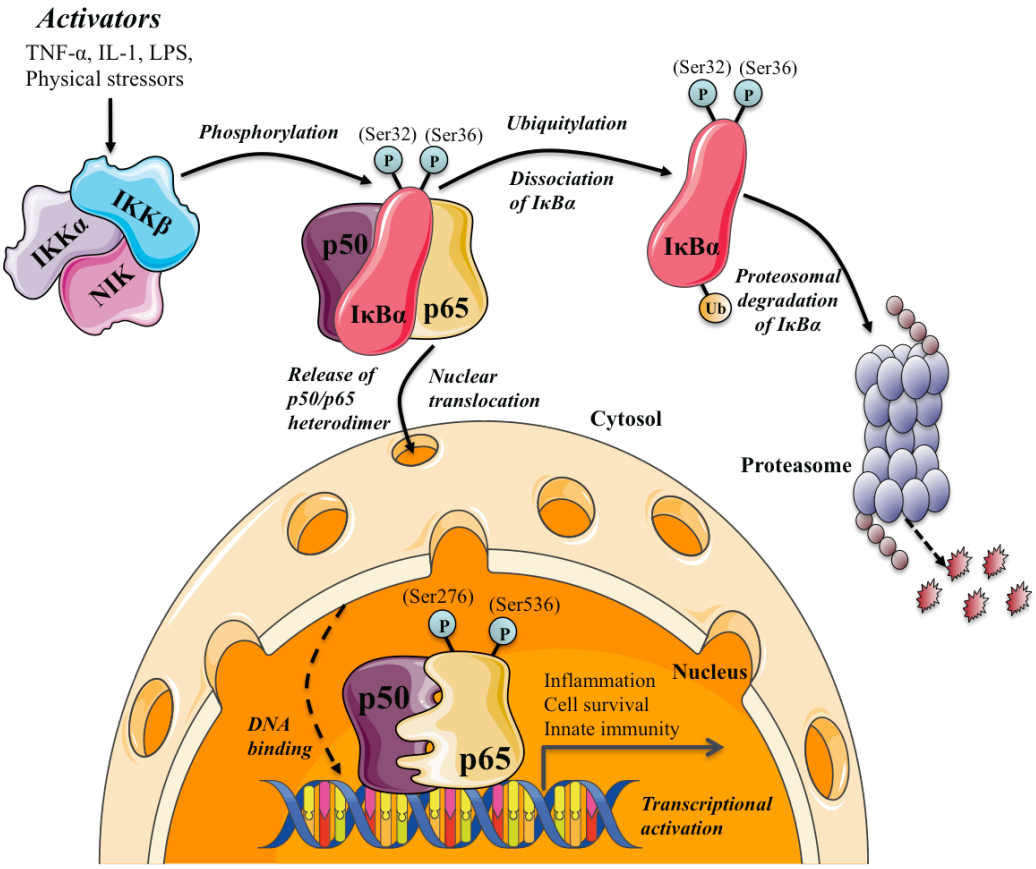


**FIGURE 1.6. NF-κB classical pathway**

Schematic representation of phosphorylation and proteasomal regulation of the classical NF-κB heterodimeric transcription factor (p50/p65). This figure was partly created with the Servier medical art library (smart.servier.com).

## 1.4 ANTIOXIDANT RESPONSE AND SIGNALLING

The homeostatic regulation of reduction and oxidation of oxygen and nitrogen products is essential for the normal, physiologic functioning of all eukaryotic cells. When the balance between oxidants and antioxidants, is tipped in the favour of the former, oxidative stress and subsequent induction of molecular damage occurs (Sies, 2015). It has long been appreciated that oxygen 'toxicity' occurs as a result of the creation of reduced forms of oxygen, causing formation of free, unpaired electrons within molecules, otherwise known as ROS (Gerschman *et*

*al.*, 1954; Halliwell, 1996). ROS and RNS are generally produced as by-products in ordinary cellular metabolism (Valko *et al.*, 2007). Their role in normally functioning cells is twofold; firstly, at low concentrations, ROS/RNS act as cell signalling intermediaries, particularly in the mitogenic response, as well as playing a role in cellular defence against infectious or noxious stimuli (Valko *et al.*, 2007). The second function, for which they are more cellular foe than friend, occurs when ROS/RNS are over-produced and the balance maintained by antioxidants, both enzymatic and non-enzymatic, is inadequate to stem the tide of these damaging free radicals (Kovacic *et al.*, 2001; Cadenas, 1997). When oxygen or nitrogen free radicals are generated in high concentrations, they are capable of inducing irreversible oxidative damage to cellular structures, nucleic acids, lipids and proteins (Navarro-Yepes *et al.*, 2014). Owing to the diverse and damaging effects on cell death and survival caused by redox imbalance, such high-level production of ROS/RNS has been implicated in numerous autoimmune, hyper-proliferative and inflammatory conditions, including atherosclerosis and IH (Schieber *et al.*, 2014).

With the numerous oxygenous and nitrogenous free radicals created by oxidative stress, an equally sophisticated and adaptable defence mechanism must act as its counter, namely the antioxidant defence system. The broad purposes of this system are to scavenge and detoxify ROS/RNS, interfere with ROS generating enzymes to prevent their over-production and sequester heavy metal ions (Masella *et al.*, 2005). Antioxidant defences exist exogenously, through dietary intake, and endogenously, in the form of enzymatic or non-enzymatic antioxidants (Halliwell, 1996). Exogenous antioxidants, in particular, various polyphenols found in fruits, vegetables and wine, are able to induce eNOS, inhibit lipid peroxidation and lipoxygenases, having significant beneficial effects for the cardiovascular system (Kanner *et al.*, 1994; Pisoschi *et al.*, 2015). Though their importance is clearly unquestionable in aiding innate systems, it has been proposed that the total cell potential for antioxidative action limits the benefit of such exogenous defences and that over-supplementation can actually induce pro-oxidant stress (Poljsak *et al.*, 2012; Poljsak *et al.*, 2013). Primary defence against deleterious free

radicals, however, is performed by the endogenous, enzymatic antioxidant systems. These enzymes, including superoxide dismutases (SOD), heme oxygenases (HO), catalase and glutathione peroxidase (GPx), act to convert harmful radicals into non-toxic by-products through electron donation or acceptance (Lu *et al.*, 2010).

Research into the regulation of redox homeostasis has been extensive and the biological and chemical actions of the involved pathways are extensively documented. However, despite the known involvement of ROS and RNS in endothelial dysfunction, these pathways remain relatively unexplored as modifiable targets in vein grafting (Powell *et al.*, 1998; Shukla *et al.*, 2012; Weaver *et al.*, 2012; Osgood *et al.*, 2014). Superoxide, and its principal producer, the NOX enzyme family, are known to be up-regulated early in the vein graft by ECs during vessel hypoxia and contribute to early endothelial dysfunction (Griendling *et al.*, 2000; Guzik *et al.*, 2005). Whereas, Peroxynitrite, a product of interaction between NO and $O_2^{\bullet-}$, is suggested to reduce bioavailability of NO within the vascular bed through the uncoupling of eNOS, having serious deleterious mitogenic effects on VSMCs (Tsapenko *et al.*, 2012; Osgood *et al.*, 2014). As alluded to earlier (in section 1.2.5.), a few studies have shown promise clinically in modifying redox regulation in vein grafting using commercially available statins (Antoniades *et al.*, 2010; Margaritis *et al.*, 2012; Spadaccio *et al.*, 2014), though these studies remain relatively scarce. Therefore, targeting oxidative stress production in VGF, at the level of transcriptional control of redox balance, may be beneficial in the prevention of ROS-induced endothelial dysfunction in CABG surgery.

### 1.4.1 TRANSCRIPTIONAL CONTROL AND REDOX BALANCE

The intricate balance between oxidant and antioxidant responses in eukaryotic cells is mediated by two master conductors. The first of these is NF-κB, which in addition to its role as a primary regulator of the immune response, is additionally responsive to redox regulation (Flohe *et al.*, 1997). It has long been recognised that oxidants, including $O_2^{\bullet-}$ and hydrogen peroxide ($H_2O_2$),

are among the numerous activators of NF-κB (Oliveira-Marques *et al.*, 2009). Both of these oxidants are produced by NOX systems, though the route to activation remains debatable (Brigelius-Flohe *et al.*, 2011). The rationale behind this comes from the overlap between activators of NOX and NF-κB. It appears that this may be explained, in part, by the effect of differing initial activating stimuli (Flohe *et al.*, 1997). Following binding of pro-inflammatory cytokines, IL-1β or TNF-α, or growth factors to their respective receptors (IL-1R, TNF-R and Toll like receptors (TLRs)), intracellular, receptor-bound phosphatidylinositol-3 kinase (PI3K) triggers downstream cascades leading to the joint activation of NOX and NF-κB (Park *et al.*, 2004; Oakley *et al.*, 2009). This cascade, although well documented for NF-κB activation, through the induction of Protein Kinase B (Akt) followed by phosphorylation of the IKK complex, remains unclear for the co-activation mechanisms of NOXs downstream of PI3K and most likely differ depending on tissue, receptor and stimulus (Lassegue *et al.*, 2010; Wenzel *et al.*, 2017). Despite this confusing picture, $O_2^{\bullet-}$, $H_2O_2$ and NF-κB activity remain inextricably linked and the concomitant activators of NF-κB, GPx's and NOX's are all of paramount importance for mounting of the redox response. Furthermore, this self-regulating NF-κB system continues to perpetuate ROS production through targeted transcription of IL-1 and TNF-α, both of which continue to activate the NOXs which were initially co-activated with NF-κB in the first place (Xu *et al.*, 2016). The chronic transcriptional response of NF-κB, in addition to pro-oxidant, self-propagating ROS production, also consists of several anti-oxidant and protective targets. Among these are members of the SOD enzyme family, which catalyse simultaneous oxidation and reduction reactions (otherwise known as dismutation) to convert $O_2^{\bullet-}$ into $H_2O_2$ (Morgan *et al.*, 2011). Owing to the complex and transient involvement of ROS at numerous places within a single pathway, as well as the dual role played by NF-κB in activation of, and protection against, oxidative stress, there remains much more to be clarified about this evolving dichotomy.

### 1.4.2 NRF2/KEAP1 SIGNALLING PATHWAY

Nuclear factor erythroid 2-related factor 2 (Nrf2), a member of the Cap 'n' Collar (Cnc) family, is another transcription factor which responds to a variety of oxidative stresses. Cnc proteins are evolutionarily conserved amongst all metazoan life, with diverse homeostatic and developmental functions (Sykiotis *et al.*, 2010). Arguably the most important of all of these is Nrf2, considered the 'master regulator' of the antioxidant and cellular defence response (Gorrini *et al.*, 2013; Vomund *et al.*, 2017). Following its discovery in 1994 (Moi *et al.*, 1994; Itoh *et al.*, 1995), and subsequent uncovering that Nrf2 was a positive regulator of the antioxidant response element (ARE), a huge number of studies propagated, to attempt to link Nrf2 to transcription of a myriad of stress responsive detoxifying enzymes, anti-inflammatory genes, proteasome production and glutathione synthesis (Venugopal *et al.*, 1996; Sykiotis *et al.*, 2010; Hybertson *et al.*, 2011). Additionally, perturbation in the regulation of Nrf2 is becoming of interest in many chronic conditions, from cancers to chronic obstructive pulmonary disorder (COPD), where oxidative stresses play vital roles (Sykiotis *et al.*, 2010; Sporn *et al.*, 2012; Niture *et al.*, 2014). With a growing appreciation for the importance of Nrf2 in conserved cellular defence responses, across tissues and species, knowledge of the molecular mechanisms of Nrf2 control and activation continues to advance.

Regulation of the activity of Nrf2 is achieved primarily through physical interaction with its innate repressor, Kelch-like ECH-associating protein 1 (Keap1), which is required for both cytosolic sequestration and continuous targeted degradation of the transcription factor (FIGURE 1.7.). Under basal conditions (i.e. absence of oxidative stress), Keap1 functions to regulate Nrf2 by three distinct, but concomitant mechanisms; firstly, in the cytosol, the Nrf2-ECH homologous domain (Neh2) and Kelch domains are bound to form a complex of a single Nrf2 and a Keap1 homodimer in a 1:2 ratio (Dinkova-Kostova *et al.*, 2005). Within the Neh2 domain, there are 2 distinct motifs to which each Kelch domain of the Keap1 dimer binds (Chen *et al.*, 2015). This

interaction is known as the “hinge and latch” model, with the first of these Neh2 motifs, ETGE, acting as a ‘latch’ with a high affinity for Kelch, in order to secure the binding of Nrf2 to Keap1 (Tong *et al.*, 2006; Kensler *et al.*, 2010). The second motif, DLG, has a much weaker affinity; however, in the absence of oxidants, it is able to bind the second Kelch to act as a ‘hinge’, fastening Nrf2 to Keap1 and exposing a Lysine rich region of Nrf2. This region can then be ubiquitinated and continually targeted for proteasomal degradation, thus, basal conditions permit only low levels of free Nrf2 and target gene transcription (Tong *et al*., 2006; Sykiotis *et al*., 2010). Secondly, Keap1 acts as an adaptor protein to the Cullin3 E3 ubiquitin ligase (Cul3), which, in the above described model, is responsible for ubiquitinating Nrf2 (Suzuki *et al.*, 2017). Thirdly, Keap1 itself is also able to shuttle between the cytosol and nucleus, though the importance and function of this process remains under question (Nguyen *et al.*, 2005; Velichkova *et al.*, 2005; Sykiotis *et al*., 2010). Nucleo-cytoplasmic shuttling of Keap1 has been suggested to play a role in the targeting of Nrf2 to specific regions of the genome, through direct interaction with chromatin (Tashiro *et al.*, 2004). However, perhaps more convincingly, it has also been reported that nuclear localisation of Keap1 either enables nuclear export of Nrf2 or targets Nrf2 for degradation from within the nucleus, consequently attenuating the antioxidant, defence response (Sun *et al.*, 2007; Niture *et al.*, 2009).

Activation of the Keap1/Nrf2 system is achieved with numerous stress-sensing mechanisms, both intrinsically, within the complex itself, and extrinsically, through stress-responsive MAPK-controlled phosphorylation (Hybertson *et al.*, 2011). Commonly, Nrf2 activation will result as a combination of these two mechanisms acting together. Firstly, upon exposure to electrophiles or oxidants, the Keap1-Cul3 complex will be inhibited and undergo a conformational change (Suzuki *et al.*, 2017). Amongst these Nrf2 inducers are Michael acceptors, isothiocyanates, heavy metals and trivalent arsenicals; all of which target the highly reactive cysteine residues (Cys) in Keap1, as such, Keap1 is considered as a true oxidant sensor (Kensler *et al.*, 2007). Additionally, Nrf2 is phosphorylated by PKC, which functions to prevent Keap1 binding and facilitate Nrf2

translocation, and sequestome-1 interaction with Keap1 may disrupt the loosely bound complex entirely (Huang *et al.*, 2002; Bloom *et al.*, 2003; Komatsu *et al.*, 2010).

Once the complex is dissociated and Nrf2 is inside the nucleus, it interacts with small Maf transcription factors and is able to bind the ARE motif within its broad range of target genes and initiate transcription (Nguyen *et al.*, 2009). Arguably most important of these, are Nrf2 targets involved in oxidant and electrophile metabolism. These include HO-1, which, in conjunction with bilirubin reductase, generates carbon monoxide and bilirubin; NADPH quinone dehydrogenase 1 (NQO1), which catalyses the reduction of quinones to reduce global ROS generation, and glutamylcysteine ligase (GCLM), which is involved in catalysis of the biosynthesis of the important antioxidant, glutathione (Baird *et al.*, 2011; Nguyen *et al.*, 2009). The list of Nrf2 target genes is extensive and still growing. Though, briefly, the transcription factor also targets genes involved in proteasome production, cell survival, molecular chaperoning, drug metabolism, nucleotide excision repair and autophagy. These far-ranging functions perhaps endow Nrf2 with the title of the most important transcription factor in protection of the organism against external stresses.

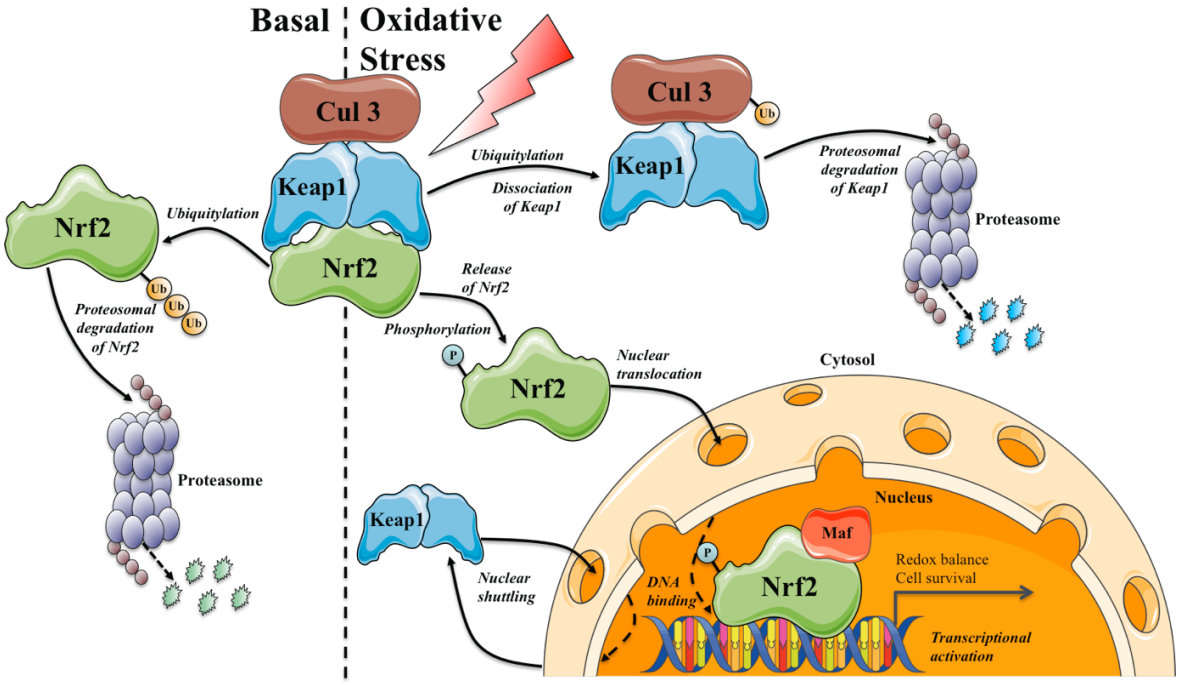


**FIGURE 1.7. Keap1/Nrf2 pathway under basal and oxidative stress conditions**

Schematic representation of activation and inhibition of the Keap1/Nrf2 pathway under stressed and basal conditions, respectively. This figure was partly created with the Servier medical art library (smart.servier.com).

## 1.5 INTERACTIONS BETWEEN THE NRF2/KEAP1 AND NF-κB PATHWAYS

Many eukaryotic transcription factors (TFs) exist, in their basal states, sequestered in the cytosol through the direct and indirect action of an inhibitory, multi-component complex, from which, dissociation must occur in order to activate the TFs (Brigelius-Flohe *et al*., 2011). As alluded to in sections 1.3.2 and 1.4.2., NF-κB and Nrf2 are no different; in their 'inactive' states, these two TFs are sequestered in the cytosol by IκBα and Keap1, respectively. Dissociation from their respective innate repressors, (i.e. TF activation) occurs under largely, but not entirely, exclusive means (Brigelius-Flohe *et al*., 2011). However, these two pathways do share similarities in the general dissociation/activation processes. In order to be inactivated, both repressors require ubiquitination and subsequent targeting for degradation; nevertheless, both the activation

sensing steps and ubiquitination machinery involved are vastly different. The study of interactions between these two critical homeostatic TFs is the subject of great interest in disease states involving oxidative stress and inflammation (Wakabayashi *et al*., 2010). Interactions between the pathways can occur directly, via protein-protein interactions, such as NF-κB and Keap1, or indirectly, due to secondary messenger actions on target gene transcription, for example via HO-1-induced Carbon Monoxide (CO) production and activation of NF-κB (Lee *et al*., 2009; Washington *et al*., 2017). Generally, under basal conditions, both pathways perform homeostatic functions in regulation of the cell cycle and maintenance of a stable redox balance (Brigelius-Flohe *et al*., 2011). In contrast, under acute pathological oxidative stress conditions, there is a shift towards transcriptional activation of NF-κB and inflammation, as well as deregulation of Nrf2, which may be in part mediated by NF-κB (Li *et al*., 2008). However, the degree of crosstalk between these two pathways in inflammatory and stressful conditions remains the subject of intensive research.

### 1.5.1 DIRECT INTERACTIONS

With similar mechanisms of action between the Nrf2 and NF-κB pathways (in their regulation by multicomponent, inhibitory complexes), it appears that much of the direct interaction occurs through modulation of their innate repressors, Keap1 and IκBα, respectively. Keap1 has been extensively shown to negatively regulate NF-κB signalling via its binding and subsequent suppression of IKKβ-induced NF-κB activation (Lee *et al*., 2009). Similar to its suppression of Nrf2, Keap1 is able to directly bind to IKKβ through its ETGE motif, acting as a 'latch' to secure itself to IKKβ (Kim *et al*., 2010). This Keap1 binding obscures IKKβ phosphorylation sites, preventing the triggering of downstream IκBα phosphorylation, whilst at the same time, ubiquitin targeting IKKβ for proteasomal degradation (Lee *et al*., 2009). In contrast, an example of a direct interaction acting in the reverse direction is the effect of NF-κB on Keap1. Yu *et al*., reported that NF-κB is able to physically associate with Keap1 and induces its translocation into

the nucleus; once within the nucleus, Keap1 is able to perform its Nrf2-repressive function and prevent the Nrf2-ARE transcriptional response (Yu *et al*., 2009). However, the mode of action of this direct NF-κB-Keap1 interaction remains to be uncovered.

### 1.5.2 INDIRECT INTERACTIONS

Numerous studies have found modulatory interactions, either repressive or activating, between the antioxidant and inflammatory pathways, most often with the use of small molecule activators of Nrf2 or chemokine-based activation of NF-κB (Jeong *et al*., 2004; Chen *et al*., 2006; Zakkar *et al*., 2009). Furthermore, studies of $Nrf2^{-/-}$ mice have been shown to express increased NF-κB activation upon inflammatory insult or traumatic injury (Wakabayashi *et al*., 2010). However, cause and effect in many of these studies cannot be realistically deduced. For instance, $Nrf2^{-/-}$ mice will have an inherently reduced capacity to cope with oxidative stress, as such, many inflammatory and pro-oxidant pathways will be activated following injury, which may, indirectly lead to activation of NF-κB, perhaps via increased NOX activity and superoxide production. What seems more compelling, is the transcriptional interplay between these two pathways and the processes of interaction occurring indirectly through genome interaction. Once NF-κB is phosphorylated at Ser276 and translocates, it binds to the transcriptional co-activator CREB-binding protein (CBP), in order to initiate transcription (Chen *et al*., 2004). At the same time, Nrf2 is unable to bind CBP (also its co-activator), thus NF-κB indirectly prevents Nrf2-ARE transcription through competitive binding to CBP (Wakabayashi *et al*., 2009). An additional mechanism of Nrf2-ARE repression is through NF-κB-mediated HDAC3 recruitment to the ARE, which functions to prevent further Nrf2 transcription (Liu *et al*., 2008). Much of what is known about the interactions between NF-κB and Nrf2 comes from the concomitant or opposing actions of their target genes. Though, as we begin to tease apart transcriptome interdependence further with new genome-wide techniques, much more will be elucidated on the pathway interactions between these two homeostatic 'master regulators' in health and disease.

## 1.6 SHEAR STRESS AND THE ENDOTHELIUM

### 1.6.1 TRANSDUCTION OF MECHANICAL FORCES IN THE VASCULATURE

Circulating blood flow applies several mechanical forces on the walls of blood vessels. Firstly, shear stress, which is the tangential frictional force acting longitudinally on the vessel wall imposed by fluid motion on a solid boundary parallel to the fluid direction (FIGURE 1.8.) (Zakkar *et al.*, 2015). It can be defined as force divided by wall area (e.g. dyn/cm$^2$) and is the force that interacts directly with the endothelium. Secondly, hydrostatic pressure is the force acting perpendicularly on the vessel wall; and, finally, circumferential stretch created by pulsatility exerts a force (or strain) on the entire circumference of the vessel wall (FIGURE 1.8.) (Zhao *et al.*, 1995).

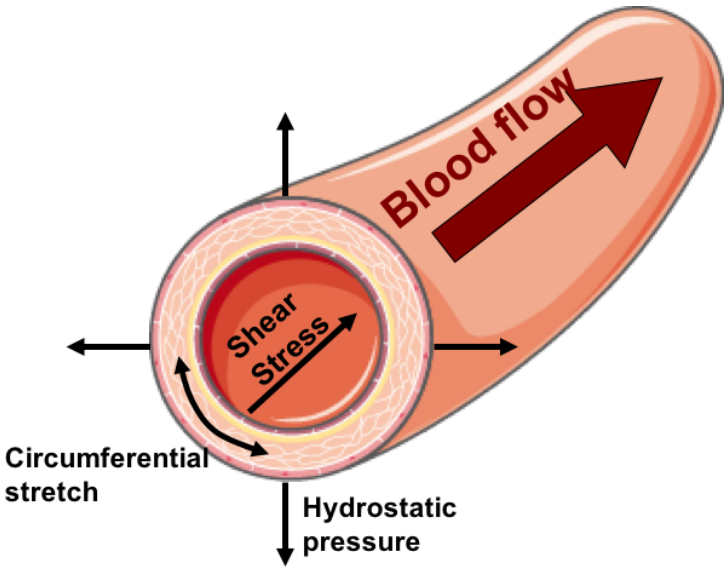


**FIGURE 1.8. Mechanical forces in the vasculature**

Mechanical forces exerted by blood flow, longitudinally (shear stress), along the wall of the vessel, and perpendicularly (hydrostatic pressure and circumferential stretch) against the vessel wall. This figure was partly created with the Servier medical art library (smart.servier.com).

Mechanotransduction through the endothelium allows the vessel to convert these mechanical, haemodynamic signals into biological responses within the vascular wall; the process requires the direct transmission of mechanical force into tangible biological functions. Integral to this conversion of mechanical force is a mechanosensory complex consisting of PECAM-1, which conducts mechanical force directly for transmission, vascular endothelial cell (VE)-Cadherin, which acts as an adaptor, and VEGF receptor 2 (VEGFR2), which activates PI3K, that in turn activates integrins (Tzima *et al.*, 2005). Integration of complex biomechanical signals by ECs also intimately involves proteins located on EC surface including G-proteins, caveolae and ion channels; small GTPases and signalling intermediaries, such as c-Src, Ras, Raf and protein kinase C (PKC); mitogen activated protein kinases, such as p38, extracellular-regulated kinase 1/2 (ERK1/2) and c-Jun N-terminal kinase (JNK); effector molecules, including nitric oxide (NO) and prostacyclin (PGI2); and, lastly, transcription factors such as KLF2, Nrf2, ATF2, NF-$\kappa$B (Noris *et al.*, 1995; Traub *et al.*, 1998; Tzima *et al.*, 2002; Resnick *et al.*, 2003; Chien, 2007; Hsieh *et al.*, 2014; Abe *et al.*, 2014; Zakkar *et al*., 2015). Diverse responses in both ECs and VSMCs are affected by the mechanotransduction pathways, from proliferation to cell-matrix interactions (Katsumi *et al.*, 2004). Shear stress has long been considered of particular importance in vascular homeostasis, due primarily to its wide-ranging impact on a number of pathologies, and also its contribution to the maintenance of normal vessel structure and functioning.

### 1.6.2 PROLONGED LAMINAR SHEAR STRESS AND PROTECTIVE SIGNALLING

Regions of the vasculature associated with a healthy phenotype are commonly characterised by a quiescent endothelium, with an anticoagulant and anti-inflammatory profile. (Boon *et al.*, 2009; Marin *et al.*, 2013). Such vascular environments are commonly seen in linear regions of vessels experiencing laminar shear stress, where blood flows in a uniform, streamlined, pulsatile pattern with the cardiac cycle, but importantly with a positive mean flow rate (Chiu *et al*., 2011). Adaptive, morphological changes of ECs are observed in linear regions of arteries resulting in the

reorganisation of F-actin filaments to confer an elongated and flatter shape (Chiu *et al.*, 1998). Typically, these portions of vessels are considered atheroprotective due to the reduced likelihood of developing atherosclerotic lesions and prolonged laminar shear stress (LSS) has long been considered the reason for this (Ku *et al.*, 1985; Frangos *et al.*, 1985; Malek *et al.*, 1999; Cunningham *et al.*, 2005; Berk, 2008).

Aside from morphological changes, prolonged LSS significantly influences the state of oxidative stress within the endothelium. The bioavailability of endothelium derived relaxing factors, NO and PGI2, is fundamental to the maintenance of a quiescent endothelium (Chiu *et al*., 2011). Under elevated, sustained LSS, endothelial NO synthase (eNOS) is upregulated and continually produces NO, supporting functions including vasodilation, inhibition of VSMC growth, inhibition of platelet aggregation and altered lipoprotein metabolism (FIGURE 1.9.) (Noris *et al.*, 1995; Traub *et al.*, 1998; Chiu *et al.*, 2005; Dardik *et al.*, 2005; Jacot *et al.*, 2008). NO also functions in the quiescent endothelium to homeostatically regulate the production and distribution of damaging ROS, such as $O_2^{\bullet-}$, lipid- and hydroxyl-radicals (Cai *et al.*, 2000). Preservation of a highly antioxidant and quiescent EC state is not dependent only on the oxidative stress system, but also requires the synergistic action of a number of transcription factors. Among the few transcription factors associated with prolonged laminar flow and protective signalling in the endothelium, none appear to be more important than KLF2. KLF2 is known to be elevated continuously for seven days *in vitro* under sustained laminar flow (Dekker *et al.*, 2002; Dekker *et al.*, 2005). Furthermore, KLF2 overexpression resulted in quiescent endothelium even in the absence of shear stress (Dekker *et al*., 2005). It was also observed that KLF2 systematically controlled numerous genes involved in migration (VEGFR2 and Semaphorin 3F (SEMA3F)), vascular tone (eNOS) and haemostasis (tissue plasminogen activator (TPA) and von Willebrand factor (vWF)) (Dekker *et al.*, 2006; Fledderus *et al.*, 2007). Interestingly, KLF2 overexpression alone was able to alter endothelial morphology to appear similar to ECs exposed to shear stress (i.e. elongated and flattened) (Dekker *et al*., 2006; Boon *et al.*, 2010).

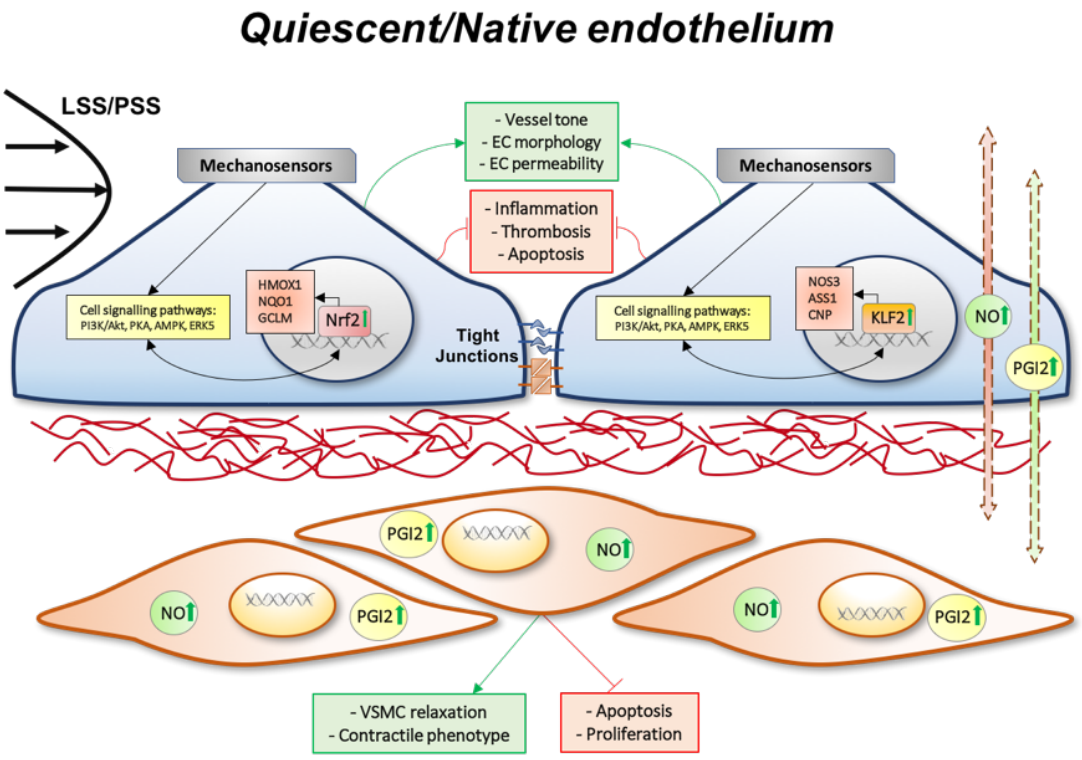


**FIGURE 1.9. Protective signalling in the quiescent endothelium**

Within the quiescent endothelium experiencing laminar shear stress (LSS) (i.e. in veins with normal flow without venous reflux, venous insufficiency or stasis and long straight portions of arteries), ECs upregulate levels of KLF2 and Nrf2 dependent genes, including eNOS and HO-1, and secrete gasotransmitters NO and PGI2.

Another element of the complex atheroprotective transcriptome is Nrf2; as mentioned earlier (section 1.4.2), Nrf2 is essential for the expression of numerous antioxidant genes including HO-1 and NQO1 (FIGURE 1.9.) (Zakkar *et al*., 2008). Regulation of Nrf2 has been inextricably linked to laminar shear stress and KLF2; the latter is not required for shear stress activation of Nrf2, but interestingly, acts to enhance its transcriptional activity (Fledderus *et al.*, 2008). Nrf2 has been shown *in vivo*, in the murine aorta, to contribute to atheroprotection via the suppression of p38 mediated VCAM1 signalling. Acting on two distinct aspects of this pathway, Nrf2 firstly inhibits the activity of an upstream MAPK kinase 3/6 (MKK3/6) and, secondly, enhances the

activity of MAPK-phosphatase 1 (MKP-1), which functions to inactivate p38 (Zakkar *et al.*, 2008). Through synergistic actions of transcription factors, KLF2 and Nrf2, as well as balanced ROS/RNS formation and scavenging, the endothelium is able to suppress chronic vascular inflammation in 'atheroprotective' portions of the vascular tree (FIGURE 1.9.).

### 1.6.3 CHRONIC INFLAMMATION AND ABNORMAL HAEMODYNAMICS

Atherosclerotic lesions are primarily localised to regions of the arterial vasculature which experience chronic oscillatory and disturbed shear stress (OSS and DSS, respectively), such as branches and bifurcations. In response to chronic OSS/DSS, activation of NF-$\kappa$B is observed both *in vitro*, using a step-flow channel, and *in vivo*, in multiple animal models, such as with the use of vascular cuffs and hyperlipidaemic models (Van der Heiden *et al*., 2010; Chiu *et al.*, 2011). Remarkably, endothelial cell specific inhibition of NF-$\kappa$B greatly reduced atherosclerotic plaque formation in apolipoprotein E knockout ($ApoE^{-/-}$) mice, indicating the crucial role of NF-$\kappa$B in atherogenesis (Gareus *et al.*, 2008). Dysfunction in the endothelium at atheroprone sites is also characterised by EC proliferation; this is in part mediated by flow-induced NF$\kappa$B activity which stimulates transcription of cyclin D1, allowing quiescent ECs to re-enter the cell cycle and become proliferative (Collins *et al.*, 2001).

The proinflammatory response mediated by JNK and p38, seen in regions of disturbed flow, is nullified by MKP-1 in the vascular endothelium of atheroprotected regions (Zakkar *et al.*, 2008; Zakkar *et al.*, 2008). Additionally, within atherosusceptible sites, JNK1 is known to have an effect on apoptosis and inflammation through the increasing expression of apoptotic facilitators, procaspase 3 and RIP1, and regulation of toll like receptor 4 (TLR4); in part explaining observation of its increased expression in atherosclerotic plaques and activation by oxidised LDL (Chaudhury *et al.*, 2010). Interestingly, JNK has been shown to induce VCAM-1 related pro-inflammatory signalling in response to aberrant shear stress through two mechanisms: firstly, through activation of activating transcription factor (ATF2) alone; and secondly, through ATF2

dependent induction of NF-$\kappa$B (Cuhlmann *et al.*, 2011). It is proposed that ECs could be sensitised to expression of other NF-$\kappa$B target genes, via the JNK-ATF2 mechanism, and thus, facilitate pro-inflammatory cascades seen in chronic vascular injury (Cuhlmann *et al.*, 2011). Abnormal and disturbed flow strongly influences the chronically inflamed environment observed in atherosclerotic lesions; however, the understanding of the molecular biology of the pathways involved under sustained, aberrant flow is complex *in vitro*, due to temporal limitations of many experimental models. Despite this, as will be elaborated upon in the next section, much that we know of the effect of shear stress on vascular inflammation comes from studies observing the acute onset of LSS and DSS.

### 1.6.4 ACUTE EXPOSURE TO HIGH SHEAR STRESS AND INFLAMMATORY ACTIVATION

Physiologically, acute increases in shear stress rates are observed relatively infrequently, such as during physiologic exertion and in therapeutic interventions, including CABG (Han *et al.*, 2012). Venous transposition into the arterial circulation is a particularly striking example of an acute increase of shear stress rates, with vECs having to adapt to up to 10-fold increased shear stress. Dramatic increases in shear stress result in the very early development of signs of vascular inflammation, with expression of MCP-1 and the infiltration of monocytes, which contribute to seeding the environment for atherogenesis (as explained in section 1.2.) (Hoch *et al.*, 1994; Stark *et al.*, 1997). Interestingly, depletion of macrophages or knock-down of ICAM1 significantly reduced rates of vein graft disease (Hoch *et al.*, 1999; Zou *et al.*, 2000), illustrating that inflammatory cells and adhesion cascades are inextricably linked to vein graft intimal hyperplasia development.

Arterial grafts are known to be comparatively unaffected by inflammatory processes in bypass (Cameron *et al.*, 1995; Taggart *et al.*, 2016; Gaudino *et al.*, 2017), further substantiating that it is the arteriovenous transposition which is distinctly responsible for creating an early inflammatory environment within the LSV graft. Moreover, acute venous arterialisation is

known to induce activation of pro-inflammatory MAPKs, ERK1/2 and p38, but not JNK, as quickly as 30 minutes post-implantation in a canine *in vivo* model of carotid artery bypass grafting (Saunders *et al.*, 2004). From literature investigating acute shear stress *in vivo*, it is evident that endothelial dysfunction is induced during bypass grafting and that, occasionally, the endothelium can be depleted; however, it is still largely unknown whether EC loss is purely a mechanical effect of increased shear stress or is in fact secondary to apoptosis and inflammation. Despite a reasonable knowledge of these acute physiological responses under shear stress, *in vivo* models of vein grafting and reperfusion are still limited in their ability to provide a truly temporal profile of the response at the molecular level. As such, it is required to investigate acute effects of shear stress *in vitro*, either using laminar or oscillatory flow (acutely, they activate very similar events), or *ex vivo*, to better understand initial and immediate responses within the vein graft endothelium.

Immediately following the onset of shear stress, *in vitro*, a plethora of biochemical events are rapidly induced. Within 30 seconds, ion channels are opened, small GTPases and kinases (PI3K and c-Src) are activated via the mechanosensory complex consisting of PECAM-1, VEGFR2 and VE-cadherin (Tzima *et al*., 2005; Ward *et al.*, 2017). At cell-cell junctions, there are responses of altered tension across these complexes; PECAM-1 senses an increase in tension, whereas VE-cadherin transduces signals from the detection of a decreased tension between ECs (Conway *et al.*, 2013). These alterations in tension are associated with a general relaxation of cell-cell attachments, as such it remains difficult to determine whether acute shear stress is in fact detected and transduced by this mechanosensing complex, the process is a passive response by the cytoskeleton or in fact whether there remains an as yet undiscovered mechanosensor upstream of the cytoskeletal modulation (Tzima *et al*., 2005). Soon after initial mechanosensation there exists a complicated, poorly characterised period of signal transduction. A rapid, transient and calcium dependent response is required for endothelial activation by shear stress involving PKC, Ion channels and cGMP, altering permeability (FIGURE

1.5.A) (as described in section 1.2.1) (Berk *et al.*, 1995). An alternative, more sustained response to acute shear is mediated in a calcium independent manner, whereby PI3K activates integrins and small GTPases, RhoA and Ras, as well as focal adhesion kinase (FAK) complexes (Ishida *et al.*, 1996; Hahn *et al.*, 2008; Hahn *et al.*, 2009). Surapisitchat et al., 2001, showed that laminar flow alone decreased JNK activation and activated ERK1/2 and p38 between 10 and 60 minutes after exposure to shear stress. Whereas, when stimulated with TNF-α and IL-1 alone for 15 minutes, all three pro-inflammatory MAPKs were activated; interestingly however, when cells were pre-exposed to flow prior to cytokine stimulation, JNK activation was inhibited (Surapisitchat *et al.*, 2001). Inhibition of JNK by flow (and subsequent expression of E-selectin) appears to be dependent on ERK1/2 activation, strongly suggesting a role for inhibitory MAPK crosstalk in response to shear stress (Berk, 2008). Finally, ERK5 (or BMK1) appears to be activated by acute shear stress and induces myocyte enhancer factor 2 (MEF2) transcription factor; however, this kinase is implicated primarily in the atheroprotective endothelial phenotype, suggesting its role is as a shear stress activated kinase, but does not necessarily confer a negative effect on the endothelium (Yan *et al.*, 1999; Pi *et al.*, 2004)

Much is evident in the literature regarding the activation of MAPKs by shear stress and the associated pro-inflammatory response that they mediate, even if the upstream events in their activation remains to be fully elucidated. However, induction of the NF-$\kappa$B transcription factor in response to acute shear stress is still relatively poorly understood. For over two decades, it has been known that NF-$\kappa$B becomes activated under conditions of acute shear stress as well as chronic oscillatory shear stress, which has allowed for a considerable amount of research into the function of NF-$\kappa$B in atherogenesis and, to a certain extent, reperfusion injury (Lan *et al.*, 1994; Van der Heiden *et al*., 2010). Acute shear stress appears to function to activate NF-$\kappa$B in an integrin dependent manner. Once integrins are activated by PI3K, they are able to begin inducing signals which include activation of small GTPases, RhoA and Ras-related C3 botulinum toxin substrate 1 (Rac1) (Bhullar *et al.*, 1998). Here we see huge similarities with inflammatory

MAPK activation by acute shear, indicating that the two pathways have concomitant and overlapping activators and perhaps functions. In turn, Rac1 induces NOX enzymes, producing ROS, which function to stimulate the critical NF-$\kappa$B kinases, IKK-$\beta$ and NIK, which together trigger classical activation of the NF-$\kappa$B pathway (Tzima *et al*., 2002; Orr *et al.*, 2008). Activation of the NF-$\kappa$B pathway by shear stress is most likely not as singular or simple as has been suggested, there exist many other elements involved for ultimate transcriptional activation, many of which perhaps remain unidentified. For example, FAKs are crucial members of the integrin-dependent shear stress induced endothelial activation mechanism, though do not explicitly stimulate NF-$\kappa$B translocation, but rather, are responsible for phosphorylation of the transcription factor, which is intimately linked to its transcriptional activity (Petzold *et al.*, 2009). Whereas, p21-activated kinase (PAK), which is also flow dependent, also functions as a crucial element in the oxidant dependent activation of NF-$\kappa$B through NIK, though, unlike Rac1, has absolutely no effect on ROS production (Orr *et al*., 2008). Interestingly, Orr et al., observed differential activation of NF-$\kappa$B under acute shear stress dependent also on the type of sub-endothelial ECM (Orr *et al.*, 2005). ECs cultured on fibronectin and fibrinogen show considerably greater NF-$\kappa$B translocation compared to those cultured on collagen type I after one-hour exposure to acute shear stress (Orr *et al*., 2005). Taken together, these studies into the flow induced activation of NF-$\kappa$B describe a relatively confusing picture with many overlapping components and perhaps many more left to be uncovered. Nevertheless, focal inhibition of acute shear stress mediated induction of NF-$\kappa$B represents an exciting therapeutic direction in the treatment of vein graft disease, reperfusion injury and even perhaps atherosclerosis.

## 1.7 RATIONALE FOR THIS THESIS

Endothelial dysfunction is induced in SVGs due to the sudden exposure to acute changes in haemodynamics once within the arterial system. Such dysfunction is causally linked to the development of late stage graft failure, and therefore, prevention of early endothelial activation in SVGs is an attractive, but currently unachievable, therapeutic strategy due to the lack of robust identification of a suitable target. NF-κB and Nrf2 are involved in endothelial dysfunction as an inducer and protector, respectively. The first aim of this thesis was to investigate endothelial cell-specific responses of NF-κB and Nrf2 pathways under conditions of acute shear stress; and, secondly, to investigate whether these pathways could be therapeutically targeted to reduce acute shear stress-induced endothelial inflammation.

### 1.7.1 HYPOTHESES

The following hypotheses were tested in this thesis:

- Acute shear stress induces a pro-inflammatory response in vECs *in vitro* and in LSV ECs *ex vivo*, which is driven by NF-κB classical pathway activation and, when this pathway is blocked, inflammation in response to acute high shear stress can be prevented.
- Acute shear stress inhibits Nrf2 activation and the antioxidant response in vECs, and pre-activation of Nrf2 in vECs prior to acute shear stress exposure prevents inflammation and exerts a protective, antioxidant effect.

### 1.7.2 EXPERIMENTAL APPROACH

The following experimental approaches were adopted to test the above hypotheses:

- Pro-inflammatory mRNA and protein profiles were studied in vECs exposed to acute high shear stress, in human umbilical vein ECs (HUVECs) *in vitro* and LSV ECs *ex vivo*.
- Activation of the NF-κB classical pathway in vECs was investigated under conditions of acute shear stress *in vitro* using HUVECs and *ex vivo* using human LSV.
- Pro-inflammatory mRNA and protein profiles were studied in vECs pre-treated with pharmacological or gene-therapy based NF-κB inhibition and subsequently exposed to acute high shear stress.
- The functional effects of NF-κB inhibition in vECs were examined, by both permeability measures and activation of the adhesion cascade, under conditions of acute high shear stress.
- Antioxidant mRNA and protein profiles were studied in vECs exposed to acute high shear stress, in HUVECs, *in vitro.*
- Activity of the Nrf2 pathway in vECs was investigated under conditions of acute shear stress *in vitro* using HUVECs.
- The effect of Nrf2 activation on EC responses to acute high shear stress was investigated directly, with an Nrf2 inducer and gene-therapy based overexpression, and indirectly, by gene-therapy-based inhibition.

# 2. MATERIALS AND METHODS

## 2.1 MATERIALS

All reagents were of the highest grade and obtained from Sigma, unless otherwise stated

### 2.1.1 REAGENTS USED IN TISSUE AND CELL CULTURE

For culture of human umbilical vein endothelial cells (HUVECs), cyropreserved c-pooled HUVECs were purchased from Promocell (catalogue number: C-12203). Ready to use Endothelial Cell Growth Medium (Promocell; catalogue number: C-22010), Endothelial Cell Basal Medium (Promocell; catalogue number: C-22210) and M-199 GlutaMax Medium (with L-Glutamine; Gibco; catalogue number: 11150059) were used to culture human umbilical vein endothelial cells (HUVECs). M-199 GlutaMax medium was also used in the culture of human LSV under perfusion, as were the reagents listed below. Other reagents used for LSV and EC culture were as follows: heat-inactivated foetal bovine serum (FBS: Gibco; catalogue number: 10082147), trypsin-ethylene diamine tetraacetic acid (PAA Laboratories; catalogue number: L11-003), L-glutamine (PAA Laboratories; catalogue number: M11-004), penicillin and streptomycin (PAA Laboratories; catalogue number: P11-010), Dulbecco's phosphate-buffered saline (DPBS: $Ca^{2+}$ and $Mg^{2+}$ free; Gibco; catalogue number: 14080055) and gelatin solution (EC *in vitro* only) (catalogue number: G1393). Pharmacological compounds used included the inhibitor of NF-κB, BAY11-7085 (Santa Cruz Biotechnology; catalogue number: sc-202490), and activator of Nrf2, Sulforaphane (Sigma Aldrich; catalogue number: S6317). Additionally, recombinant human Tumour Necrosis Factor-α (TNF-α) (Miltenyi; catalogue number: 130-094-017), was used as an inducer of inflammation and NF-κB.

Roswell Park Memorial Institue-1640 medium (RPMI-1640 buffered with 25mM HEPES; Gibco; catalogue number: 42401018) was used for the culture of THP-1 cells (ATCC® TIB-202™). Other reagents used in THP-1 culture were as follows: heat-inactivated foetal bovine serum (Gibco; catalogue number: 10082147), trypsin-ethylene diamine tetraacetic acid (PAA Laboratories;

catalogue number: L11-003), L-glutamine (PAA Laboratories; catalogue number: M11-004), penicillin and streptomycin (PAA Laboratories; catalogue number: P11-010).

### 2.1.2 IMMUNOCHEMICAL REAGENTS

The immunochemical reagents used in experiments outlined in this thesis are listed in TABLE 2.1, TABLE 2.2 & TABLE 2.3; whilst the company locations are outlined in TABLE 2.4. Abbreviations used in all tables are as follows: WB – Western blotting; ICC – Immunocytochemistry; and IF – Immunofluorescence.

| ANTIBODY | SPECIES | WORKING CONCENTRATION | COMPANY | CATALOGUE # |
|---|---|---|---|---|
| Anti-NF-κB (p65) (c-20) | Rabbit | WB: 0.1μg/mL<br>ICC/IF: 0.2μg/mL<br>IF (*en Face*): 0.33μg/mL | Santa Cruz BT | Sc-372 |
| Anti-Phospho p65(Ser276) | Rabbit | WB: 0.4μg/mL | Santa Cruz BT | Sc-101749 |
| Anti-Phospho p65(Ser536) | Rabbit | WB: 0.4μg/mL | Santa Cruz BT | Sc-33020 |
| Anti-IκBα (c-21) | Rabbit | WB: 0.2μg/mL<br>ICC: 0.4μg/mL | Santa Cruz BT | Sc-371 |
| Anti-Nrf2 (c-20) | Rabbit | WB: 0.2μg/mL | Santa Cruz BT | Sc-722 |
| Anti-Nrf2 (h-300) | Rabbit | WB: 0.2μg/mL | Santa Cruz BT | Sc-13032 |
| Anti-MCP-1 | Rabbit | ICC: 3.33μg/mL<br>IF (*en face*): 9.99μg/mL | Abcam | Ab9669 |
| Anti-GAPDH | Mouse | WB: 3.33μg/mL | Millipore | MAB374 |
| Anti-Lamin A/C (h-110) | Rabbit | WB: 0.2μg/mL | Santa Cruz BT | Sc-6215 |
| FITC-Conjugated Anti-vWF | Sheep | ICC/IF: 200μg/mL<br>IF (*en face*): 200μg/mL | Abcam | Ab8822 |
| Anti-VE-Cad | Mouse | ICC/IF: 4μg/mL | Santa Cruz BT | Sc-9989 |
| Anti-Keap1 | Goat | WB: 0.4μg/mL | Santa Cruz BT | Sc-15246 |
| Anti-HO-1 | Mouse | WB: 4μg/mL | Abcam | Ab13248 |
| Anti-mouse IgG | | ICC/IF: equal to concentration of primary Ab used | | |
| Anti-rabbit IgG | | ICC/IF: equal to concentration of primary Ab used | | |

**TABLE 2.1. Details of primary antibodies**

| ANTIBODY | SPECIES | WORKING CONCENTRATION | COMPANY | CATALOGUE # |
|---|---|---|---|---|
| Anti-Mouse Alexa Fluor 488 | Goat | ICC/IF: 1:200 | Invitrogen | A-11001 |
| Anti-Rabbit Alexa Fluor 568 | Goat | ICC/IF: 1:200<br>IF (*en face*): 1:200 | Invitrogen | A-11011 |
| Anti-Rabbit IgG HRP | Swine | WB: 1:2000 | Dako | P0217 |
| Anti-Mouse IgG HRP | Goat | WB: 1:2000 | Dako | D0486 |

**TABLE 2.2. Details of secondary antibodies**

| STAIN/DYE | WORKING CONCENTRATION | COMPANY | CATALOGUE # |
|---|---|---|---|
| TO-PRO 3 | IF (*en face*): 1:1000 | Invitrogen | T3605 |
| DAPI Dilactate | ICC/IF: 1:1000 | Invitrogen | D3571 |
| Fluoromount-G | Applied dropwise | Invitrogen | 00-4958-02 |

**TABLE 2.3. Details of fluorescent nuclear labels and mounting medium**

| COMPANY | LOCATION |
|---|---|
| Abcam | Cambridge, UK |
| Santa Cruz BT | Dallas, USA |
| Invitrogen | Carlsbad, USA |
| Dako | Santa Clara, USA |
| Millipore | Burlington, USA |

**TABLE 2.4. Locations of companies where immunochemical reagents were purchased**

### 2.1.3 ADENOVIRUSES

Four recombinant replication incompetent adenoviral constructs were used in this project:

- Wild-type porcine IκBα overexpressing recombinant adenovirus (WT-IκBα) kindly gifted by Dr Mark Bond, University of Bristol. The original WT-IκBα was constructed as stated in Wrighton *et al.*, 1996. Homology between the amino acid sequences of human and porcine IκBα is greater than 90% and the porcine IκBα adenoviral construct has in fact been found to be more effective in human ECs than porcine (Wrighton *et al.*, 1996; Rupec *et al.*, 1999).
- GFP-tagged, wild-type human Nrf2 overexpressing recombinant adenovirus (WT-Nrf2) kindly gifted by Professor Paul Evans, University of Sheffield. The original WT-Nrf2 was constructed as stated in Kraft *et al.*, 2004.
- GFP-tagged, dominant negative (DN) human Nrf2 overexpressing recombinant adenovirus (DN-Nrf2) kindly gifted by Professor Paul Evans, University of Sheffield. The original DN-Nrf2 was constructed as stated in Kraft et al, 2004.
- Silent expression cassette (rAd66) was used as a control for three viruses above (WT and DN adenoviruses)

All adenovirus preparations were produced and titrated by Dr Graciela Sala-Newby and Mrs Jill Tarlton (University of Bristol). Briefly, viral preparations were purified on a caesium chloride gradient and aliquots were stored at -80°C until use. The number of plaque-forming units (pfu) per mL was calculated by end-point dilution in HEK293 cells (Anderson *et al.*, 2000).

## 2.2 CULTURE OF HUVECS

HUVECs were cultured in endothelial cell growth medium (ECGM) supplemented with endothelial cell growth supplement mix, containing final concentrations of 0.004 ml/ml endothelial cell growth supplement, 0.1 ng/ml recombinant human epidermal growth factor, 1ng/ml recombinant human basic fibroblast growth factor, 90µg/ml heparin, 1µg/ml hydrocortisone, 100µg/ml penicillin, 100iu/ml streptomycin and 2mM L-Glutamine at 37°C in 5% $CO_2$. ECs were quiesced for 18 hours in 2% FBS (v/v) endothelial cell basal medium (ECBM) supplemented with 100µg/mL penicillin, 100IU/mL streptomycin and 2mM L-Glutamine; but lacking the growth factors listed above.

### 2.2.1 CELL PASSAGE

On reaching confluence, cells were passaged using trypsin digestion. Briefly, cells were washed once with DPBS, incubated with trypsin-EDTA (0.05%(w/v) trypsin, 0.02%(w/v) EDTA) at 37°C for 3-4 minutes or until all adherent cells were displaced. ECGM was added to the trypsin at a ratio of 1:2 to neutralise trypsin activity. The cell suspension was centrifuged at 300g for 5 minutes, the supernatant discarded, and the cell pellet re-suspended in 1mL pre-warmed ECGM. Cell suspensions were divided 1:3 and cultured in ECGM at 37°C in 5% $CO_2$. Cells were used for experiments between passage 2-6.

### 2.2.2 CRYOPRESERVATION AND RESUSCITATION

For storage, cells were trypsinised as in 2.2.1 and resuspended in 1mL 10% (v/v) dimethyl sulphoxide (DMSO) in ECGM and the cell suspension pipetted into cryovials (ThermoFisher; catalogue number: 5000-1020). Cryovials were immediately stored at -80°C in a freezing container that freezes cells at a rate of -1°C/minute; the following day, cells were transferred into liquid nitrogen for long term storage. For resuscitation, cells were thawed quickly using a 37°C waterbath, upon defrosting, transferred immediately into 20-25mL pre-warmed ECGM in

flasks and incubated at 37°C in 5% $CO_2$. ECGM was replaced 16-24 hours later to ensure removal of DMSO.

### 2.2.3 CELL COUNTING

Cells were counted using a Neubauer haemocytometer and the concentration of cells per mL was calculated with the following formula:

$$\text{Average cells per } 1mm^2 = \text{Cell №} \times 10^4 = \text{Cells/mL}$$

## 2.3 CULTURE OF THP-1 CELLS

THP-1 monocytic-like cells were cultured in suspension in RPMI medium supplemented with 10% FBS(v/v), 100µg/mL penicillin, 100IU/mL streptomycin and 2mM L-Glutamine.

### 2.3.1 CELL SUBCULTURE

For subculturing, every 3 to 4 days, cell density was assessed by counting so as to not exceed a density above $1 \times 10^6$ cells/mL. Briefly, any loosely adhered cells were dislodged using a cell scraper and the cell suspension was centrifuged at 300g for 5 minutes, the supernatant was discarded, and cell-pellet re-suspended in 1mL pre-warmed RPMI medium, a further 14mL was added to cell suspension, prior to cell counting as described in 1.2.4. Cells were then seeded into flasks containing 20mL of pre-warmed RPMI at a density of $1 \times 10^5$ cells/mL. For cryopresevation, cells were subcultured as described in 2.3.1 and resuspended at a density of $1 \times 10^5$ cells/mL in 1mL 10% (v/v) DMSO in RPMI medium and the cell suspension pipetted into cryovials. Cells were resuscitated as in 2.2.2, into 20mL of pre-warmed RPMI medium.

## 2.4 OVEREXPRESSION OF NRF2, KEAP1, NF-κB AND IκBα

### 2.4.1 ECTOPIC OVEREXPRESSION OF WT- IκBα, WT-NRF2 AND DN-NRF2 IN HUVECS

Overexpression of WT or DN forms of IκBα or Nrf2 were achieved using recombinant adenoviruses described above in 2.1.3. The empty cassette (rAd66) was used as the negative control. Firstly, HUVECs were seeded in 6 well plates for assessment of overexpression or onto 1% gelatin-coated glass slides at a density of $2x10^5$/slide and cultured for 24 hours, as in 2.5.1., for shear stress exposure. The empty-cassette adenovirus (rAd66), and DN-Nrf2, WT-Nrf2 or WT-IκBα containing adenoviruses were diluted in ECBM to achieve a final concentration of $1x10^7$ pfu/mL. Cells were cultured with adenoviruses for 18 hours and after washing cells with DPBS fresh ECBM added for a further 48 hours to enable maximal expression of viral proteins. Expression of Ad-WT-Nrf2 and Ad-DN-Nrf2 was assessed by visualising GFP protein under a fluorescence inverted microscope. Cells were then analysed immediately for overexpression by WB or subjected to shear stress prior to analysis by either qPCR or ICC.

## 2.5 SHEAR STRESS INDUCTION IN PARALLEL PLATE FLOW CHAMBER

### 2.5.1 CELL CULTURE

HUVECs were cultured and passaged as previously described in 2.2. Menzel standard glass microscope slides (1mm thickness) (Thermo Scientific; catalogue number: 10144633A) were sterilised in 70%(v/v) ethanol and air-dried in cell culture ready quadriPERM® slide tray plates (Sarstedt; catalogue number: 94.6077.308). A physical barrier area to cell growth was established by adhering reusable flexiPERM® cell culture chambers (Sarstedt; catalogue number: 94.6032.039) to the glass slide surface. The established growth area was coated with 700µl 1%(w/v) gelatin for 1 hour at 37°C; the gelatin solution was then aspirated, prior to washing the slide with DPBS and subsequent addition of 3mL pre-warmed ECGM. Cells were

seeded at a density $2.5\times10^5$/slide and cultured using ECGM (described in section 2.1.1) for 48 hours (unless otherwise stated) at 37°C and 5% $CO_2$ until 100% confluence was achieved, then quiesced in ECBM overnight. For shear stress exposure, M-199 GlutaMax medium, supplemented with 2% FBS (v/v), 100µg/mL penicillin and 100IU/mL streptomycin, was used.

### 2.5.2 SHEAR STRESS

Endothelial cell exposure to shear stress was achieved by placing the cells on the glass slides into a parallel plate flow chamber (FIGURE 2.1.) (PPFC) constructed by Dr. Stephen White, Manchester Metropolitan University (based on Castier *et al.*, 2009). The chambers were made from Polymethyl methacrylate (Perspex/Acrylic glass) in-house at the University of Bristol mechanical workshop.

Using sterile forceps, glass slides coated with cultured ECs were placed into the slide groove of the PPFC base plate followed by a silicon gasket (0.25mm thick, white solid silicon sheeting from Tyms seals and gaskets; catalogue number: TYM0115) around the cell area, ensuring that the gasket did not come into contact with the cells. After pipetting 1 mL of pre-warmed M-199 medium onto cell area, the top-plate was carefully placed onto the gasket (See FIGURE 2.1). Once assembled in groups of three, chambers were mounted into the frame and clamps were tightened using a torque wrench to create a seal around silicon gaskets. M-199 medium was aspirated into a 30mL pipette attached to silicon tubing loops (1.58mm internal diameter, silicon tubing, VWR; catalogue number: 228-1066, and 1.42mm internal diameter peristaltic pump tubing, Elkay Laboratory products; catalogue number: 116-MEDI-056), which in turn were attached to chambers by plastic cannulae/male luer fitting (3mm outer diameter, World Precision Instruments; catalogue number: 13162-100). Frames and chambers were placed into incubators at 37°C and 5% $CO_2$ (FIGURE 2.2.B.). Cells were exposed to laminar shear stress at 0.5 or 12 dyn/cm$^2$ using a multi-channel peristaltic pump (Watson-Marlow; 323E manual pump driver, catalogue number: 036.3124.00U, 314D pumphead, catalogue number: 033.4411.000). Shear stress rates used, were to simulate approximate venous (0.5dyn/cm$^2$) and arterial (12dyn/cm$^2$) shear stresses. Time-points of 30 and 90 minutes were selected to assess nuclear and cytosolic movement of transcription factors and their repressors. Time-points of 90 and 120

minutes were selected in order to detect an mRNA transcriptional response. Finally, time-points of 4 and 6 hours were selected to detect a target protein response and allow for mRNA translation.

Shear stress rates were calculated for a slit die assuming the viscosity of water at 37°C, using the following equation:

$$\tau = 6\mu Q / wh^2$$

Where τ represents Shear Stress; $\mu$, viscosity; $Q$, flow rate; $w$, width and $h$, height (of the silicon gasket) and assuming the viscosity of water at 37°C.

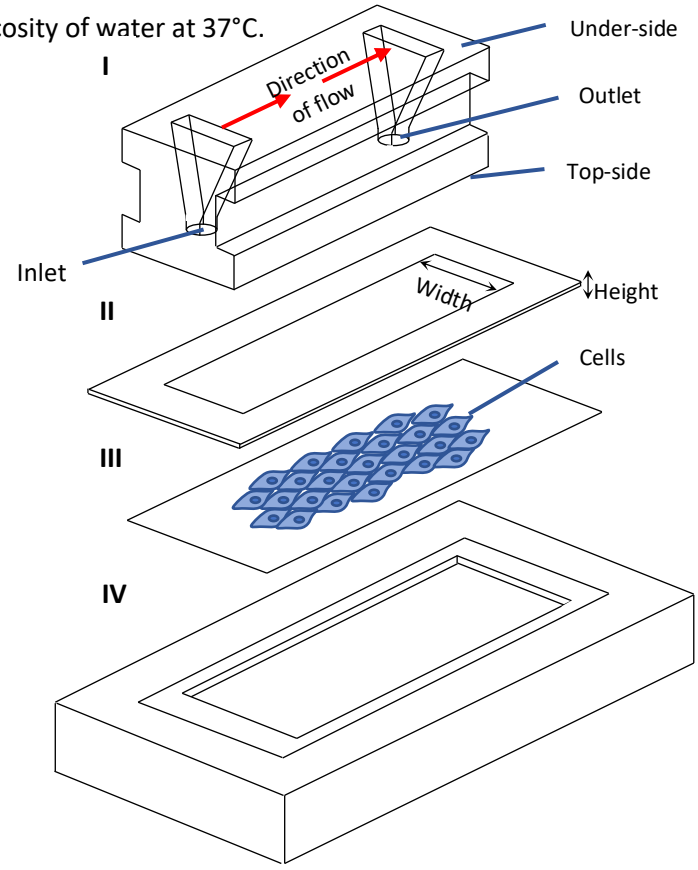


**FIGURE 2.1. Schematic diagram of the parallel plate flow chamber**

I. Top-plate of flow rig containing ports and openings for both inlet and outlet (image drawn upside down to visualise openings). Arrows represent the direction of flow.
II. Silicon gasket; used to seal plates together and provide the correct width and height (indicated by black arrows) of the slit dye for calculation of shear stress, using the equation above.
III. Glass slide with HUVECs (blue) cultured on 1% gelatin within restricted growth area
IV. Base plate for glass slide.

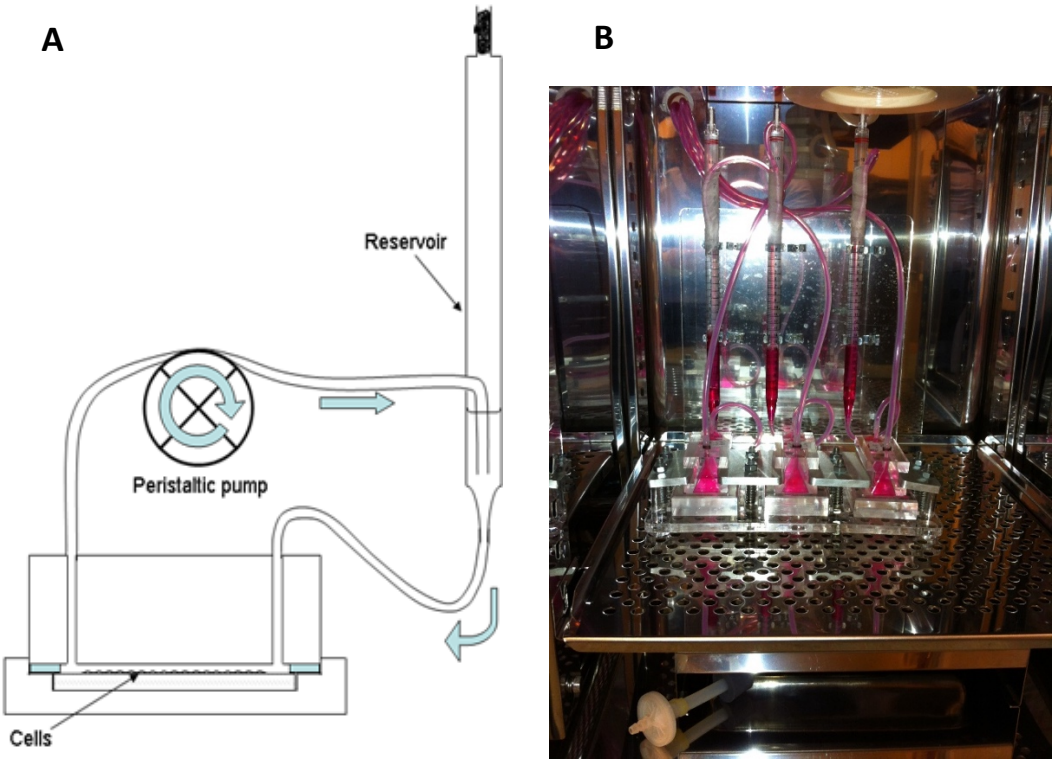


**FIGURE 2.2. Parallel plate flow chamber model**

A. Cross section through parallel plate flow chamber (adapted from White *et al.*, 2011)
B. Parallel plate flow chambers *in-situ*

## 2.6 *IN VITRO* REAL-TIME MONOCYTE ADHESION ASSAY

Monocyte adhesion to an endothelial monolayer, *in vitro*, was assessed in real-time using the Bioflux 200 microfluidic channel system (Fluxion; catalogue number: 950-0092). Briefly, the Bioflux 200 system uses pressurised, sterile air, pumped through a fully-enclosed tubing, plate and microfluidic circuit to generate a modifiable shear stress through microfluidic channels, which are viewable under a microscope (FIGURE 2.3.).

ECs up to passage 4 were cultured as in 2.2. Prior to seeding ECs into the microfluidic channel system of the Bioflux 200 48-well, low shear plates (Fluxion; catalogue number: 910-0004), channels were coated with 1μg/mL (w/v) bovine fibronectin (Sigma; catalogue number: F1141) for 1 hour at 37°C and 5% $CO_2$. Unbound fibronectin was then removed from the wells and

flushed out of the channels with ECGM. ECs were seeded very quickly into the channels to prevent cell aggregation and blocking of microfluidic capillaries. ECs were seeded with viewing channels constantly in view under the ThermoFisher EVOS FL microscope (ThermoFisher, AMF4300). Seeding was performed into the outlet well and ECs were flushed through the channels with a shear stress of 5dyn/cm$^2$ for less than 5 seconds (until ECs entered the viewing channels), and a cell density of 4×10$^7$ cells/mL in a total volume of 10μL of ECGM. ECs were cultured in the channels for 48 hours at 37°C and 5% $CO_2$ with ECGM. Following these 48 hours, and prior to exposure to high shear stress, ECs were labelled with 10μmol/L CellTracker™ CM-DiI (ThermoFisher; catalogue number: C7000) red fluorescent probe for three-hours, concurrently with pre-treatment of ECs with either 20μmol/L NF-κB inhibitor, 20μmol/L BAY11-7085, or 0.2% (v/v) DMSO vehicle control at 37°C and 5% $CO_2$. ECs were then exposed to unidirectional, pulsatile shear stress (at 12 dyn/cm$^2$ and 1 hertz(Hz)) for 6 hours at 37°C and 5% $CO_2$ using the Bioflux 200 system. THP-1 cell labelling was achieved by incubation of 3x10$^6$ THP-1 cells/mL with 10μmol/L Calcein AM (ThermoFisher, catalogue number: C1430) for 30 minutes, in a 6-well plate. Cells were then centrifuged at 300g for 5 minutes, to remove unbound Calcein AM, and re-suspended at the same density of 3x10$^6$ cells/mL. Following labelling of THP-1 cells and exposure of HUVECs to 6 hours of shear stress, Calcein AM-labelled THP-1 cells at a density of 3×10$^6$ cells/mL were flowed over confluent endothelial monolayers (at 1dyn/cm$^2$) for 10 minutes and viewing channels were imaged in real-time using a Zeiss AxioObserver Z1 inverted fluorescent microscope. Adhered THP-1 cells were enumerated after 10 minutes and divided by the total number of ECs in viewing channels to give a percentage of adhered monocytes.

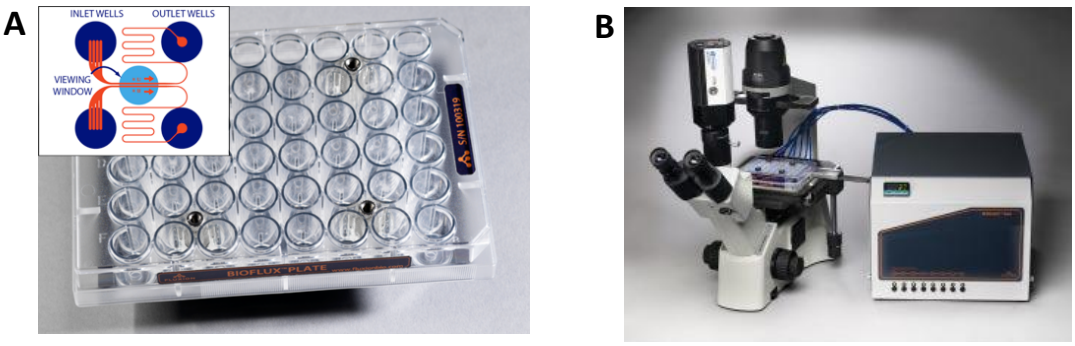


**FIGURE 2.3. Bioflux 200, 48-well plate and integrated system**

A. 48-well plate with schematic of paired inlet and outlet wells, complete with viewing window containing microfluidic channels
B. Integrated Bioflux system consisting of a highly accurate electro-pneumatic pump, tubing and the Bioflux pressure interface attached to the 48-well plate. Images from bioflux.fluxion.com

## 2.7 *EX VIVO* HUMAN LONG SAPHENOUS VEIN PERFUSION MODEL

Surplus segments of surgically prepared human LSV resected during CABG surgeries (Ethics number: REC 14/EE/1097) were placed into M-199 GlutaMax medium, supplemented with 10% FBS (v/v), 100µg/mL penicillin and 100IU/mL streptomycin. Segments of LSV were used immediately after resection, additionally segments with minimal side-branches and clips were preferred. Appropriate length segments for either *en face* preparation, intimal RNA extraction, *ex vivo* monocyte adhesion or histology processing were cut transversely for use as static/baseline control and maintained in M-199 medium until the bioreactor was operating. For use in the bioreactor, segments of 6cm were cut transversely at each end to ensure minimal prior contact to the vessel in order to limit endothelial damage across vessel length. Vein segments were cannulated with Male Luer Fittings (1.5mm (1/16”) outer diameter, (World Precision Instruments; catalogue number: 13160-100) and secured with sterile 4-0 mersilk surgical suture (Ethicon; catalogue number: W586H). Secured segments were then attached to

a perfusion circuit consisting of an in-house designed bioreactor, silicon tubing (FIGURE 2.4.A.) (suppliers as above in 2.3.2) and a multi-channel peristaltic pump. The perfusion system was maintained at 37°C and 5% $CO_2$ (FIGURE 2.4.B.). Vein segments were perfused with pre-warmed M199 culture medium under mean arterial flow rate of 100mL/min, which equated to a shear stress of 12dyn/cm$^2$, as calculated by the equation for shear through a non-deformable cylinder:

$$\tau=4\mu Q/\pi r^3$$

where τ represents Shear Stress; $\mu$, viscosity; $Q$, flow rate; $\pi$, pi; $r$, radius (the radius of the outer diameter of the cannula, 1.6mm, was used) and assuming the viscosity of water at 37°C.

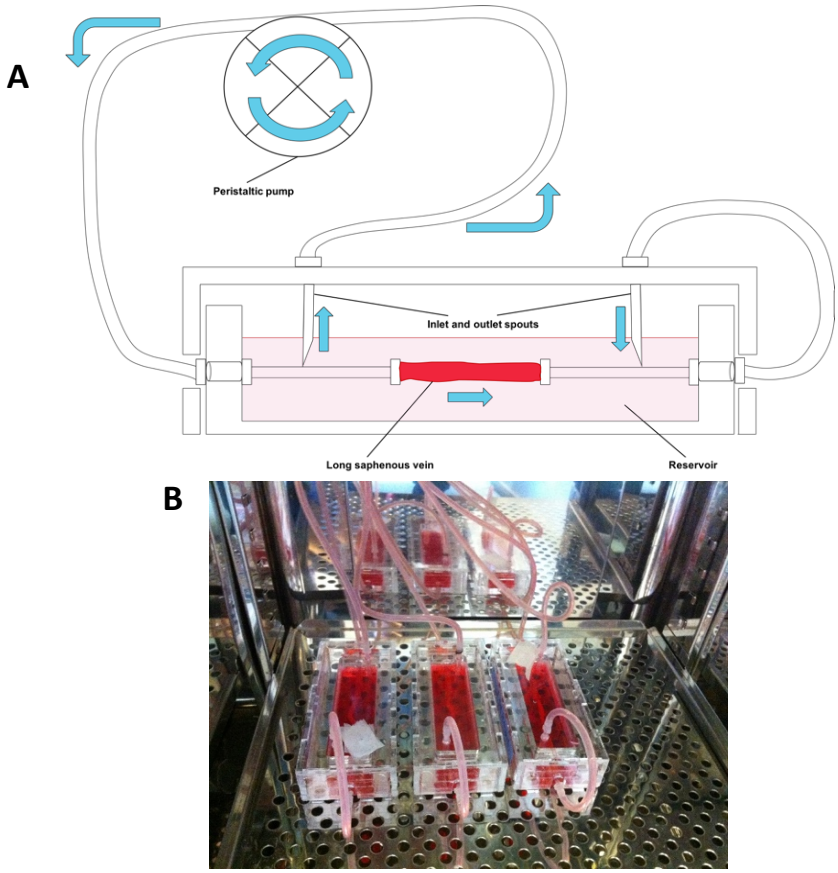


**FIGURE 2.4.** ***Ex Vivo*** **perfusion system**

A. Cross section of *ex vivo* perfusion system
B. Image of 3 *ex vivo* perfusion rigs for exposure of LSV to regulated levels of shear stress using a peristaltic pump

### 2.7.2 *EN FACE* PREPARATION

For immunofluorescent analysis of the saphenous vein endothelium, a procedure involving confocal microscopy and microdissection was developed and optimised. Sections of vein (static control segments or segments exposed to flow in the bioreactor) were cut transversely into approximately 1cm lengths, washed once in DPBS and dissected longitudinally using fine forceps and fine spring scissors. The vessel was pinned to dental wax using 100A minutien pins (Fine Science Tools; catalogue number: 2600210) with the luminal surface facing upwards, the dental wax was arched slightly to tauten the luminal surface and fixed using 10%(v/v) formalin/distilled water for 48 hours (FIGURE 2.5.A.). Following fixation, tissue was transferred to PBS for microdissection. Microdissection was performed, mostly with tissue free-floating in PBS, using an Olympus SZ-PT stereomicroscope. Briefly, the intimal layer of the vessel was peeled gently away from adventitial and medial layers using fine forceps and, if necessary, further microdissection with spring scissors was performed to ensure thin, flat intimal sections for immunofluorescent analysis (FIGURE 2.5.B.).

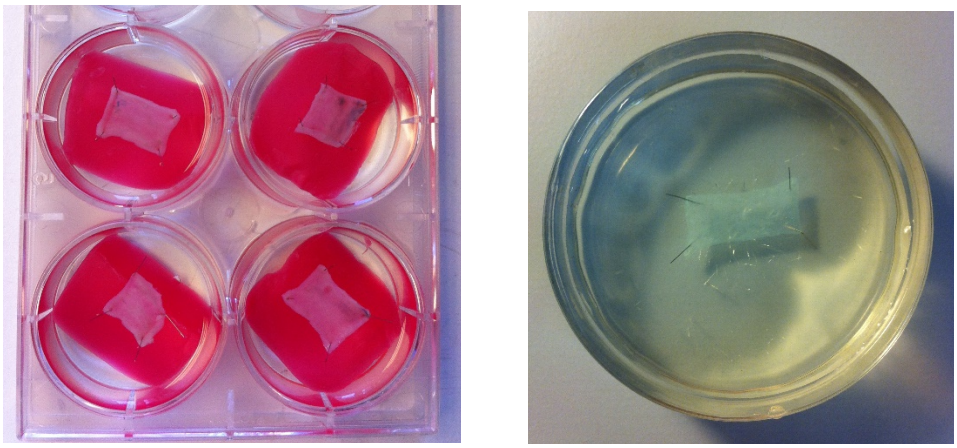

**FIGURE 2.5.** ***En face*** **preparation of LSV**

A. LSV pinned to dental wax and fixed in a 6-well plate
B. *En face* prepared segment, pinned to sylgard coated glass petri dish for confocal imaging

### 2.7.3 INTIMAL RNA EXTRACTION

For extraction of RNA from endothelial cells of the long saphenous vein, a technique was used which involves the flushing of the lumen of the vessel with a severe lysis buffer, in this case, Qiazol (Qiagen; catalogue number: 79306), to disrupt cells in the intimal layer, predominantly endothelial cells (Nam *et al.*, 2009; Chen *et al.*, 2015). Briefly, segments were cut transversely into 2-3cm lengths and washed in ice-cold DPBS. Using a 1mL syringe and 18-gauge unbevelled needle with the tip inserted a few millimetres into the vessel lumen, the vessel was flushed with ice-cold DPBS. Finally, the lumen was quickly flushed (3-6 seconds) with 350µL of ice-cold Qiazol and the eluate was collected in a 1.5mL Eppendorf tube. This eluate was subjected to the RNA isolation protocol as in section 2.10.2.

### 2.7.4 *EX VIVO* MONOCYTE ADHESION

Following exposure to high shear stress, or maintenance in a static condition in M199 medium, for 6 hours, veins were sectioned transversely into approximately 1cm segments. Vessels were then dissected as above and pinned to a sterile glass petri dishes coated with sylgard silicone elastomer. Pinned samples were incubated with $1\times10^6$ THP-1 cells labelled with 10µM Calcein AM for 15 minutes then washed thoroughly with DPBS, twice. Veins were then placed directly into Immersol W2010 aqueous immersion medium (Zeiss; catalogue number: 444969) on a glass slide with the luminal side facing downwards, a coverslip placed on top and viewed immediately with the Zeiss AxioObserver Z1 fluorescent microscope. Due to the undulating and uneven endothelial surface of the LSV, sequential Z-stack images were taken to ensure sufficient coverage of the endothelial surface was captured, with individual slices separated by 1µm gaps and the depths of Z-stacks ranging from 5µm to 100µm. Z-stacks were taken at 5 equally distributed points across the surface of the vessel, i.e. four at the four points of a cross and one centrally. Z-Stacks were then processed, and maximum intensity projections were produced in

order to create a 2D image from a 3D stack. Total numbers of adhered cells were then counted using the 'Identify Primary Objects' feature with CellProfiler 2.0. software (See section 2.7.5.).

### 2.7.5 VALIDATION OF AUTOMATED THP-1 CELL ENUMERATION

CellProfiler was used to count the number of adhered monocytes to the LSV endothelial surface. CellProfiler is an open-source, freely available software and allows automated, quantitative and reproducible analysis of light microscopy images (Carpenter *et al*., 2006). The method used was the 'Identify Primary Objects' module (see TABLE 2.5.), which employed a two-class thresholding approach, whereby object detection works in an almost binary way, as there are large differences in intensities between objects and background in the image. Size limitation was also a very important feature to factor in to the enumeration due to the clumped nature of the adhered monocytes.

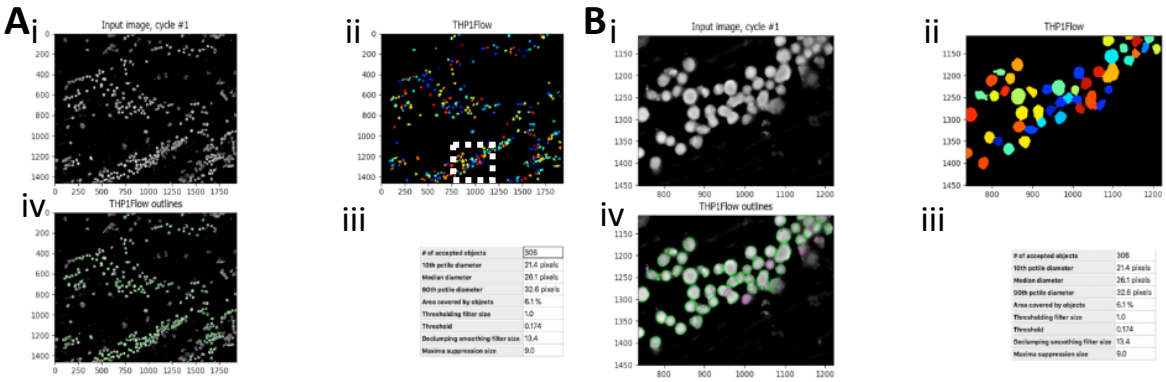


**FIGURE 2.6. CellProfiler output from adhered monocyte counts**

CellProfiler was used for automated counting of adhered THP-1 cells to the endothelial surface, outputs of the analysis are shown here to prove validity of the method. Clockwise from top left, panels include grayscale original image (i), randomly assigned colour representation of image showing segmentation (ii), quantitative data outputs (iii) and original image with segmented outlines (iv).

A. *Identify primary objects* – Identification and counts of labelled monocytes. Magnified region represented by dotted white box
B. Magnification of A

## 2.8 IMMUNOCYTOCHEMISTRY

### 2.8.1 DUAL IMMUNOCYTOCHEMISTRY FOR MCP-1/IκBα AND VE-CADHERIN

HUVECs were cultured on glass slides, as in section 2.5.1., and either exposed to shear stress or maintained in static conditions. Slides were washed twice with ice-cold DPBS prior to fixation in 500µL of 3% (w/v) paraformaldehyde/PBS for 10 minutes. Following fixation, slides were washed three times for 5 minutes each, in PBS. Permeabilisation was achieved by incubation in 0.1% (v/v) Triton X-100/PBS three times for 5 minutes each. Slides were again washed once for 5 minutes in PBS and blocked for 45 minutes with 20% (v/v) goat serum/PBS at RT. Cells were washed for 5 minutes with PBS and then incubated with 120µL of 3.33µg/mL rabbit anti-MCP-1 IgG (Abcam; catalogue number: ab9669), 120µL of 0.4µg/mL rabbit anti-IκBα IgG (Santa Cruz Biotechnology; catalogue number: sc-371), or rabbit anti-IgG isotype controls at matched concentrations to primary antibodies, diluted in 1% (w/v) bovine serum albumin (BSA)/PBS overnight at 4°C. The following day, slides were washed three times in PBS for 5 minutes each and incubated with 120µL AlexaFluor568 conjugated goat anti-rabbit IgG (Invitrogen; catalogue number: A-11001) diluted 1:200 in 1% (w/v) BSA/PBS for 1 hour at RT. From this point onwards, care was taken to prevent direct exposure to either sunlight or artificial light by covering slide boxes with aluminium foil. Slides were washed three times for 5 minutes in PBS and incubated with 120µL of 4 µg/mL mouse anti-VE-Cadherin (F-8) IgG (Santa Cruz Biotechnology; catalogue number: sc-9989), or mouse anti-IgG isotype controls at matched concentrations to primary antibodies, diluted in 1% (w/v) BSA/PBS for 1 hour at RT. Slides were washed three times for 5 minutes in PBS and incubated with 120µL AlexaFluor488 conjugated goat anti-Mouse IgG (Invitrogen; catalogue number: A-11011) diluted 1:200 in 1% (w/v) BSA/PBS for 1 hour at RT. Nuclei were stained using 1:1000 dilution of DAPI-dilactate (Invitrogen; catalogue number: D3571) in PBS for 1 hour. Following three final 5-minute washes in PBS, the remaining PBS was carefully removed and slides were mounted with Fluoromount-G (Invitrogen, catalogue

number: 00-4958-02) and then stored in the dark at 4°C until imaging was performed with the Zeiss AxioObserver Z1 fluorescent microscope using a 20x lens coupled with an AxioCamMRC Zeiss camera.

Image analysis was performed using CellProfiler2.0 software (Carpenter *et al*., 2005). Quantification of arbitrary fluorescence intensity (or 'Integrated Fluorescence Intensity' as defined by CellProfiler) was calculated as total fluorescence across the objects (cells) divided by the total number of cells. Measurements of cell morphological features were also calculated with CellProfiler; these measurements are also expanded on in TABLE 2.5. For each condition, 20 fields were imaged across each slide, which equated to approximately 2000 cells per condition.

### 2.8.2 IMMUNOCYTOCHEMISTRY ANALYSIS

Immunocytochemistry images were analysed using CellProfiler (Carpenter *et al.*, 2006). CellProfiler has a toolbox of executable modules which are user-configured and run consecutively in a logical pipeline format. The primary pipeline utilised for image analysis consisted of 12 modules, outlined in TABLE 2.5., below. Briefly, the user selects a number of modules depending on quantitation required from the image sets. Each module used requires the user to define a number of image-processing settings, including thresholding, de-clumping objects and smoothing.

| MODULE | SETTINGS | FUNCTION |
|---|---|---|
| Identify Primary Objects | Global thresholding using Otsu approach; based on object size | Detect Nuclei using DAPI image |
| Identify Secondary Objects | Watershed method across the image; Adaptive thresholding using Otsu approach | Detect cell boundaries using Nuclei as seed; using primary stain (e.g. MCP-1/VE-Cadherin) |
| Identify Tertiary Objects | Subtraction | Subtract 1° object from 2° object to give cytosolic area |
| Measure Object Intensity | Select primary stain (of interest) and objects | Measures of intensities for each cell individually in total cell, nucleus and cytosol |
| Measure Object Neighbours | Select secondary stain (i.e. VE-Cadherin) and objects | Measures proximity of objects, percent of objects in contact and other neighbour features |
| Measure Image Area Occupied | Select objects to measure | Measures of total area covered by cells and sum of cell perimeters |
| Measure Image Intensity | Select primary stain (of interest) and objects | Measures of intensities of all cells/nuclei/cytosol |
| Calculate Math | Select features to define | Calculate ratio of intensity between nucleus and whole cell |
| Calculate Math | Select features to define | Calculate ratio of intensity between cytosol and whole cell |
| Display Histogram | Select features to define | Provide histogram representation of intensity – for normal distribution |
| Overlay Outlines | Select overlays | Overlay nuclei and cell outlines over primary stain |
| Export to Spreadsheet | Select features to export | Export all data into excel format |

**TABLE 2.5. Modules used in CellProfiler-based immunocytochemistry analysis**

### 2.8.3 VALIDATION OF AUTOMATED MCP-1 AND IκBα INTENSITY ANALYSIS

MCP-1/IκBα immunocytochemistry image sets were analysed for whole cell integrated fluorescence intensity (sum of intensities divided by number of cells per image). For the running of the analysis, the MCP-1/IκBα (red) channel was used as the primary stain for quantification. Initially, nuclei were identified, using the DAPI nuclear stain, to represent 'seed' regions (FIGURE 2.7.A. and E). To determine cell boundaries, edges of MCP-1/IκBα immunofluorescence were expanded from seed regions (nuclei), with a boundary-based algorithm, until the intensity threshold detected crosses the lower limit, i.e. the cell/staining extremity (FIGURE 2.7.B. and F.). The final stage of segmentation of cellular compartments is a subtraction of nuclei from the whole cell (FIGURE 2.7.C. and G). Intensity of MCP-1/IκBα immunofluorescence and morphology data were then quantified for each cell compartment (nuclei, cytosol and whole cell). However, for quantification in this thesis, whole cell fluorescence was used.

---

**FIGURE 2.7. Outputs from CellProfiler MCP-1/IκBα analysis**

Clockwise from top left, panels include grayscale original image (i), randomly assigned colour representation of image showing segmentation (ii), quantitative data outputs or outlines (iii) and original image with outlines or image representing subtraction of nuclei from whole cell (iv).

A. *Identify Primary objects* – Identification of seed regions from DAPI nuclear stain
B. *Identify Secondary objects* – Grows from seed region to boundary of cells from using MCP-1 immunofluorescence and step A as the seed
C. *Identify tertiary objects* – Subtracts nuclei from whole cell to give cytosol segmentation
D. *Display Histogram* – Outputs integrated intensity in the form of histogram for normality
E. Magnification of A
F. Magnification of B
G. Magnification of C

White dotted box represents magnified area for E, F and G

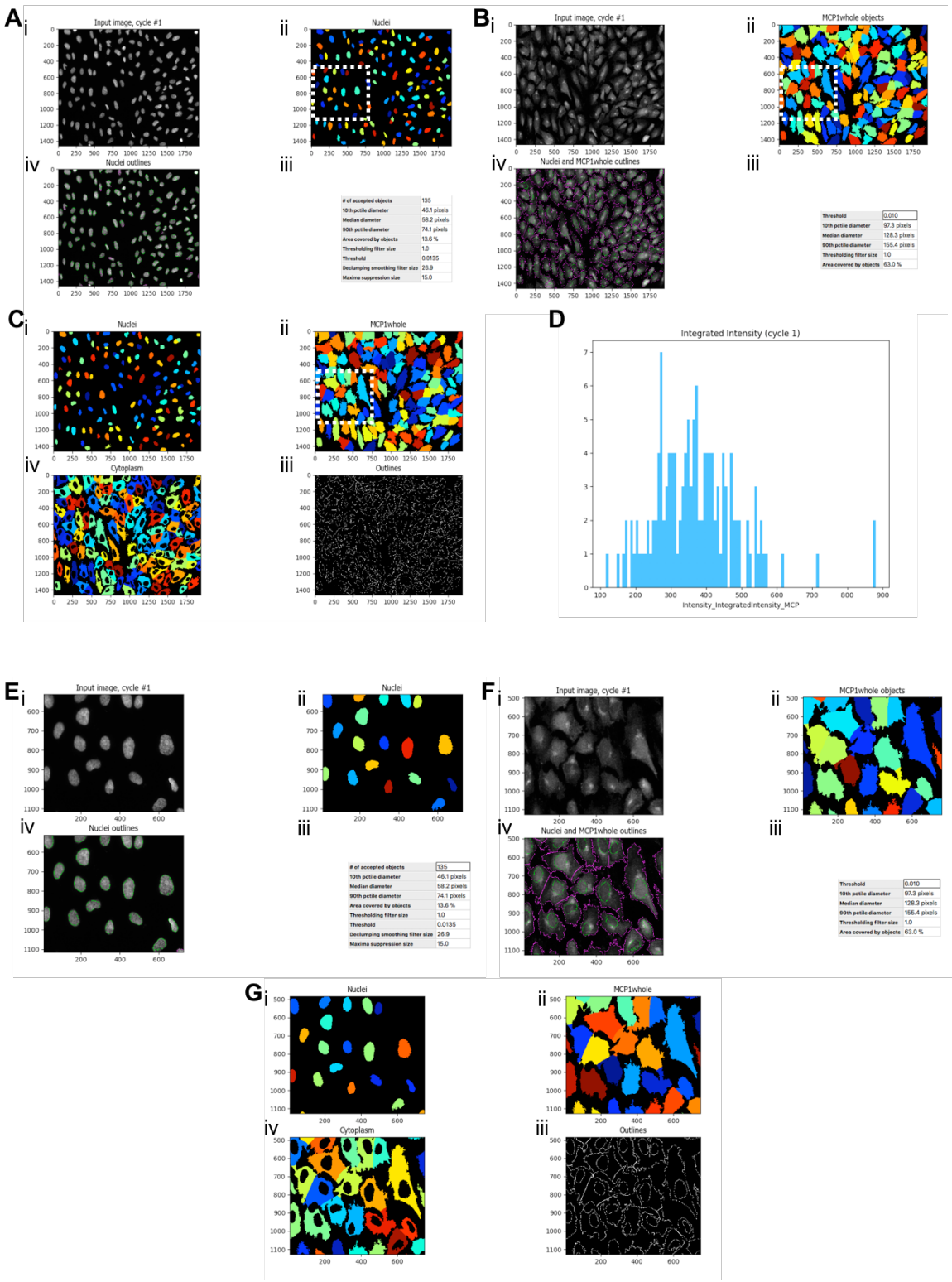
A
i
Input image, cycle #1
ii
Nuclei
iii
iv
Nuclei outlines
# of accepted objects 135
10th pctile diameter 46.1 pixels
Median diameter 58.2 pixels
90th pctile diameter 74.1 pixels
Area covered by objects 13.6 %
Thresholding filter size 1.0
Threshold 0.0135
Declumping smoothing filter size 26.9
Maxima suppression size 15.0
B
i
Input image, cycle #1
ii
MCP1whole objects
iii
iv
Nuclei and MCP1whole outlines
Threshold 0.010
10th pctile diameter 97.3 pixels
Median diameter 128.3 pixels
90th pctile diameter 155.4 pixels
Thresholding filter size 1.0
Area covered by objects 63.0 %
C
i
Nuclei
ii
MCP1whole
iii
Outlines
iv
Cytoplasm
D
Integrated Intensity (cycle 1)
Intensity_IntegratedIntensity_MCP
E
i
Input image, cycle #1
ii
Nuclei
iii
iv
Nuclei outlines
# of accepted objects 135
10th pctile diameter 46.1 pixels
Median diameter 58.2 pixels
90th pctile diameter 74.1 pixels
Area covered by objects 13.6 %
Thresholding filter size 1.0
Threshold 0.0135
Declumping smoothing filter size 26.9
Maxima suppression size 15.0
F
i
Input image, cycle #1
ii
MCP1whole objects
iii
iv
Nuclei and MCP1whole outlines
Threshold 0.010
10th pctile diameter 97.3 pixels
Median diameter 128.3 pixels
90th pctile diameter 155.4 pixels
Thresholding filter size 1.0
Area covered by objects 63.0 %
G
i
Nuclei
ii
MCP1whole
iii
Outlines
iv
Cytoplasm

### 2.8.4 VALIDATION OF AUTOMATED VE-CADHERIN CELL-CELL CONTACT ANALYSIS

Analysis of VE-Cadherin immunocytochemistry, in order to quantify endothelial barrier organisation, was done using CellProfiler software. The feature quantified was 'Percent touching', which gives a quantifiable measure of cell-cell contacts and gaps between cells, which was used as a surrogate marker to illustrate disruptions to the endothelial barrier. As it is a percentage calculation, 100% represents an entirely intact endothelial monolayer without distinguishable gaps. The analysis pipeline used was a similar process to that outlined in TABLE 2.5, with the key difference being that the primary stain used was VE-Cadherin. The other differences are in the thresholding strategies for detection of object edges and addition of a 'measure object neighbours' module. Also, here, an adaptive, watershed thresholding approach was used, which is preferred when there is a clear and distinct boundary between objects and the intensity gradient drops off or increases sharply at the border. Finally, the 'measure object neighbours' module expands object borders outwardly by a nominal, specified distance and quantifies features of neighbouring objects based on adjacent pixels.

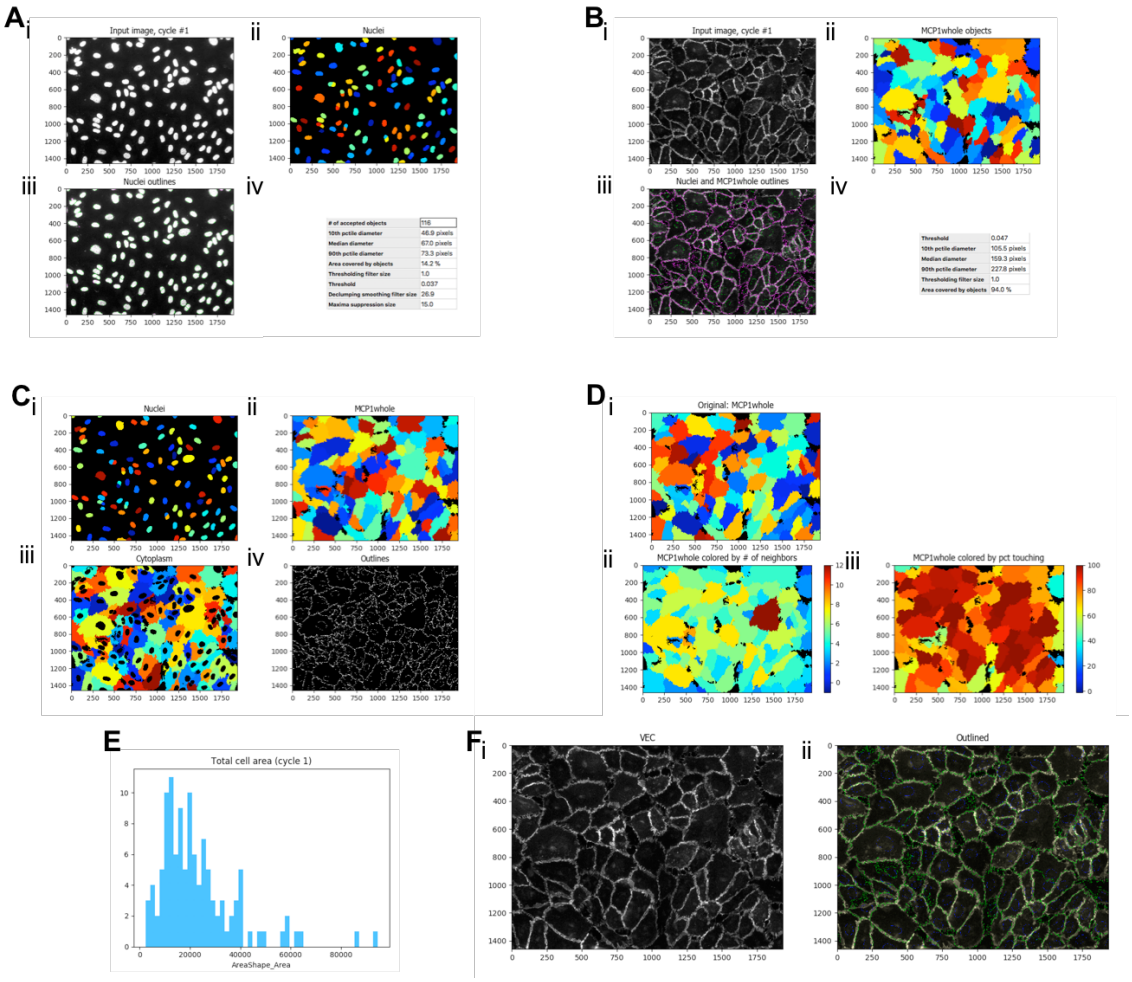


**FIGURE 2.8. Outputs from CellProfiler VE-Cadherin analysis**

Clockwise from top left, panels include grayscale original image (i), randomly assigned colour representation of image showing segmentation (ii), original image with outlines or image representing subtraction of nuclei from whole cell (iii) and quantitative data outputs, visualisation of quantification or outlines (iv).

A. *Identify Primary objects* – Identification of seed regions from DAPI nuclear stain
B. *Identify Secondary objects* – Grows from seed region to boundary of cells from using VE-Cadherin immunofluorescence and step A as the seed (N.B. MCP1whole (title) only represents naming system, as this pipeline was adapted from earlier (2.8.3)).
C. *Identify tertiary objects* – Subtracts nuclei from whole cell to give cytosol segmentation
D. *Measure object neighbours* – Measurement outputs including number of adjacent object neighbours (iii) and percent touching by object (iv)
E. *Display Histogram* – Outputs histogram of total cell area to show distribution
F. *Display outlines* – Final representation of original image (i) and original image complete with nuclear outline (blue) and outer border outline (green) superimposed

## 2.9 IMMUNOFLUORESCENCE ON TISSUE SAMPLES

### 2.9.1 LSV DUAL *EN FACE* NF-κB/MCP-1 AND vWF IMMUNOFLUORESCENCE

*En Face* prepared segments of LSV were maintained free-floating, in a total volume of 500μL per well at 4°C (unless stated otherwise), throughout the procedure, 24-well plates with the luminal side facing upwards. Firstly, segments were permeabilised with 0.2%(v/v) TritonX-100/PBS overnight at 4°C. Segments were then blocked in 20%(v/v) goat serum/PBS for 1 hour at RT. Primary antibody incubation was performed with 300μL of 1.33μg/mL rabbit anti-NF-κB IgG (Santa Cruz Biotechnology; Catalogue number: sc-372) or 300μL of 9.99μg/mL Rabbit anti-MCP-1 IgG (Abcam; catalogue number: ab9669), or rabbit anti-IgG isotype controls at matched concentrations to primary antibodies, diluted in 1%(v/v) BSA/PBS for 48 hours. After washing segments at RT, three times for 5 minutes with PBS with continual agitation, they were incubated with 1:200 dilution of AlexaFluor 568 conjugated goat anti-rabbit IgG in 1%(v/v) BSA/PBS overnight. Following three 5-minute washes in PBS, segments were incubated with 200μg/mL FITC-conjugated sheep anti-vWF IgG (Abcam; Catalogue number: ab8822), or sheep anti-IgG isotype controls at matched concentrations to primary antibodies, diluted in 1%(v/v) BSA/PBS overnight. Segments were washed three times for 5 minutes with PBS. Lastly, segments were incubated for one hour at RT with TO-PRO3 iodide (ThermoFisher; Catalogue number: T3605) diluted 1:1000 in PBS. Samples were maintained in PBS at 4°C until confocal imaging was performed. For confocal microscopy, segments were placed onto a Sylgard (Dowsil; Catalogue number: 101697) coated petri dish and pinned at four corners as in FIGURE 2.5.B. and submerged in PBS for imaging with a water immersion lens. The Leica SP8 AOBS confocal scanning microscope attached to a Leica DM6000 upright epifluorescence microscope and 25x dipping lens were used for all *en face* imaging (Leica). Due to the undulating and uneven endothelial surface of the LSV, sequential Z-stack images were taken to ensure sufficient area of the endothelial surface was captured, with individual slices separated by 500nm gaps and the

depths of Z-stacks ranging from 15μm to 100μm. Z-stacks were taken at five equally distributed points across the surface of the vessel, i.e. the four points of a cross and one centrally.

### 2.9.2 IMARIS *EN FACE* IMMUNOFLUORESCENCE ANALYSIS FOR NUCLEAR NF-κB

Quantitative analysis of Z-stacks as 2D maximum intensity projections was not possible due to underlying VSMCs beneath the endothelial monolayer which also expressed the proteins of interest. As such, a protocol was designed to quantitatively analyse ECs alone, whilst removing underlying VSMCs, in 3D, using Bitplane Imaris software. *En face* image sets from section 2.7.2 were analysed with the procedure outlined in TABLE 2.6 below.

| MODULE | SETTINGS | FUNCTION |
|---|---|---|
| 3D volume reconstruction | N/A | Create volume view of nuclei |
| Surface rendering | Threshold based on Absolute intensity; Smoothing objects to a resolution of 0.2μM | Create surface rendered nuclei from nuclear stain |
| Split touching objects | Set seed point diameter of 6μM | Sets centre point of automatically detected objects and separates touching objects/nuclei |
| Classify seed points | Based on intensities of objects ('Quality'), user defined | Allows removal of some nuclei based on intensity |
| Classify surface | Based on ellipticity of objects (oblate/flattened at poles), user defined | Allows removal of some nuclei based on their shape (e.g. VSMC nuclei – much longer and thinner) |
| Cut surfaces | Cutting in 3D; to remove or separate further touching objects | Allows user to clip overlapping/joined objects manually |
| Surface selection | Select new surface (i.e. with all unwanted objects removed) | To define quantitative measures for only nuclei of interest (EC) |
| Export statistics | Select features to export | Export all morphometric and intensity data to Excel |

**TABLE 2.6. Process of Imaris 3D *en face* immunofluorescence analysis**

### 2.9.3 VALIDATION OF IMARIS 3D ANALYSIS PROCESS

Due to the extremely contoured and uneven surface topology of the LSV, it was necessary, in order to capture enough ECs in one plane, to image the endothelium with Z-stacks. Using equally spaced, consecutive 'slices' through the Z-plane, Z-stacks give the user a volumetric, three-dimensional representation of the surface of the vessel and the underlying cellular architecture. The imaging method used here was optimised to have consecutive slices through Z separated by 500nm spacing between slices and an image resolution of 110nm. This allowed for the capturing of very high-resolution 3D images of the LSV endothelium which, when re-constructed as a volume, were not subject to information loss and avoided the need for computationally expensive deconvolution techniques.

With the optimised image capturing complete, it was necessary to define an analysis method which allowed for true quantification and extraction of measurable features from the 3D volumes of nuclei. To analyse specifically the nuclear compartment required the use of Imaris Bitplane software, which permits the user to analyse object specific characteristics in 3D that would not be possible with another analysis method. Using Imaris the intensity of NF-κB immunofluorescence in LSV EC nuclei only was analysed, whilst removing underlying nuclei of other cell types from the analysis. This required first, the volumetric reconstruction of Z-stacks (FIGURE 2.9.A. and B.), and segmentation of all nuclei as surface rendered 'objects' (FIGURE 2.9.C.).

The process of filtering out of nuclei underneath the endothelial surface was then performed in three independent steps. Firstly, 'seed points' were identified based on object size and 'quality', which is the intensity at the centre of the 'seed point' (grey spheres) (FIGURE 2.9.D.). For the second stage, filtering of nuclei was performed based on their shape, in particular their oblate ellipticity, whereby objects that were more elongated (i.e. a large major axis length and small minor axis), were removed from the final analysis (FIGURE 2.9.E.). Finally, the semi-automated

algorithm-based segmentation was complete and the new surface objects were created (FIGURE 2.9.F.). However, this algorithm-based segmentation was often not absolute, due to the fact that some nuclei were in very close proximity or some underlying nuclei did not satisfy the shape-based criteria mentioned above. As such, it was necessary to manually select and remove some objects from the analysis or 'cut' objects that were touching in order to split them (FIGURE 2.9.G. and H.). Following the segmentation of only EC nuclei and removal of all other nuclei (blue and red objects respectively in FIGURE 2.9.I.), quantification of intensity could be performed volumetrically within the defined EC nuclei for NF-κB (red) (FIGURE 2.9.J.).

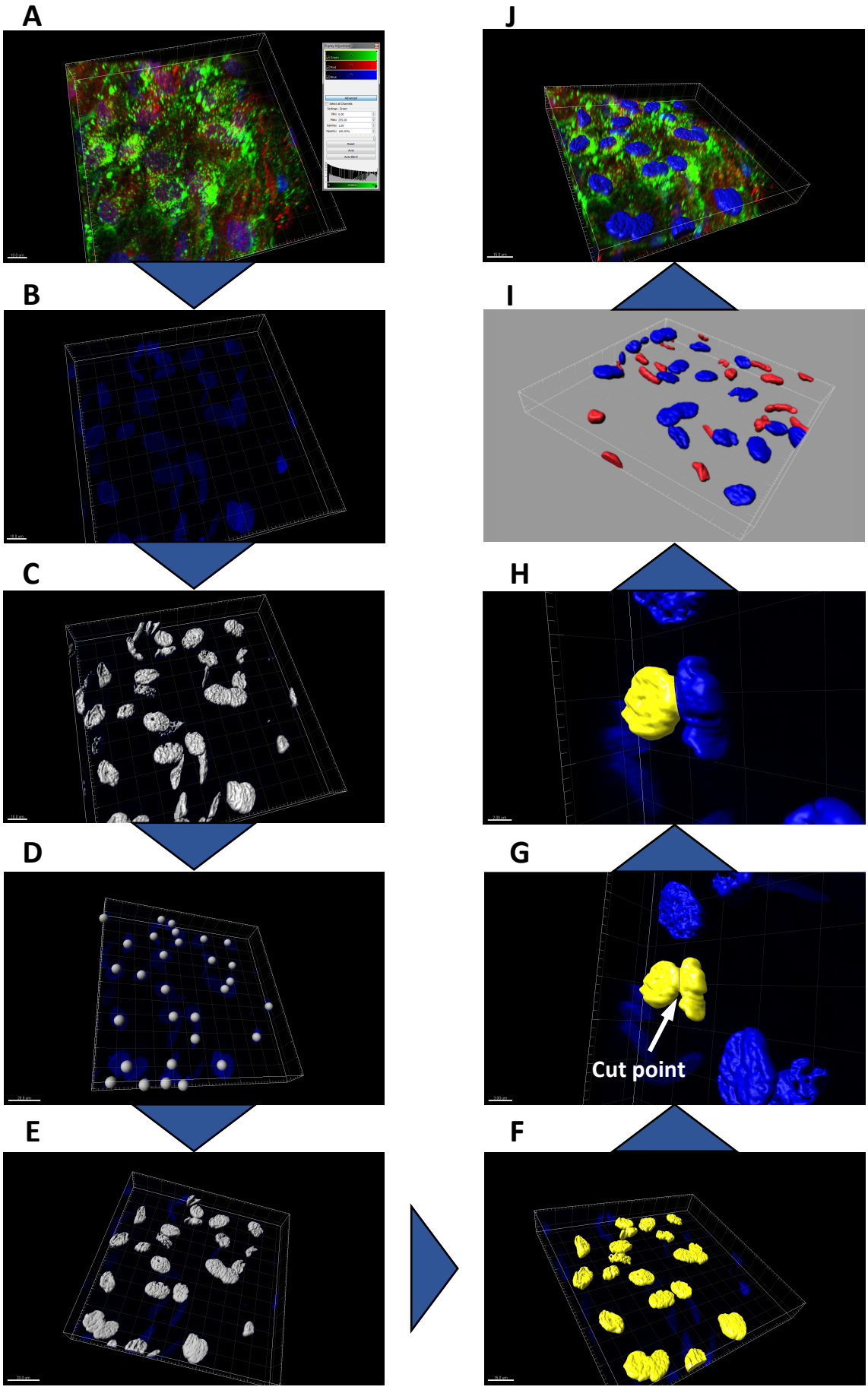
A
J
B
I
C
H
D
G
Cut point
E
F

**FIGURE 2.9. Validation of Imaris 3D endothelial cell analysis process**

Imaris utilises 3D volumetric images (Z-stacks used here) to allow segmentation and quantification of images. The process represented here demonstrates the workflow undertaken for quantitative, volumetric analysis of solely the surface cells of the LSV, whilst removing the nuclei underneath the surface cell layer, from the analysis.

A. *3D volume reconstruction* – *En face* prepared LSV, with all three channels represented in volume (Red: NF-κB; Green: vWF; Blue: TO-PRO3 (nuclear stain)).
B. 3D volume reconstruction – Nuclear stain only.
C. *Surface rendering* – Creation of surface rendered and smoothed nuclei (Grey) for segmentation.
D. *Classify Seed points and Split touching objects* – Semi-automated object detection allowing user defined inclusion or exclusion of objects based on 'Quality' or intensity of objects – each object should be individually represented by a grey sphere (set to 6μM for seed point (approx. lower boundary size of nuclei)).
E. *Classify surfaces* – Removal of nuclei based on a morphological or intensity-based characteristic, in this case, oblate ellipticity (i.e. flat and elongated compared to a spheroid).
F. *Surface selection* – Create new surface rendered selection with only objects of interest.
G. *Cut surfaces* – Manual removal or clipping of objects – line in the yellow object (two adjoined nuclei), represents user defined 'cut' line (white arrow pointing to thin black line in the centre of the adjoining nuclei) for separation.
H. *Cut surfaces* – Separated objects – now considered as two independent nuclei
I. Two distinct sets of nuclei segmented, blue representing EC nuclei, red representing other.
J. Final image to represent selected surface rendered objects on original image – Intensity and morphology statistics for all three channels to be exported from selected/segmented objects only.

### 2.9.4 VALIDATION OF MCP-1 *EN FACE* IMMUNOFLUORESCENCE

Due to the discontinuous nature of MCP-1 staining and the difficulty in defining the borders of the ECs in the LSV, *en face*, it was a challenge to find a suitable analysis method for these 3D data sets. Having tried numerous 3D analysis suites, including Imaris, CellProfiler and Volocity, ultimately, the preferred analysis method was using the '3D Object Counter' module in FIJI/ImageJ. This module works based upon the user defined intensity threshold in order to segment objects (Bolte *et al.*, 2006). The distribution of MCP-1 staining was highly localised to the perinuclear region and very intense at these points, as such, the threshold used was relatively high (50 AFI (out of 255 total)) and object volume was relatively low (1000 voxels), in order to best segment these regions only (Supplementary video 2. shows MCP-1 LSV *en face* staining with segmented objects overlaid). Only the MCP-1 channel was used for analysis. Due also to the high threshold setting, this also ensures that only the endothelial signal will be detected because, owing to the depth of the tissue, signal from underlying cells was much weaker and not significant enough to surpass the threshold, therefore the analysis was not often confounded by the analysis of non-endothelial (i.e.VSMC/fibroblast) MCP-1.

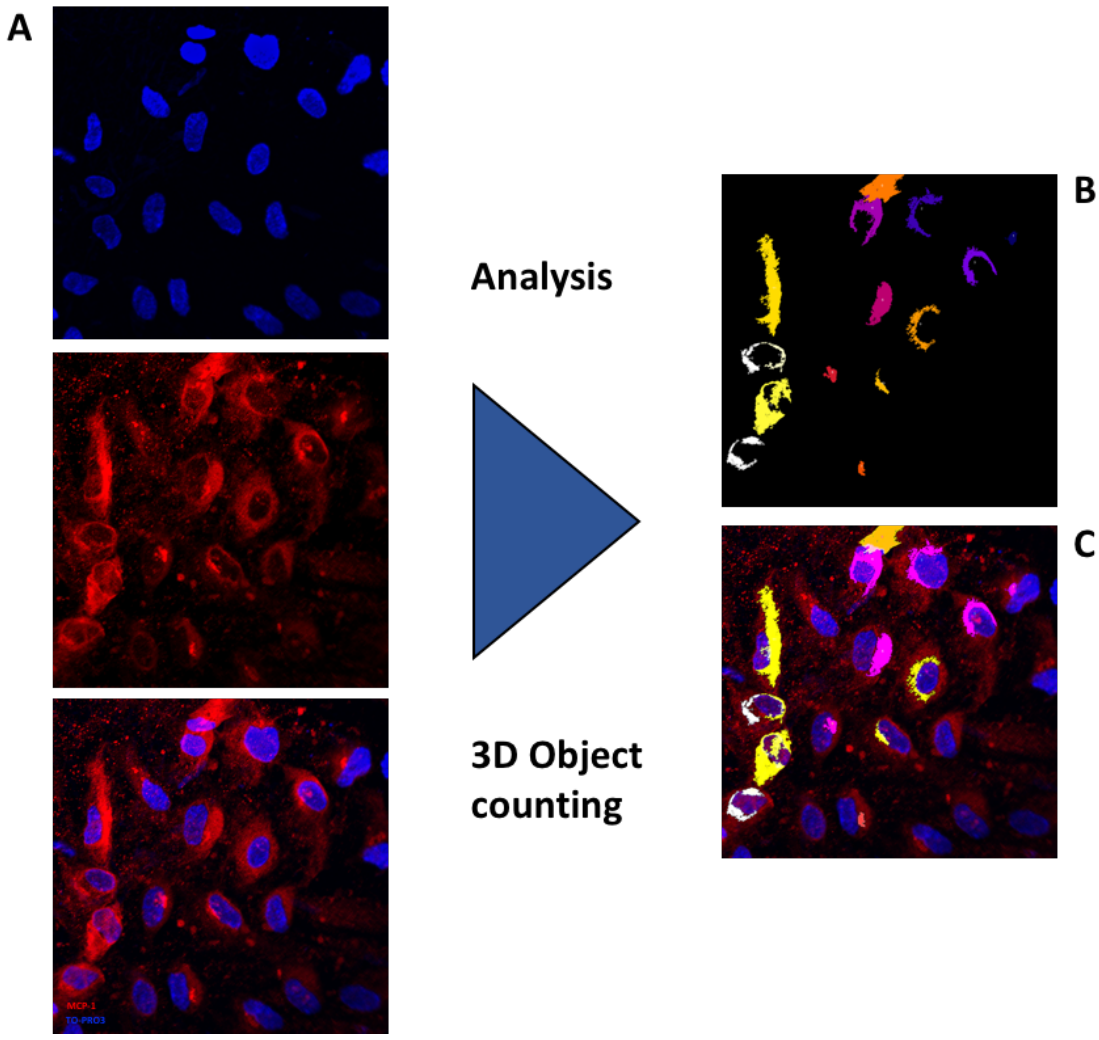


**FIGURE 2.10. FIJI-based analysis of MCP-1 en face immunofluorescence**

FIJI '3D Object counter' uses Z-stacks as its input to segment objects that cross the user-defined intensity threshold.

A. Column of images represent maximum intensity projections (MIP) from Z-stacks of MCP-1 (red) and nuclei (blue)
B. MIP of coloured 3D object map calculated by FIJI (colour coding is randomly assigned)
C. Overlay of *en face* immunofluorescence and 3D object map

## 2.10 MOLECULAR BIOLOGY

### 2.10.1 RNA EXTRACTION

Total RNA extraction and purification was performed using the miRNeasy Mini kit (Qiagen; catalogue number: 217004). Cultured cells were washed twice in ice-cold DPBS and lysed in 350 or 700µL Qiazol lysis reagent for approximately 30 seconds and then wells or slides were scraped using the rubber insert of a 1mL syringe. Lysates were kept on ice or stored at -80°C until purification.

### 2.10.2 RNA PURIFICATION AND QUANTIFICATION

RNA was purified following the manufacturer's instructions. Briefly, samples were mixed with chloroform at a ratio of 1:0.2 (sample:chloroform) and centrifuged at 4°C for 15 minutes at 12,000g. Once separated, the upper layer of chloroform from each sample was carefully removed and mixed with 1.5 volumes of absolute (100%) ethanol and the remaining phenol discarded. Samples were then transferred to purification columns and centrifuged at 12,000g; after three washes with wash buffer RNA samples were collected in 30µl RNAse free water and stored at -80°C until required.

Total RNA was quantified using the QIAxpert spectrophotometer system (Qiagen; catalogue number: 9002340). The RNA concentration (ng/mL) was obtained by measuring absorbance at 260nm. RNA contamination with ethanol or phenol was determined by measuring the ratio of absorbance at 260/230, with a ratio of ≤1.8 suggesting high levels of contamination. Contamination with nucleic acid was determined by the ratio of absorbance at 260/280, with a ratio <2.0 indicating high nucleic acid levels. If significant contamination was detected, samples were discarded.

### 2.10.3 QUANTITATIVE RT-PCR (RT-qPCR)

Reverse transcription was on 80-500ng/mL purified RNA performed using the transcriptor first strand cDNA synthesis kit (Roche; catalogue number: 04896866001). Firstly, RNA secondary structures were removed. To do so, RNA levels were normalised to the same concentration with variable volumes of RNAse free water and RNA, and subsequently incubated with 2µL random hexamer primers for 10 minutes at 65°C using a thermal block cycler (Bio-Rad; model number: C1000). Secondly, according to manufacturer's instructions, 4µL of reaction buffer, 0.5µL protector RNase inhibitor, 2µL deoxynucleotide mix and 0.5µL reverse transcriptase enzyme were added to each RT reaction to give final concentrations of: 1x, 20U, 1mM and 10U, respectively. Reactions were then incubated for 10 minutes at 25°C, 30 minutes at 55°C and 5 minutes at 85°C. A total of 20µL cDNA was synthesised and cDNA samples were stored at -20°C until analysis. Quantitative PCR analysis was performed using the LightCycler 480 real-time PCR instrument (Roche) and LightCycler 480 SYBR Green I Master (Roche; catalogue number: 04707516001). Each 10µL reaction, in white 96-well plates (Greiner Bio-one; catalogue number: 669 285), consisted of: 5µL SYBR Green, 3µL PCR grade water, 1µL primer sets (0.5 µL of both forward and reverse primers) and 1µL cDNA, water (as internal PCR control) or blank RT reaction sample (RT control). Plates were sealed (Greiner Bio-one; catalogue number: 676040) and centrifuged for 15 seconds at 250g (Labnet; Mini PCR plate spinner; catalogue number: C1000). The PCR program conditions (TABLE 2.7.) were as follows:

| STEP | SUB-STEP | TEMPERATURE/°C | TIME |
|---|---|---|---|
| **Pre-Incubation** | - | 95 | 5 min |
| **Amplification (45 cycles)** | Denaturing | 95 | 10 sec |
| | Annealing | 60 | 10 sec |
| | Elongation | 72 | 10 sec |
| **Melting** | - | 95 | 5 sec |
| | | 65 | 1 min |
| | | 97 | Continuous |
| **Cooling** | - | 40 | -1.5°C/sec |

**TABLE 2.7. RT-qPCR program conditions**

PCR reactions were run in triplicate to allow for variation within wells and the average $C_T$ (Cycles of Threshold) values were used for calculating fold changes in expression. This value corresponds to the number of cycles whereby the amplified cDNA template reaches a detection threshold and is therefore only a relative measure of amplicon concentration. $C_T$ values within sample triplicates never differed by more than 1 cycle. The following equation was used to determine the relative expression difference between experimental and control conditions (or fold change):

$$Fold\ change = 2^{-\Delta C_T}$$

*where* $\Delta C_T = C_{T\ experimental} - C_{T\ control}$

To determine non-specific product contamination, melting curves were analysed. All primers used gave single melting curves indicating that only one PCR product was being amplified.

### 2.10.4 PRIMER DESIGN AND SEQUENCES

Design of primers for qPCR analysis was done using Primer-BLAST software. Filters for design included:

- specificity for solely the target gene and its transcript variants
- a product size of between 95 and 200 base pairs
- an optimal melting temperature of 65°C
- an optimal primer size of between 22 and 26 base pairs
- a primer GC content of 40-65%
- a requirement for the spanning of exon-exon junctions or separation of the primer pair by at least one intron on the corresponding genomic DNA
- lack of secondary structures
- lack of primer dimers

| GENE NAME | FORWARD SEQUENCE *(5'->3')* | REVERSE SEQUENCE *(5'->3')* |
|---|---|---|
| β-Tubulin (TUBB1) | GCTGGACCGCATCTCTGTGTACT | TTACCTGCCCCAGACTGACCAAAT |
| Monocyte chemoattractant protein 1 (CCL2/MCP-1) | CTCAGCCAGATGCAATCAATGCCC | TTCTTTGGGACACTTGCTGCTGGT |
| Interleukin 6 (IL-6) | AAATTCGGTACATCCTCGACGGCA | TTTTCACCAGGCAAGTCTCCTCAT |
| Interleukin 8 (IL-8) | TGTGAAGGTGCAGTTTTGCCAAGG | AATTTCTGTGTTGGCGCAGTGTGG |
| Intercellular adhesion molecule 1 (ICAM-1) | GCAGACAGTGACCATCTACAGCTT | GCCTCACACTTCACTGTCACCTC |
| E-Selectin (SELE) | TCAGCTCTCACTTTGGTGCTTCTCA | TGCTGACAATAAGCACTGGCCTCA |
| Vascular cell adhesion molecule 1 (VCAM-1) | GGCCCAGTTGAAGGATGCGGG | AGAGCACGAGAAGCTCAGGAGAA |
| Haem Oxygenase 1 (HMOX1/HO-1) | GAGACGGCTTCAAGCTGGTGATGG | TTCTGGGAAGTAGACAGGGGCGAA |
| NADPH quinone dehydrogenase 1(NQO-1) | GTGGTTTGGAGTCCCTGCCATTCT | ACTGCCTTCTTACTCCGGAAGGGT |
| Glutamate cysteine ligase, modifier subunit (GCLM) | TCAACCCAGATTTGGTCAGGGAGT | CAGCTGTGCAACTCCAAGGACTGA |

**TABLE 2.8. List of primer sequences**

## 2.11 WESTERN BLOTTING

### 2.11.1 SDS PROTEIN EXTRACTION

Cells were washed twice with ice-cold DPBS and lysed using 1% Sodium Dodecyl Sulphate (SDS) lysis buffer (50mM Tris-HCl (pH 6.8), 10% (v/v) glycerol and 1% (w/v) SDS). Tissue culture wells or glass slides were rubbed with the insert of a 1mL syringe and samples were used immediately or stored at -80°C.

### 2.11.2 NUCLEAR AND CYTOSOLIC PROTEIN FRACTIONATION

Cells were washed twice with ice-cold DPBS and lysed using the NE-PER Nuclear and Cytoplasmic extraction reagents (Thermo-Fisher Scientific; catalogue number: 78835), volumes used were as per manufacturer's instructions. Briefly, cells were lysed directly with buffer CER-I and rubbed with the insert of a 1 mL syringe. Samples were vortexed and stored on ice for 10 minutes, after which time buffer CER-II was added, tubes were vortexed and kept on ice for a further 1 minute and vortexed again. Following addition of both cytoplasmic buffers, samples were centrifuged at 14,000g for 10 minutes, the supernatant was transferred to a clean tube and stored at -80°C until analysis. The pellet was resuspended in ice-cold NER and vortexed for 15 seconds and placed on ice for 10 minutes; these steps were repeated 4 times until the nuclear pellet was largely dispersed. Samples were centrifuged a final time for 10 minutes at 14,000g; the supernatant was collected in a clean tube and stored at -80°C until analysis.

### 2.11.3 PROTEIN ASSAY

The concentration of protein in samples was determined using the Micro Bicinchoninic Acid (BCA) assay kit (Thermo-Fisher scientific; catalogue number: 23235). To clear bottom 96-well plates, 2.5µL of protein lysate was added to 145µL of HPLC grade water. Bovine serum albumin (BSA) at concentrations of 0, 0.1, 0.25, 0.5, 1.0, 2.5, 5.0 and 10µg/mL were used for production of a standard curve. All samples and standard measurements were conducted in duplicate.

Following addition of protein lysate or BSA, 150µL of Micro BCA reagents were added (combined solution of reagents A:B:C in a ratio of 25:24:1) and the plate was incubated at 37°C for 1 hour; after which time plates were read at 560nm using an ELISA plate reader (LabTech; catalogue number: LT-5000MS) and the protein concentrations of samples were calculated from the linear range of the standard curve.

### 2.11.4 POLYACRYLAMIDE GEL ELECTROPHORESIS (PAGE)

All PAGE analyses were performed using the Biorad Mini format 1-D electrophoresis system (Biorad; catalogue number: 1658004). Using the sample concentrations calculated in 2.11.3, 5-20µL of the protein lysates were diluted using HPLC grade water to standardise the sample volume and protein concentration to ensure equal loading. Laemmli sample buffer (Biorad; catalogue number: 161-0737) supplemented with 5% (v/v) β-mercaptoethanol was added to samples (at a ratio of 1:1) prior to heating at 95°C for 5 minutes. For approximation of protein size, 10µL of BLUeye pre-stained protein ladder (Geneflow; catalogue number: S6-0024) supplemented supplemented with 2.5% (v/v) β-mercaptoethanol was also heated at 95°C for 5 minutes and loaded with protein samples. Samples were loaded onto 4-15% Mini-PROTEAN TGX stain-free gels (Biorad; catalogue number: 456-1084) and subjected to electrophoresis at 300V for 15-25 minutes in 1×Tris/Glycine/SDS (TGS) running buffer (Biorad; catalogue number: 161-0772). Following electrophoresis, the precast gel packs were opened using a gel opening lever; gels were wetted with running buffer, removed carefully and placed on the UV transilluminator tray of the ChemiDoc XRS+ imaging system (Biorad; catalogue number: 1708265). Using ImageLab software, stain-free gels were activated and imaged to be used as a loading control for densitometry.

### 2.11.5 PROTEIN TRANSFER AND PROTEIN DETECTION

Following gel imaging, gels were transferred to a Trans-Blot turbo nitrocellulose transfer pack (Biorad; catalogue numbers: 170-4158, 170-4159) and, using the Trans-Blot turbo transfer

system, electrophoretic protein transfer was performed as per the manufacturer's instructions. Non-specific binding was blocked by placing 0.2µM Nitrocellulose membranes in 5% (w/v) fat-free milk powder in PBS with Tween (PBS-T; 137mM NaCl, 0.1% (v/v) Tween 20; pH 7.6) for 30 minutes. Following blocking, membranes were incubated and rocked with primary antibodies (see TABLE 2.1.) diluted in 5% milk/PBS-T for 1 hour at room temperature or overnight (16-18 hours) at 4°C. Blots were then washed three times for 5, 10 and 30 minutes in PBS-T then incubated and rocked in HRP-conjugated secondary antibody (see TABLE 2.2.) in 5% milk/PBS-T for 1 hour at room temperature. Membranes were washed a further three times as above and then incubated with 3mL of Luminata Forte Western HRP substrate (Merck Milipore; catalogue number: WBLUF0500) for 3 minutes. Finally, membranes were imaged using the ChemiDoc XRS+ imaging system according to the manufacturer's instructions. Western blots were exposed using this system for between 2-90 seconds, most commonly, experiments were run in triplicate and all WBs were exposed at the same time to avoid any bias in densitometric analysis.

### 2.11.6 DENSITOMETRY

The protein band density was determined using ImageLab software and the ChemiDoc XRS+ system and results were expressed as the adjusted sum of pixel intensities following global (whole gel) background subtraction. The density of protein bands detected was normalised using the Stain-Free loading control for each sample.

## 2.12 NF-κB ACTIVITY ASSAY

Cells were lysed as in 2.11.1 for whole cell lysates. To detect active NF-κB (p65) protein, the TransAM p65 DNA-binding ELISA kit (Active Motif; catalogue number: 40096) for 96 strip-well reactions was used. All incubations were performed at RT. Briefly, cell extracts were incubated and gently rotated in wells for 1 hour, extracts were removed, and a primary antibody to NF-κB (provided in kit) was added to wells at a dilution of 1:1000 for 1 hour. The primary antibody was

washed and replaced with a HRP conjugated secondary antibody for 1 hour. Wells were washed, and the developing solution was added for approximately 5 minutes, or until wells turned a blue colour. Finally, a stop solution was added, wells were covered and, for quantitative analysis of NF-κB activity, the final absorbance was read at 450nm. Absorbance was expressed as arbitrary units and calculated relative to static control samples, normality range was verified by standard curve.

### 2.13 STATISTICAL ANALYSIS

For experiments where only two groups were analysed, data were subjected to a paired, two-tailed t-test. For experiments where more than two groups were analysed, a one- or two-way ANOVA was used depending on the number of independent variables, followed by post-hoc pairwise comparisons with Bonferroni correction for multiple comparisons. If data-sets were large enough (for example for immocytochemical analyses, where 20 images were per sample were analysed), normal distribution was assessed with the D'Agostino-Pearson test; all data assessed passed normality tests. Sample number (*n)* when referring to *in vitro* use of HUVECs refers to pooled vials of HUVECs, each with a different lot number (i.e. pooled from new/different donors). Sample number (*n*) when referring to *ex vivo* use of LSV refers to tissue resected from different patients, each with a unique ethics number. The cut-off value for statistical significance was 0.05. Data are presented as means±SEM. All statistical analysis was performed with GraphPad Prism 7.0.

# 3. NF-κB ACTIVATION IN VENOUS ENDOTHELIUM IN RESPONSE TO ACUTE HIGH SHEAR STRESS

## 3.1 INTRODUCTION

Veins grafted into the arterial circulation are known to undergo pro-inflammatory activation, characterised by increased expression of chemokines and adhesion molecules, though the exact underlying mechanisms for this activation are still not fully understood (Ascione *et al.*, 2000; Zou *et al.*, 2000; Christiansen *et al.*, 2004; Kwei *et al.*, 2004). Endothelial expression of adhesion molecules, ICAM-1, VCAM-1 and E- and P-Selectins, in the vein graft, allows circulating leukocytes to adhere to and infiltrate the vascular wall soon after implantation (Hoch *et al.*, 1994; Golledge, 1997; Hoch *et al.*, 1999; Kwei *et al.*, 2004). It is also recognised that the triggering of the adhesion cascade, and subsequent leukocyte extravasation, contributes further to the pro-proliferative response of medial VSMCs through the direct secretion of growth factors and the action of inflammatory cytokines and growth factors on MMP induction (Newby *et al.*, 2000; Newby, 2005; Newby, 2008; Wan *et al.*, 2012).

Over thirty years ago, Pearce *et a*l. recognised the importance of the acute phase, immediately after implantation, on the inflammatory insult experienced by the vein graft endothelium in a canine interposition bypass model (Pearce *et al.*, 1985). They observed a significant neutrophilic response accompanied by a degree of endothelial loss within 6 hours after implantation of the vessel, which was reduced with anti-inflammatory pre- and post-treatments. Very few subsequent studies, however, have evaluated acute inflammatory changes in vein grafts, with many focussing on the inflammatory processes occurring less acutely, after 24 hours post-implantation (Golledge *et al.*, 2000; Kwei *et al.*, 2004; Nguyen *et al.*, 2016).

The transcription factor, NF-κB has been implicated in a great number of cardiovascular pathologies, including atherosclerosis, heart failure, ischaemia/reperfusion injury and cardiac hypertrophy (Van Der Heiden *et al*., 2010). Due to its myriad roles in cellular behaviour, NF-κB activity in such disease models can be either protective or pathogenic; or, in the case of atherogenesis, both, depending upon the cell-type (Hayden *et al.*, 2008; Lawrence, 2009; Van

der Heiden *et al*., 2010). NF-κB has been proposed to be involved in the systemic inflammatory response which occurs during cardiopulmonary bypass and CABG surgery, owing to the systemic production of cytokines and inflammatory mediators, including IL-1, IL-6, IL-8 and TNF-α, all of which are target genes of the classical NF-κB, p50/p65, transcription factor (Wan *et al.*, 1997; Ascione *et al.*, 2000; Zhang *et al.*, 2004; Hinokiyama *et al.*, 2006; Miyake *et al.*, 2006; Suleiman *et al.*, 2008; Miyake *et al.*, 2014). In addition, to its role in co-ordinating acute and chronic inflammation in numerous cell types in the vasculature, NF-κB is also known to be mechanoresponsive (Lan *et al.*, 1994; Bhullar *et al.*, 1998; Lehoux *et al.*, 2006). Consequently, it was hypothesised that acute high shear stress induces a pro-inflammatory response in vECs *in vitro* and in LSV ECs *ex vivo*, which is driven by NF-κB classical pathway activation and, when this pathway is blocked, inflammation in response to acute high shear stress can be prevented.

## 3.2 RESULTS

### 3.2.1 ENDOTHELIAL CELL PRO-INFLAMMATORY RESPONSE TO ACUTE SHEAR STRESS *IN VITRO*

#### 3.2.1.1 AHSS ACTIVATED A PRO-INFLAMMATORY GENE PROFILE IN HUVECS

To initially validate the model of pro-inflammatory acute shear stress, *in vitro*, fully confluent monolayers of HUVECs were exposed to AHSS at 12dyn/cm$^2$ for 90 and 120 minutes. Relative mRNA transcript levels of four pro-inflammatory genes, MCP-1, IL-6, IL-8 and ICAM-1, were quantified in HUVECs exposed to AHSS and compared to the mRNA levels present in HUVECs maintained in static culture, using RT-qPCR. Significant increases of between 3- to 7-fold in relative levels of all four pro-inflammatory gene mRNA transcript levels were observed, at both time-points as a result of AHSS, compared to static controls (FIGURE 3.1.).

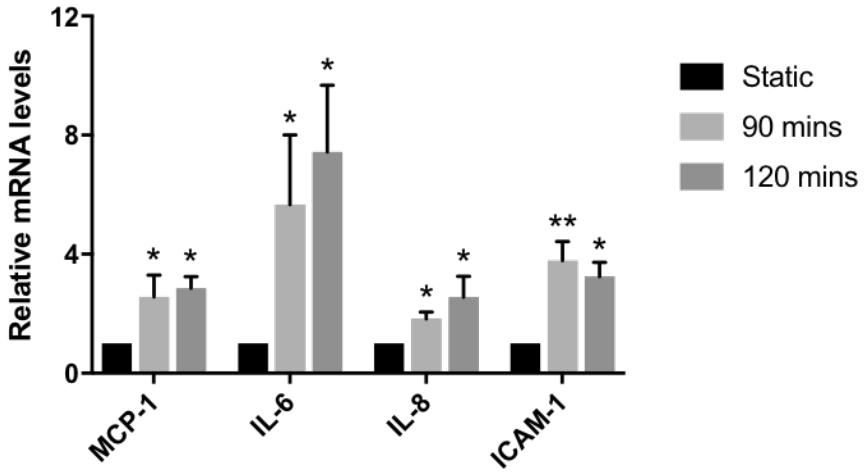


**FIGURE 3.1. AHSS induced pro-inflammatory mRNA transcript profiles in HUVECs**

MCP-1, IL-6, IL-8 and ICAM-1 mRNA levels quantified by RT-qPCR from HUVECs exposed to 90 and 120 minutes of AHSS (12dyn/cm$^2$). mRNA levels were normalised to β-tubulin and expressed as a fold-change relative to static control. * indicates $p<0.05$, ** indicates $p<0.01$ vs. static control, One-way ANOVA followed by post-hoc pairwise comparisons with Bonferroni correction for multiple comparisons, n=6.

#### 3.2.1.2 LOW SHEAR STRESS DID NOT INDUCE A PRO-INFLAMMATORY GENE PROFILE

To further validate the pro-inflammatory effect of AHSS, fully confluent monolayers of HUVECs were exposed to acute low shear stress (ALSS) at 0.5dyn/cm$^2$ for 90 and 120 minutes. Relative mRNA transcript levels of four pro-inflammatory genes, MCP-1, IL-6, IL-8 and ICAM-1, in HUVECs exposed to ALSS were then compared to the levels present in HUVECs maintained in static culture, by RT-qPCR. No significant increase in relative levels of all four pro-inflammatory gene mRNA transcript was observed, at either time-point, under ALSS, compared to static controls (FIGURE 3.2.).

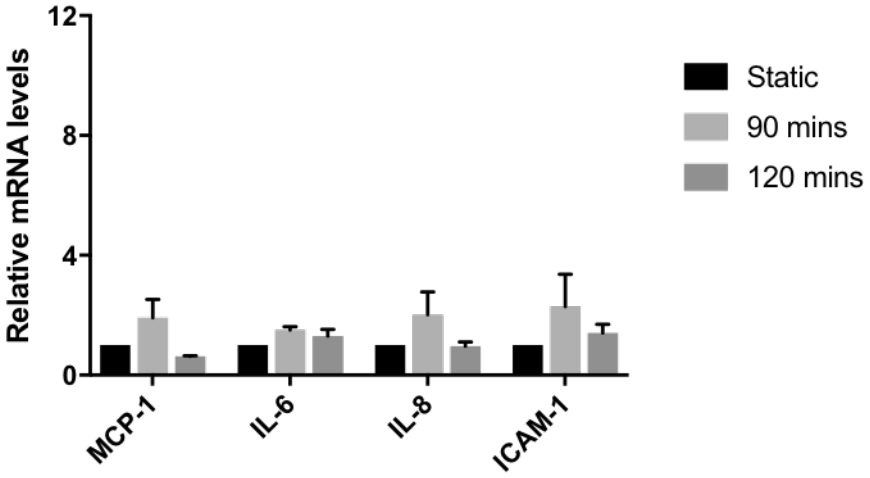


**FIGURE 3.2. ALSS did not induce pro-inflammatory mRNA profiles in HUVECs**

MCP-1, IL-6, IL-8 and ICAM-1 mRNA levels quantified by RT-qPCR in HUVECs exposed to 90 and 120 minutes of ALSS (0.5 dyn/cm$^2$). mRNA levels were normalised to β-tubulin and expressed as a fold-change relative to static control. One-way ANOVA followed by post-hoc pairwise comparisons with Bonferroni correction for multiple comparisons, n=6.

#### 3.2.1.3 AHSS INCREASED MCP-1 PROTEIN LEVELS

Having established that AHSS, not ALSS, resulted in increased MCP-1, IL-6, IL-8 and ICAM-1 mRNA levels, it was necessary to evaluate whether protein levels were also increased under AHSS exposure, at slightly later time-points than mRNA analysis to allow for protein translation. MCP-1 was chosen as a representative pro-inflammatory protein as its involvement in VGF, via monocyte recruitment to the endothelium and direct mitogenic effects on VSMCs, has been well-established (Stark *et al.*, 1997; Schepers *et al.*, 2006; Fu *et al.*, 2012). As such, immunocytochemical analysis for MCP-1 was performed to determine whether the increased pro-inflammatory mRNA expression, in HUVECs exposed to AHSS, resulted in augmented protein production. HUVECs were exposed to AHSS at 12dyn/cm$^2$ for 4 and 6 hours, then fixed and analysed by immunofluorescence. Mean arbitrary fluorescence intensity (AFI) of MCP-1 staining (red) was quantified in the whole cell using CellProfiler (FIGURE 3.3.A.) (sections 2.9.2. and 2.9.3.). VE-Cadherin staining (green) was utilised as evidence of a confluent endothelial monolayer and therefore quantification was not required.

Analysis revealed that basal levels of MCP-1 protein, in static control cells, were relatively low and expression was ubiquitously present throughout cells, though, most prominently at a distinct perinuclear site. However, following exposure to AHSS for 4 hours a significant increase in MCP-1 protein level was observed, compared to static controls (FIGURE 3.3.A. and B.). By 6 hours, MCP-1 levels had returned to basal levels of static controls.

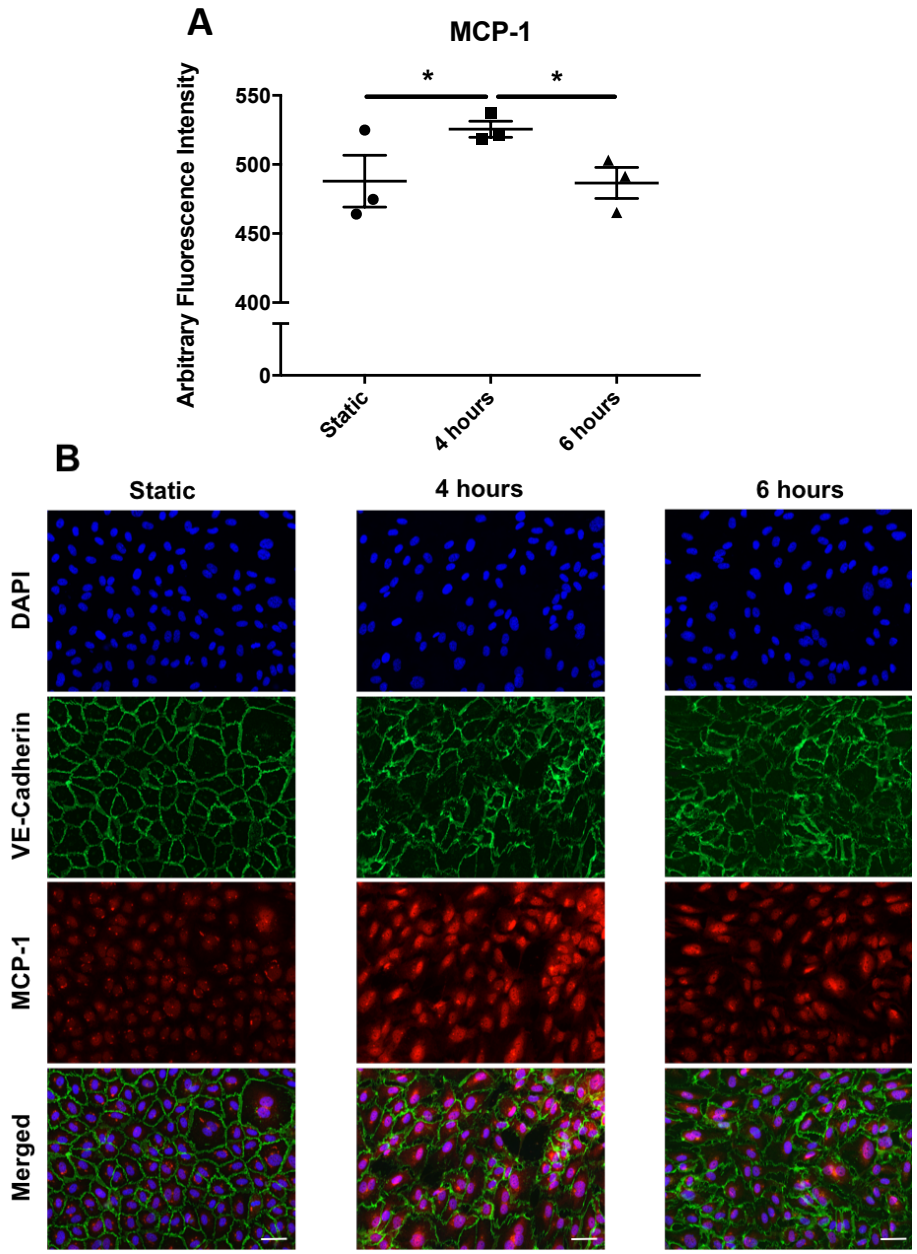


**FIGURE 3.3. MCP-1 levels were increased in response to AHSS**

MCP-1 protein quantified by immunofluorescence in HUVECs exposed to AHSS for 4 and 6 hours, compared with static controls.

A. Whole cell arbitrary fluorescence intensity (AFI) of MCP-1 staining by ICC and quantified by CellProfiler2.0. * indicates $p<0.05$, One-way ANOVA followed by post-hoc pairwise comparisons with Bonferroni correction for multiple comparisons, n=3.

B. Representative images of MCP-1 protein detected by immunofluorescence, co-stained for VE-Cadherin (green), MCP-1 (red) and nuclei/DAPI (blue). Scale bars represent 15μm and apply to all images.

### 3.2.2 PRO-INFLAMMATORY RESPONSE OF EX VIVO LSV ECs TO ACUTE SHEAR STRESS

#### 3.2.2.1 AHSS ACTIVATED MCP-1 IN HUMAN LSV ECs

Once the pro-inflammatory response to AHSS was established in ECs *in vitro*, it was necessary to determine whether this response was corroborated in human LSV, *ex vivo*. LSV sections resected from patients during CABG surgery were exposed to AHSS (as described in the methods (section 2.7.)) using a flow apparatus or maintained in static conditions. Pro-inflammatory mRNA transcript levels were analysed by RT-qPCR. As with *in vitro* mRNA analysis of pro-inflammatory response, the four genes analysed were MCP-1, IL-6, IL-8 and ICAM-1. A significant increase in relative MCP-1 mRNA transcript levels was observed following exposure to AHSS for 120 minutes, but not at 90 minutes (FIGURE 3.4.A.). No significant difference in the relative levels of IL-6, IL-8 and ICAM-1 were detected after 120 minutes AHSS exposure (FIGURE 3.4.B., C. and D., respectively).

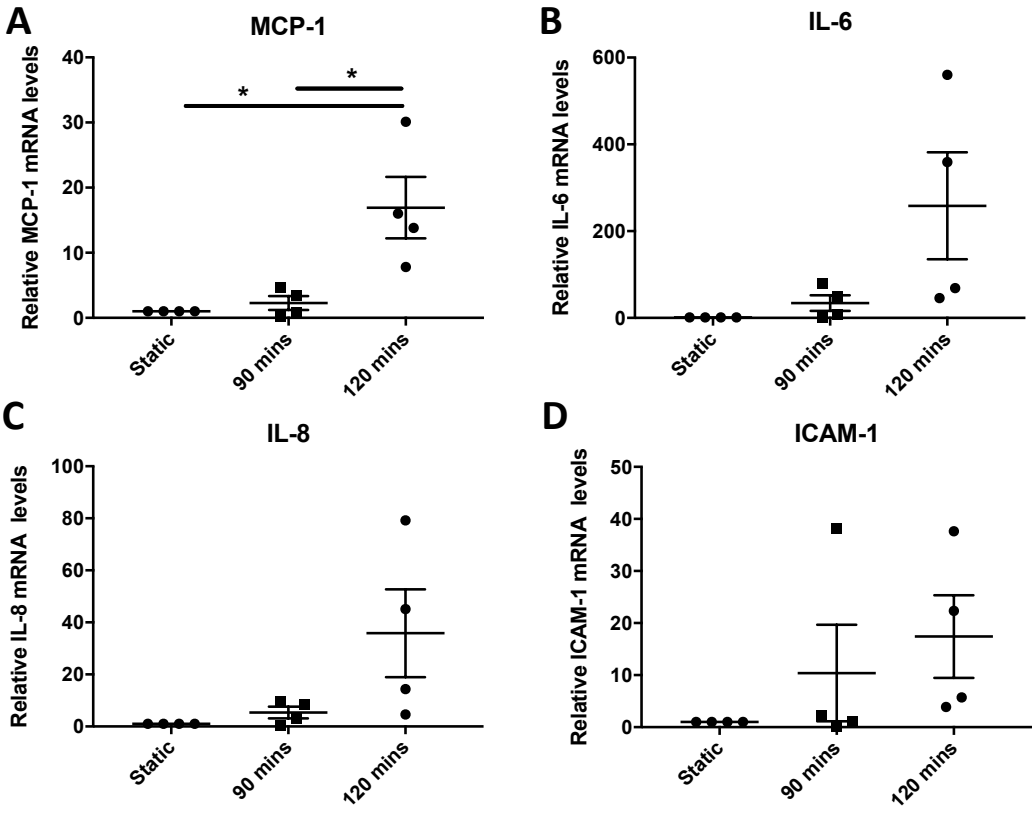


**FIGURE 3.4. MCP-1 transcript levels were increased in LSV ECs within vein segments under AHSS, ex vivo**

Quantification of MCP-1, IL-6, IL-8 and ICAM-1 mRNA levels (A, B, C and D, respectively) in LSV ECs exposed to AHSS for 90 and 120 minutes, by RT-qPCR. mRNA levels were normalised to β-tubulin and expressed as a fold-change relative to static control. * indicates $p<0.05$, One-way ANOVA followed by post-hoc pairwise comparisons with Bonferroni correction for multiple comparisons, n=4.

#### 3.2.2.2 AHSS INCREASED LEVELS OF MCP-1 PROTEIN IN THE LSV ENDOTHELIUM

Having observed a significant increase in MCP-1 mRNA transcript levels in LSV ECs following 120 minutes exposure to AHSS and increases in protein levels of MCP-1 *in vitro* in responses to AHSS, levels of MCP-1 protein were evaluated using *en face* staining of the LSV endothelium (described in detail in 2.7.2. and 2.9.). Segments of fresh LSV were exposed to AHSS for 6 hours or maintained in static conditions. LSV segments were subjected to *en face* immunofluorescence analysis for MCP-1. Mean AFI of MCP-1 staining (red) was quantified in 3D using FIJI, which evaluated the highly localised MCP-1 staining found in the perinuclear regions of LSV ECs (Supplementary videos 1 and 2 show images in Z-stack and images with segmented objects, respectively). Whole cell MCP-1 immunofluorescence was not analysed, as in 3.2.1.3., owing to the discontinuous nature of the staining in *en face* prepared LSV. vWF co-staining (green) was used as an EC marker to identify the surface layer of cells as ECs.

At baseline (static), MCP-1 levels in LSV ECs were very low and very few cells showed detectable levels of MCP-1 protein (FIGURE 3.5.A.). In contrast, intense perinuclear MCP-1 protein staining was observed almost ubiquitously after 6 hours of AHSS exposure (indicated by white arrows in FIGURE 3.5.B.). In agreement with data from ICC and RT-qPCR (sections 3.2.1.3. and 3.2.2.1., respectively), *en face* immunoanalysis revealed that MCP-1 was significantly increased following 6 hours AHSS exposure in the LSV endothelium, compared with static control samples (FIGURE 3.5.A. and B.)

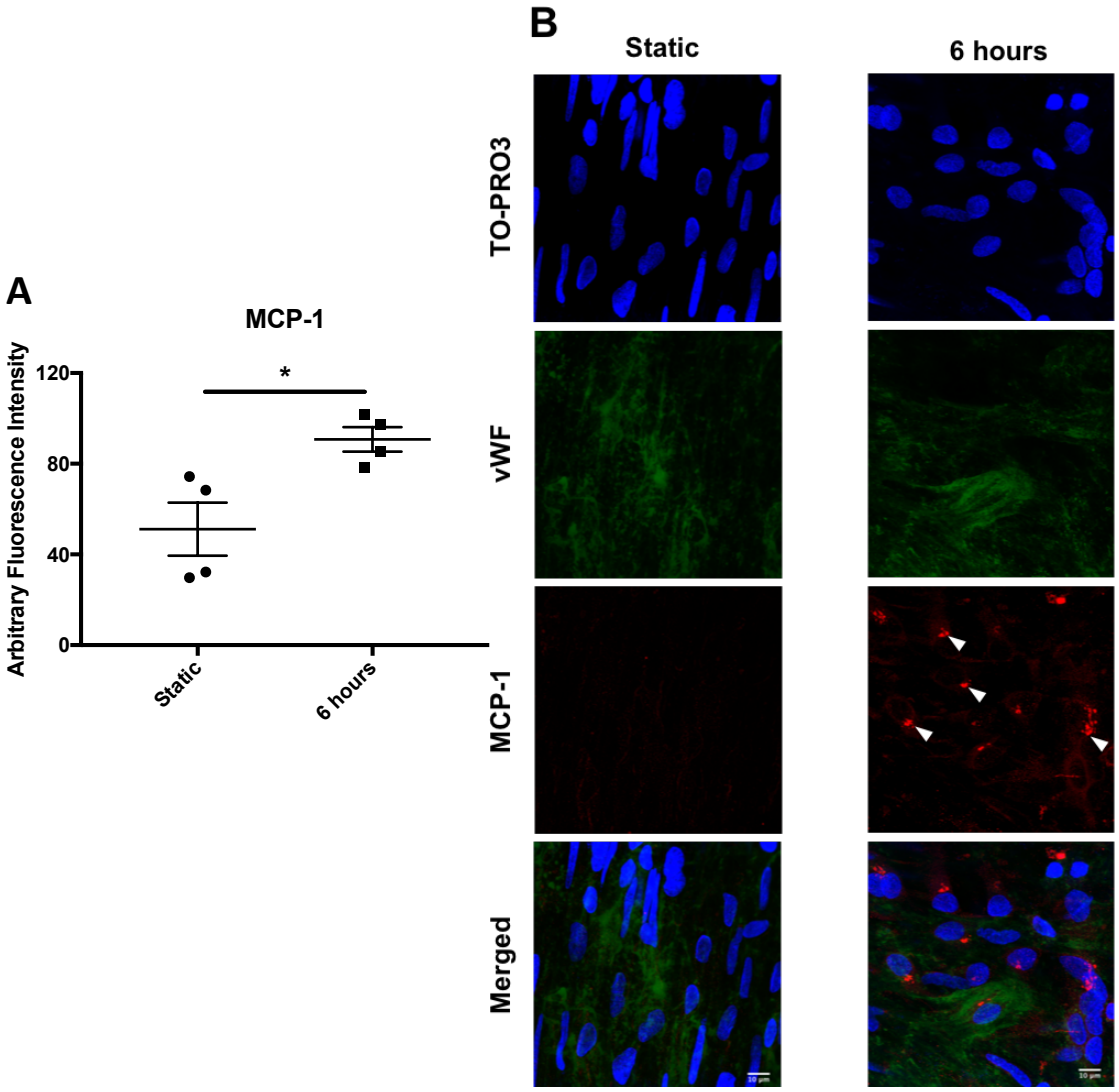


**FIGURE 3.5. AHSS exposure increased levels of MCP-1 in the LSV endothelium**

Total MCP-1 levels were quantified as mean arbitrary fluorescence intensity in the LSV endothelium following exposure to AHSS for 6 hours or maintenance in static conditions.

A. Mean arbitrary fluorescence intensity of immunofluorescence for MCP-1 in *en face* prepared LSV endothelium, as calculated using FIJI/ImageJ. * indicates $p<0.05$; two-tailed, two sample t-test, n=4.

B. Representative maximum intensity projection (MIP) images of immunofluorescence for MCP-1 protein *en face*, co-stained for MCP-1 (red), vWF (green) and TO-PRO3/nuclei (blue). White arrows on MCP-1 panel indicate perinuclear MCP-1 protein within LSV ECs. Scale bars represent 10μm and apply to all images.

### 3.2.3 NF-κB RESPONSE TO AHSS - *IN VITRO*

#### 3.2.3.1 AHSS ACTIVATED THE NF-κB CLASSICAL PATHWAY

Having shown that vECs responded to AHSS with up-regulation of numerous pro-inflammatory markers, at the mRNA and protein level, both *in vitro* and *ex vivo*, the underlying mechanism of up-regulation was investigated. The four genes previously shown to be upregulated by AHSS are target genes of the transcription factor, NF-κB (p65), as such, it was selected as a potential driver of this response. In addition to this, NF-κB has a known role in inflammation regulation and as a mechano-stimulated transcription factor (Pahl, 1999; Lehoux *et al*., 2006).

HUVECs were exposed to AHSS at 12dyn/cm$^2$ for 30 and 90 minutes or maintained in static conditions. Cells were lysed into distinct cellular compartments, giving cytosolic and nuclear fractions. Analysis of these fractions by Western blotting revealed a significant, 3-fold increase in nuclear NF-κB levels comparative to static controls, following exposure to AHSS for both 30 and 90 minutes (FIGURE 3.6.A. and C.). This was associated with a significant reduction in levels of cytosolic IκBα at both time-points, relative to static controls (FIGURE 3.6B. and C.). There were no significant changes in levels of cytosolic NF-κB, as seen in the representative blots (data not shown for nuclear IκBα due to extremely low detection levels) (FIGURE 3.6.C.).

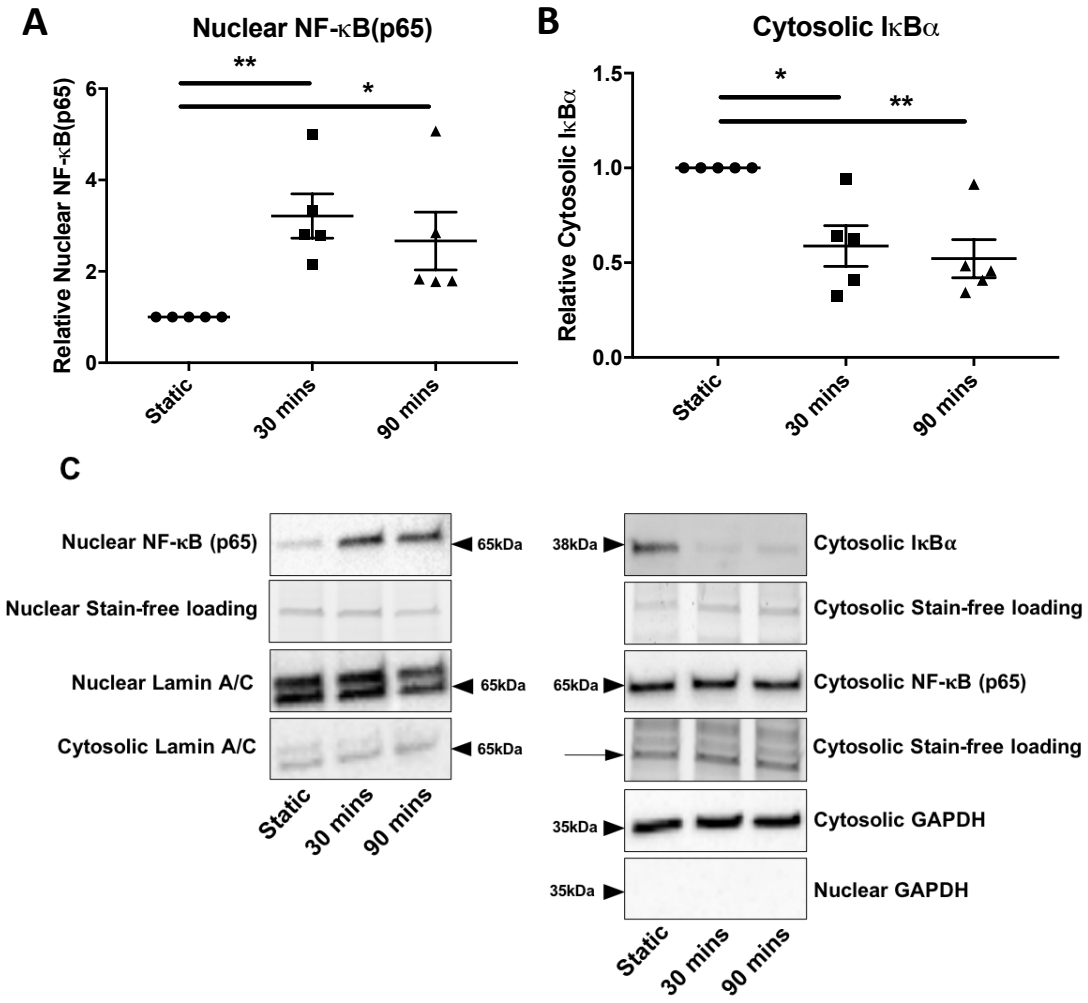


**FIGURE 3.6. AHSS activated NF-κB classical pathway**

Relative levels of nuclear NF-κB and cytosolic IκBα were quantified in fractionated cell lysates by Western blotting. Approximate molecular weights, in kDa, are indicated centrally, next to representative blots. * indicates $p<0.05$, ** indicates $p<0.01$, One-way ANOVA followed by post-hoc pairwise comparisons with Bonferroni correction for multiple comparisons, n=5.

A. Relative nuclear NF-κB protein level, normalised to stain free loading controls and expressed as a fold change relative to static.
B. Relative cytosolic IκBα protein level, normalised to stain free loading controls and expressed as a fold change relative to static.
C. Representative blots with complementary loading controls. Anti-clockwise from top left: nuclear NF-κB and loading control; nuclear and cytosolic LaminA/C; nuclear and cytosolic GAPDH; cytosolic NF-κB and loading control; cytosolic IκBα and loading control. Arrow with tail represents loading band analysed where two bands can be seen.

#### 3.2.3.2 AHSS ACTIVATION OF NF-κB TRANSCRIPTIONAL ACTIVITY

Nuclear translocation of NF-κB and cytosolic degradation of IκBα are necessary, but often not sufficient, to induce transcriptional activation of NF-κB. Covalent modifications to the transcription factor enhance DNA binding and recruitment of co-factors required for complete transcriptional activation (Chen *et al.*, 2004). As such, the transcriptional activity of NF-κB under AHSS and covalent changes to the transcription factor, between static controls and cells exposed to shear, were compared. HUVECs were either subjected to AHSS at 12dyn/cm$^2$ for 30 and 90 minutes or maintained in static conditions, after which, protein levels of phosphorylated NF-κB (phospho-NF-κB) at Serine residue 276 (Ser276), and transcriptional motif (κB) binding by NF-κB, were analysed.

Western blot analysis and the ELISA-based DNA binding assay revealed low basal levels of phospho-NF-κB, and very little κB-binding in static controls, respectively. Following 30 minutes exposure to AHSS a small, but significant, increase in phosphorylation of NF-κB was observed, which decreased again by 90 minutes (FIGURE 3.7.A. and B.). This finding was supported by an increased binding of NF-κB to the κB binding motif after shear stress exposure for 30 minutes, which also reduced by 90 minutes to below basal levels (FIGURE 3.7.C.). Finally, these data corroborate the nuclear translocation findings from WB presented above (section 3.2.3.1.).

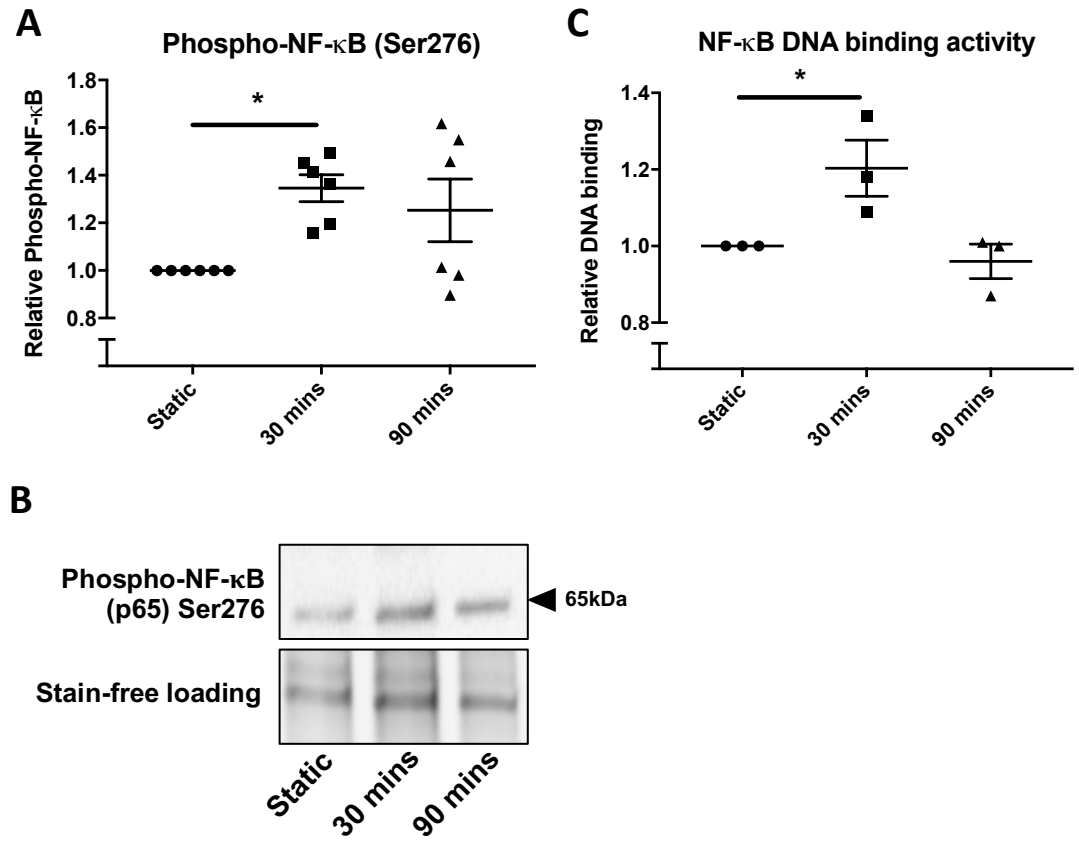


**FIGURE 3.7. AHSS promoted transcriptional activation of NF-κB**

Relative levels of the phosphorylated form of NF-κB (Ser276) were detected by Western blot analysis and NF-κB DNA binding affinity to the κB oligonucleotide was examined an ELISA-based TransAm activity assay. * indicates $p<0.05$, One-way ANOVA followed by post-hoc pairwise comparisons with Bonferroni correction for multiple comparisons, n=3-6.

A. Relative Phospho-NF-κB (Ser276) protein levels, normalised to stain free loading controls and expressed as a fold change relative to static.
B. Phospho-NF-κB (Ser276) representative blot and stain free loading control.
C. Relative binding affinity of NF-κB for the κB oligonucleotide, expressed as a fold change of optical density relative to static.

### 3.2.4 NF-κB RESPONSE TO AHSS IN THE LSV ENDOTHELIUM - *EX VIVO*

#### 3.2.4.1 AHSS TRIGGERED NF-κB TRANSLOCATION LSV ECS

Having shown that NF-κB is activated in venous ECs *in vitro*, in response to AHSS, NF-κB activation was evaluated in the LSV endothelium, using an *ex vivo* perfusion model. Briefly, segments of LSV were exposed to AHSS at 12dyn/cm$^2$ for 30 and 90 minutes or maintained in static conditions. As in section 3.2.2.2, LSV segments were subsequently prepared for *en face* immunofluorescent analysis (Supplementary video 3 shows NF-κB immunofluorescent within Z-stack images). To quantify nuclear translocation of NF-κB, mean AFI was evaluated in LSV EC nuclei only (red), in 3D, using Imaris (described in detail in 2.7.2. and 2.9.). Co-staining with vWF (green) was used to identify the surface layer of cells as ECs.

In static conditions, nuclear NF-κB protein levels were low and very few EC nuclei appeared positive for NF-κB. AHSS exposure induced a significant increase in nuclear NF-κB translocation in LSV ECs after 30 minutes, which increased further after 90 minutes exposure, to over two-fold greater than static, baseline levels (FIGURE 3.8.A.). This effect is clearly observed in the representative image at 90 minutes, where almost all nuclei are stained positive for NF-κB (FIGURE 3.8.B.).

---

**FIGURE 3.8. AHSS induced NF-κB translocation in LSV ECs**

Mean arbitrary fluorescence intensity (MFI) of immunofluorescence for NF-κB protein was calculated in ECs from LSV samples exposed to 30 and 90 minutes shear stress or maintained in static conditions.

A. Mean arbitrary fluorescence intensity calculated from volumetric analysis of LSV EC nuclei using Imaris software; * indicates $p<0.05$, ** indicates $p<0.01$, **** indicates $p<0.0001$, One-way ANOVA followed by post-hoc pairwise comparisons with Bonferroni correction for multiple comparisons, n=5.
B. Representative MIP images of NF-κB protein detected by immunofluorescence, showing NF-κB localisation in LSV EC nuclei, co-stained for NF-κB (red), vWF (green) and nuclei/TO-PRO3 (blue). Scale bars represent 10μm and apply to all images.

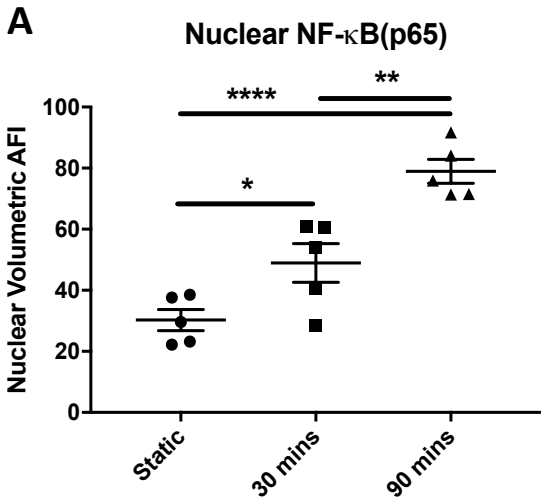
A
Nuclear NF-κB(p65)
Nuclear Volumetric AFI
100
80
60
40
20
0
****
**
*
Static
30 mins
90 mins

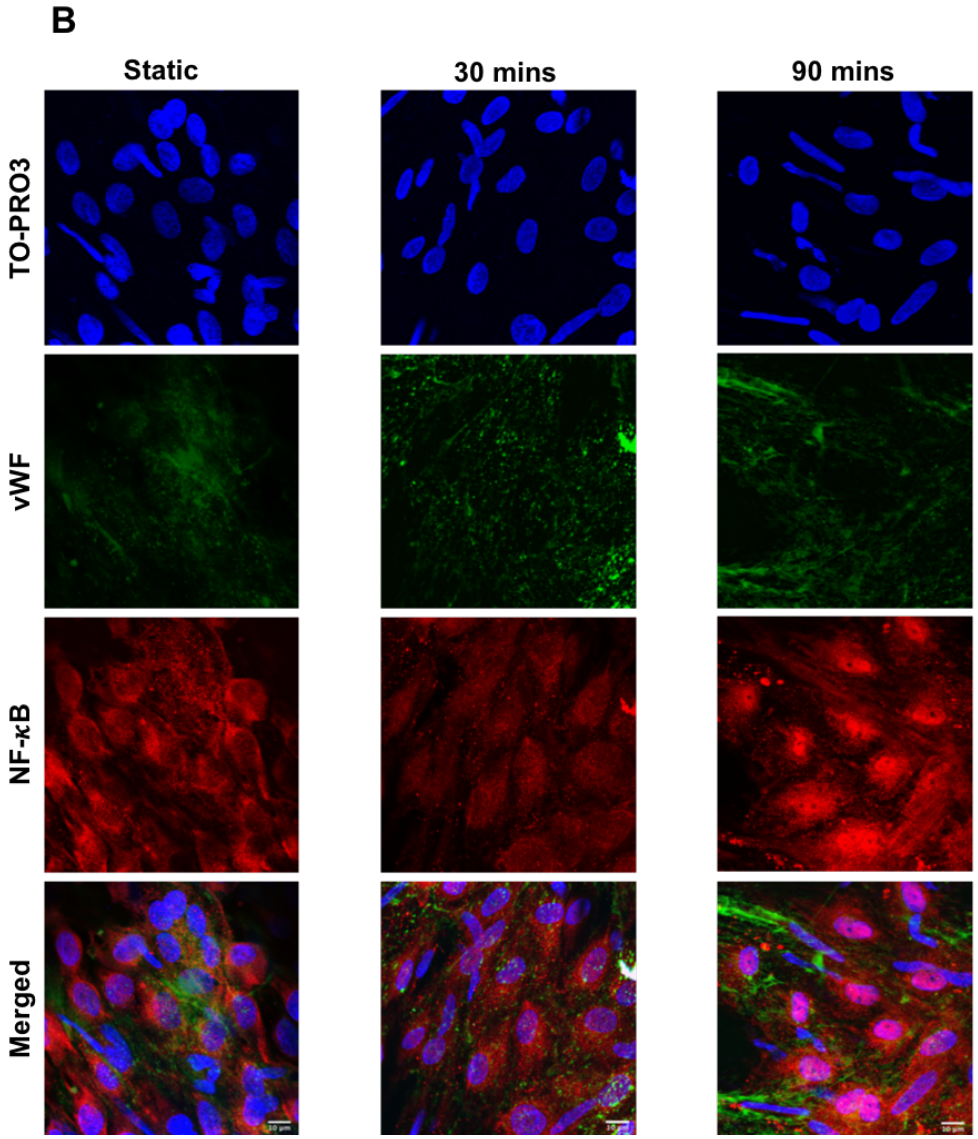
B
Static
30 mins
90 mins
TO-PRO3
vWF
NF-κB
Merged

### 3.2.5 NF-κB INHIBTION AND vEC RESPONSE TO AHSS – *IN VITRO*

#### 3.2.5.1 PHARMACOLOGICAL INHIBITION OF NF-κB, AND RESPONSE TO TNF-α STIMULATION

BAY11-7085 is a known, specific inhibitor of the NF-κB classical pathway, due to its targeted modulatory effects on the activation loop of IKK-β (of the IKK complex), which acts to prevent phosphorylation of IκBα and its dissociation from the p50/p65 NF-κB heterodimer (Pierce *et al.*, 1997). To validate BAY11-7085, the TNF-α induced gene response was assessed with and without the presence of the inhibitor in a dose-dependent manner. The effect on NF-κB target gene expression was then measured using RT-qPCR for the same target genes as the original Pierce *et al.* paper; MCP-1, VCAM-1, E-Selectin and IL-8. HUVECs were pre-treated with 0.2% (v/v) DMSO-control (equivalent to maximal concentration of inhibitor) or varying concentrations of BAY11-7085 (1.25, 2.5, 5, 10 and 20 μmol/L) for one hour. Following pre-treatment cells were stimulated with 10ng/mL TNF-α for one hour. With the two highest doses (10 and 20μmol/L), there was a significant reduction in the mRNA levels of all four target genes following TNF-α stimulation (FIGURE 3.9.). As such, the highest dose of 20μmol/L was selected for use in all subsequent experiments in this thesis.

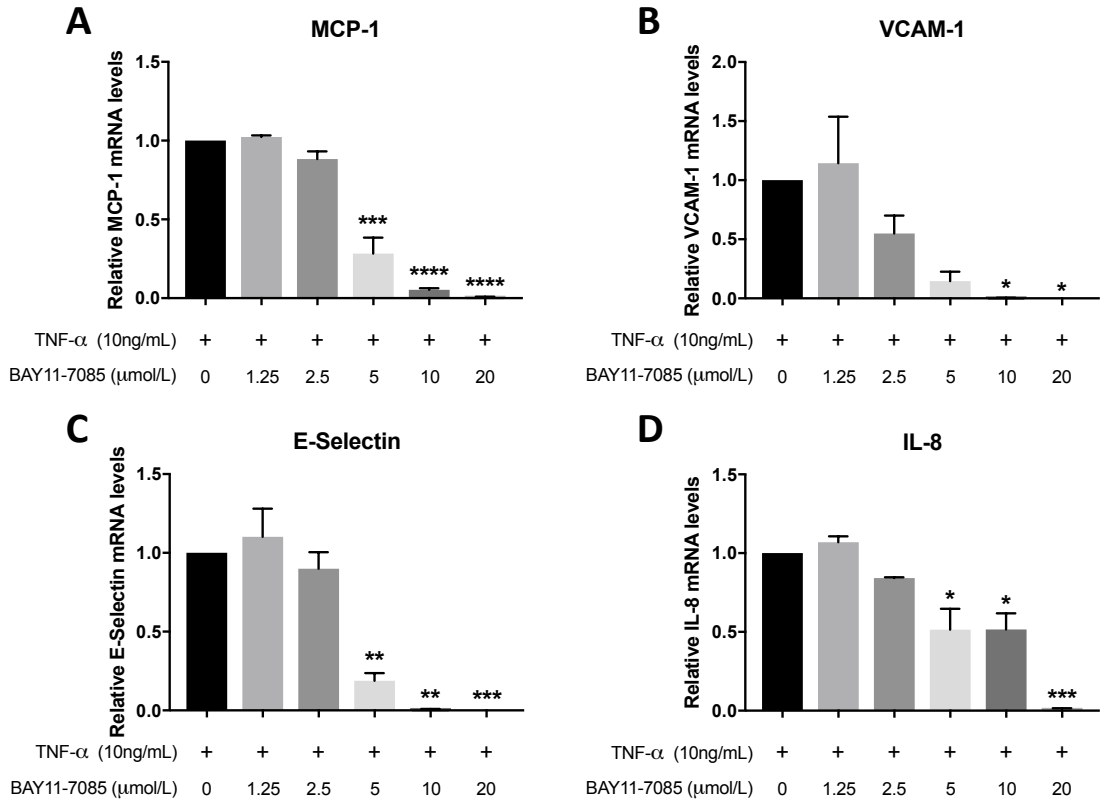


**FIGURE 3.9. BAY11-7085 prevented TNF-α induced gene response**

Quantification of MCP-1, VCAM-1, E-Selectin and IL-8 mRNA levels (A, B, C and D, respectively) in HUVECs pre-treated with DMSO control (BAY11-7085 0μmol/L) or increasing concentrations of BAY11-7085 prior to stimulation with 10ng/μL TNF-α for 1 hour, using RT-qPCR. mRNA levels were normalised to β-tubulin and expressed as a fold-change relative to DMSO control. * indicates $p<0.05$, ** indicates $p<0.01$, *** indicates $p<0.001$, **** indicates $p<0.0001$, One-way ANOVA followed by post-hoc pairwise comparisons with Bonferroni correction for multiple comparisons, n=3.

#### 3.2.5.2 BAY11-7085 PRE-TREATMENT REDUCED PRO-INFLAMMATORY RESPONSES TO AHSS *IN VITRO*

Having shown both the induction of a pro-inflammatory response and activation of the NF-κB classical pathway in ECs under conditions of AHSS, it was hypothesised that inhibition of NF-κB activation would be associated with a reduction of the pro-inflammatory gene response under AHSS. HUVECs were pre-treated for one hour with 20μmol/L BAY11-7085 or 0.2% (v/v) DMSO control, prior to exposure to AHSS for 90 and 120 minutes, or maintenance in static conditions. The pro-inflammatory gene response was measured by the relative levels of MCP-1, IL-6, IL-8 and ICAM-1 mRNA and expressed as a fold change from DMSO static control.

mRNA levels of MCP-1, IL-6 and ICAM-1 in DMSO treated cells (controls) all significantly increased after 120 minutes AHSS, relative to DSMO treated static control, as in section 3.2.1.1 (FIGURE 3.10.). BAY11-7085 was not able to reduce basal levels of mRNA compared to DMSO treated static control. However, under AHSS, mRNA transcript levels of all pro-inflammatory, except IL-8, genes were significantly reduced with NF-κB inhibition, compared with DMSO treated controls, at equivalent time-points (FIGURE 3.10.)

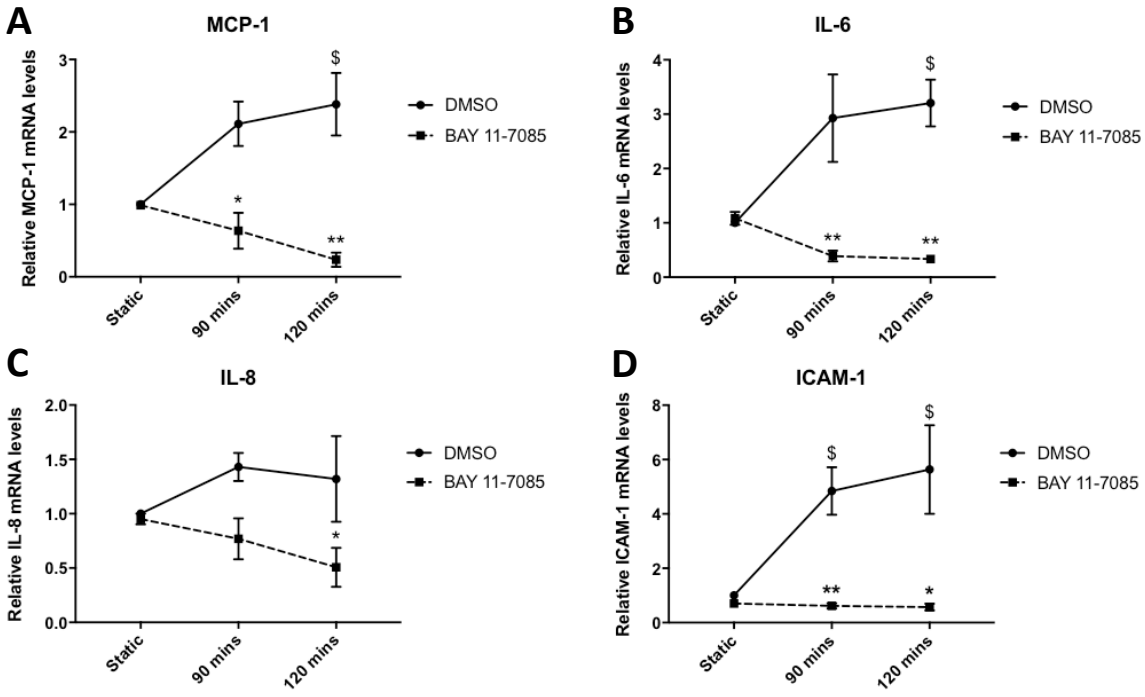


**FIGURE 3.10. NF-κB inhibition attenuated the pro-inflammatory mRNA response under conditions of AHSS**

Quantification of MCP-1, IL-6, IL-8 and ICAM-1 mRNA (A, B, C and D, respectively) in HUVECs exposed to 90 and 120 minutes of AHSS, with or without inhibition of NF-κB by BAY11-7085 pre-treatment using RT-qPCR. mRNA levels were normalised to β-tubulin and expressed as a fold-change relative to DMSO treated, Static control. * indicates $p<0.05$, ** indicates $p<0.01$ vs. DMSO control samples (equivalent time-points), $ indicates $p<0.05$ vs. DMSO static control, Two-way ANOVA followed by post-hoc pairwise comparisons with Bonferroni correction for multiple comparisons, n=3.

#### 3.2.5.3 ADENOVIRAL-MEDIATED OVEREXPRESSION OF IκBα

In addition to pharmacological inhibition of NF-κB, a gene-therapy based approach was also adopted. This approach employed adenoviral-mediated overexpression using a wild-type form of the NF-κB, innate repressor, IκBα (WT-IκBα). The WT-IκBα adenoviral overexpression functions to sequester NF-κB in the cytosol and prevent its translocation, and thus, any activation of the pathway.

Increasing concentrations of virus (pfu/mL) were used to determine the optimum infection efficiency in the overexpression of IκBα, compared to rAd66 empty viral cassette controls. HUVECs were infected with either WT-IκBα adenovirus or rAd66 control adenovirus at 3 different concentrations ($1\times10^6$, $1\times10^7$ and $1\times10^8$ pfu/mL), IκBα protein expression was then analysed by Western blotting. Optimal overexpression of IκBα was achieved with the highest concentration of $1\times10^8$ pfu/mL WT-IκBα adenovirus, as such, this concentration was used for all subsequent experiments within this chapter (FIGURE 3.11.A. and B.).

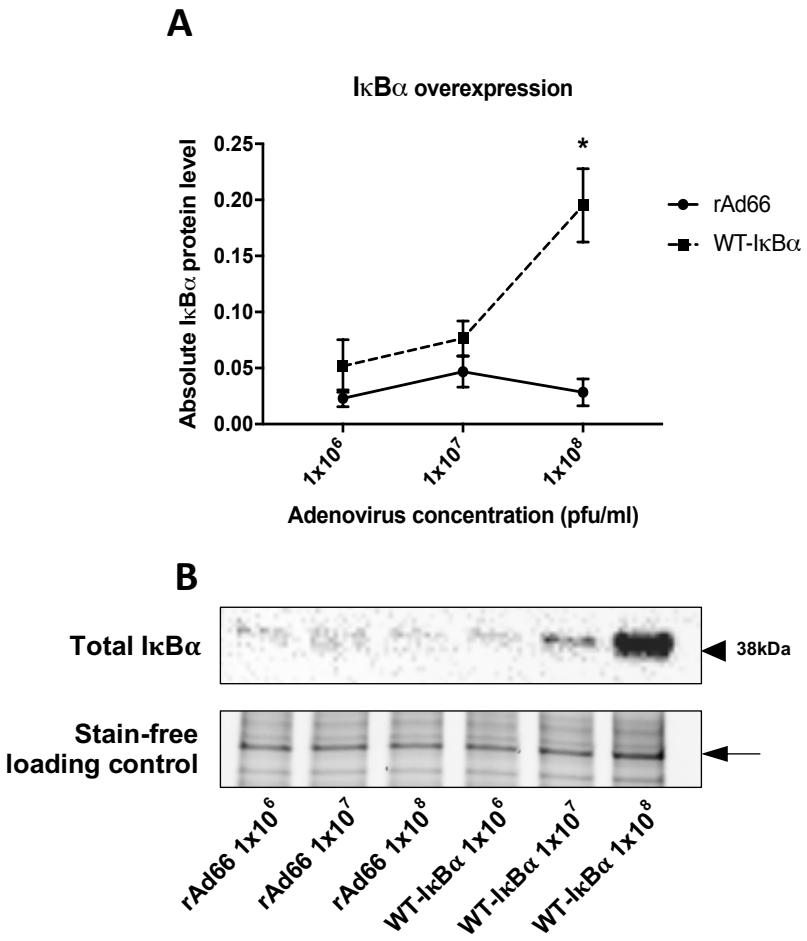


**FIGURE 3.11. Overexpression of IκBα was achieved optimally with the highest dose of WT-IκBα adenovirus**

IκBα protein levels were compared in HUVECs infected with WT-IκBα or rAd66 adenoviruses, by Western blot analysis. * indicates $p<0.05$, vs. rAd66 control samples (equivalent concentrations), Two-way ANOVA followed by post-hoc pairwise comparisons with Bonferroni correction for multiple comparisons, n=3.

A. IκBα protein levels, normalised to stain free loading controls and expressed as mean pixel intensity within a given volume
B. Representative IκBα blot and stain free loading control. Arrow with tail represents loading band analysed

#### 3.2.5.4 OVEREXPRESSION OF IκBα ABROGATED AHSS-INDUCED PRO-INFLAMMATORY mRNA RESPONSE

After validating adenoviral mediated over-expression of IκBα protein, HUVECS were infected with the WT-IκBα adenovirus and then exposed to AHSS at 12dyn/cm$^2$ for 90 and 120 minutes and pro-inflammatory mRNA (MCP-1, IL-6, IL-8 and ICAM-1) levels were quantified by RT-qPCR.

mRNA transcript levels of IL-6, IL-8 and ICAM-1 did not significantly increase under AHSS exposure in rAd66 control samples, despite a tendency to increase; only MCP-1 significantly increased significantly by 90 minutes (FIGURE 3.12.). Nevertheless, increase in levels of MCP-1, IL-6 and IL-8 were significantly blocked with adenoviral overexpression of WT-IκBα following exposure to 90 minutes AHSS. Of these three genes, only MCP-1 was significantly reduced following 120 minutes exposure to AHSS (FIGURE 3.12.). ICAM-1 was not significantly reduced with WT-IκBα overexpression at either time point.

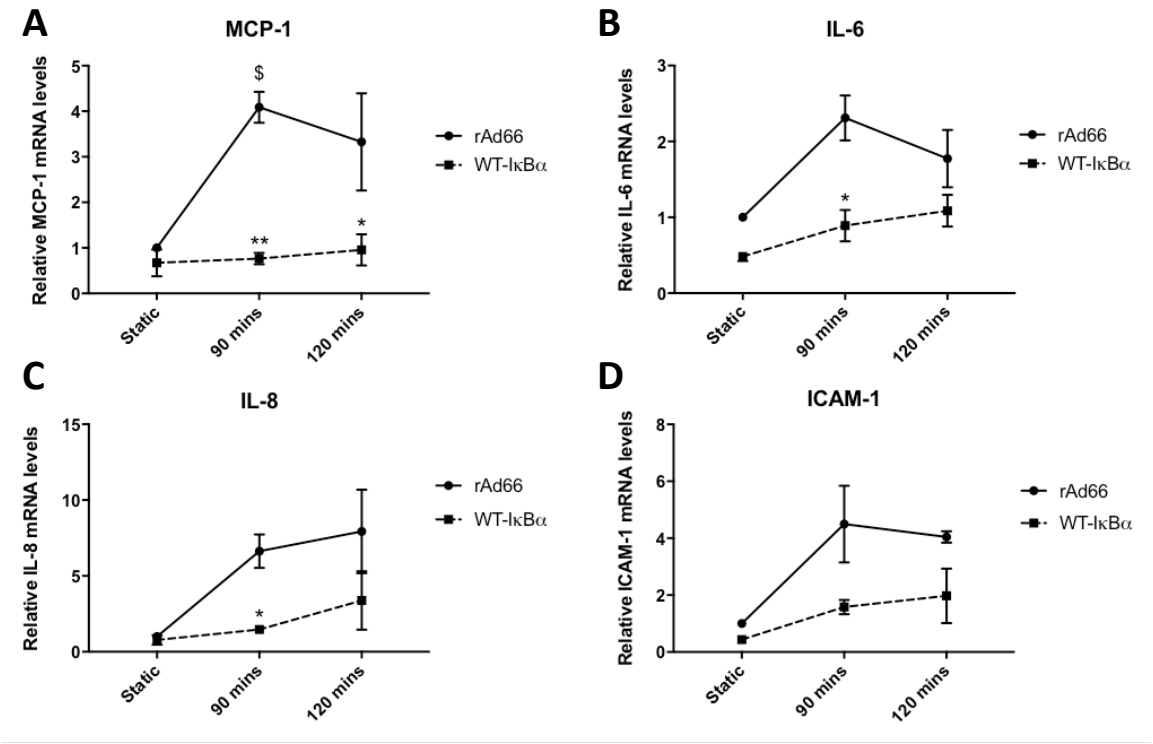


**FIGURE 3.12. Overexpression of IκBα prevented some pro-inflammatory gene responses under AHSS**

Quantification of MCP-1, IL-6, IL-8 and ICAM-1 mRNA (A, B, C and D, respectively) in HUVECs exposed to 90 and 120 minutes of AHSS, with or without inhibition of NF-κB by overexpression of WT-IκBα using RT-qPCR. mRNA levels were normalised to β-tubulin and expressed as a fold-change relative to rAd66 static control. * indicates $p<0.05$, ** indicates $p<0.01$ vs. rAd66 control samples (equivalent time-points), $ indicates $p<0.05$ vs. rAd66 static control, Two-way ANOVA followed by post-hoc pairwise comparisons with Bonferroni correction for multiple comparisons, n=3.

#### 3.2.5.5 OVEREXPRESSION OF IκBα REDUCED MCP-1 PROTEIN LEVELS UNDER AHSS

Having demonstrated that adenoviral-mediated overexpression of IκBα reduced mRNA levels of MCP-1 under AHSS, MCP-1 protein levels were examined by immunofluorescence, with and without WT- IκBα overexpression. HUVECS were infected as above and then exposed to 4 or 6 hours of AHSS 12dyn/cm$^2$, or maintained in static conditions, prior to detection of MCP-1 by immunofluorescence, as in section 3.2.1.3.

MCP-1 protein levels in control-transfected cells tended to reduce with the application of AHSS, as opposed to increasing, as was observed in FIGURE 3.3. However, with overexpression of the NF-κB repressor, IκBα, there was a significant, transient reduction in MCP-1 protein levels at 4 hours compared with rAd66 control, which had then tended to increase again by 6 hours, roughly to levels of control-transfected cells (FIGURE 3.13.A., B. and C.).

---

**FIGURE 3.13. IκBα overexpression reduced MCP-1 under AHSS**

Quantification of MCP-1 arbitrary fluorescence intensity (AFI) levels in HUVECs exposed to AHSS with or without overexpression of WT-IκBα.

A. Whole cell AFI of MCP-1 staining as assessed by immunofluorescence and quantified by CellProfiler2.0. * indicates $p<0.05$ vs. rAd66 control samples (equivalent time-point), Two-way ANOVA followed by post-hoc pairwise comparisons with Bonferroni correction for multiple comparisons, n=3.
B. Representative images of MCP-1 protein detected by immunofluorescence in ECs infected with rAd66 empty viral vector adenovirus control; co-stained for VE-Cadherin (green), MCP-1 (red) and nuclei/DAPI (blue). Scale bars represent 15μm and apply to all images.
C. Representative images of MCP-1 protein detected by immunofluorescence in ECs infected with WT-IκBα-overexpressing adenovirus; co-stained for VE-Cadherin (green), MCP-1 (red) and nuclei/DAPI (blue). Scale bars represent 15μm and apply to all images.

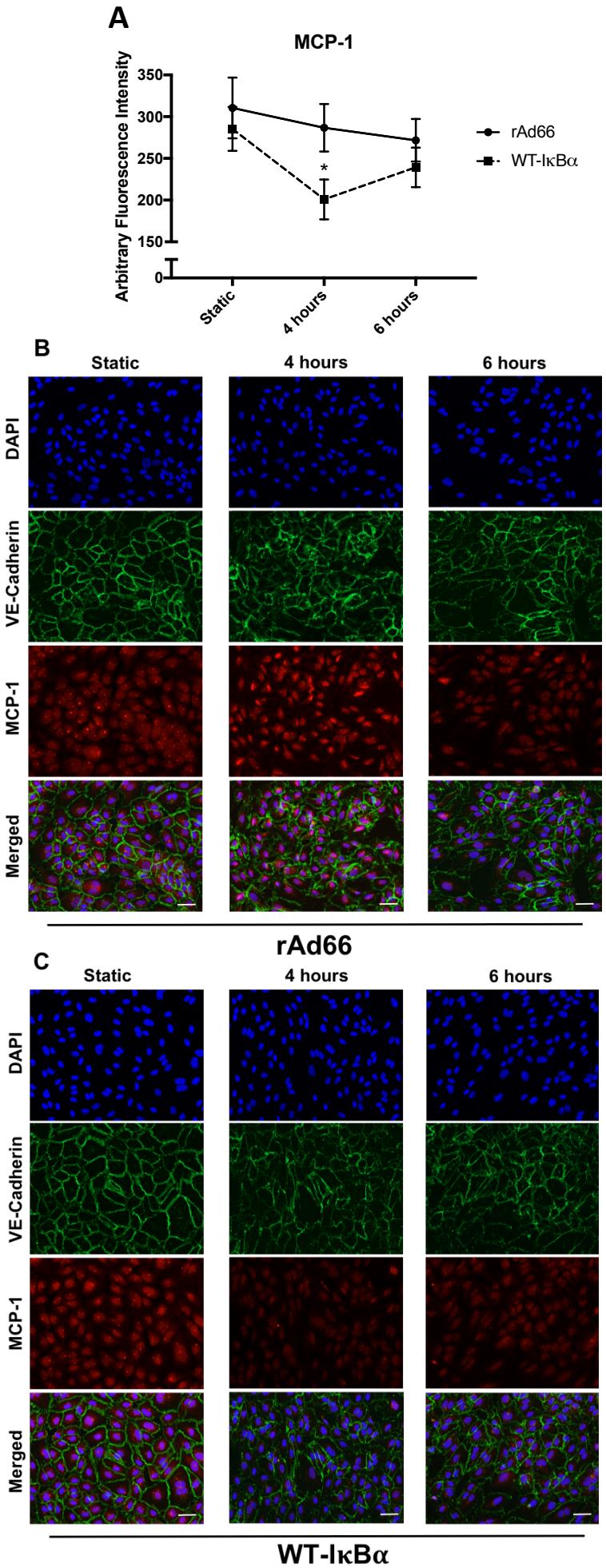
A
MCP-1
Arbitrary Fluorescence Intensity
350
300
250
200
150
0
Static
4 hours
6 hours
rAd66
WT-IκBα
*
B
Static
4 hours
6 hours
DAPI
VE-Cadherin
MCP-1
Merged
rAd66
C
Static
4 hours
6 hours
DAPI
VE-Cadherin
MCP-1
Merged
WT-IκBα

#### 3.2.5.6 IκBα LEVELS INCREASED UNDER AHSS AFTER OVEREXPRESSION OF IκBα

Inhibition of NF-κB dependent gene transcription was shown to be effective by two independent methods, both pharmacological and gene-therapy based, at the gene-expression and protein level. However, having also seen that MCP-1 reduction, by IκBα overexpression, was transient, The potentially transient nature of IκBα expression under flow was also evaluated by immunofluorescence. Experimental conditions were repeated as above (section 3.2.5.5.). Again, it was observed by a different method that, with adenoviral overexpression of WT-IκBα, expression levels of IκBα at static were significantly increased in comparison to rAd66 controls (FIGURE 3.14.A.). Interestingly, however, levels of IκBα actually increased following AHSS exposure with the WT-IκBα overexpressing adenovirus compared to both rAd66 controls and WT-IκBα static control (FIGURE 3.14.A., B. and C.)

---

**FIGURE 3.14. IκBα overexpression increased levels of IκBα under AHSS**

IκBα arbitrary fluorescence intensity (AFI) levels in HUVECs exposed to AHSS with or without overexpression of WT-IκBα.

A. Whole cell AFI of IκBα protein detected by immunofluorescence and quantified by CellProfiler2.0. * indicates $p<0.05$, ** indicates $p<0.01$, *** indicates $p<0.001$ vs. rAd66 control samples (equivalent time-points); $ indicates $p<0.05$, $$ indicates $p<0.01$ vs. WT-IκBα static control; Two-way ANOVA followed by post-hoc pairwise comparisons with Bonferroni correction for multiple comparisons, n=3.
B. Representative images of IκBα protein detected by immunofluorescence in ECs infected with rAd66 empty viral vector control; co-stained for VE-Cadherin (green), MCP-1 (red) and nuclei/DAPI (blue). Scale bars represent 15μm and apply to all images
C. Representative images of IκBα protein detected by immunofluorescence in ECs infected with WT-IκBα-overexpressing adenovirus; co-stained for VE-Cadherin (green), MCP-1 (red) and nuclei/DAPI (blue). Scale bars represent 15μm and apply to all images.

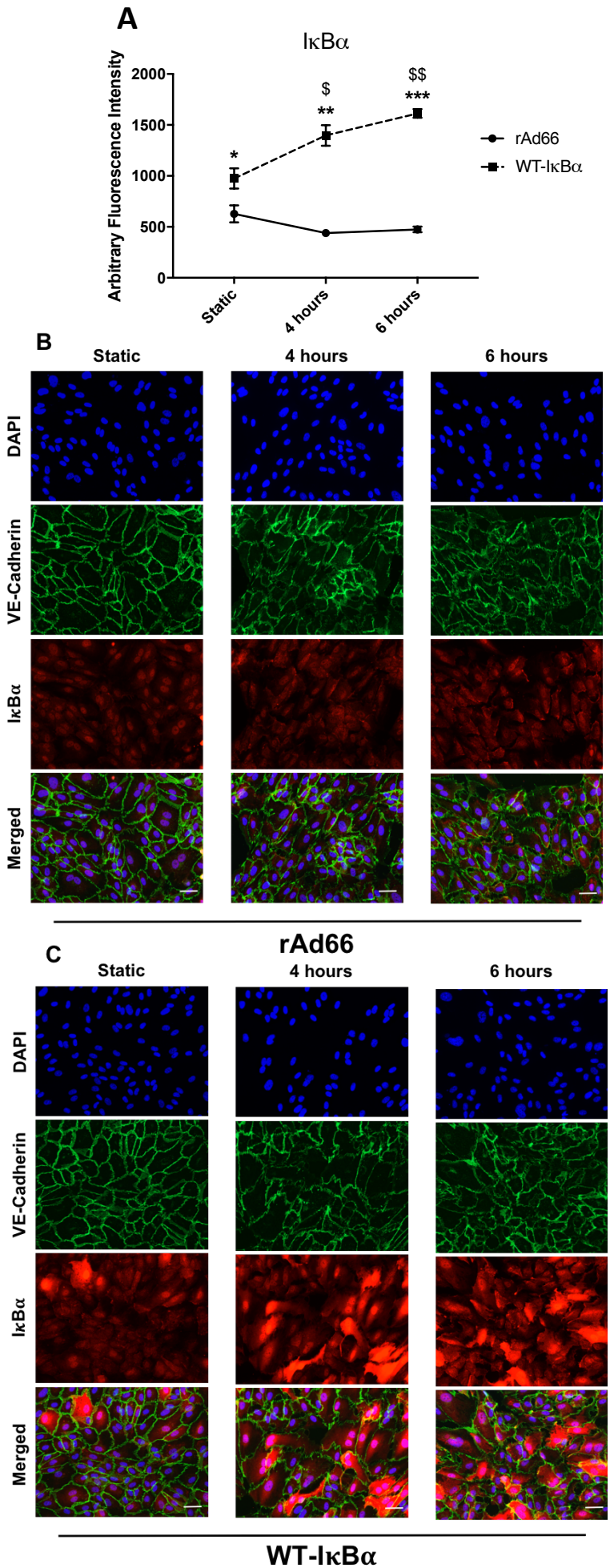
A
IκBα
Arbitrary Fluorescence Intensity
2000
1500
1000
500
0
*
**
$
***
$$
rAd66
WT-IκBα
Static
4 hours
6 hours
B
Static
4 hours
6 hours
DAPI
VE-Cadherin
IκBα
Merged
rAd66
C
Static
4 hours
6 hours
DAPI
VE-Cadherin
IκBα
Merged
WT-IκBα

### 3.2.6 NF-κB INHIBTION AND vEC RESPONSE TO AHSS – *EX VIVO*

#### 3.2.6.1 BAY11-7085 REDUCED MCP-1 PROTEIN LEVELS UNDER AHSS IN LSV ECs

Following the observation that NF-κB inhibition reduced the pro-inflammatory response to AHSS in ECs in culture, MCP-1 levels were investigated in LSV ECs exposed to AHSS, *ex vivo*. Upon collection of the vessel, appropriate length segments were cut, cannulated, and treated with 50μmol/L BAY11-7085, or 0.5%(v/v) DMSO, for 3 hours prior to exposure to AHSS at 12dyn/cm$^2$ for 6 hours using the *ex vivo* perfusion model. Following shear stress exposure, MCP-1 protein levels were investigated in *en face* prepared LSV ECs using immunofluorescent analysis.

Following 6 hours exposure to AHSS in DMSO control samples, MCP-1 protein levels were significantly increased in LSV ECs compared to both static controls (BAY11-7085 and DMSO). With BAY11-7085 pre-treatment MCP-1 levels under shear conditions were significantly reduced, back to static control levels (FIGURE 3.15.A. and B.).

---

**FIGURE 3.15. BAY11-7085 pre-treatment prevented increases in AHSS-driven MCP-1 production in LSV ECs**

*En face* immunofluorescent analysis was used to investigate MCP-1 protein levels in LSV ECs exposed to AHSS, with and without pre-inhibition of NF-κB using BAY11-7085.

A. Integrated fluorescence intensity of immunofluorescence for MCP-1 protein, calculated using FIJI; * indicates $p<0.05$, Two-way ANOVA followed by post-hoc pairwise comparisons with Bonferroni correction for multiple comparisons, n=4.
B. Representative maximum intensity projection (MIP) images of immunofluorescence for MCP-1 protein *en face*, co-stained for MCP-1 (red), vWF (green) and TO-PRO3/nuclei (blue). Scale bars represents 10μm.

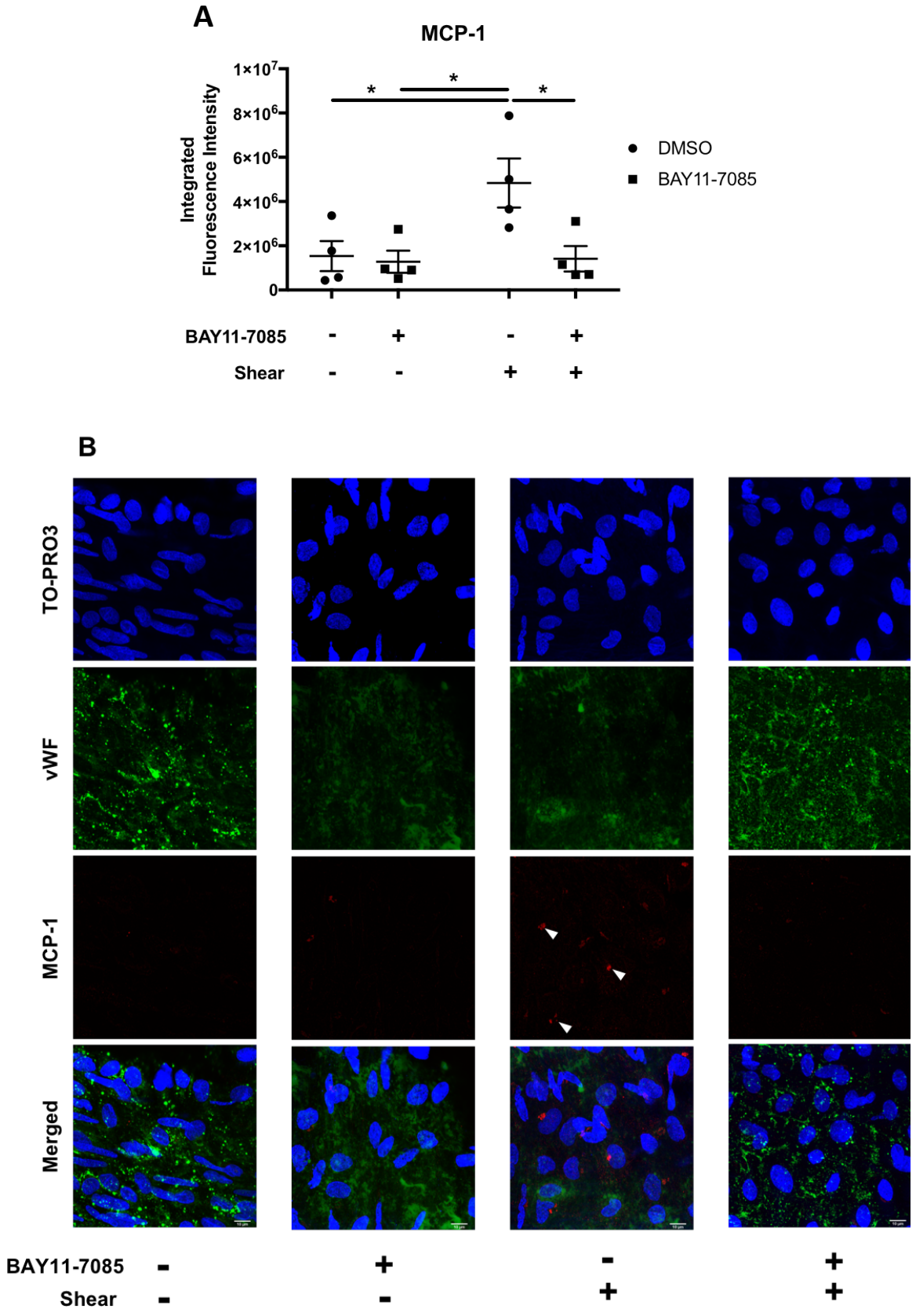
A
MCP-1
Integrated Fluorescence Intensity
1×10^7
8×10^6
6×10^6
4×10^6
2×10^6
0
*
*
*
DMSO
BAY11-7085
BAY11-7085 - + - +
Shear - - + +
B
TO-PRO3
vWF
MCP-1
Merged
BAY11-7085 - + - +
Shear - - + +

### 3.2.7 NF-κB INHIBTION AND vEC PHENOTYPIC RESPONSE TO TNF-α AND AHSS

#### 3.2.7.1 BAY11-7085 REDUCED TNF-α-INDUCED LOSS OF VE-CADHERIN CELL-CELL CONTACT

Permeability regulation to solutes and lipoproteins into the vascular wall is an integral property of a functional endothelium. To firstly address the relationship between NF-κB activation and endothelial integrity, TNF-α was utilised in order to initially interrogate the effects NF-κB activation and inhibition on endothelial monolayer structure and closely simulate the endothelial inflammatory activation under AHSS. Regulation of permeability is maintained by an intricate network of intercellular contacts situated in the cleft between endothelial cells, functioning as a selectively permeable barrier, amongst these homophilic cell-to-cell contacts VE-Cadherin is crucially important. Consequently, to examine endothelial barrier integrity, VE-Cadherin contact attachment and organisation of the endothelial barrier structure, were assessed by immunofluorescence. This is used here as a surrogate, quantitative measure of cell-cell contact and quantification of gaps in the endothelial monolayer structure.

HUVECs were pre-treated with 0.2% (v/v) DMSO-control or 20 μmol/L of BAY11-7085 for 3 hours. Following pre-treatment, cells were stimulated with 10ng/mL TNF-α for 18 hours then subjected to immunofluorescence analysis for VE-Cadherin. Immunofluorescence analysis revealed that, in DMSO-treated controls, 18 hours of TNF-α stimulation significantly disrupted VE-Cadherin cell-cell contacts, as shown by the reduced percentage of objects (cells) in contact with neighbouring objects (cells). This disruption was rescued, however, with NF-κB inhibition using BAY11-7085 pre-treatment (FIGURE 3.16.A. and B.).

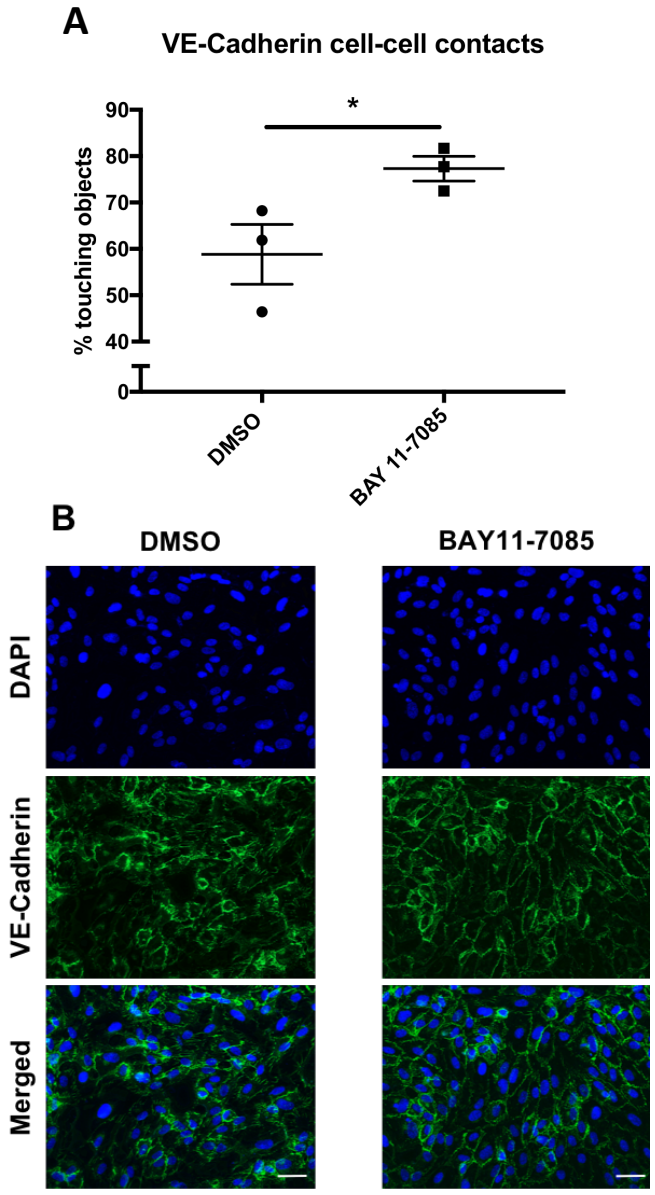


**FIGURE 3.16. BAY11-7085 protected against TNF-α induced cell-cell contact**

Immunofluorescence for VE-Cadherin protein was used to quantify the percentage of ECs in contact with one another following chronic TNF-α stimulation, with and without a pre-treatment to inhibit NF-κB, using BAY11-7085 or DMSO, respectively.

A. Percentage of objects touching was calculated with immunofluorescence for VE-Cadherin protein, using CellProfiler; * indicates $p<0.05$, two-tailed, two-sample t-test, n=3.

B. Representative images of VE-Cadherin protein detected by immunofluorescence for both DMSO and BAY11-7085 treated ECs; co-stained for VE-Cadherin (green) and nuclei/DAPI (blue). Scale bars represent 15μm and apply to all images.

#### 3.2.7.2 OVEREXPRESSION OF IκBα REDUCED AHSS-INDUCED LOSS OF ENDOTHELIAL CELL-CELL CONTACT

To address the contribution of NF-κB to VE-Cadherin cell-cell contact in the context of AHSS, IκBα was over-expressed via adenoviral-mediated delivery. Cells were then exposed to 4 or 6 hours of HSS at 12dyn/cm$^2$ or maintained in static conditions. Subsequently, HUVECs were analysed immunocytochemically as above (section 3.2.7.1.).

Immunofluorescence analysis demonstrated in rAd66-infected control samples, that 4 hours of AHSS exposure significantly reduced the number of VE-cadherin positive EC cell-cell contacts, which subsequently recovered by 6 hours (FIGURE 3.17.A. and B.). Whereas, overexpression of IκBα prevented the flow-induced loss of EC cell-cell contact after 4 hours AHSS, relative to rAd66 controls (FIGURE 3.17.A. and C.).

---

**FIGURE 3.17. IκBα overexpression reduced AHSS induced disruption of endothelial barrier**

Immunofluorescence for VE-Cadherin protein was used to quantify the percentage of ECs in contact with one another following 4 and 6 hours exposure to AHSS, with and without adenoviral-mediated overexpression of IκBα.

A. Percentage of objects touching was calculated with immunofluorescence for VE-Cadherin protein, using CellProfiler; * indicates $p<0.05$ vs. WT-IκBα 4 hours; $ indicates $p<0.05$ vs. rAd66 static control, Two-way ANOVA followed by post-hoc pairwise comparisons with Bonferroni correction for multiple comparisons, n=3.
B. Representative images of VE-Cadherin cell-cell contact detected by immunofluorescence in ECs infected with rAd66 empty viral vector control; co-stained for VE-Cadherin (green) and nuclei/DAPI (blue). Scale bars represent 15μm and apply to all images.
C. Representative images of VE-Cadherin cell-cell contact detected by immunofluorescence in ECs infected with WT-IκBα-overexpressing adenovirus; co-stained for VE-Cadherin (green) and nuclei/DAPI (blue). Scale bars represent 15μm and apply to all images.

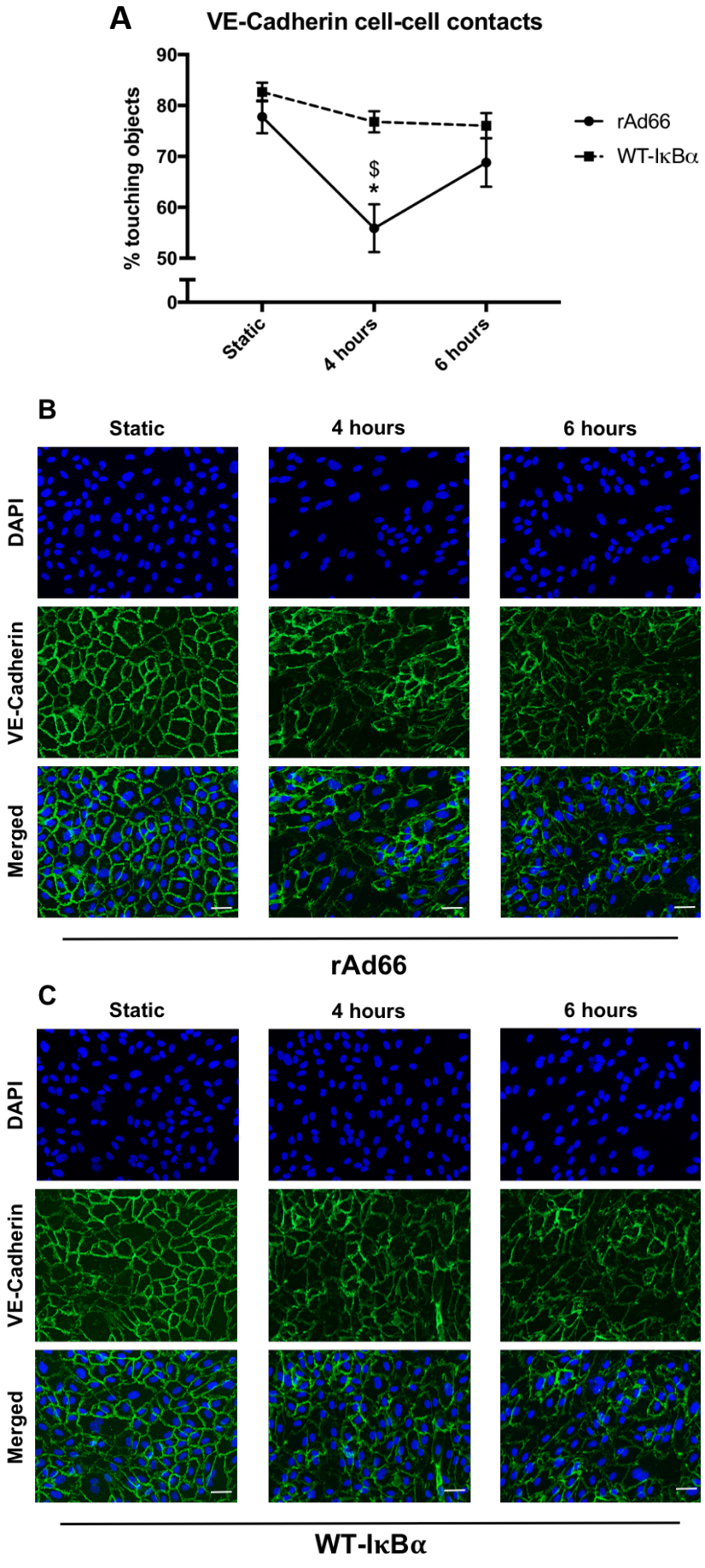
A
VE-Cadherin cell-cell contacts
% touching objects
90
80
70
60
50
0
Static
4 hours
6 hours
* $
rAd66
WT-IκBα
B
Static
4 hours
6 hours
DAPI
VE-Cadherin
Merged
rAd66
C
Static
4 hours
6 hours
DAPI
VE-Cadherin
Merged
WT-IκBα

### 3.2.7.3 EC ELONGATION UNDER AHSS IS ALTERED BY IκBα OVEREXPRESSION

Elongation and increased ellipticity of ECs are considered a hallmark of arterial ECs, primarily resulting from prolonged exposure to high shear stress, whereas, venous ECs are generally much rounder in comparison (Aitsebaomo *et al*., 2008). Consequently, the shape of ECs was analysed as a marker of 'arterialisation' of vECs when NF-κB was inhibited through over-expression of IκBα, both under static and AHSS conditions. As in section 3.2.7.2, adenoviral mediated overexpression of IκBα was performed in HUVECs, prior to exposure to AHSS for 4 and 6 hours or maintenance in static conditions. Cells were then subjected to immunofluorescent analysis for VE-cadherin using CellProfiler. From this analysis, two features were obtained, the mean eccentricity and the mean major axis (longest) length of objects in an image. Major axis length simply refers to the length (in pixels) along the longest axis of a shape. Whereas, eccentricity refers to the flat- or round-ness of a shape and, as indicated in FIGURE 3.18.C., eccentricity (ε) is calculated on a scale of 0 to 1, where ε equal to 0 represents and 1 represents a line (though 0 and 1 are degenerate cases).

Elongation, represented by length of the major axis in number of pixels, was significantly increased in static conditions in WT-IκBα infected cells, compared to rAd66 static controls (FIGURE 3.18.A., D. and E.). Following exposure to AHSS, EC elongation increased in both groups after 4 hours, to roughly similar levels, and, in both cases elongation was significantly increased relative to rAd66 static controls. Eccentricity, represented in FIGURE 3.18.C., however, was increased only after 6 hours of AHSS in both IκBα overexpression and rAd66 control groups and there was no difference observed between treatment groups, suggesting that it is AHSS, not NF-κB inhibition, which affects EC morphology (FIGURE 3.18.B.). No change was observed in alignment of ECs with the direction of flow in either group or at either time-point (data not shown).

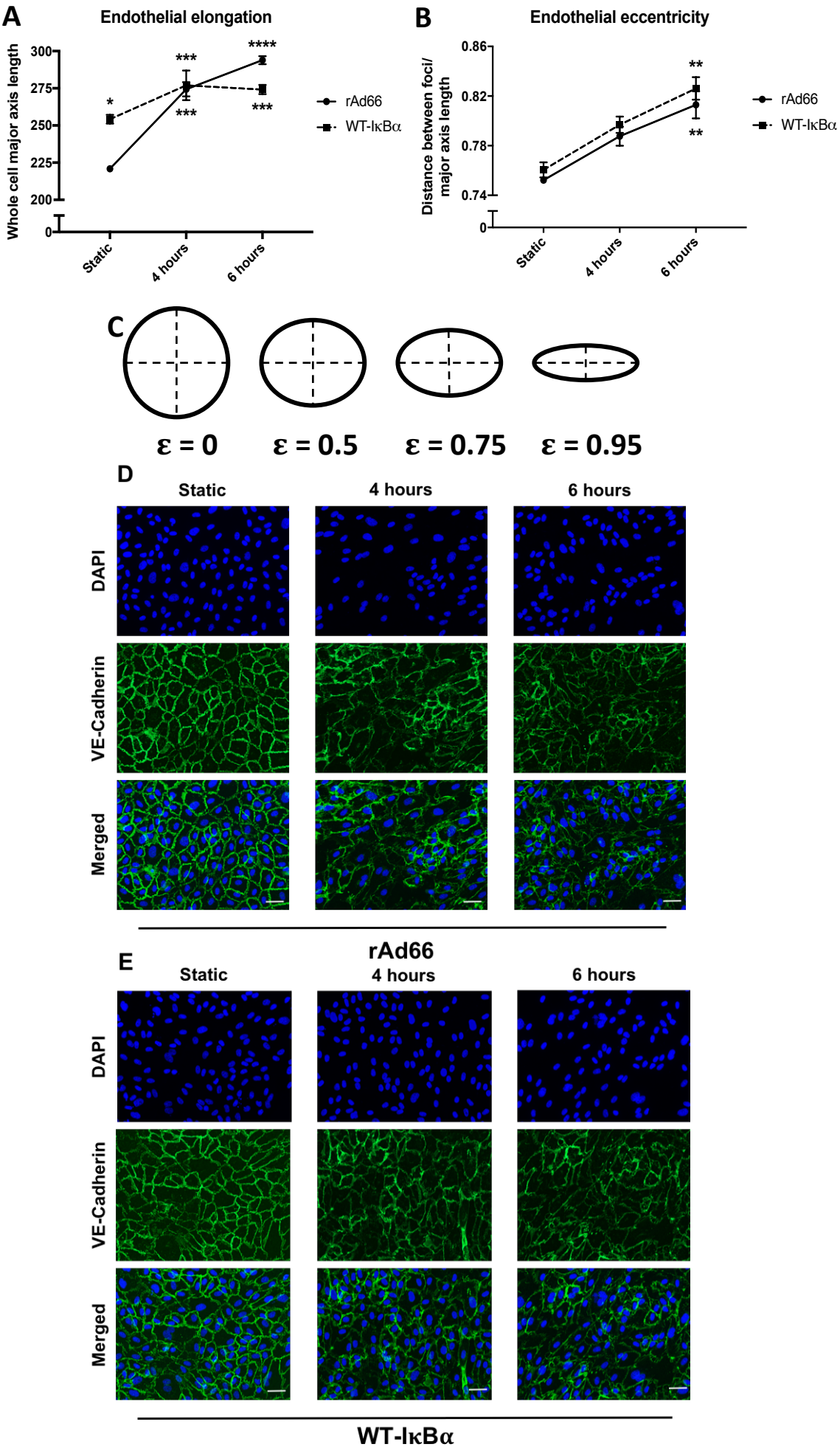
A
Endothelial elongation
Whole cell major axis length
300
275
250
225
200
0
Static
4 hours
6 hours
rAd66
WT-IκBα
B
Endothelial eccentricity
Distance between foci/ major axis length
0.86
0.82
0.78
0.74
0
C
ε = 0
ε = 0.5
ε = 0.75
ε = 0.95
D
Static
4 hours
6 hours
DAPI
VE-Cadherin
Merged
rAd66
E
Static
4 hours
6 hours
DAPI
VE-Cadherin
Merged
WT-IκBα

**FIGURE 3.18. AHSS, not IκBα overexpression, altered endothelial shape under flow**

Endothelial cell morphology characteristics under AHSS conditions with and without overexpression of IκBα; as shown by major axis length (A) and eccentricity (B and C).

A. Endothelial elongation as a measure of the major axis length. * indicates $p<0.05$, ** indicates $p<0.01$, *** indicates $p<0.001$ vs. rAd66 static control; Two-way ANOVA followed by post-hoc pairwise comparisons with Bonferroni correction for multiple comparisons, n=3.
B. Endothelial eccentricity. ** indicates $p<0.01$ vs. respective static controls; Two-way ANOVA followed by post-hoc pairwise comparisons with Bonferroni correction for multiple comparisons, n=3.
C. Diagrammatic representation of eccentricity measures.
D. Representative images of VE-Cadherin detected by immunofluorescence in ECs infected with rAd66 empty viral vector control; co-stained for VE-Cadherin (green) and nuclei/DAPI (blue). Scale bars represent 15μm and apply to all images.
E. Representative images of VE-Cadherin detected by immunofluorescence in ECs infected with WT-IκBα-overexpressing adenovirus; co-stained for VE-Cadherin (green) and nuclei/DAPI (blue). Scale bars represent 15μm and apply to all images.

#### 3.2.7.4 NF-κB INHIBITION REDUCED AHSS-INDUCED MONOCYTE ADHESION *IN VITRO*

A hallmark of the vascular inflammatory response is the initiation of the adhesion cascade, leading to attachment of circulating monocytes to the endothelial surface and, ultimately, their extravasation into the vascular wall (Ley *et al.*, 2007). Owing to the significantly reduced pro-inflammatory response to AHSS seen with NF-κB inhibition, including diminished expression of MCP-1 and ICAM-1, the effect of NF-κB inhibition on the endothelial-monocyte interaction was evaluated. Prior to the onset of AHSS, cells were incubated for 3 hours with 20μmol/L BAY11-7085, or 0.2%(v/v) DMSO, and 10μmol/L CM-DiI red fluorescent cell probe, concurrently. HUVECs were then exposed to pulsatile, laminar shear stress at 12dyn/cm$^2$ and 1 hertz (Hz) frequency for 6 hours. Calcein-labelled (10μmol/L) THP-1 cells were then flowed over the activated ECs at a shear stress of 1dyn/cm$^2$ and pulsatile frequency of 1Hz for 10 minutes whilst being imaged in real-time, using the Fluxion Bioflux microfluidic system. THP-1 monocytic cell-endothelial cell interactions were then evaluated in real-time (Supplementary video 4. shows adhesion in real time). A significant reduction of adhered monocytes was observed after AHSS when ECs were pre-treated with NF-κB inhibitor, BAY11-7085, as compared with the DMSO control group (FIGURE 3.19.A. and B.).

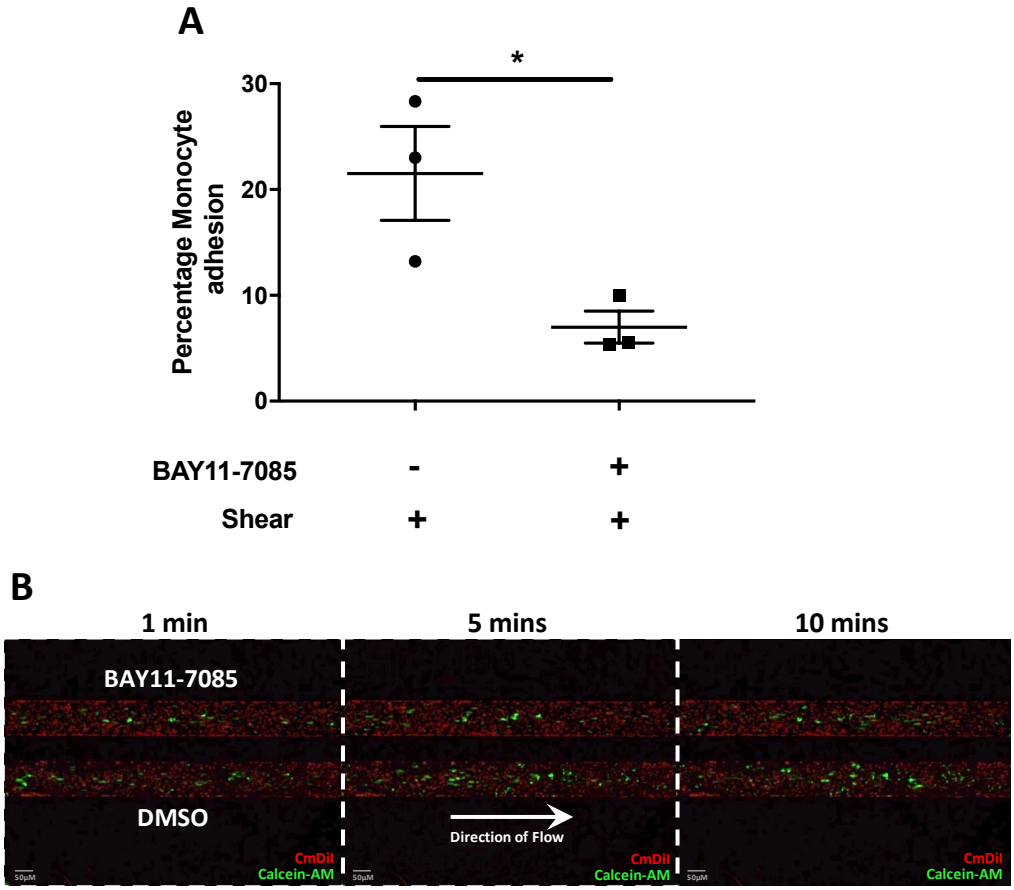


**FIGURE 3.19. BAY11-7085 pre-treatment reduced AHSS-induced monocyte adhesion**

Percentage of monocytes adhered to an endothelial monolayer was calculated by the number of adhered Calcein-labelled monocytes as a proportion of the total number of ECs, with and without treatment with NF-κB inhibitor.

A. Percentage of monocytes adhered to ECs after 10 minutes of incubation, with and without BAY11-7085 pre-treatment. * indicates $p<0.05$; two-tailed, two sample t-test, n=3.

B. Representative fluorescence images showing real-time monocyte (Calcein-AM, green fluorescent probe) adhesion to an endothelial monolayer (CM-DiI, red fluorescent probe) after 1, 5 and 10 minutes dynamic co-culture. Scale bars represent 50μm.

#### 3.2.7.5 NF-κB INHIBITION REDUCED AHSS-INDUCED MONOCYTE ADHESION TO THE LSV ENDOTHELIUM

Having shown a reduction AHSS-induced monocyte adhesion *in vitro,* corroboration of this finding in an *ex vivo* setting with human LSV sections exposed to AHSS, was attempted. LSV segments were pre-treated with 50μmol/L BAY11-7085, or 0.5%(v/v) DMSO, for 3 hours. Vein sections were then exposed to AHSS for 6 hours using the *ex vivo* perfusion model. Following AHSS exposure, veins were then incubated in static conditions with THP-1 monocytes for 15 minutes to permit adhesion.

No difference was noted in static controls treated with BAY11-7085 or DMSO (FIGURE 3.20.A. and B.). However, exposure to AHSS significantly enhanced monocyte adhesion to the venous endothelial surface compared to levels observed in static controls and BAY11-7085 pre-treatment suppressed this back to static control levels (FIGURE 3.20.A. and B.).

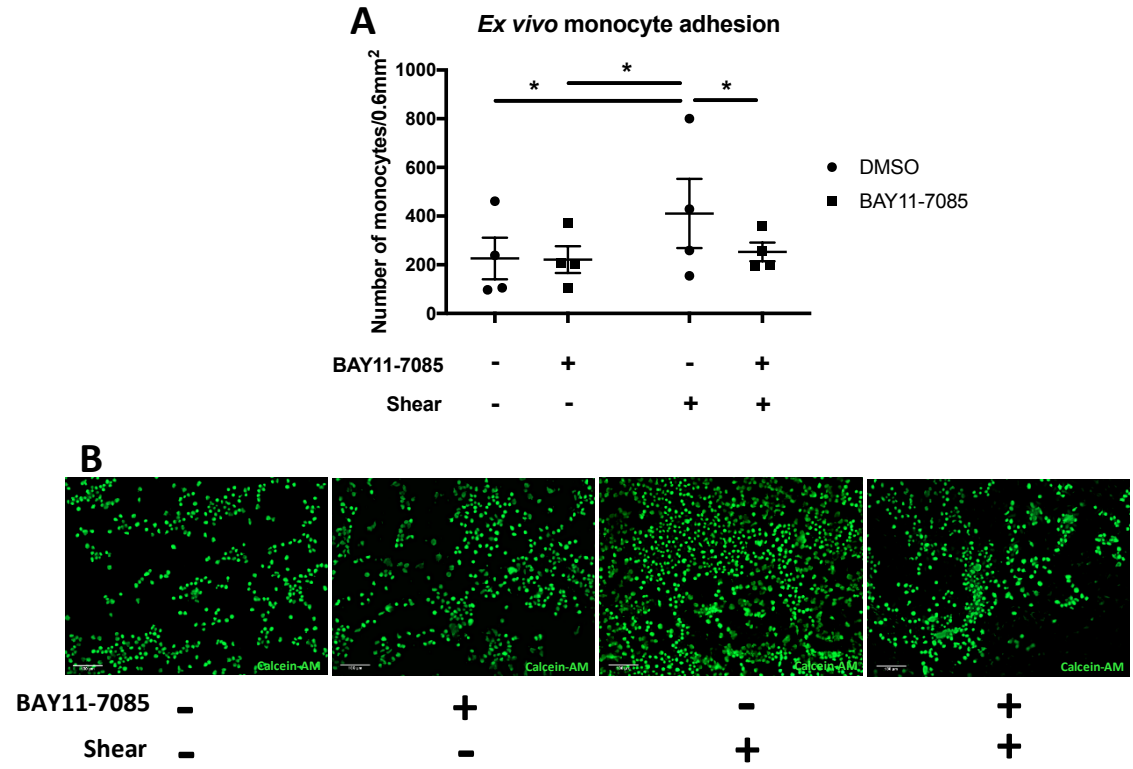


**FIGURE 3.20. BAY11-7085 retarded AHSS-induced monocyte adhesion to the LSV endothelium**

Calcein-labelled monocytes adhered to the LSV endothelium, both with and without NF-κB inhibition, were enumerated following exposure to AHSS or maintenance in static conditions and represented as a total number of monocyte adhered within a given area (0.6mm$^2$) of the endothelium.

A. Mean number of monocytes adhered to the LSV endothelium in 5 equally spaced images taken across the luminal surface. * indicates $p<0.05$; Two-way ANOVA followed by post-hoc pairwise comparisons with Bonferroni correction for multiple comparisons, n=4.

B. Representative MIP images of adhered monocytes (green). Scale bars represent 100μm.

## 3.3 DISCUSSION

### 3.3.1 INTRODUCTORY SUMMARY

Immediately after grafting of the LSV into the arterial circulation during CABG surgery, ECs become activated in response to altered haemodynamics, the precise impact of this on vein graft outcome still remains unclear. Many *in vivo* and *ex vivo* studies into IH development have focussed on reduction of lesion development at late time-points, and the early adaptive response of the vein graft is often overlooked or is considered to be of less consequence (Stark Stark *et al.*, 1997; Shintani *et al.*, 2002; Kwei *et al.*, 2004; Jiang *et al.*, 2009; Owens, 2010). An improved knowledge of the initiation and regulation of the acute response to grafting is therefore necessary for the design of therapies which may successfully affect both acute and chronic stages of vein graft pathogenesis.

Activation of the endothelium requires the convergence of numerous elements of the adaptive and innate immune responses, from antigenic responses to secretion of chemokines (Pober *et al.*, 2007; Gimbrone *et al.*, 2016). It is recognised that such immune responses are triggered in the vein graft and many chemokines and cytokines have been implicated at various stages in the vein graft remodelling process (Ward *et al.*, 2017). Several *in vivo* studies have explored the actions of MCP-1 and vein graft-monocyte interactions in the development of vein graft disease, both acutely and chronically (Weber *et al.*, 1999; Roque *et al.*, 2002; Schober *et al.*, 2004; Schepers *et al.*, 2006, 2006; Fu *et al.*, 2012). Furthermore, Golledge *et al*. investigated the role played by biomechanical forces on acute endothelial activation in the vein graft. They were able to demonstrate that, after only 45 minutes of acute arterial, haemodynamic stimulation, there was an induction of ICAM-1 expression in the vein graft endothelium (Golledge *et al.*, 1997; Golledge *et al.*, 2000). However, the elements which drive the regulation of this inflammatory network acutely in the vein graft endothelium, are relatively poorly defined (Deshmane *et al.*, 2009).

Co-ordination of EC inflammatory activation is hugely complex and falls generally into two temporally distinct phases. Type I activation is a rapid response to harmful inflammatory stimuli, which is $Ca^{2+}$-dependent and typically lasts less than 10 minutes, post-stimulus (Pober *et al.*, 2007). Whereas, type II activation is induced by more prolonged inflammatory stress stimuli; this type of activation, in response to biomechanical- or cytokine-induced stimulation, involves the convergence of MAPK, AP-1 and NF-κB signalling (Pober *et al.*, 2007). These processes have been extensively characterised in cultured ECs and, as such, both types of EC activation have been observed in response to pro-inflammatory acute shear stress stimulation (Lan *et al.*, 1994; Baeuerle *et al.*, 1994; Khachigian *et al.*, 1995; Bhullar *et al.*, 1998; Ahmad *et al.*, 1998; Dong *et al.*, 2002; Hay *et al.*, 2003). However, the actions of these distinct EC activation processes have been scarcely explored in the vein graft endothelium, where acute EC activation is known to occur. In this chapter, EC type II activation in the LSV endothelium in response to AHSS was investigated; focussing on the NF-κB classical pathway.

### 3.3.2 PRO-INFLAMMATORY ACTIVATION OF vECs UNDER AHSS

The development and characterisation of the endothelial inflammatory response to shear stress was established by many formative studies into mechanosensation and mechanotransduction (Dewey *et al.*, 1981; Shyy *et al.*, 1994; Nagel *et al.*, 1994; Li *et al.*, 1996; Gimbrone *et al.*, 1997; Takahashi *et al.*, 1997; Kim *et al.*, 2001; Chiu *et al.*, 2004; Li *et al.*, 2005). In these studies, the pro-inflammatory transcriptional output of cytokines and adhesion molecules were used as surrogate markers for shear-activated ECs. In this chapter, known NF-κB target genes, MCP-1, IL-6, IL-8 and ICAM-1, were chosen as transcriptional markers of inflammation owing to their recognised roles in vein grafting and shear stress responsiveness (Pahl, 1999; Ascione *et al.*, 2000; Crook *et al.*, 2000; Chiu *et al.*, 2004; Schepers *et al.*, 2006; Nguyen *et al.*, 2016). Finally, MCP-1 was selected as the inflammatory marker to be examined in depth, as the chemokine has been relatively well established as partly causative in vein graft disease and, when the MCP-1

pathway is blocked, the potential implications for the resolution of IH are profound (Stark *et al.*, 1997; Roque *et al.*, 2002; Schepers *et al.*, 2006; Fu *et al.*, 2012). In response to AHSS (at 12dyn/cm$^2$) for 90 minutes and 2 hours, transcript levels of all pro-inflammatory markers were increased in ECs in culture, consistent with previous studies (Resnick *et al.*, 1995; Shyy *et al.*, 1994). Whereas ECs exposed to ALSS (at 0.5 dyn/cm$^2$) did not up-regulate pro-inflammatory transcripts at either time-point. Thus, validating a venous, but not arterial, pro-inflammatory response to AHSS, and corroborating the formative mechanotransduction studies mentioned above.

Following confirmation of a pro-inflammatory response to AHSS in venous ECs in culture, it was necessary to examine the same transcriptional response in LSV ECs *ex vivo*. In the LSV, only transcript levels of MCP-1 were significantly increased after 2 hours exposure to flow. The observed increased in MCP-1 increased at the transcript level in LSV ECs was also supported by augmented MCP-1 protein levels, following AHSS exposure for 6 hours. Schepers et al. demonstrated increased levels of endothelial MCP-1 and monocyte-endothelial interactions in a murine interpositional vein graft model, 6 hours after implantation of the vessel (Schepers *et al*., 2006). These concordant findings, from a human *ex vivo* model and murine *in vivo* model, support the hypothesis that it is early exposure to an altered haemodynamic environment which is the trigger for initiation of adhesion and inflammation (Schepers *et al*., 2006). However, levels of the other pro-inflammatory mRNA transcripts, IL-6, IL-8 and ICAM-1, did not increase by 120 minutes, most likely due to the variability between samples. Increased experimental repeats are required in future experiments as the relative fold increase compared with static control was reasonably large. It is possible that these results may have been confounded by the analysis of a mixed population of vascular cells due to the EC RNA isolation method. Currently, no reliable method exists to directly isolate EC RNA from a vessel without mechanically removing the cells first, by trypsination, scraping or collagenase digestion and bead detection, which may affect gene expression (Jaffe *et al.*, 1973; Vara *et al.*, 2005; Luo *et al.*, 2016). However, Nam et al. utilise

a method which allows the instant isolation of RNA from the intima, producing RNA largely from ECs (Nam *et al*., 2009). Although this technique is imperfect, owing to the extraction of intimal RNA, not solely EC RNA, it allows the immediate transcriptional state of the intima and ECs within it to be assessed. As such, the transcriptional response of the endothelium to AHSS, examined in the LSV, may have been influenced by the presence of a pre-existing neointima, containing diffuse VSMCs and fibroblasts (Wan *et al*., 2012; Prim *et al.*, 2016).

Further *in vitro* evidence of the acute nature of the pro-inflammatory response to shear showed that, after 4 hours of high shear, HUVECs had upregulated MCP-1 protein levels; a transient response which was lost *in vitro* by 6 hours. This was entirely in-keeping with a previous observation of a biphasic regulation of MCP-1 expression to shear stress, whereby transcript levels initially peaked after approximately 2 hours and reduced to below baseline levels by 4 hours (Shyy *et al*., 1994). This initial spike, described by Shyy *et al*., was followed by a second increase in levels after 24 hours (Shyy *et al*., 1994). The potential reasons for this complex regulation may relate to the enhancer regions within the promoter of MCP-1, which contains multiple *cis*-regulatory elements acting to control transcription of the chemokine (Ueda *et al.*, 1994; Shyy *et al.*, 1995; Shyy *et al.*, 1995; Ueda *et al.*, 1997; Yadav *et al.*, 2010). Two NF-κB binding sites exist upstream of the transcriptional initiation site, which are both bound by NF-κB following cytokine-mediated activation via IL-1β or TNF-α (Ueda *et al.*, 1997; Yadav *et al.*, 2010). Shyy *et al*. also discovered the existence of two further *cis*-regulatory elements in the proximal promoter region of MCP-1, which, under shear stress conditions (after 8 hours), are bound to by the *trans*-acting factor, AP-1 (Shyy *et al.*, 1995). Furthermore, it has been proposed that cytokine-mediated MCP-1 expression requires the combined action of both NF-κB and AP-1 (Martin, 1997). Consequently, the biphasic shear stress regulation of MCP-1 expression, at the transcript and protein levels, may be acutely driven by the action of NF-κB and later by the involvement of AP-1, between 8 and 24 hours (long after the latest time-points observed here).

### 3.3.3 ACTIVATION OF NF-κB UNDER AHSS

Having established that ECs were activated under AHSS, both *in vitro* and *ex vivo,* the potential mechanism for the EC activation observed in the LSV endothelium was investigated. The NF-κB classical pathway was chosen owing to its established role in the initiation of EC activation in atherogenic lesions, as well as it's shear stress responsiveness (Lan *et al.*, 1994; Khachigian *et al.*, 1995; Bhullar *et al.*, 1998; Hay *et al.*, 2003; Lehoux *et al.*, 2006). Initially characterised *in vitro* by Lan *et al*., NF-κB is activated as quickly as 30 minutes after the onset of 12dyn/cm$^2$ shear stress, with a peak at 60 minutes. These results are in concurrence with the data presented in this chapter, whereby a peak of NF-κB nuclear translocation at 30 minutes after AHSS onset and a reduction by 90 minutes were observed, though nuclear levels of NF-κB were still significantly above that of static controls at 90 minutes.

The reciprocal reduction in IκBα levels due to degradation of the innate inhibitor are another hallmark of the activation of the NF-κB classical pathway (Hayden *et al.*, 2008). This was confirmed by the findings within this chapter, in which a significant reduction in the cytosolic levels of IκBα was observed at both 30 and 90 minutes after AHSS onset. Previous studies have shown, however, that after an initial decrease, there is a recovery of IκBα expression to near baseline levels after 60 minutes exposure to AHSS (Bhullar *et al.*, 1998). This disparity between the current data and previous findings may be explained by the use of ECs from different vascular beds and species. Bhullar *et al*. examined the IκBα response to shear stress with bovine arterial ECs (BAECs), as opposed to HUVECs used here. This discrepancy in the length of NF-κB classical pathway activation under shear stress, may be due to the fact that arterial ECs are innately less responsive to inflammatory, biomechanical stimulation compared with venous ECs. This most likely explains the rapid and transient degradation of IκBα in aECs compared to the more persistent reduction of IκBα in vECs (Aitsebaomo *et al.*, 2008; Zakkar *et al.*, 2011).

Translocation of NF-κB into the nucleus upon activation is necessary, but not always sufficient, to evoke a transcriptional response (Karin *et al.*, 2000). Additional post-translational modifications are often required in order to reduce the affinity of interactions between NF-κB and the IκB proteins or to mount an effective transcriptional response (Hayden *et al.*, 2008). Amongst the most important of the positive regulatory modifications is inducible phosphorylation. In response to AHSS, phosphorylation of NF-κB at Serine residue 276 (Ser-276) was observed transiently after 30 minutes and decreased again after 90 minutes AHSS exposure. Whereas, no change was observed in phosphorylation at Ser-536 (data not shown) under AHSS, Observation of covalent modification to NF-κB under AHSS provides further support to the conclusion that the NF-κB classical pathway is activated. As only one of the two primary phosphorylation sites were modified under flow, alteration of this site (Ser 276) provides a possible approach for the therapeutic targeting of flow-activated NF-κB in the vein graft endothelium.

Ser-276 is located within the Rel Homology domain (RHD) of NF-κB (p65), which is directly responsible for DNA binding at the κB site and NF-κB subunit hetero-dimerisation (Hayden *et al*., 2008). Whilst the Ser-536 phosphorylation site is located within the transcription activation domain (TAD) of NF-κB, responsible for regulation of transcriptional activity (Christian *et al.*, 2016). Inducible phosphorylation at Ser-276 enhances the oligomerisation properties of NF-κB with transcriptional co-activators (p300 and CREB-binding protein (CBP)) and promotes the transcriptional response via a disruption of negative transcriptional regulator, Histone Deacetylase (HDAC1) complex (Chen *et al.*, 2004). Phosphorylation at this site after 30 minutes exposure to AHSS is consistent with the observation that there was an increased binding affinity to the κB-oligonucleotide. A lack of phosphorylation at Ser-536, however, may be explained by the observation that Ser-536 phosphorylation has been linked to the resolution of inflammation, through promotion of increased NF-κB turnover and a subsequent reduction in its activity

(Christian *et al.*, 2016). It is entirely possible that, however, due to the rapid temporal dynamics of NF-κB covalent modifications, phosphorylation at Ser-536 may have been missed by time-point selection either before 30 minutes or between 30 and 90 minutes. Mutational analyses of both of these residues would be an intriguing follow up, to attempt to uncover whether the NF-κB response was abrogated under shear stress with one or both phosphorylation sites altered.

Replication of the observations presented in formative studies by Bhullar *et al*. and Lan *et al*., *in vitro*, led to the development of a novel *en face* preparation method combined with novel 3D imaging and analysis in this chapter. This method was developed in order to interrogate NF-κB nuclear translocation, *ex vivo*, in the LSV endothelium. Using this technique, a significant increase in nuclear levels of NF-κB in LSV ECs under AHSS was apparent, following exposure for both 30 and 90 minutes. Nuclear translocation was more pronounced at 90 minutes in LSV ECs, compared with the observed 30 minutes, *in vitro*. This later NF-κB translocation in LSV ECs also supports the observation that NF-κB target gene transcript levels increase only after 2 hours, as opposed to 90 minutes in the *in vitro* setting. This provides the first evidence that NF-κB is activated in the LSV endothelium in response to the exposure to acute arterial haemodynamics and not, as Hinokiyama *et al*. suggest, in response to vein graft harvest and surgical preparation (Hinokiyama *et al.*, 2006).

### 3.3.4 NF-κB INHIBITION AND THE PRO-INFLAMMATORY RESPONSE

Having established that NF-κB was activated, and MCP-1 levels were increased concurrently in the LSV endothelium following AHSS exposure, the proposed mechanism was then directly explored via inhibition of NF-κB before the onset of arterial flow, *in vitro* and *ex vivo*. Firstly, *in vitro* results showed that inhibition of NF-κB, both pharmacologically and using an adenovirus-mediated gene delivery approach to overexpress IκBα (WT-IκBα), prior to shear exposure, prevented the subsequent transcriptional response of MCP-1 (as well as IL-6, IL-8 and ICAM-1).

Furthermore, with WT-IκBα infection, there was a reduction in MCP-1 protein levels after 4 hours of AHSS, an effect which was lost after 6 hours. Finally, the increase in MCP-1 levels at 4 hours in rAd66 control samples was not observed as in untreated cells (as mentioned above). This may have been due to a heightened initial inflammatory response caused by the innate immune response induced by exposure to the adenoviral vectors (Gregory *et al.*, 2011).

In addition, these results were replicated in the LSV, *ex vivo*, whereby pre-treatment with an NF-κB inhibitor, significantly reduced MCP-1 protein levels to baseline after 6 hours exposure to flow. This observation was further substantiated, functionally, both *ex vivo* and *in vitro*; wherein, NF-κB pre-inhibition abrogated AHSS-induced monocyte adhesion to the venous endothelium. These data not only validate the mechanistic involvement of NF-κB in AHSS-driven inflammation, but also provide an exciting therapeutic target in the treatment of vein graft inflammation, as many pharmacological inhibitors of NF-κB are already approved for clinical use (Gilmore *et al.*, 2006; Miller *et al.*, 2010). Whilst NF-κB inhibition poses certain problems systemically, due to the pleiotropicity and homeostatic functions of the pathway, the harvest of autologous LSV uniquely sidesteps these problems, as it is possible to use the inhibitor locally, prior to implantation (Fraser, 2006).

Several studies have shown that *in vivo*, local NF-κB inhibition, using a decoy *cis*-element (κB-oligodeoxynucleotide(κB-ODN)), siRNA-mediated knockdown or alternative gene therapy approach to overexpress IκBα, limits IH development in multiple vein graft models (Shintani *et al.*, 2002; Miyake *et al.*, 2006; Wang *et al.*, 2007; Miyake *et al.*, 2007). These studies propose the same conclusions for their observed results; that it is the actions of NF-κB inhibition on reduction of medial VSMC proliferation and migration, which is ultimately responsible for reducing IH formation. The role of NF-κB in the acute adaptive response of the vein graft to its new environment is largely overlooked. Perhaps a combined approach of acute, rapid-acting, pharmacological NF-κB inhibition, locally in the LSV endothelium, in conjunction with a

prolonged, gene therapy approach, may represent a further improved therapeutic strategy in IH reduction. Therapeutic strategies to target the vein graft endothelium, in particular NF-κB, will be expanded upon in the general discussion

In addition to the problems associated with systemic inhibition of NF-κB, there also exists the necessity for opposing apoptotic conditions between ECs and VSMCs in the vein graft. It has been suggested that, in vein graft VSMCs, NF-κB activation and anti-apoptotic functions, induced by cyclical stretch and oxidative stress, acts to counterbalance the action of pro-apoptotic p38-MAPK pathways triggered under these conditions (Mayr *et al.*, 2002; Lehoux *et al.*, 2006; Castier *et al.*, 2009; Pedrigi *et al.*, 2017). Thus, when NF-κB is inhibited in vein graft VSMCs, the protective, anti-apoptotic role played by the transcription factor against cell death is lost and the balance is tipped in the favour of apoptosis. This indirect effect of increased apoptosis in VSMCs positively contributes to reduced intimal cell density and vessel wall thickness; features which are beneficial for IH reduction (Moore *et al.*, 2001; Lehoux *et al.*, 2006). In contrast, the loss of anti-apoptotic functions of NF-κB in ECs, and the potentially concomitant increased action of pro-apoptotic pathways, may be detrimental to the LSV endothelium, and thus, vein graft patency; which clearly represents a tentative aspect of this study.

Owing to the extremely acute time-points addressed here and the investigation of the role of NF-κB in EC activation and inflammation, apoptosis was not focussed upon in LSV ECs in response to AHSS. Though it appears that, from observational, preliminary work performed, that even with a functionally active (and anti-apoptotic) NF-κB pathway, EC denudation may still occur under AHSS. This suggests that the anti-apoptotic activity of NF-κB is not sufficient to prevent EC loss. This gap in knowledge, regarding the potential mechanisms of denudation of the endothelium in the adaptive vein graft response, represents a substantial challenge in the field. Whether denudation is purely due to the mechanical effects of high shear stress, is a

mechanistic consequence of activation of the endothelium, is due to a loss of focal adhesions, or is to the result of loss of anti-apoptotic and protective pathways, remains to be answered.

This question of the effect of NF-κB inhibition on later-stage EC preservation was loosely addressed by Miyake et al. in two *in vivo* models of IH. They propose that NF-κB inhibition helps to promote endothelial function and integrity in both a vein graft and balloon-catheter arterial injury model (Miyake *et al.*, 2006; Miyake *et al.*, 2014). However, direct damage to the native endothelium was not assessed in either model, either acutely or in a more prolonged context. Firstly, the murine vein graft was distended upwards of 300mmHg for 10 minutes in order to transfect the vessel with the κB-oligodeoxynucleotide (ODN); a pressure which induces considerable activation in the endothelium and stimulates considerable EC loss within 2 hours after grafting (Angelini *et al.*, 1990; Hinokiyama *et al*., 2006; Miyake *et al*., 2006). In contrast, arterial injury models are known to almost entirely disrupt the integrity of the endothelium leaving very little intact endothelium (Xu, 2004). Both studies by Miyake *et al*., assessed endothelial properties of relaxation and endothelial coverage 28 days after implantation, making the results into EC function difficult to interpret, as the monolayer may have been primarily composed of new or re-endothelialised cells (Xu *et al.*, 2003; Miyake *et al*., 2006; Miyake *et al*., 2014). Nonetheless, they also show an increase in active B-Cell lymphoma 2 (Bcl2) apoptosis regulator after 1 week in the remaining ECs, following treatment with κB-ODN containing nanospheres, suggesting that NF-κB inhibition in ECs may not affect the protective, anti-apoptotic functions of NF-κB (Miyake *et al*., 2014). This suggests that perhaps if the vein graft were to be minimally manipulated (i.e. not distended at high pressure as Miyake *et al*. did), then NF-κB inhibition may, in fact, be able to help preserve an intact monolayer upon grafting through promotion of NF-κB-driven Bcl2-mediated anti-apoptotic pathways. Thus, the preservation of a functional vein graft endothelium, with and without NF-κB inhibition, at later

time-points than those observed in the current results, and earlier than the 1 week in the study by Miyake et al., would certainly be of necessity for future investigations.

NF-κB is known to have conflicting functions in both survival and inflammation, particularly under shear stress stimulation at acute and prolonged time-points (Partridge *et al.*, 2007; Orr *et al.*, 2008). It is not evident whether, beyond the acute phase of NF-κB inhibition proposed here (first 6 hours), there will be a delayed action of NF-κB or whether ECs will have been sensitised to, and therefore protected against, the effects of high shear stress. Prolonged exposure to high shear stress in ECs in culture, beyond 16 hours, activates cytoprotective transcriptional pathways, involving the switching of NF-κB to a pro-survival phenotype by PKCζ and ERK1/2, as well as the activation of cytoprotective transcription factors, Nrf2 and Klf2 (Partridge *et al*., 2007; Boon *et al.*, 2009; Mason, 2016). It may be possible that, beyond the initial activation phase in the vein graft endothelium (between 0-8 hours), ECs are sensitised to inflammatory flow stimulation and exhibit a cytoprotective phenotype. Certainly, data related to overexpression of IκBα, presented here, suggests that beyond the acute phase of shear exposure, there is a shift in EC phenotype towards protection and away from inflammation. This effect is shown particularly strongly by the transient disruption of endothelial cell-cell contacts, indicative of a leaky and activated endothelium, at 4 hours, and the subsequent recovery of the monolayer integrity by 6 hours, as well as the acute and transient response of MCP-1 to flow. Sensitisation of ECs to pro-inflammatory shear and the switching of NF-κB to a pro-survival phenotype may also partially explain the observation of Miyake *et al*., whereby acute NF-κB inhibition led to later enhancement of Bcl2-mediated pro-survival pathways in the vein graft endothelium (Miyake *et al*., 2014).

As with the studies of Miyake *et al*. mentioned above, the benefit of inhibiting acute EC activation at the transcriptional level, is that it provides a more comprehensive inhibition of inflammatory processes in vein grafts, despite the potential pleiotropic problems addressed

earlier. Prevention of the MCP-1 and adhesion cascade response represents a critical feature in the inhibition of vein graft inflammation. Many studies have linked the inhibition of the MCP-1/CC-motif receptor 2 (CCR2) axis with an improved outcome following induction of various injurious *in vivo* cardiovascular pathologies, from vein grafting to femoral artery wire-induced injury (Schober *et al.*, 2004; Schepers *et al.*, 2006; Fu *et al.*, 2012). Initially, in response to vascular injury, MCP-1 functions as part of the early, complex network of chemokines, including IL-8, RANTES, Fractalkine and CC-chemokine ligand 5 (CCL5), that drive the arrest and adhesion of circulating monocytes to the endothelium (Gerszten *et al.*, 1999; Charo *et al.*, 2004). This is then followed by a secondary surge in MCP-1 levels approximately 1 week after implantation of the graft (Stark *et al.*, 1997; Schepers *et al*., 2006).

Involvement of the MCP-1/CCR2 axis, and subsequent recruitment of monocytes, has been widely recognised as integral in the inflammatory-driven development of IH in the vein graft (Schober *et al.*, 2004). Inhibition of the pathway, with a competitive CCR2 receptor antagonist (7ND-MCP-1) or homozygous $CCR2^{-/-}$ knockout rodent vein graft models, both show reductions in intimal thickness up to 28 days after surgery (Roque *et al.*, 2002; Schepers *et al*., 2006). Interestingly, both of these studies highlight the importance of MCP-1 as a potent mitogenic stimulus for VSMCs and emphasise the significant impact that the paracrine actions of MCP-1 have in IH development (Roque *et al*., 2002; Schepers *et al*., 2006). However, more recently, Fu et al. have suggested that alteration of the MCP-1/CCR2 axis in graft intrinsic VSMCs is of no bearing in enhancing VSMC proliferation or, ultimately, IH progression (Fu *et al*., 2012). They go further to suggest that it is, in fact, solely the depletion of this chemokine axis in graft extrinsic monocytes, which influences IH development in the vein graft (Fu *et al.*, 2012). Despite this contention, if the MCP-1/CCR2 axis can be reduced, both acutely and chronically, in the vein graft endothelium via NF-κB inhibition, then monocyte adhesion, mediated by MCP-1 and a multitude of other related factors, can altogether be prevented, thus preventing the ensuing mitogenic actions of invading monocytes (Weber *et al.*, 1999). Thus, targeting of the MCP-

1/CCR2 axis and other chemokines upstream, at the gene regulatory level, via NF-κB, represents a more wide-ranging therapeutic target in the prevention of initiation of the inflammation and ensuing deleterious monocyte adhesion.

### 3.3.5 CONCLUSION

The present chapter explored the pro-inflammatory activation of the venous endothelium under acute arterial shear stress, and the involvement of the NF-κB classical pathway in the co-ordination of this response. In order to investigate these questions, parallel experiments were carried out in vECs, both in culture and in the LSV. It was initially established that AHSS induced a pro-inflammatory response in vECs in both settings, demonstrated by increased pro-inflammatory cytokine production, monocyte adhesion and reduced cell-cell contacts between ECs. Most importantly, this study has, for the first time, identified NF-κB as a major orchestrator of this pro-inflammatory response to arterial haemodynamic stimulation in the vein graft endothelium. Further to this, it was shown that inhibition of this pathway prior to AHSS onset was sufficient to abrogate the pro-inflammatory response, both observationally and functionally. Taken together, these findings indicate the crucial role played by NF-κB in the control of the acute adaptive response of the vein graft endothelium to arterial flow, as well as providing insight into the pertinence of NF-κB inhibition in the prevention of this response. Moreover, several novel techniques to interrogate endothelial behaviour in cells in culture and human vessels have been developed to enable the analyses in this chapter, including analysis of monolayer structure *in vitro* and *en face* preparation and analysis of the endothelium in tissue. Further investigation as to the applicability of acute NF-κB inhibition in the treatment of vein graft inflammation *ex vivo* and *in vivo*, using the techniques developed in this chapter, would certainly help to elucidate the longer-term effects of such a therapeutic strategy in treatment of vein graft failure.

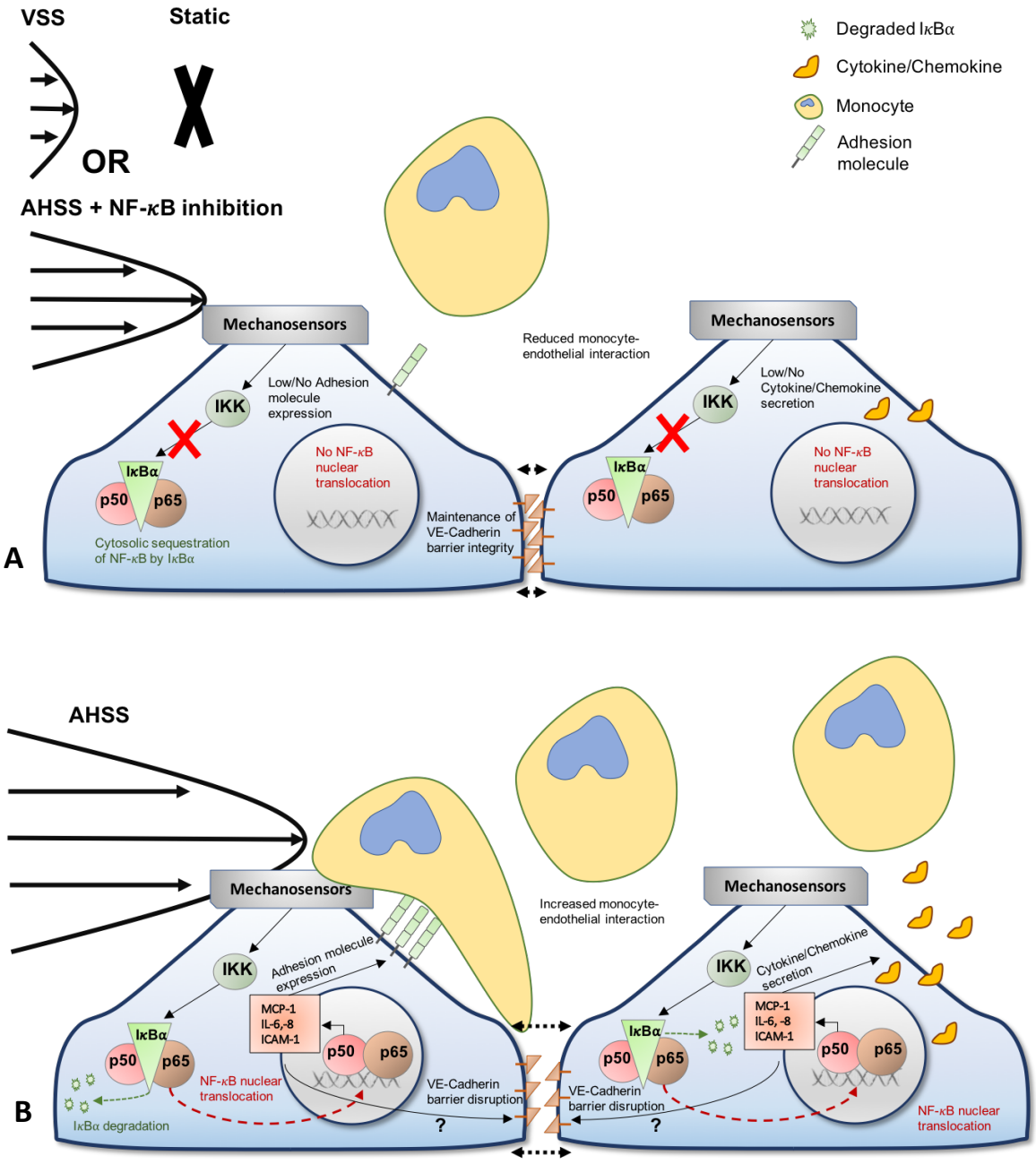


**FIGURE 3.21. EC involvement of the NF-κB classical pathway under acute shear stress**

Summary diagrams to represent findings from Chapter 3 to indicate the activity of NF-κB in ECs under (A) anti-inflammatory static conditions, venous shear stress or AHSS with NF-κB inhibition and (B) pro-inflammatory AHSS without NF-κB inhibition. Black block arrows represent pathway activation, black dotted arrows represent endothelial cell-cell contact organisation, green arrows represent degradation and red arrows represent nuclear translocation.

# 4. NRF2/KEAP1 RESPONSE TO ACUTE HIGH SHEAR STRESS IN VENOUS ENDOTHELIAL CELLS

## 4.1 INTRODUCTION

Underlying many vascular pathologies is a co-ordinated response to injury. Such injury can be commonly attributed to mechanical disruption of the vascular wall due to, for example, the actions of stenting and graft harvest, and deleterious haemodynamic stimulation, such as that following graft implantation or stent placement (Papaharalambus *et al.*, 2007). Both of which induce damage to the endothelium, resulting in a loss of its homeostatic functions, causing increases in solute permeability, loss of vasomotor tone and promotion of leukocytic adhesion (Gimbrone *et al.*, 2016). Loss of endothelial homeostasis in the vasculature is a feature implicated in the development of all vascular pathologies, and it may be partly explained by alterations of the balance from physiological redox regulation, towards pathological redox production (Brigelius-Flohe *et al.*, 2011). Imbalance between the scavenging and oxidation of physiological gasotransmitters, such as NO and carbon monoxide (CO), and their conversion into oxygen radicals, including $O_2^{\bullet -}$ and $ONOO^-$, is of paramount importance in the pathogenesis of atherosclerosis and IH (Jeremy *et al.*, 2004; Mustafa *et al.*, 2009; Brigelius-Flohe *et al.*, 2011). Excess production of ROS enhances inflammation-induction through the indirect induction of cytokine production, and more directly induces dysregulation of VSMC apoptosis, proliferation and migration, monocyte adhesion and extravasation, and, ultimately, vascular lesion formation (Papaharalambus *et al.*, 2007).

Ordinarily, ROS generation is counterbalanced by the antioxidant and cytoprotective systems through redox regulation of transcription, either by Nrf2 and NF-κB (Brigelius-Flohe *et al.*, 2011). Activation of these transcriptional systems is entirely context and stimulus dependent. However, their protective functions are primarily to promote enzymatic activities aimed towards elimination of deleterious ROS, co-operation to perform actions in drug and food metabolism, as well as removing harmful damaged proteins and DNA (Baird *et al.*, 2011). Induction of signalling via the Nrf2-ARE system promotes the transcription of numerous enzymes involved in

responses to electrophilic, oxidative or heavy-metal based stresses, including GCLM, GCLC and NQO1. Though perhaps the most important of these in the cardiovascular system is HO-1, which is responsible for diverse vascular homeostatic functions from inflammatory protection to thrombosis prevention (Durante, 2010). Using an experimental murine model of interpositional vein grafting, HO-$1^{-/-}$ mice developed a significantly increased intimal area, rich with VSMCs, within 10 days post-operatively, which demonstrates the anti-proliferative and cytoprotective dual actions of HO-1 upregulation in the vein graft wall (Yet *et al.*, 2003). This anti-proliferative action of HO-1 in VSMCs is thought to be mediated directly through its ability to arrest VSMC cell-cycle progression. It is possible however, that this response was also partly the result of an indirect effect of improved endothelial protection and re-endothelialisation, induced by a lack of HO-1 activity in native ECs and endothelial progenitor cells (EPCs) (Durante, 2010).

Numerous other studies have highlighted an anti-inflammatory role for Nrf2, independently, through the suppression of signalling via TNF-$\alpha$, IL-1$\beta$, p38 and NF-$\kappa$B (Chen *et al.*, 2006; Zakkar *et al.*, 2009; Ahmed *et al.*, 2017). Within protected regions of the vasculature, typically exposed to prolonged laminar shear stress, vascular inflammation is generally at very low basal levels, as Nrf2 and Klf2 function synergistically to suppress inflammation through promotion of the antioxidant and cellular defence responses (Fledderus *et al.*, 2008; Zakkar *et al*., 2009). Whereas, at atherosusceptible regions of the arterial tree, which are exposed to chronic disturbed or low shear stress, Nrf2 is suppressed and there is an increase in the activity of the p38-VCAM-1 axis (Zakkar *et al*., 2009). However, pharmacological induction of Nrf2 was able to partly reverse this deleterious, inflammatory effect of disturbed shear, suggesting that, in conjunction with other effectors and in certain biomechanical contexts, Nrf2 activation can prevent endothelial inflammation.

The anti-inflammatory and mechanoresponsive potential of Nrf2 in the prolonged or chronic context, as well as it's crucial role in cellular defence, have clearly been well defined previously

(Fledderus *et al.*, 2008; Zakkar *et al*., 2009; Ali *et al.*, 2009; Boon *et al*., 2009). As such, the activity and modulation of this pathway in ECs under acute biomechanical stimulation was assessed in this chapter. It was hypothesised that acute shear stress prevents activation of Nrf2 and its transcriptional response in vECs. Pre-activation of Nrf2 in vECs, prior to acute shear stress exposure, prevents a pro-inflammatory response and exerts a protective effect via an Nrf2 transcriptional response. To investigate this, firstly, the activation of the Nrf2/Keap1 pathway in ECs subjected to AHSS was assessed, *in vitro*, by cellular localisation of the transcription factor and its innate repressor, Keap1. Secondly, endothelial expression of Nrf2 target genes and pro-inflammatory genes were quantified in ECs subjected to AHSS with activation and inhibition of Nrf2 prior to the onset of high flow.

## 4.2 RESULTS

### 4.2.1 NRF2/KEAP1 RESPONSE TO AHSS

#### 4.2.1.1 AHSS UPREGULATED mRNA LEVELS OF NRF2 TARGET GENES

To initially validate whether Nrf2 was activated in ECs as a result of exposure to AHSS, the levels of Nrf2 target, ARE mRNA transcripts were compared in HUVECs with and without exposure to AHSS. HUVECs were exposed to AHSS at 12dyn/cm$^2$ for 90 and 120 minutes or maintained in static conditions. mRNA levels of HO-1, GCLM and NQO-1, were then quantified by RT-qPCR and expressed relative to static controls.

A significant increase in the level of HO-1 and GCLM mRNAs was detected in ECs exposed to AHSS for both 90 and 120 minutes, relative to static; however, no significant difference was detected in NQO-1 (FIGURE 4.1.).

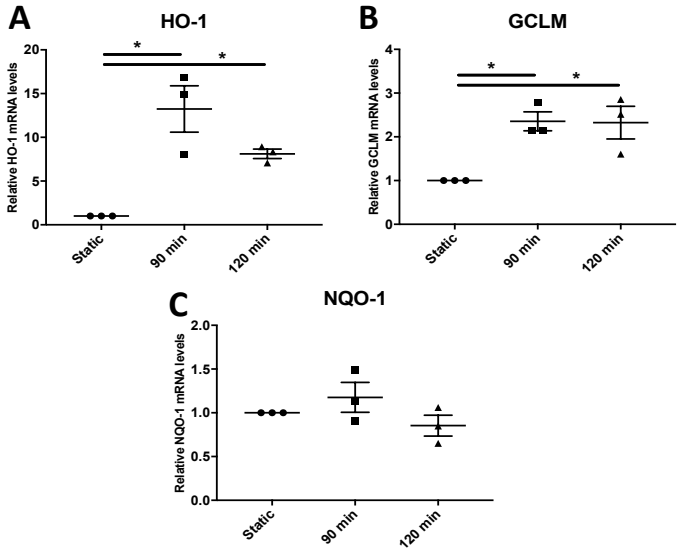


**FIGURE 4.1. AHSS upregulated mRNA levels of HO-1 and GCLM, but not NQO-1.**

Relative mRNA levels of HO-1, GCLM and NQO-1 (A, B and C, respectively) from HUVECs exposed to AHSS for 90 and 120 minutes or maintained in static conditions. mRNA levels were normalised to β-tubulin and expressed as a fold-change relative to static control. * indicates $p<0.05$, One-way ANOVA followed by post-hoc pairwise comparisons with Bonferroni correction for multiple comparisons, n=3.

#### 4.2.1.2 AHSS UP-REGULATED HO-1 PROTEIN LEVELS

With the establishment of increased mRNA levels of HO-1 and GCLM, it was necessary to investigate whether this effect was observed at the protein level. HO-1 was chosen as a representative protein of the Nrf2 response owing to the large (approximately 12-fold) increase in HO-1 mRNA levels following 90 minutes exposure to AHSS. Briefly, HUVECs were exposed to AHSS at 12dyn/cm$^2$ for 4 and 6 hours, or maintained in static conditions, then HO-1 protein levels were quantified by Western blotting.

At baseline (static), HO-1 protein levels were consistently low across samples and a significant increase in HO-1 protein level was observed after exposure to AHSS for 4 and 6 hours compared to static controls (FIGURE 4.2.).

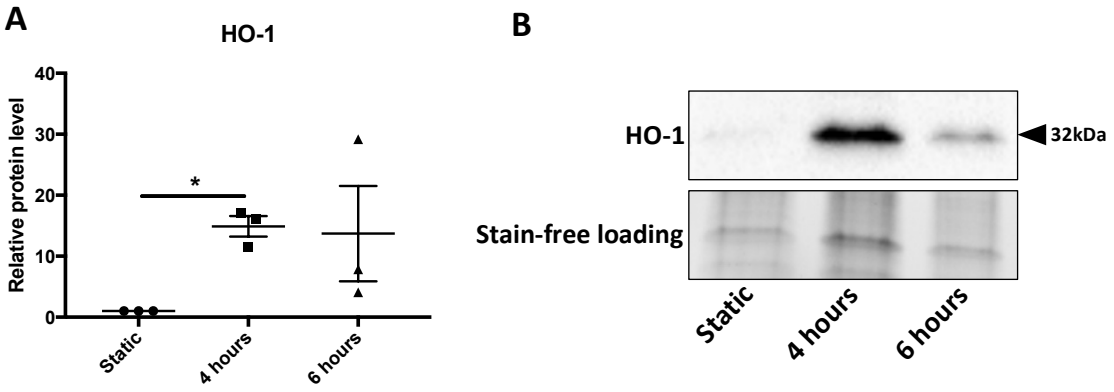


**FIGURE 4.2. AHSS increased HO-1 protein levels at 4 hours**

Relative protein levels of HO-1 were quantified by Western blotting from HUVECs exposed to AHSS for 4 and 6 hours, then normalised to stain free loading controls and expressed as a fold change relative to static. Approximate molecular weight in kDa is indicated adjacent to representative blots. * indicates $p<0.05$ vs. Static control, One-way ANOVA followed by post-hoc pairwise comparisons with Bonferroni correction for multiple comparisons, n=3.

A. Relative HO-1 protein level, normalised to stain free loading controls and expressed as a fold change relative to static
B. Representative HO-1 blot and complementary loading control

#### 4.2.1.3 AHSS PROMOTED THE NUCLEAR EXPORT OF NRF2/KEAP1

Having observed increased levels of Nrf2 target gene mRNAs in ECs following exposure to AHSS, the activation of the Nrf2 transcription factor was evaluated by examining Nrf2/Keap1 cellular localisation as an indicator of activity, using nuclear/cytosolic fractionation and Western blotting. The levels of Nrf2 and Keap1 were assessed in both the nuclear and cytosolic compartments of ECs exposed to AHSS at 12dyn/cm$^2$ for 30 and 90 minutes and compared to ECs maintained in static conditions.

Western blot analysis revealed that relative levels of Nrf2 in the cytosol remained constant at both time-points (FIGURE 4.3.A. and E.). In contrast, it was revealed that nuclear levels of Nrf2 remained constant after 30 minutes of AHSS exposure and subsequently decreased after 90 minutes (FIGURE 4.3.B. and E.). Interestingly, an increase was observed in cytosolic levels of Keap1 after 30 minutes exposure to AHSS, which had reduced by 90 minutes (FIGURE 4.3.C. and E.). This was supported by the observation that Keap1 also appeared to be exported from the nucleus, as nuclear levels were decreased after exposure to AHSS for 90 minutes, relative to static (FIGURE 4.3.D. and E.). Validation of the nuclear and cytosolic fractionation was demonstrated by very low levels of the nuclear marker, Lamin A/C, present in the cytosolic fraction and absence of cytosolic marker, GAPDH, in the nuclear fraction.

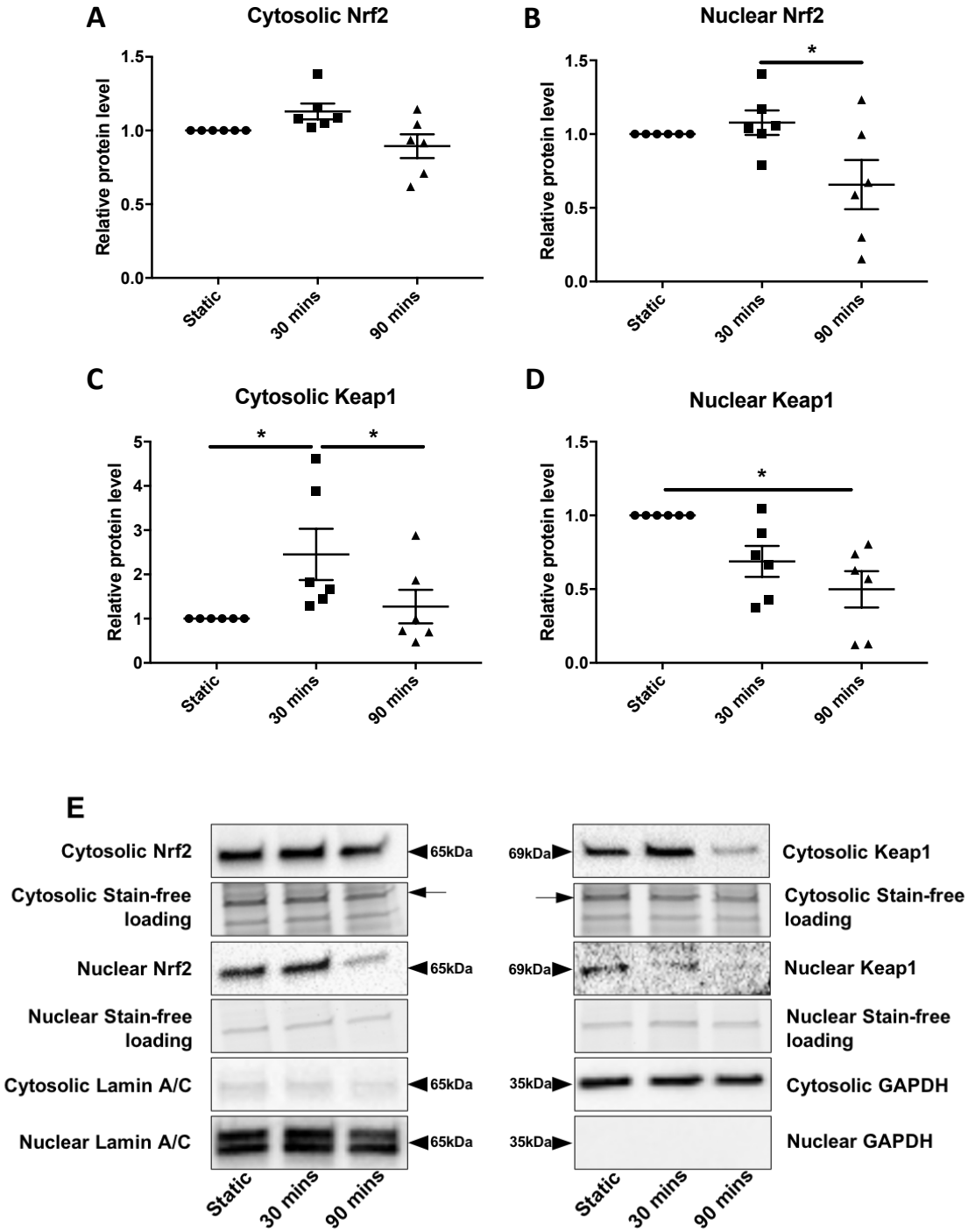
A
Cytosolic Nrf2
Relative protein level
1.5
1.0
0.5
0.0
Static
30 mins
90 mins
B
Nuclear Nrf2
*
Relative protein level
1.5
1.0
0.5
0.0
Static
30 mins
90 mins
C
Cytosolic Keap1
*
*
Relative protein level
5
4
3
2
1
0
Static
30 mins
90 mins
D
Nuclear Keap1
*
Relative protein level
1.5
1.0
0.5
0.0
Static
30 mins
90 mins
E
Cytosolic Nrf2
65kDa
Cytosolic Stain-free loading
Nuclear Nrf2
65kDa
Nuclear Stain-free loading
Cytosolic Lamin A/C
65kDa
Nuclear Lamin A/C
65kDa
Static
30 mins
90 mins
69kDa
Cytosolic Keap1
Cytosolic Stain-free loading
69kDa
Nuclear Keap1
Nuclear Stain-free loading
35kDa
Cytosolic GAPDH
35kDa
Nuclear GAPDH
Static
30 mins
90 mins

**FIGURE 4.3. AHSS triggers the nuclear export of Nrf2 and Keap1**

Relative levels of nuclear and cytosolic Nrf2 and Keap1 were quantified in cell fraction lysates by Western blotting. Detected bands were quantified by densitometry, normalised using band detected on stain free gel and expressed as relative protein level. Approximate molecular weights in kDa are indicated adjacent to representative blots. * indicates $p<0.05$, One-way ANOVA followed by post-hoc pairwise comparisons with Bonferroni correction for multiple comparisons, n=6.

A. Relative cytosolic Nrf2 protein level, normalised to stain free loading controls and expressed as a fold change relative to static.
B. Relative nuclear Nrf2 protein level, normalised to stain free loading controls and expressed as a fold change relative to static.
C. Relative cytosolic Keap1 protein level, normalised to stain free loading controls and expressed as a fold change relative to static.
D. Relative nuclear Keap1 protein level, normalised to stain free loading controls and expressed as a fold change relative to static.
E. Representative blots with complementary loading controls. Anti-clockwise from top left: cytosolic Nrf2 and loading control; nuclear Nrf2 and loading control; nuclear and cytosolic LaminA/C; nuclear and cytosolic GAPDH; nuclear Keap1 and loading control; cytosolic Keap1 and loading control. Arrow with tail represents loading band analysed where two bands can be seen.

### 4.2.2 PHARMACOLOGICAL ACTIVATION OF NRF2 AND THE ENDOTHELIAL RESPONSE TO AHSS

#### 4.2.2.1 SULFORAPHANE INDUCED NRF2 TRANSLOACTION

Sulforaphane (SFN) is an isothiocyanate found in cruciferous vegetables and is a known, potent activator of the Nrf2-driven antioxidant response (Thimmulappa *et al.*, 2002). The compound has also been effectively shown to have anti-inflammatory functions against cytokine-induced inflammation (Garstkiewicz *et al.*, 2017). The effect of SFN concentration on Nrf2 nuclear translocation was initially examined to validate the efficacy of the dosages to be used in this thesis. HUVECs were treated with varying concentrations of SFN (0.1, 0.5, 1, 2.5 and 5 μmol/L) or DMSO, at a standardised maximal concentration (0.05% (v/v)), for 4 hours. Following the 4-hour treatment, cells were fractionated into compartments, as above, using a nuclear/cytosolic lysis approach.

Significantly increased Nrf2 nuclear translocation, relative to DMSO, was observed with 5μmol/L of SFN, only (FIGURE 4.4.). However, for all subsequent experiments in this chapter, two concentrations were utilised, a low concentration of 1μmol/L, based on previous literature (Zakkar *et al*., 2008), and a high concentration of 5μmol/L, based on results observed here.

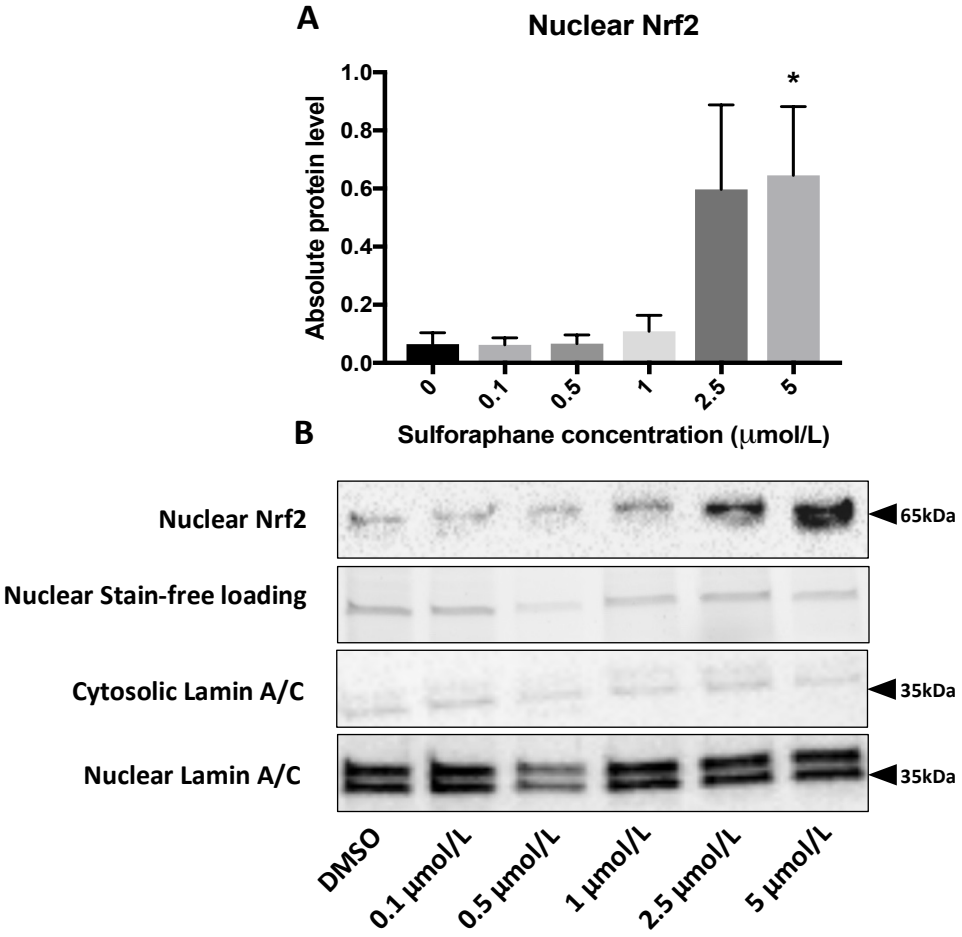


**FIGURE 4.4. Sulforaphane induced Nrf2 translocation at the maximal dosage.**

Quantification of protein levels of nuclear Nrf2 from HUVECs treated with varying concentrations of SFN (0.1, 0.5, 1, 2.5 and 5μmol/L) or DMSO (0.05% (v/v), represented graphically as 0), by Western blot analysis. Detected bands were quantified by densitometry, normalised using band detected on stain free gel and expressed as relative protein level. Approximate molecular weights in kDa are indicated adjacent to representative blots. * indicates $p<0.05$, vs. DMSO, Two-way ANOVA followed by post-hoc pairwise comparisons with Bonferroni correction for multiple comparisons, n=3.

A. Relative levels of nuclear Nrf2 protein normalised to stain-free loading control
B. Representative Western blots of nuclear fractions for Nrf2 and nuclear protein, lamin A/C. Stain-free gel used as loading control.

#### 4.2.2.2 SULFORAPHANE AND AHSS SYNERGISTICALLY ACTIVATED ARE-mRNA PRODUCTION

Having observed increased levels of ARE-genes during the acute shear stress response, the same genes were assessed, with and without SFN pre-treatment at both high and low concentrations. HUVECs were pre-treated with 1 or 5μmol/L SFN or DMSO (0.05% (v/v)) for 4 hours, and subsequently exposed to AHSS for 90 and 120 minutes. After which time, relative mRNA levels of HO-1, GCLM and NQO-1 were measured by RT-qPCR.

Treatment of HUVECs in static conditions with 5μmol/L SFN significantly increased the levels of HO-1 and GCLM, relative to DMSO controls, thus supporting the above observations of increased nuclear Nrf2 at this dosage. GCLM levels were also increased with 1μmol/L SFN treatment in static conditions, compared to DMSO-treated controls (FIGURE 4.5.). Levels of both HO-1 and GCLM in HUVECs treated with 5μmol/L SFN remained significantly greater than DMSO treated controls, following the application of 90 minutes of AHSS. As observed previously NQO-1 levels remained unchanged by exposure to AHSS, additionally SFN treatment had no effect on NQO-1 mRNA levels (FIGURE 4.5.).

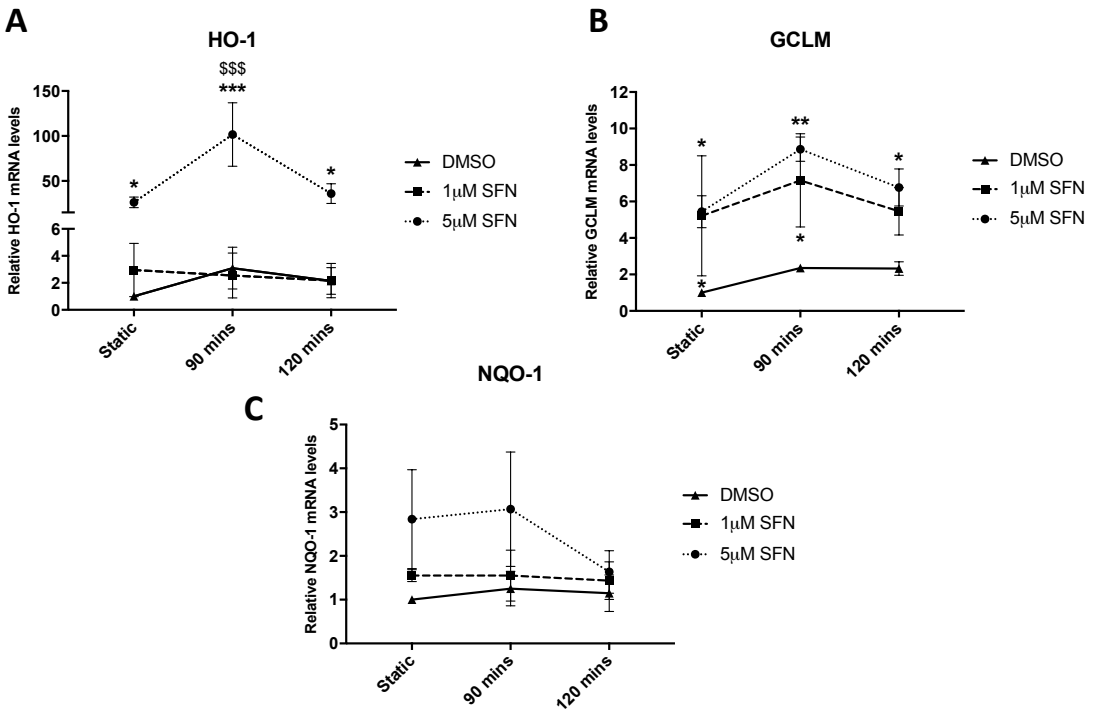


**FIGURE 4.5. SFN pre-treatment increased levels of HO-1 and GCLM, which remained enhanced with AHSS exposure.**

Relative mRNA levels of HO-1, GCLM and NQO-1 (A, B and C, respectively) in HUVECs pre-treated with either 1 and 5μmol/L SFN, or DMSO (0.05% (v/v)), and subsequently exposed to AHSS for 90 and 120 minutes or maintained in static conditions. mRNA expression data were normalised to β-tubulin and expressed as a fold-change relative to DMSO static control. * indicates $p<0.05$, ** indicates $p<0.01$ and *** indicates $p<0.001$ vs. DMSO control (equivalent time-point); $$$ indicates $p<0.001$ vs. 1μM SFN (equivalent time-point), Two-way ANOVA followed by post-hoc pairwise comparisons with Bonferroni correction for multiple comparisons, n=3.

#### 4.2.2.3 SULFORAPANE DID NOT REDUCE PRO-INFLAMMATORY mRNA LEVELS IN ECs EXPOSED TO AHSS

Many reports have linked SFN treatment to a reduction in inflammation following TNF-α induced activation of NF-κB and in other pro-inflammatory contexts (Kim *et al.*, 2010; Garstkiewicz *et al.*, 2017; Liu *et al.*, 2017). Consequently, it was examined whether SFN pre-treatment attenuated endothelial inflammatory responses in response to pro-inflammatory AHSS. As above in section 4.2.2.2, HUVECs were pre-treated with two concentrations of SFN (1 and 5μmol/L) or DMSO (0.05% (v/v) – vehicle control) for 4 hours, and subsequently exposed to AHSS for 90 and 120 minutes. After which time, relative mRNA levels of MCP-1, IL-6 and IL-8 were evaluated by RT-qPCR.

As was observed in section 3.2.1.1., AHSS exposure led to a significant induction in mRNA levels of MCP-1, IL-6 and IL-8 at both time-points. Following AHSS stimulation at both time-points, 1μmol/L SFN pre-treatment only significantly reduced levels of MCP-1 transcripts, relative to DMSO treated controls (FIGURE 4.6.A.). Pre-treatment with 5μmol/L of SFN was not able to reduce mRNA levels of pro-inflammatory genes, and, in fact, increased mRNA levels of IL-8 under both static and flow conditions (FIGURE 4.6.C.).

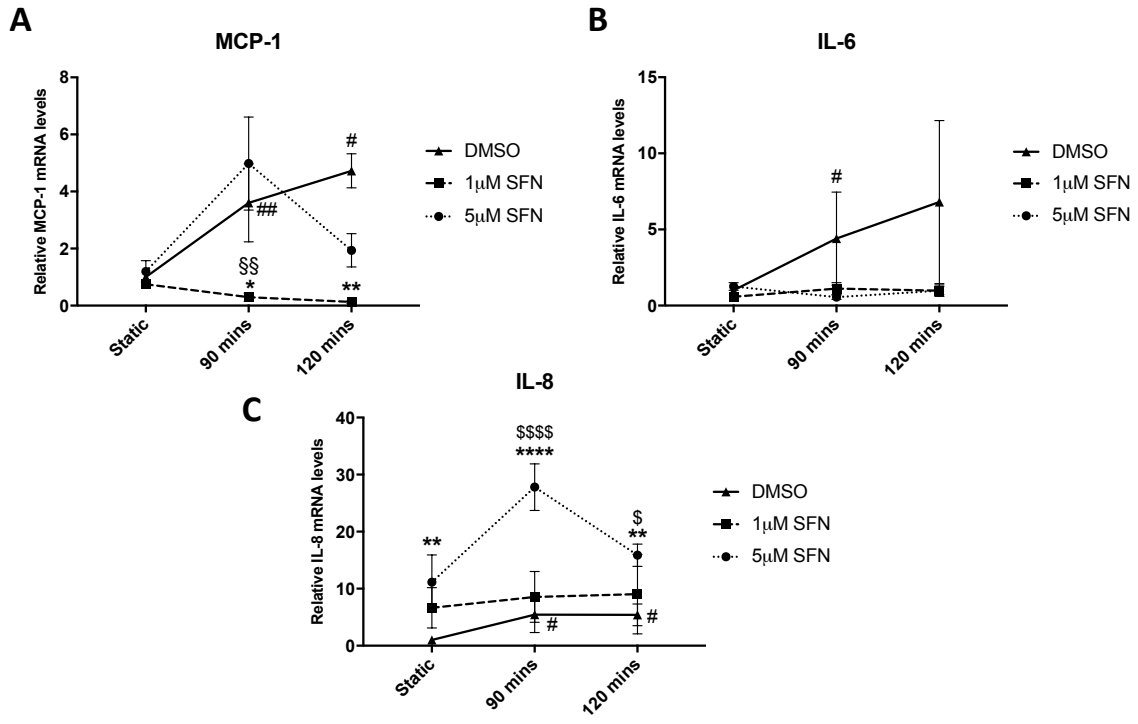


**FIGURE 4.6. SFN pre-treatment did not consistently reduce pro-inflammatory levels as a result of AHSS**

Relative levels of MCP-1, IL-6 and IL-8 (A, B and C, respectively) from HUVECs pre-treated with either 1 and 5μmol/L SFN, or DMSO (0.05% (v/v)), and subsequently exposed to AHSS for 90 and 120 minutes or maintained in static conditions. mRNA expression data were normalised to β-tubulin and expressed as a fold-change relative to DMSO static control. * indicates $p<0.05$, ** indicates $p<0.01$ and **** indicates $p<0.0001$ vs. DMSO control (equivalent time-point); §§ indicates $p<0.01$ vs. 5μM SFN (equivalent time-point); $ indicates $p<0.05$ and $$$$ indicates $p<0.0001$ vs. 1μM SFN (equivalent time-point); # indicates $p<0.05$ and ## indicates $p<0.01$ vs. DMSO-treated, static control (utilised only as evidence of pro-inflammatory induction in DMSO controls), Two-way ANOVA followed by post-hoc pairwise comparisons with Bonferroni correction for multiple comparisons, n=3.

### 4.2.3 EFFECT OF ADENOVIRAL-MEDIATED OVEREXPRESSION OF NRF2 ON THE ENDOTHELIAL RESPONSE TO AHSS

#### 4.2.3.1 VALIDATION OF ADENOVIRAL-MEDIATED OVEREXPRESSION OF NRF2 PROTEIN

In addition to pharmacological activation of Nrf2 with SFN, the effect of overexpression of Nrf2 was also investigated. This gene-therapy based method of Nrf2 overexpression was used in order to increase the levels of Nrf2 protein, thus leading to a baseline increase in the activity of the pathway prior to the onset of AHSS. Adenoviral-mediated overexpression of a wild-type form of Nrf2 (WT-Nrf2), containing an EGFP tag to directly observe transfection was utilised. Increasing concentrations of virus (pfu/mL) were used to test the optimum infection efficiency in the overexpression of Nrf2, compared to rAd66 empty viral vector control and validate overexpression. Briefly, HUVECs were cultured in the presence of either $1x10^5$, $1x10^6$ or $1x10^7$ pfu/mL WT-Nrf2 adenovirus or $1x10^7$ pfu/mL rAd66 control adenovirus for 18 hours. Following removal of the virus, cells were cultured for a further 48 hours and then Nrf2 protein expression analysed by Western blotting and fluorescence microscopy.

Firstly, microscopy analysis of the GFP-tagged adenovirus showed that a more pronounced overexpression was achieved at with WT-Nrf2, compared with rAd66 controls and the lower concentrations of WT-Nrf2. The distribution also appeared to be generally homogenous throughout the whole cell (i.e. both nuclear and cytosolic), with the exception of a portion of cells (indicated with arrows), that appeared to contain high nuclear levels of the protein (FIGURE 4.7.C.). Secondly, WB analysis showed significantly increased levels of Nrf2 in HUVECs transfected with WT-Nrf2 at concentrations of both $1x10^6$ and $1x10^7$ pfu/mL, compared with both rAd66 controls and $1x10^5$pfu/mL WT-Nrf2; Nrf2 protein levels were over 20-fold higher with $1\times10^7$ pfu/mL WT-Nrf2, compared even with $1x10^6$pfu/mL. As above in section 4.2.2.1., two concentrations ($1x10^6$ and $1x10^7$ pfu/mL) were chosen to assess the activity-dependent effect of Nrf2 activation under shear stress.

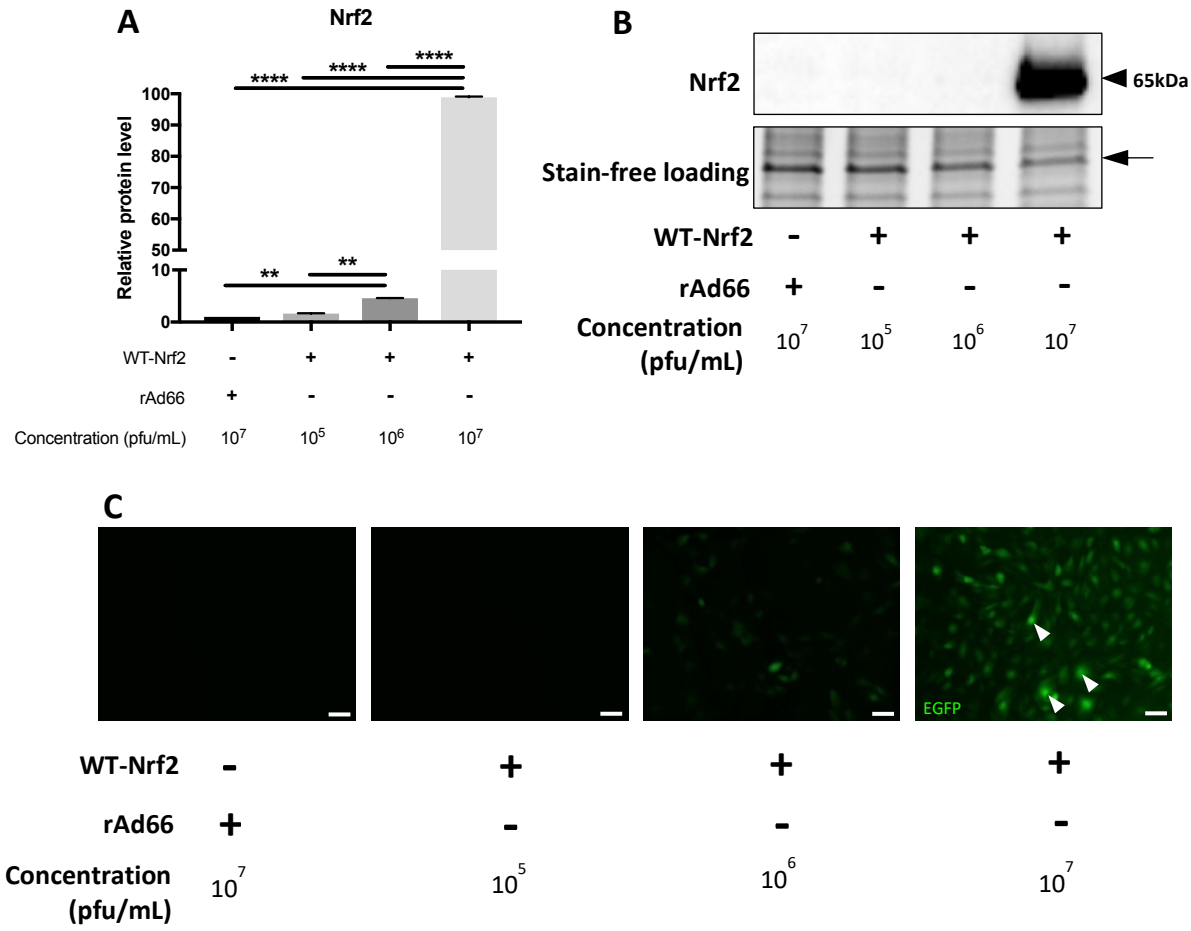


**FIGURE 4.7. Validation of adenoviral-mediated overexpression of WT-Nrf2**

Relative Nrf2 protein levels were compared in HUVECs infected with WT-Nrf2 or rAd66 control adenoviruses at varying concentrations, by Western blot analysis and EGFP assessment viewed under fluorescent light. ** indicates $p<0.01$ and **** indicates $p<0.0001$, One-way ANOVA followed by post-hoc pairwise comparisons with Bonferroni correction for multiple comparisons, n=3.

A. Relative levels of Nrf2 protein, quantified by WB analysis using SCBT Nrf2 h-300 antibody, normalised to stain free loading control and expressed relative to rAd66 ($10^7$) control.
B. Representative Nrf2 blot and stain free loading control. Arrow with tail represents band analysed.
C. Representative images of EGFP-tagged WT-Nrf2 and RAd66 at varying concentrations, viewed under fluorescent light. Arrows show cells containing high nuclear levels of Nrf2, scale bars represent 15μm.

#### 4.2.3.2 OVEREXPRESSION OF NRF2 AND AHSS INCREASED HO-1-mRNA LEVELS

To further investigate the regulation of the antioxidant response under shear stress, and its promotion via Nrf2 activation, the effect of adenoviral-mediated overexpression of Nrf2 was examined under AHSS. HUVECs were infected for 18 hours with $1x10^6$ and $1x10^7$ pfu/mL of WT-Nrf2 containing adenovirus, or rAd66 empty viral cassette control at $1x10^7$ pfu/mL; cells were then cultured for an additional 48 hours. After exposure to AHSS at 12dyn/$cm^2$ for 90 and 120 minutes, relative mRNA levels of HO-1, GCLM and NQO-1 were evaluated by RT-qPCR.

Owing to variability between independent experiments and data-points, only mRNA levels of GCLM were significantly increased in rAd66 controls under AHSS, HO-1 did not significantly increase as in section 4.2.1.1., though NQO-1 remained constant which is in concurrence with previous results. mRNA levels of all three antioxidant response genes were significantly increased following infection of HUVECs with $1x10^7$ pfu/mL WT-Nrf2 compared to rAd66 control, under static conditions, providing further validation of Nrf2 protein overexpression. Only levels of HO-1 were maintained significantly above rAd66 control samples following application of shear stress, at both viral concentrations (FIGURE 4.8.A.). Levels of both GCLM and NQO-1 remained above controls, but not significantly (FIGURE 4.8.B. and C.).

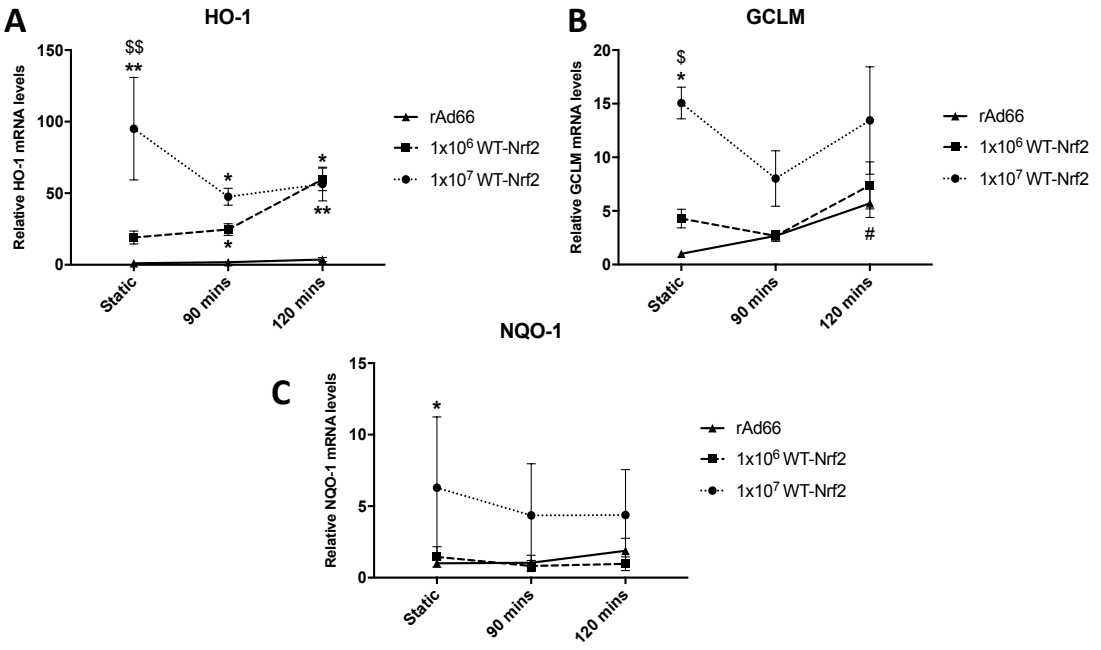


**FIGURE 4.8. Overexpression of Nrf2 increased HO-1 mRNA levels both in static and flow conditions**

Relative mRNA levels of HO-1, GCLM and NQO-1 (A, B and C, respectively) from HUVECs infected with WT-Nrf2 containing- or rAd66 control-adenoviruses, at $1x10^6$ pfu/mL and $1x10^7$ pfu/mL, and subsequently exposed to AHSS for 90 and 120 minutes or maintained in static conditions. mRNA expression data were normalised to β-tubulin and expressed as a fold-change relative to rAd66 static control. * indicates $p<0.05$, ** indicates $p<0.01$ and *** indicates $p<0.001$ vs. rAd66 control (equivalent time-point); $ indicates $p<0.05$, $$ indicates $p<0.01$ vs. $1x10^6$ WT-Nrf2 (equivalent time-point), Two-way ANOVA followed by post-hoc pairwise comparisons with Bonferroni correction for multiple comparisons, n=3.

#### 4.2.3.3 DOSE DEPENDENT EFFECTS OF OVEREXPRESSION OF NRF2 ON AHSS-INDUCED PRO-INFLAMMATORY mRNA LEVELS

To attempt to corroborate the unexpected observations seen with SFN pre-treatment and exposure to AHSS, mRNA levels of pro-inflammatory genes were assessed with and without overexpression of WT-Nrf2 using two different adenoviral concentrations (performed as above in Section 4.2.2.5.).

As expected, mRNA levels of all three pro-inflammatory genes increased following exposure to AHSS in control cells infected with rAd66. Firstly, MCP-1 levels were reduced following exposure to AHSS for 90 and 120 minutes with overexpression of WT-Nrf2, at $1x10^6$pfu/mL, in concurrence with SFN pre-treatment at 1μM (FIGURE 4.9.A.). However, WT-Nrf2 overexpression at $1x10^7$pfu/mL induced a significant increase in levels of all pro-inflammatory genes in static conditions (FIGURE 4.9.A., B. and C.). This elevation was maintained under shear stress for both MCP-1 and IL-8; though levels of IL-8 were most pronounced of all pro-inflammatory genes after 120 minutes with WT-Nrf2 at $1x10^7$pfu/mL (FIGURE 4.9.C.).

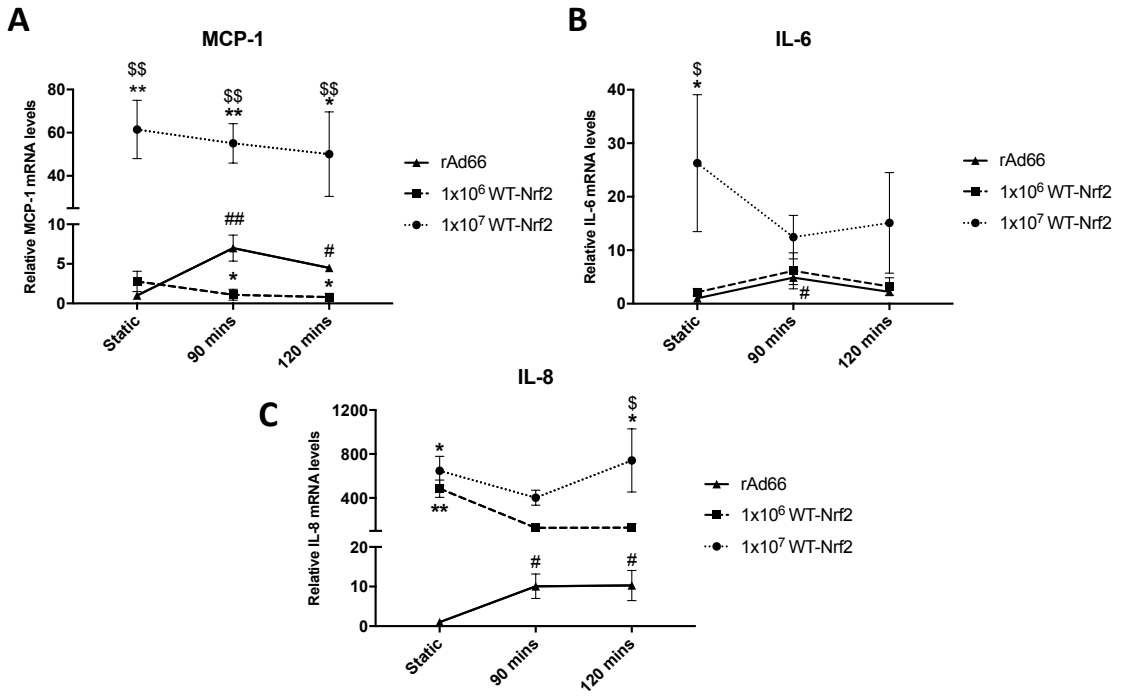


**FIGURE 4.9. Dose-dependent effect of Nrf2 overexpression of Nrf2 on inflammatory mRNA expression**

Relative mRNA levels of MCP-1, IL-6 and IL-8 (A, B and C, respectively) from HUVECs infected with WT-Nrf2 containing- or rAd66 control-adenoviruses, at low ($1x10^6$ pfu/mL) and high ($1x10^7$ pfu/mL) viral concentrations, and subsequently exposed to AHSS for 90 and 120 minutes or maintained in static conditions. mRNA expression data were normalised to β-tubulin and expressed as a fold-change relative to rAd66 static control. * indicates $p<0.05$ and ** indicates $p<0.01$ vs. rAd66 control (equivalent time-point); $ indicates $p<0.05$, $$ indicates $p<0.01$ vs. $1x10^6$ WT-Nrf2 (equivalent time-point); # indicates $p<0.05$ and ## indicates $p<0.01$ vs. rAd66 static control (utilised only as evidence of pro-inflammatory induction in rAd66 controls), Two-way ANOVA followed by post-hoc pairwise comparisons with Bonferroni correction for multiple comparisons, n=3.

### 4.2.4 EFFECT OF INHIBITION OF NRF2 ON THE ENDOTHELIAL RESPONSE TO AHSS

#### 4.2.4.1 VALIDATION OF DOMINANT-NEGATIVE NRF2 OVEREXPRESSION

To date, the majority of Nrf2 research has focussed upon its role in cytoprotection, consequently there has been little cause for the development of Nrf2 inhibitors. As such, an adenoviral-mediated overexpression approach was utilised here to attempt to inhibit Nrf2 under conditions of injurious AHSS stimulation. To do so, an adenovirus encoding a dominant negative form of Nrf2 (DN-Nrf2) with an EGFP-tag, was used. The DN-Nrf2 adenovirus contains a mutant Nrf2 which lacks the N-terminal transcriptional activation domain, but the C-terminal DNA-binding and heterodimerisation domains are retained (Kraft *et al.*, 2004). It has been demonstrated that this DN-Nrf2 mutant protein competes with endogenous Nrf2 for both co-factor interactions and binding to the ARE-motif (Alam *et al.*, 1999).

Increasing adenoviral concentrations ($1x10^5$, $1x10^6$ and $1x10^7$ pfu/mL) of DN-Nrf2 were evaluated against a maximal concentration of rAd66 control adenovirus ($1x10^7$ pfu/mL). HUVECs were infected with adenoviruses for 18 hours and cultured for a further 48 hours, after which point ECs were analysed for levels of both DN-Nrf2 and endogenous Nrf2 by Western blotting, as well as for the presence of EGFP expression, by fluorescence microscopy. Infecting with $1x10^7$ pfu/mL of DN-Nrf2 significantly increased DN-Nrf2 expression and reduced endogenous Nrf2 levels, compared to rAd66 viral controls (FIGURE 4.10.A. and B., respectively). Confirmation of this was observed by increased EGFP expression, viewed under fluorescent light, following infection with the maximal concentration of DN-Nrf2 (FIGURE 4.10.D.).

---

**FIGURE 4.10. Adenoviral-overexpression of DN-Nrf2 reduced endogenous Nrf2**

Relative DN-Nrf2 and endogenous Nrf2 protein levels were compared in HUVECs infected with DN-Nrf2 or rAd66 control adenoviruses at varying concentrations, by Western blot analysis and EGFP assessment, viewed under fluorescent light. * indicates $p<0.05$ and ** indicates $p<0.01$, One-way ANOVA followed by post-hoc pairwise comparisons with Bonferroni correction for multiple comparisons, n=3.

A. Relative levels of DN-Nrf2 protein (lower band at 25-30kDa), quantified by WB analysis using SCBT Nrf2 c-20 antibody, normalised to stain free loading control and expressed relative to RAd66 ($10^7$) control.

B. Relative levels of endogenous Nrf2 (upper band at 65kDa), quantified by WB analysis using SCBT Nrf2 c-20 antibody, normalised to stain free loading control and expressed relative to RAd66 ($10^7$) control.

C. Representative Nrf2 (DN-form and endogenous) blot and stain free loading control.

D. Representative images of EGFP-tagged DN-Nrf2 and rAd66 at varying concentrations, viewed under fluorescent light. Arrows show cells containing high nuclear levels of Nrf2, scale bars represent 15μm.

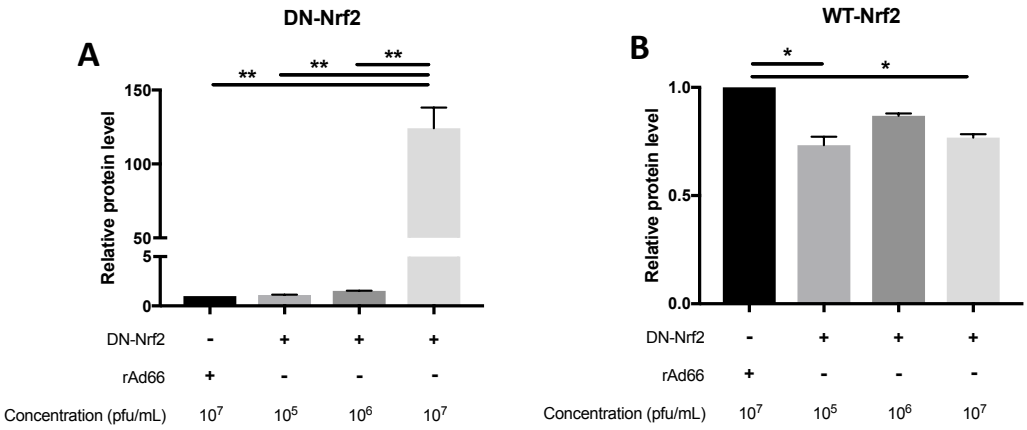


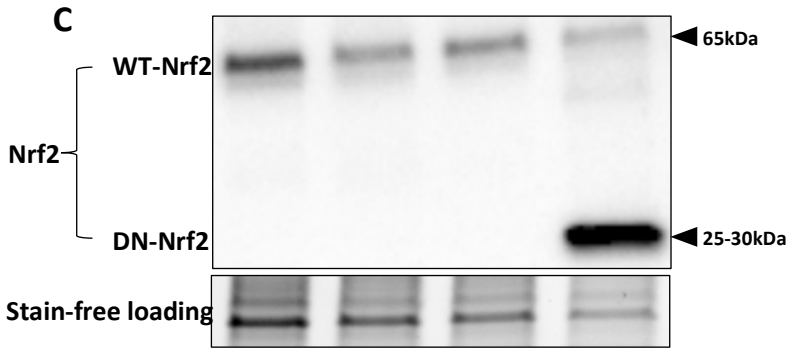


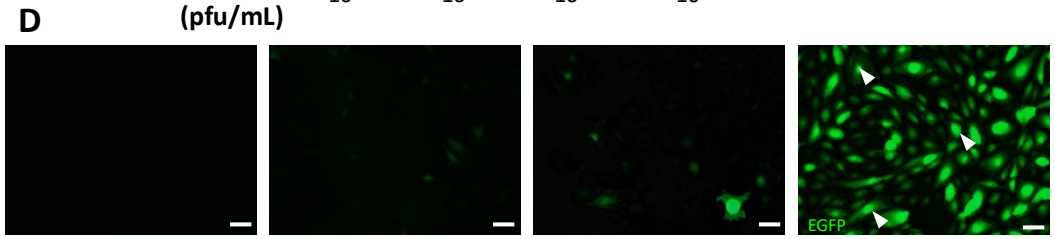

#### 4.2.4.2 DN-NRF2 REDUCED ANTIOXIDANT mRNA LEVELS

Having observed increased antioxidant and pro-inflammatory mRNA transcripts under shear stress, following Nrf2 activation, it was essential to assess the levels of these genes with inhibition of Nrf2 and application of shear stress. To do this, HUVECs were infected either with DN-Nrf2 or rAd66 control virus (both at concentration of $1x10^7$ pfu/mL) for 18 hours and subsequently cultured for a further 48 hours. HUVECs were then exposed to shear stress at 12dyn/$cm^2$ for 90 and 120 minutes and antioxidant mRNA (HO-1, GCLM and NQO-1) levels assessed by RT-qPCR.

Levels of all antioxidant genes were significantly reduced, following the application of flow, in DN-Nrf2 overexpressing ECs relative to rAd66 controls (FIGURE 4.11.A., B. and C.). However, only NQO-1 levels were reduced under static conditions as well, suggesting that in the case of HO-1 and GCLM, overexpression of DN-Nrf2 alone was not sufficient to prevent the basal Nrf2 transcriptional response of these genes (FIGURE 4.11.A. and B.).

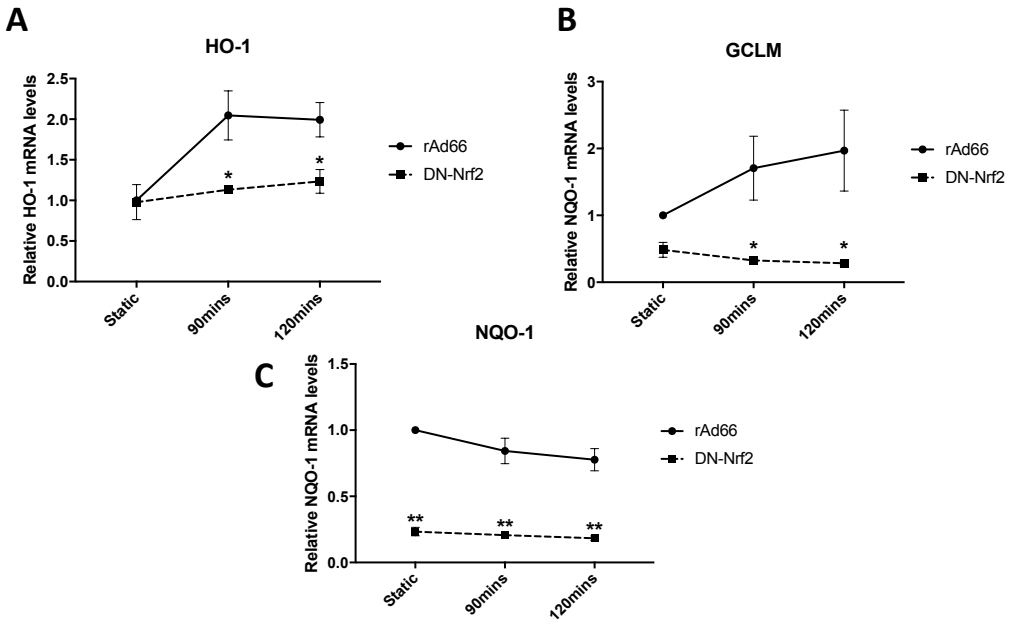


**FIGURE 4.11. DN-Nrf2 overexpression reduced antioxidant levels in ECs subjected to AHSS**

Relative mRNA levels of HO-1, GCLM and NQO-1 (A, B and C, respectively) from HUVECs infected with DN-Nrf2 containing- or rAd66 control-adenoviruses at $1x10^7$ pfu/mL, and subsequently exposed to AHSS for 90 and 120 minutes or maintained in static conditions. mRNA expression data were normalised to β-tubulin and expressed as a fold-change relative to rAd66 static control. * indicates $p<0.05$ and ** indicates $p<0.01$ vs. rAd66 control (equivalent time-point), Two-way ANOVA followed by post-hoc pairwise comparisons with Bonferroni correction for multiple comparisons, n=3.

#### 4.2.4.3 DN-NRF2 HAD NO EFFECT ON PRO-INFLAMMATORY mRNA LEVELS FOLLOWING AHSS EXPOSURE

HUVECs were infected with either DN-Nrf2 or rAd66 adenoviruses at $1x10^7$ pfu/mL, as above, and following exposure to AHSS for 90 and 120 minutes, pro-inflammatory mRNA levels were assessed by RT-qPCR. levels of all three pro-inflammatory genes (MCP-1, IL-6 and IL-8) remained unchanged by DN-Nrf2 overexpression both in static and flow conditions (FIGURE 4.12.A., B., and C.).

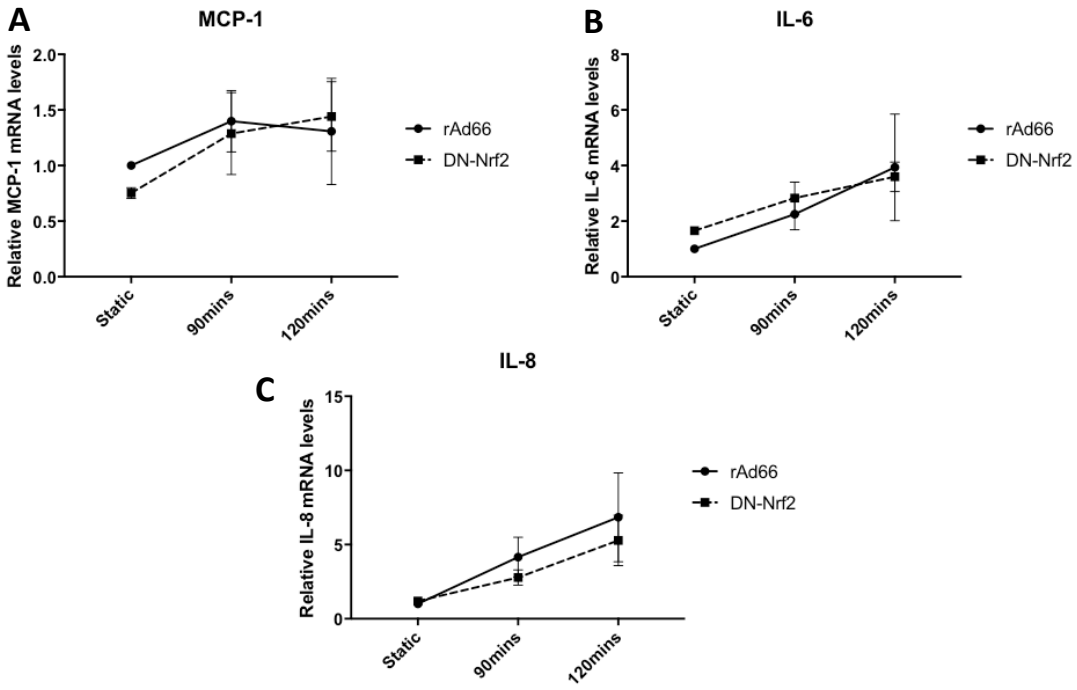


**FIGURE 4.12. DN-Nrf2 overexpression did not affect levels of pro-inflammatory genes**

Relative mRNA levels of MCP-1, IL-6 and IL-8 (A, B and C, respectively) from HUVECs infected with DN-Nrf2 containing- or rAd66 control-adenoviruses, at $1x10^7$ pfu/mL, and subsequently exposed to AHSS for 90 and 120 minutes or maintained in static conditions. mRNA expression data were normalised to β-tubulin and expressed as a fold-change relative to rAd66 static control. Two-way ANOVA followed by post-hoc pairwise comparisons with Bonferroni correction for multiple comparisons, n=3.

## 4.3 DISCUSSION

### 4.3.1 INTRODUCTORY SUMMARY

Maintenance of a quiescent, healthy endothelium in the grafted LSV is essential for the improvement of graft longevity (Osgood *et al.*, 2014). The activation of ECs is a significant contributor to the early pathogenesis of intimal hyperplasia (Motwani *et al.*, 1998). Within the vein graft, the loss of endothelial homeostasis contributes to the initiation of VSMC dysfunction and enhanced proliferation, as well as enhanced solute permeability and leukocyte recruitment to the vascular wall (Motwani *et al*., 1998; Owens, 2015).

It is widely recognised that oxidative stress plays an integral role in the development of many cardiovascular pathologies, with lipid peroxidation and direct mitogenic effects of ROS being the most well-defined examples in vein grafts (Jeremy *et al.*, 2004; Margaritis *et al.*, 2012; Weaver *et al.*, 2012). In dysfunctional ECs, the balance between the normal functions of oxygen-based gasotransmitters, such as NO and CO, and detrimental effects of ROS is tipped in the favour of the latter, thus reducing bioavailability of physiological gasotransmitters and subsequently reducing EC function (Shukla *et al.*, 2012). This imbalance is further exaggerated in the venous endothelium by the arterial transposition of the LSV, as the endothelium has to adapt to approximately three-fold increases in oxygen concentration, relative to venous circulation (Joddar *et al.*, 2015). As such, many clinical and experimental vein grafting studies have pursued therapeutic angles aimed at the reduction of ROS production, firstly, by antioxidants, such as vitamins C, D and E, and also NO-donating nitroaspirins (Jeremy *et al.*, 1997; Antoniades *et al.*, 2003; Wan *et al.*, 2007; Antoniades *et al.*, 2010). However, these studies have thus far been disappointing, perhaps partly owing to the potential negative, pro-oxidant behaviours of many vitamins and the fact that up to 50% of CABG patients may develop aspirin resistance after surgery (Kempfert *et al.*, 2009; Joddar *et al.*, 2011).

Studies of statin-based therapies, in both CABG patients and ECs *in vitro*, have revealed the benefits of statins beyond their lipid lowering functions, particularly in relation to the stress response involved in vascular disease (Cannon *et al.*, 2004; Antoniades *et al.*, 2010; Antoniades *et al*., 2011; Kocarslan *et al.*, 2016; Yuan *et al.*, 2017). Several studies have reported positive clinical outcomes and strongly indicate that the indirect, pleiotropic effects of statins on redox regulation can promote EC function and even enhance cell survival under injurious mechanical stimulation (Kulik *et al.*, 2008; Ali *et al.*, 2009; Margaritis *et al.*, 2014). These cytoprotective, redox-based effects of statins have been suggested to function through both Klf2- and Nrf2-dependent mechanisms, via distinct actions on eNOS and HO-1, respectively (Ali *et al*., 2009; Margaritis *et al*., 2014). Such studies into the effects of statins, and other antioxidant compounds, in the vein graft highlight the potential that endothelial cytoprotection and redox state modulation may play in the maintenance of a functional LSV endothelium following grafting.

Despite evidence from the wider cardiovascular field regarding the importance of Nrf2-dependent cytoprotection and antioxidant response, direct therapeutic targeting of Nrf2 has not been robustly evaluated. Dietary antioxidants, including sulforaphane and many vitamins, are commonly recognised as strong activators of the Nrf2-driven cytoprotective response. Consequently, these types of compounds represent exciting angles for treatment of vascular pathologies which are driven partly by oxidative stress, such as vein graft disease and coronary artery disease, owing to their ready availability and relative safety (Papaharalambus *et al.*, 2007; Kulik *et al.*, 2009; Bocci *et al.*, 2015). Using an *ex vivo* LSV organ culture model, Joddar et al. were able to show that treatment with the dietary supplement and Nrf2 inducer, Protandim, reduced IH progression and limited VSMC proliferation through induction of catalase and HO-1 (Joddar *et al*., 2011). Increased HO-1 has also been associated with both direct and indirect effects on VSMC proliferation in a murine graft model, which may be explained partly by the direct action on CO and the subsequent effect on VSMC cell cycle arrest, or as an indirect action of reduced

inflammation (Durante, 2010; Washington *et al.*, 2017). However, such studies into the antioxidant/Nrf2 response in the vein graft observed primarily VSMC responses to Nrf2 activation and seem to neglect the endothelial response, which remains of paramount importance to ultimate graft patency.

The cytoprotection afforded to ECs by Nrf2 is seen primarily at atheroprotected sites of the arterial tree, where the endothelium is exposed to prolonged laminar shear stress; at such sites there are readily available reserves of NO and CO, whose production is vital for normal endothelial function at these sites (Lehoux *et al.*, 2006; Boon *et al*., 2009). Both NO and CO are able to directly influence the production of one another by increasing levels of HO-1 and binding to eNOS, respectively (Washington *et al*., 2017). The transcriptional regulation of levels of both gasotransmitters relies on the concomitant actions between Klf2 and Nrf2, which convey true atheroprotection at portions of the vasculature exposed to prolonged protective shear (Fledderus *et al*., 2007; Ali *et al*., 2009).

### 4.3.2 NRF2 TARGET GENE RESPONSE UNDER AHSS

In the maintainance of bioavailability of NO and CO, the protective effect of mechanical stimulation in these endothelial regions is due also to the Nrf2-dependent induction of a number of antioxidant response element (ARE) genes (Satta *et al.*, 2017). These ARE genes, collectively acting to promote cell survival, are composed primarily of two types, firstly, those that are induced and respond upon pro-oxidant insult; and, secondly, those that are responsible for maintaining basally low-levels of oxidants under non-stressed conditions (Nguyen *et al.*, 2009). In this study, the ARE genes chosen (HO-1, GCLM and NQO-1) were all highly inducible in the stress-response, but also have basal protective functions, responsible for breaking the highly pro-oxidant heme into CO and bile products, production of antioxidant glutathione (GSH) and reduction of quinones, respectively (Nguyen *et al.*, 2009; Franklin *et al.*, 2009; Suzuki *et al.*, 2017). Somewhat unexpectedly, owing to the acuteness of the time-points evaluated, mRNA

and protein levels of HO-1 were increased following EC exposure to pro-inflammatory acute high shear stress. Acute shear exposure *in vitro* is recognised to increase ROS levels, which, in turn, is one of the primary inducers of ARE gene expression, which perhaps explains these transcriptional responses (Hsieh *et al.*, 2009; Hsieh *et al.*, 2014; Chistiakov Chistiakov *et al.*, 2017). There was no transcriptional response of NQO-1, however, which may indicate that there was not yet any protein/DNA damage induced by shear stress sufficient enough to promote an NQO-1 response, as increased levels have been observed following exposure to prolonged shear in HUVECs in culture, suggesting that NQO-1 transcription is mechanically responsive (Jaiswal, 2000; Fledderus *et al.*, 2008).

Interestingly, however, there was no increase in nuclear Nrf2 levels following 30 minutes of shear stress and, in fact, after 90 minutes, there was a reduction in nuclear Nrf2. This is contrary to Hsieh *et al*.'s findings that, following 120 minutes of shear exposure, Nrf2 nuclear translocation increased in a PI3K, PKC and ROS-dependent manner (Hsieh *et al*., 2009). However, their study presents primarily representative Western blots (no graphical data) from only a single sample and, as such, the results must be interpreted with caution (Hsieh *et al*., 2009). Despite this discrepancy between transcriptional response and Nrf2 localisation, there was a significant nuclear export effect of Keap1 observed in the presence of acute shear stress, suggesting that the repressive control of Nrf2 by its association with Keap1 was diminished. Warabi *et al*. showed elegantly that shear stress exposure improves Nrf2 stability via lipid peroxidation by NOX action, and they propose that this, in turn, is able to oxidatively modify Keap1 to induce its dissociation from Nrf2 (Warabi *et al.*, 2007; McSweeney McSweeney *et al.*, 2016). Additionally, covalent modification of Nrf2, by PKC-induced phosphorylation at Serine residue 40, is recognised to further stabilise Nrf2 and further supress its association with Keap1, which may possibly explain the increased ARE mRNA response, but reduced nuclear Nrf2 (McSweeney *et al*., 2016). Taken together, these data and prior observations suggest that Nrf2

can be transcriptionally active, despite nuclear translocation not increasing beyond constitutive levels.

### 4.3.3 NRF2 ACTIVATION AND THE PRO-INFLAMMATORY RESPONSE TO AHSS

In addition to the cytoprotective role of Nrf2, activation of the transcription factor has been shown to reduce inflammation in several distinct contexts, including cytokine- and LPS-driven inflammatory stimulation (Kim *et al.*, 2010; Ahmed *et al.*, 2017). The action of HO-1 is responsible for a large proportion of the anti-inflammatory effects observed by activation of Nrf2 (Washington *et al*., 2017). Both directly, via NF-κB inhibition in a hepatic injury model or foam cell macrophages, for instance, or indirectly through the actions of its bile-based metabolites, biliverdin and bilirubin, which have been proposed to reduce TNF-α and ox-LDL driven endothelial dysfunction (Kawamura *et al.*, 2005; Ahmed *et al*., 2017). However, to date, very few studies have investigated the role of Nrf2 in inflammation induced by mechanical stimulation. Zakkar *et al.* demonstrated that, at atheroprotected regions of the arterial tree exposed to prolonged, high, laminar shear stress, Nrf2 actions were responsible for the suppression of p38-VCAM1 signalling that was differentially observed in the atheroprone regions (Zakkar *et al*., 2009). It was also illustrated in this study that Nrf2 activation with sulforaphane (SFN) was able to reverse the pro-inflammatory, p38-VCAM1 response observed under conditions chronic, injurious shear stress, *in vivo* (Zakkar *et al*., 2009). Therefore, owing to its known mechano-responsivity and dual cytoprotective and anti-inflammatory actions, the effect of Nrf2 activation was evaluated here under pro-inflammatory AHSS stimulation, *in vitro*.

To do this initially, the effect of SFN pre-treatment on the reduction of inflammation (shown by pro-inflammatory mRNA levels (MCP-1, IL-6 and IL-8)) under AHSS was assessed. The findings observed here were somewhat unexpected, it was hypothesised initially that activation of Nrf2 would prevent AHSS-driven inflammation, at both the lower and higher concentrations of the compound (1 and 5μmol/L, respectively). However, at 1μmol/L, only MCP-1 levels were reduced

significantly under acute shear, relative to DMSO control; an observation which was corroborated with adenoviral-mediated overexpression of WT-Nrf2 at $1x10^6$pfu/mL. In the context of acute shear-induced inflammation in the vein graft, introduced in chapter 3, this inhibitory effect of Nrf2 activation on MCP-1 mRNA level is encouraging, as MCP-1 is proposed to be one of the primary, inflammatory influences stimulating IH progression (Schepers *et al*., 2006). What is of more concern, however, is the effect that Nrf2 activation, at a higher concentration (i.e. hyper-activation), either with gene-therapy based overexpression or a pharmacological method, has on inflammatory mRNA levels. Using both methods of Nrf2 activation (SFN at 5μmol/L or WT-Nrf2 at $1x10^7$pfu/mL) increased mRNA levels of IL-8 in static conditions, alone, and, following the application of acute shear, IL-8 levels remained significantly above control levels. Additionally, with WT-Nrf2 at $1x10^7$pfu/mL, MCP-1 levels were also significantly increased, both in static and shear conditions. These data suggest that the anti-inflammatory effects of Nrf2 activation were entirely dose- and context-dependent.

#### 4.3.4 NRF2 HYPER-ACTIVATION

The importance of context regarding Nrf2 and inflammation is also highlighted in studies of the NLRP3 inflammasome. Typically, the NACHT, LRR and PYD domain containing protein 3 (NLRP3) inflammasome is responsible for protection of the host against bacterial infection by the induction of a specific type of cell-death, known as Pyroptosis, but also recognises and responds to a wide range of deleterious stimuli, including oxidative stress and ROS (Ahmed *et al*., 2017). In the acute context, activity of the NLRP3 inflammasome is advantageous in protection of a tissue against pathogenic infection; whereas, chronic inflammasome activation has been linked to atherogenesis and chronic kidney disease (Hennig *et al.*, 2018). Recent studies associating Nrf2 activation with reduced acute inflammasome function observed that small-compound Nrf2 activators, such as tert-butylhydroquinone (tBHQ), can negatively regulate inflammasome

expression and activity via Nrf2-dependent ARE induction, in a similar fashion to that seen with SFN stimulation (Liu *et al*., 2017; Garstkiewicz *et al*., 2017).

Additionally, Nrf2 is able to directly regulate the expression of numerous pro-inflammatory genes, to the extent that the presence of an ARE-binding motif has been identified in the IL-6 promoter region (Wruck *et al.*, 2011; Kobayashi *et al.*, 2016). Despite the action of Nrf2 having largely been observed as anti-inflammatory (Kim *et al*., 2010; Ahmed *et al*., 2017), observation of Nrf2 crosstalk with the inflammasome and transcriptional targeting of genes positively involved in inflammation, appear to be the only limited evidence for the potential pro-inflammatory actions of Nrf2. However, the mechanisms behind these potential pro-inflammatory actions of Nrf2 remain unclear and are likely interconnected at multiple levels of regulation (Hennig *et al.*, 2018). One possible explanation for the pro-inflammatory response seen with Nrf2 hyperactivation, could be related to overactivity of HO-1. In addition to MCP-1 and IL-8, HO-1 mRNA levels were significantly increased in both $1x10^7$pfu/mL of WT-Nrf2 and 5μmol/L SFN, in static and shear conditions. When HO-1 is overactive, there is excessive production of CO, a by-product of haem catalysis, which, in physiological conditions, is a normally functioning gasotransmitter; however, when CO is produced in excess, it becomes severely pro-inflammatory, such as can be seen in cigarette smokers (Washington *et al*., 2017). It would be interesting, in future, to assess levels of HO-1 activity and CO production under AHSS, to pick apart further, this unexpected effect.

Many studies into inflammation and Nrf2, however, have scarcely explored the negative role played by Nrf2 hyper-activation, such as has been done in investigations into the function of Nrf2 in cancer. In this growing body of evidence into the contradicting functions of Nrf2 in cancer, the paradox holds that, at physiological levels, Nrf2 protects tissues against tumour development through its cytoprotective, antioxidant actions; whilst, hyper-activation of Nrf2, seen in many tumours, in fact protects and favours tumour cell growth (Lau *et al.*, 2008; Rotblat

*et al.*, 2012; Sporn *et al.*, 2012; Huang *et al.*, 2015; Menegon *et al.*, 2016). Although it is difficult to translate the oncogenic environment into a vascular one, nevertheless, the importance of experimental setting and quantity may be relevant. This paradox is highlighted by Sporn *et al*. with the Fumarate paradigm. Fumarate is a necessary, physiologic metabolite produced during the Krebs cycle which is both anti-carcinogenic and anti-inflammatory; it is also a potent Nrf2 activator through sequestration of Keap1 and, at low doses, Fumarate inducing therapeutics, like many other Nrf2 activators, can prevent the development of tumours (Sporn *et al.*, 2012). However, with the loss of the enzyme which catalyses the breakdown of Fumarate, Fumarate Hydratase, there are huge increases in intracellular Fumarate, Keap1 becomes continuously sequestered and Nrf2 is hyper-activated, leading to uncontrolled tumourigenesis (Sporn *et al*., 2012). This unconstrained activity in cancer studies emphasises the importance of context and dose dependency with Nrf2 activation.

As with the Fumarate paradigm, the results in this chapter concur, to some extent, with the dose-dependency notion in the activation of Nrf2. At the lower concentration of both WT-Nrf2 and SFN, low level activation of Nrf2 prevented the increase in MCP-1 mRNA levels under flow. However, at the higher concentrations of both virus and compound, there was a significant pro-inflammatory response, which, in certain cases, was increased further with the application of acute shear stress. This effect cannot be explained merely as one of cytotoxicity induced by high concentrations of virus or compound, as the vehicle control samples (DMSO and rAd66 empty vector adenovirus) used here were always at the maximal concentration. One other possible explanation for the observation of dose-dependent pro-inflammatory induction by Nrf2 hyper-activation, may be related to the interaction between Keap1 and the NF-κB pathway. Lee *et al.* showed that Keap1, and its associated complex (Cul3 and Ring box 1 (Rbx1)), functions as an E3 Ubiquitin Ligase for IKKβ of the NF-κB classical pathway (Lee *et al.*, 2009). This Keap1 complex, under basal conditions, functions to ubiquitinate IKKβ and target it for degradation, thus limiting NF-κB driven pro-inflammatory signalling. Following depletion of Keap1, IKKβ was stabilised and

accumulated, which led to an activation of NF-κB-dependent transcription, entirely independently of the actions of Nrf2 (Lee *et al*., 2009).

The relevance of this to pro-inflammatory signalling activation in the present study is because, firstly, Keap1 was inactivated and depleted following acute shear stress exposure, shown by nucleo-cytosolic shuttling and an increase in ARE mRNA transcription. And secondly, both pharmacological and gene-therapy based methods of Nrf2 activation lead to a dysregulation or inactivation of Keap1 by ubiqutination or electrophilic alteration (Zhang *et al.*, 2005; Hong *et al.*, 2005). Consequently, there is an unrestrained activation of Nrf2 in ECs exposed to flow when high levels of Nrf2 activation are already present, such as with high concentrations of SFN and WT-Nrf2. There may also be a de-regulation and loss of Keap1-dependent negative regulation of pro-inflammatory NF-κB signalling, as, in this experimental context, Keap1 is being 'doubly' inactivated, by both shear stress and Nrf2 hyper-activation. Together, these models, of excessive CO production or dysregulation of Keap1-dependent NF-κB signalling conservation, may partly explain why Nrf2 hyper-activation, with high concentrations of activators and acute shear stress, leads to an increase in inflammation. However, further direct evidence regarding Keap1 inactivation and potential degradation on shear-induced inflammation would be necessary, in the presence of either NF-κB or proteasome inhibitors, to unequivocally create the association between Keap1 inactivation and NF-κB signalling under AHSS-driven inflammation and Nrf2 hyper-activation.

### 4.3.5 CONCLUSION

The purpose of the current chapter was to evaluate the feasibility of activation of the cytoprotective, antioxidant signalling system, driven by Nrf2/Keap1, as a potential target in the resolution of EC inflammation induced by acute shear stress. There appears to be an antioxidant transcriptional response, of ARE genes, under acute shear that is regulated not by the translocation of Nrf2, but perhaps by the nuclear export of its repressor, Keap1. Furthermore,

activation of Nrf2 prior to shear stress exposure, induced divergent inflammatory responses dependent on the concentration of the activator, be it adenoviral or pharmacological. With low-level Nrf2 activation, there appeared to be a degree of inflammation resolution in response to shear; whereas, when Nrf2 was hyper-activated, the opposite effect was observed, and inflammation was increased. Although the mechanism remains unclear, further investigation into the activity of HO-1 and dysregulation of Keap1-dependent NF-κB inhibition may certainly provide some clues as to the role of Nrf2 in acute vascular injury and inflammation.

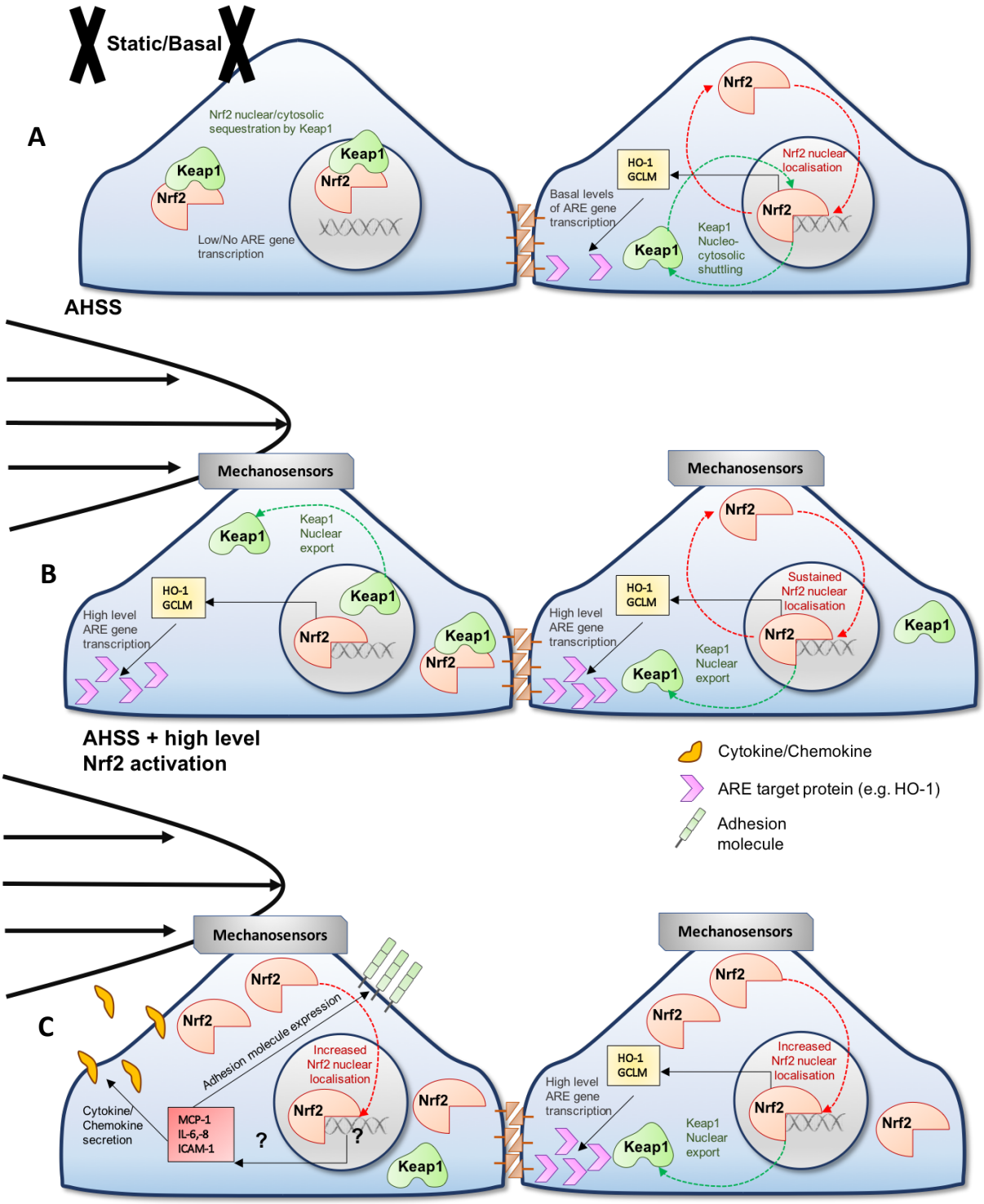


**FIGURE 4.13. EC involvement of the Nrf2/Keap1 pathway under acute shear stress**

Summary diagrams to represent findings from Chapter 4 to indicate the activity of Nrf2 in ECs under (A) static conditions, (B) AHSS with low/no Nrf2 activation and (C) AHSS with Nrf2 hyperactivation. Black block arrows represent pathway activation, green arrows represent Keap1 nucleo-cytosolic movement and red arrows represent Nrf2 nucleo-cytosolic movement.

# 5. GENERAL DISCUSSION

## 5.1 INTRODUCTORY SUMMARY

Endothelial cell dysfunction and vascular inflammation are major contributors to vein graft failure. Vascular inflammation in vein grafts is driven by the innate immune response to a complex cytokine milieu, interactions with circulating leukocytes, generation of harmful oxygen radicals, vessel damage during surgical harvest and injurious haemodynamic stimulation (Sabik, 2011). Following initiation of vascular inflammation, the effects of the arteriovenous transposition are transduced from the endothelium to VSMCs in the medial layer of the LSV. This partly contributes to enhanced VSMC migration and proliferation, ultimately leading to IH development, accelerated atherosclerosis and vein graft failure (Newby *et al.*, 2000). The molecular mechanisms leading to the initiation of, and transition between, each distinct phase of vein graft disease, however, are not yet fully elucidated.

When adapting to an entirely new haemodynamic environment, including approximately 10-fold increased shear stress rates, the adaptive ability of the LSV endothelium is pushed beyond its innate capacity. This early, adaptive response to altered flow begins a harmful spiral towards endothelial inflammatory activation, defined by the induction of inflammatory cytokines and chemokines, loss of vasomotor tone, increase in permeability, monocyte adhesion and extravasation which can ultimately result in dysfunction of ECs and surrounding VSMCs, leading to the initiation of IH pathogenesis (Golledge, 1997; Kwei *et al*., 2004; Schepers *et al*., 2006). However, to date, no therapeutic approaches have proved successful in preventing VGF, which may partly be due to the complexity of the physical and molecular environment that immediately ensues following implantation. The introduction of practices such as low-pressure vessel distension and the use of the 'no-touch' technique, have enhanced long term patency of vein grafts (Angelini *et al*., 1990; De Souza *et al*., 2002), but not eradicated graft failure. Interestingly, both of these surgical techniques focus primarily on the preservation of the endothelium prior to, and immediately after, implantation of the graft (Wise *et al.*, 2016).

## 5.2 HYPOTHESES, AIMS AND IMPLEMENTATION

This thesis aimed to investigate the vEC response to increased haemodynamic stimulation experienced by saphenous vein grafts by subjecting vEC to AHSS using *in vitro*- and tissue-based models. The focus of the investigations was into the role of two transcription factors, NF-κB and Nrf2, which were independently evaluated, to characterise their responses under AHSS and assess the therapeutic potential of their use as targets for the reduction of biomechanically-induced EC inflammation.

It was hypothesised, that the exposure of vECs to AHSS induces inflammation involving both pro-inflammatory actions of NF-κB and inactivation of the protective Nrf2 pathway. And secondly, that independent inhibition of NF-κB and activation of Nrf2 will prevent the vEC pro-inflammatory response to AHSS.

Two parallel studies were employed to test these hypotheses. Firstly, *in vitro* and *ex vivo* models of AHSS, using HUVECs and human LSV respectively, were utilised to determine the involvement of NF-κB in AHSS-driven inflammation. Subsequently the potential of NF-κB inhibition as a prevention for acute vein graft inflammation was investigated. Secondly, the activity of the Nrf2/Keap1 pathway in the adaptive shear response was explored in HUVECs subjected to AHSS, *in vitro,* to investigate whether exogenous activation of Nrf2 prevented AHSS-driven inflammation.

## 5.3 NF-κB PATHWAY INVOLVEMENT IN vEC ACTIVATION

Initially, it was necessary to validate several previous formative mechanotransduction studies by investigating whether, in the model used here, vECs exposed to AHSS up-regulated pro-inflammatory chemokine and cytokines (Dewey *et* al., 1981; Shyy *et al*., 1994; Davies, 1997; Chiu *et al*., 2004; Chiu *et al*., 2011). Initial results corroborated these studies, showing that AHSS increased the levels of a number of pro-inflammatory genes (MCP-1, IL-6, IL-8, ICAM-1) at the transcript and protein levels, in both vECs in culture and in the LSV endothelium, as shown by *en face* imaging methods. When addressing the potential involvement of NF-κB in the co-ordination of this pro-inflammatory response to AHSS, it was demonstrated that NF-κB was activated, and translocated to the nucleus, as quickly as 30 minutes after the onset of AHSS *in vitro* and *ex vivo*. Next, a causative link between these two elements was investigated. Using pharmacological and adenoviral-based approaches, it was shown that the pro-inflammatory response to shear stress was abrogated, *in vitro* and in human LSV ECs by the inhibition of the NF-κB classical pathway. This observation was also substantiated in functional assessments of endothelial inflammation, whereby NF-κB inhibition was able to reduce AHSS-driven endothelial-monocyte interaction and rescue AHSS-induced disruption of EC cell-cell contacts, which provided additional and functional evidence for the involvement of NF-κB inhibition in vein graft inflammation. These findings suggest a critical role for the NF-κB classical pathway in acute vein graft inflammation caused by AHSS and suggest that inhibition of this pathway offers the potential to reduce endothelial inflammation under such conditions.

Endothelial monolayer integrity and permeability represent a critical feature which must be regulated in the dysfunctional vein graft endothelium. It is widely reported that acute shear stress triggers significant changes in permeability to albumin, modified-LDL and dextran-based solutes across the endothelial barrier, as quickly as one hour after exposure; an effect which is lost after chronic shear exposure when the endothelial barrier has 'strengthened' again (Jo *et*

*al.*, 1991; Warboys *et al.*, 2010; Tarbell, 2010). Here, it was demonstrated that the *in vitro* inhibition of NF-κB prevented shear stress-induced disruption of EC cell-cell contact after four hours, albeit by a surrogate measure of VE-Cadherin adherens junction (AJ) structure. EC barrier integrity of controls also recovered to equivalent levels to those observed in cells with NF-κB inhibition, which supports the concept of a transient reduction in shear-induced permeability proposed by Warboys and colleagues (Warboys *et al.*, 2010).

These findings, regarding the role of NF-κB in vein graft EC inflammation, illustrate the rapid and transient nature of the process when induced by acute increases in shear stress. Observations of MCP-1 protein expression under flow at six hours, transient MCP-1 reduction with NF-κB inhibition and transitory endothelial barrier disruption, all highlight the fact that the acute period immediately after flow onset is vital to maintaining a mostly functional endothelium. However, the *ex vivo* evidence presented here suggests that this transitory inflammation occurs slightly later in the LSV endothelium *ex situ*, and perhaps this will be later still in the *in vivo* setting. This tight window of opportunity, whereby inhibition may be vital to prevent an EC inflammatory response, appears to lie between 0-4 hours and 0-6 hours, *in vitro* and *ex vivo*, respectively. These findings in the LSV offer some insight into the critical temporal nature of this acute inflammatory period after arteriovenous transposition, highlighted by Pearce *et al.* and Golledge *et al.* over two decades ago (Pearce *et al.*, 1985; Golledge, 1997). In addition to the timing of EC inflammation in the vein graft, these findings also elucidate a possible mechanism behind vein graft EC activation and offer a potential therapeutic target for pharmacological modulation. However, further investigation into the temporal dynamics of acute inflammation, and its progression to a more chronic response, would help reveal more about the transience of endothelial inflammation in the context of numerous other inflammatory factors and the length of NF-κB inhibition necessary to achieve effective inflammatory reduction.

In the future, local pre-treatments of the LSV immediately upon harvest may offer an exciting therapeutic possibility. This is particularly pertinent when inhibiting NF-κB, as the pathway plays critical and hugely pleiotropic roles throughout various tissues of the body (Lawrence, 2009). As such, the local method of pre-treating solely the vessel avoids the possible complications associated with systemic NF-κB inhibition *in vivo*, such as disruption to homeostatic and normal cell cycle functions (Fraser, 2006). Alternatively, if longer term NF-κB inhibition is necessary to prevent neointimal formation, as Miyake *et al*. suggest, a dual therapeutic approach could be adopted, the *in-situ* graft pre-treatment, prior to implantation may be performed first; and, if necessary, drug-eluting nanoparticles, targeted to adhesion molecules (ICAM-1 or VCAM-1) for instance, may also be used to specifically act upon the dysfunctional endothelium (Arruebo *et al.*, 2007; Yang *et al.*, 2013).

Finally, gene-therapy approaches may also be utilised for localised inhibition of the vein graft upon harvest (George *et al.*, 2011; Wan *et al*., 2012). The use of recombinant adenoviruses, however, triggers adaptive immune responses. Thus, the use of helper dependent adenoviruses, lacking viral coding sequences may represent a viable option when trying to limit immune responses and induce longer expression of the transgene (Vetrini *et al.*, 2010). This approach, combined with the pre-treatment, would provide acute and prolonged NF-κB inhibition throughout the graft, thus preventing NF-κB induced mitogenic effects seen in neointimal lesions *in vivo* in the prolonged context (Miyake *et al*., 2006; Vetrini *et al*., 2010; Miyake *et al*., 2014).

## 5.4 NRF2 PATHWAY INVOLVEMENT IN vEC ACTIVATION

In a parallel study, the involvement of another transcription factor, Nrf2, in response to pro-inflammatory AHSS was assessed. Initially, the activation of Nrf2 target (ARE) genes was examined under AHSS in vECs *in vitro*, which revealed an increase in the mRNA levels of ARE

genes, HO-1 and GCLM, and HO-1 at the protein level. This led to the investigation of the activity, by cellular localisation, of both Nrf2 and its repressor, Keap1. Interestingly, and despite the increases in ARE gene transcript levels, Nrf2 appeared to be exported from the nucleus following 90 minutes of AHSS exposure. This nuclear export of Nrf2 was associated with nuclear export and subsequent cytosolic increase of Keap1 following 30 minutes AHSS exposure. Together, these transcriptional and cellular localisation data suggest that the Nrf2 pathway is acutely activated by AHSS, perhaps by a dissociation from Keap1 within the nucleus. In the light of these results, it was examined whether exogenous activation of Nrf2, before EC exposure to AHSS, could reduce the inflammatory response induced by AHSS. Results showed that, high level activation (or hyperactivation) of Nrf2, using either a pharmacological or adenoviral-mediated approach, greatly increased the levels of pro-inflammatory mRNA transcripts in vECs subjected to AHSS. Whereas, low level activation of Nrf2 was only able to reduce mRNA transcript levels of MCP-1. Moreover, the inhibition of the Nrf2 pathway, using a dominant-negative adenovirus, had no effect on pro-inflammatory mRNA transcript levels, despite reducing transcript levels of ARE genes, HO-1, GCLM and NQO-1, in vECs subjected to AHSS. These results represent a new insight into the activity of Nrf2 in vECs exposed to AHSS and suggest that the pathway may play a role in acute vascular inflammation. However, further investigation into the effects that Nrf2 hyperactivation in vECs exposed to various inflammatory mechanical stimuli is necessary to substantiate this.

Investigating the regulation and activation of the cytoprotective Nrf2 pathway under acute arterial shear stress, surprisingly revealed a discrepancy between the ARE-gene response and Nrf2 localisation following shear stress exposure. Under pro-inflammatory AHSS stimulation, HO-1 was increased, indicative of the ARE-gene response, at both the mRNA transcript and protein level by two and four hours, respectively. Unexpectedly, this was not associated with increased nuclear translocation of Nrf2, but, in fact, an increased nuclear export of the Nrf2 repressor, Keap1. Despite this, transcriptional regulation of HO-1, however, is not necessarily

attributable to Nrf2; there is some evidence that NF-κB also plays a role in the control of HO-1 regulation, due to its dual roles in inflammation regulation and stress-response (Durante, 2010). In contrast, GCLM, which is also upregulated here at the transcript level under AHSS, is regulated primarily by the actions of Nrf2 and the gene does not contain a κB oligonucleotide consensus sequence; though, interestingly, transcriptional regulation of the catalytic subunit is controlled by both TFs (Dickinson *et al.*, 2004). The fact that GCLM is transcribed almost exclusively by Nrf2, and that levels increase in response to AHSS, suggests that Nrf2 is in fact transcriptionally active. To add further complexity to the current Nrf2 target gene picture, there is also evidence that the transcriptome controlled by AP-1 also contains many parallel genes, as there exists an AP-1 consensus sequence within the ARE motif (Biswas *et al.*, 2014). Stress response regulation is clearly an extremely complex series of finely-tuned, yet overlapping elements and, consequently, these data must be interpreted with caution, because, although plausible, the findings are still in their preliminary stage. Further investigation would be necessary to examine true Nrf2 transcriptional activation, such as evaluation of Nrf2 phosphorylation at Ser40 as an indicator of active and dissociated Nrf2, an ARE-luciferase assay and perhaps an Nrf2-ARE binding assay.

It is thought that exogenous Nrf2 activation, either with gene-therapy-based or pharmacological approaches, could protect ECs against the inflammatory effects of AHSS. However, high-level activation of Nrf2 (hyperactivation), with sulforaphane pre-treatment (5μmol/L) and adenoviral-mediated WT-Nrf2 overexpression ($1x10^7$pfu/mL), concomitantly with AHSS, increased MCP-1, IL-6 and IL-8 mRNA transcript levels in vECs exposed to AHSS. However, there was a reduction of MCP-1 transcript levels following shear stimulation with the lesser degree of Nrf2 activation. As alluded to earlier, these findings emphasize caution when investigating Nrf2 activation and that, as in many oncology studies, hyper-activation of Nrf2 and dysregulation of Keap1 may promote inflammation and harm, rather than protection (Lau *et al*., 2008; Sporn *et al.*, 2012; Menegon *et al*., 2016).

The findings presented here, regarding the possible pro-inflammatory function of Nrf2 in acute shear, represent a contrasting view from the widely accepted notion that Nrf2 possesses anti-inflammatory potential. It has been well established that Nrf2 activation can prevent p38-mediated VCAM-1 signalling in TNF-$\alpha$ stimulated ECs, *in vitro*, and in portions of the arterial vasculature exposed to chronic, low shear stress, *in vivo* (Zakkar *et al*., 2009). The same study also observed an increase in TNF-$\alpha$-driven induction of VCAM-1 transcript levels in cells overexpressing the same DN-Nrf2 form, used here (Zakkar *et al*., 2009). It is well understood that Nrf2 is induced by a variety of mechanical stimuli, however, these stimuli are largely of the prolonged and protective type, under which, Nrf2 acts to positively regulate redox balance, which, in turn is thought to prevent inflammation (Lee *et al.*, 2015; Kobayashi *et al.*, 2016). Nevertheless, in the context of acute shear stress, no increase in pro-inflammatory transcript levels following Nrf2 inhibition was observed in this study, though there was when Nrf2 was hyperactivated, indicating that dual Nrf2 activation exogenously and under shear stress, paradoxically, induces inflammation. This suggests that, under acute shear, Nrf2 does not play an integral role in the subsequent inflammatory response, unless it is hyper-activated. Though this may be less to do with Nrf2 hyperactivity than the inactivation of Keap1 and its possible degradation, thus preventing Keap1 from regulating the NF-$\kappa$B pathway through Keap-1 dependent IKK$\beta$ degradation; or, alternatively, due to excessive HO-1 activity and CO production (Lee *et al.*, 2009; Washington *et al*., 2017). Whilst these findings did not support the anti-inflammatory role of Nrf2 pre-activation in the context of acute shear, they are able to provide some initial insight into the stimulation- and dose-dependent effects of Nrf2 regulation in early mechanotransduction events. The results described here also highlight that much more detailed study into the actions of Nrf2 activation in human LSV tissue, particularly upon exposure to acute arterial haemodynamics, is needed, in order to translate these findings from an EC mechanical adaptive response, to findings genuinely translatable to vein grafting.

## 5.5 FUTURE WORK

### 5.5.1 NF-κB AND VEIN GRAFT FAILURE

In order to truly establish the role played by NF-κB in driving AHSS-induced inflammation in the vein graft endothelium, *in vivo* porcine translational studies, employing either an interpositional or coronary vein graft, would be necessary to corroborate the *ex vivo* findings presented in Chapter 3. Further to this, it would be of great interest to validate, firstly, whether the NF-κB inhibitor, BAY11-7085, was capable of reducing chemokine and cytokine expression and monocyte-endothelial interaction acutely in the vein graft, using an *in vivo* model. Secondly, it would be pertinent in such a model, to assess the therapeutic efficacy of an acute vein graft pre-treatment on a longer-term outcome, such as neointimal size or monocyte infiltration into the vein graft wall. Lastly, using the tissue-based models established in this thesis, evaluating the effect that NF-κB pre-inhibition has on endothelial preservation and apoptosis at later time-points (>24 hours) represents a currently unexplored and essential area for the continuation of this work.

### 5.5.2 NRF2 AND THE AHSS RESPONSE

Having established that Nrf2 hyperactivation induced a pro-inflammatory response under AHSS, it became clear that Nrf2 activation did not represent a viable strategy to retard acute vein graft inflammation. However, further temporal characterisation of the basal activity of the Nrf2/Keap1 axis under shear stress stimulation *in vitro*, beyond 30 minutes-six hours, may provide some important detail as to how ECs switch from an inflammatory-prone to a protected phenotype. Furthermore, since *ex vivo* responses may differ from *in vitro* experiments, investigation of the Nrf2 response to AHSS in the LSV endothelium may be of interest in better defining the role of Nrf2 in early shear, mechanotransduction events.

### 5.5.3 NF-κB AND NRF2: POTENTIAL CROSSTALK

Finally, with the known involvement of ROS and NOXs in the shear stress mediated activation of NF-κB, it is conceivable that there is a role for antioxidant response pathway involving Nrf2, via crosstalk in the activation of NFκB. The interaction between NF-κB activation and Nrf2 remains poorly understood; NF-κB is known to disrupt the transcriptional activity and binding of Nrf2 to antioxidant response elements (ARE) through interaction with Creb-binding protein (CBP) (Liu *et al.*, 2008). However, Liu *et al*. were only able to establish a unidirectional mechanism of interaction (i.e. from NF-κB to Nrf2). In contrast, Lee *et al*. established a link between the two pathways which worked in the opposite direction, whereby, a Keap1-dependent complex functioned to regulate IKKβ activity, by ubiqutination, independently of Nrf2 (Lee *et al*., 2009). As suggested earlier, this interaction may offer a possible explanation for the findings associated with Nrf2 hyperactivation and this would represent a logical further investigation in the AHSS context.

## 5.6 CONCLUSION

In summary, the results of this thesis have demonstrated that acute exposure of vECs to arterial levels of shear stress is associated with the induction of a pro-inflammatory response, both *in vitro* and *ex vivo*, which was driven by activation of the NF-κB classical pathway. Inhibition of the NF-κB classical pathway, was able to prevent AHSS-induced inflammation. Activation of the Nrf2/Keap1 cytoprotective signalling system, *in vitro*, was also seen in response to AHSS, which, when activated at low-levels or hyper-activated, prior to shear stress exposure, initiated highly divergent pro-inflammatory responses. The findings with regards to Nrf2, raise many interesting questions as to the role of Nrf2 in the early, adaptive shear stress response and mechanotransduction.

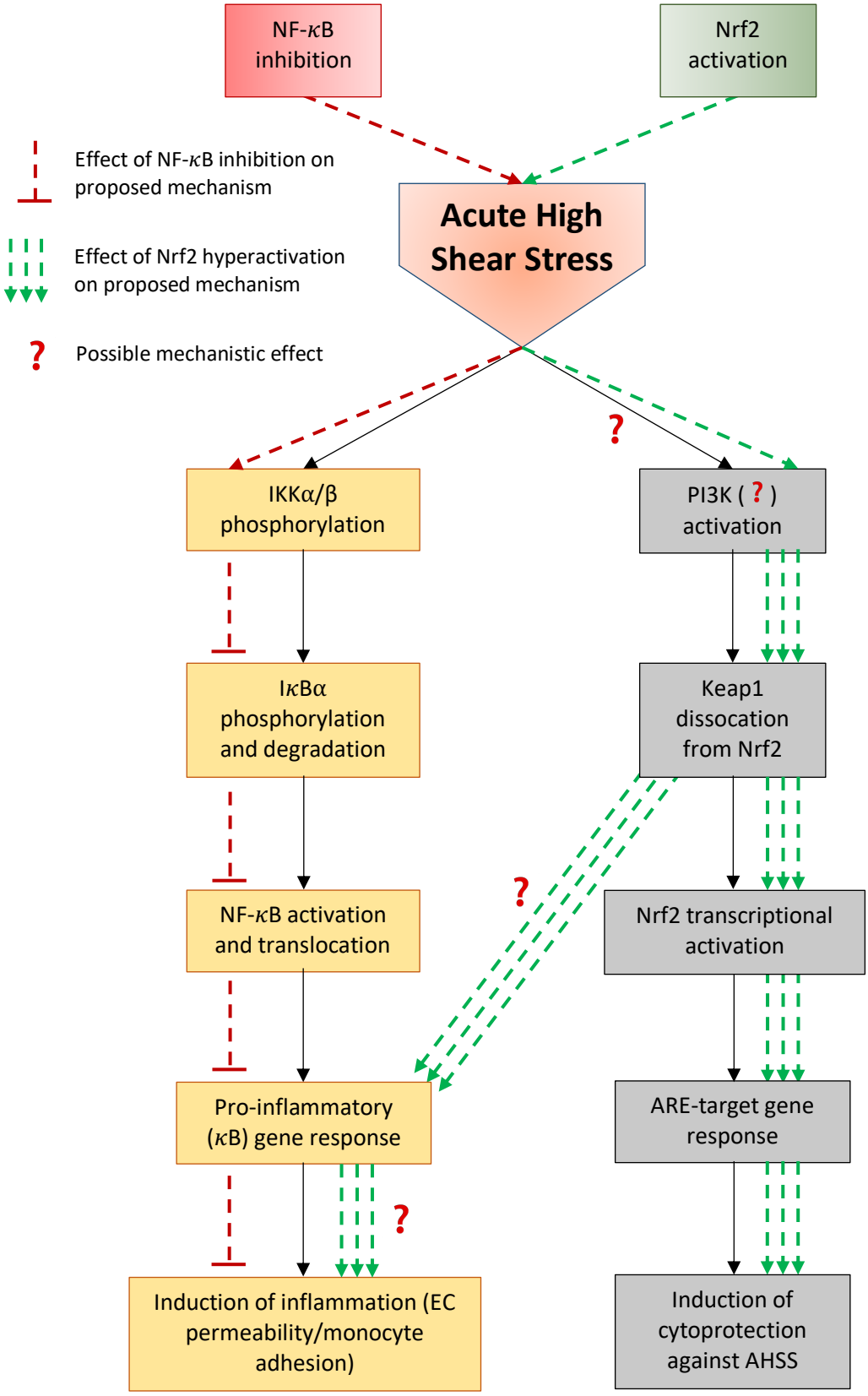
NF-κB inhibition
Nrf2 activation
Effect of NF-κB inhibition on proposed mechanism
Effect of Nrf2 hyperactivation on proposed mechanism
? Possible mechanistic effect
Acute High Shear Stress
?
IKKα/β phosphorylation
PI3K ( ? ) activation
IκBα phosphorylation and degradation
Keap1 dissocation from Nrf2
NF-κB activation and translocation
?
Nrf2 transcriptional activation
Pro-inflammatory (κB) gene response
ARE-target gene response
?
Induction of inflammation (EC permeability/monocyte adhesion)
Induction of cytoprotection against AHSS

**FIGURE 5.1. Mechanistic summary figure**

A summary of the working model for this thesis, including the potential mechanisms of activation (black arrows) of the NF-κB classical pathway (left-hand side) and Nrf2/Keap1 pathway (right-hand side) in vECs exposed to AHSS. Additionally, the effects that NF-κB inhibition (red arrows) and Nrf2 hyperactivation (green arrows) are included, as well as a proposed mechanistic explanation and link (red question mark) between the pathways to explain how Nrf2 hyperactivation increased pro-inflammatory gene transcripts.

# 6. APPENDIX

**SUPPLEMENTARY FIGURE 1. IgG CONTROL IMAGES FOR IMMUNOCYTOCHEMISTRY**

All immunocytochemistry analysis was performed in conjunction with concentration- and species-matched Anti-IgG control antibodies. Here, the Anti-IgG control images are presented for MCP-1 and VE-Cadherin, at primary antibody concentrations of 3.33μg/mL and 4μg/mL, respectively.

Anti-IgG controls clearly show no non-specific staining, as such, representative images are entirely black.

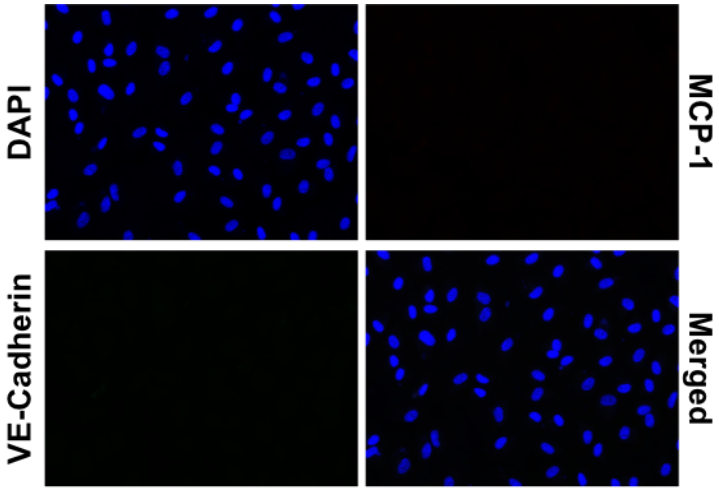

**SUPPLEMENTARY FIGURE 2. IgG CONTROL IMAGES FOR MCP-1 *EN FACE* IMMUNOFLUORESCENCE**

All NF-κB immunofluorescent analysis was performed in conjunction with concentration- and species-matched Anti-IgG control antibodies. Here, the Anti-IgG control images are presented for MCP-1 and vWF, at primary antibody concentrations of 3.33μg/mL and 200μg/mL, respectively.

Anti-IgG controls clearly show no non-specific staining, as such, representative images are entirely black.

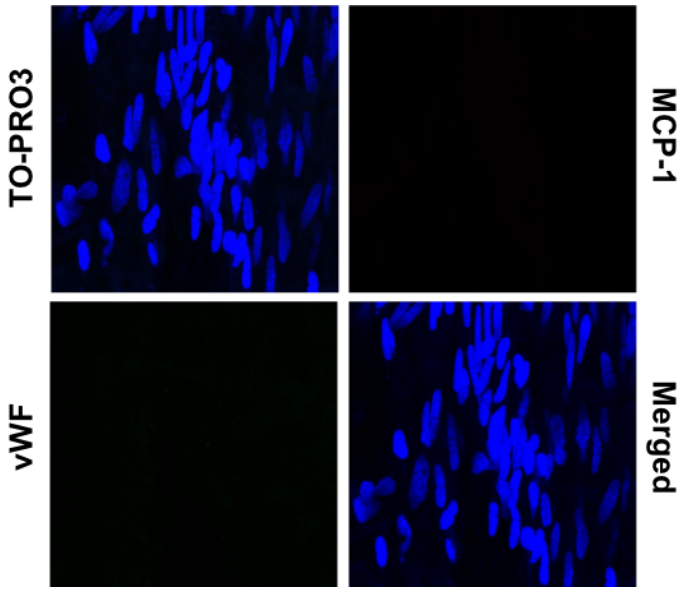

**SUPPLEMENTARY FIGURE 3. IgG CONTROL IMAGES FOR NF-κB *EN FACE* IMMUNOFLUORESCENCE**

All NF-κB immunofluorescent analysis was performed in conjunction with concentration- and species-matched Anti-IgG control antibodies. Here, the Anti-IgG control images are presented for NF-κB and vWF, at primary antibody concentrations of 0.33μg/mL and 200μg/mL, respectively.

Anti-IgG controls clearly show no non-specific staining, as such, representative images are entirely black.

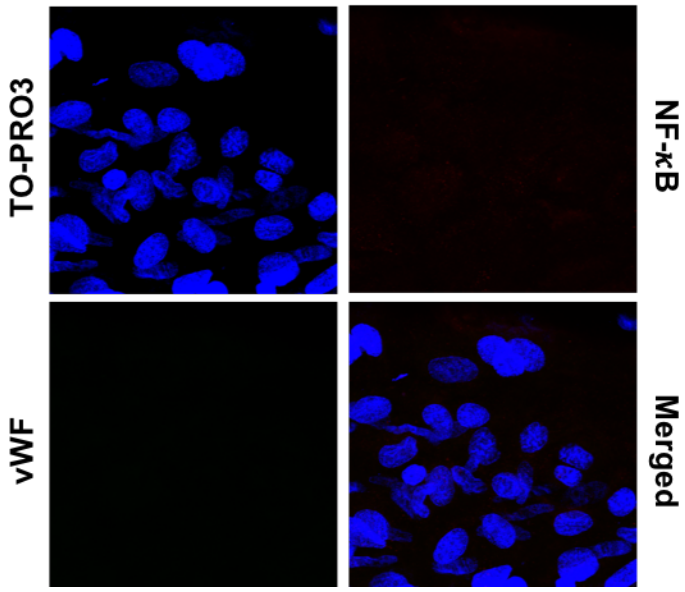

**SUPPLEMENTARY VIDEO 1. Z-STACK OF MCP-1 *EN FACE* IMMUNOFLUORESCENCE**

MCP-1 protein immunofluorescence in the LSV endothelium, described in sections 2.7.2., 2.9.1., 2.9.4. and 3.2.2.2., was assessed using *en face* preparation and immunofluorescent analysis of portions of the LSV. Confocal microscopy was used to acquire Z-stacked image sets at 5 equally-distributed points across the endothelial surface. Supplementary video 1. shows a representative Z-stack from LSV immunofluorescence staining for MCP-1 (red), vWF (green) and TO-PRO3/nuclei (blue) from a portion of LSV which was exposed to 6 hours AHSS in section 3.2.2.2. The video pans from the bottom to top, showing first the underlying VSMCs and then ECs, marked by vWF co-staining (green).

**SUPPLEMENTARY VIDEO 2. Z-STACK OF MCP-1 *EN FACE* IMMUNOFLUORESCENCE WITH MCP-1 SEGMENTATION OVERLAID**

As above, MCP-1 protein immunofluorescence in the LSV endothelium, described in sections 2.7.2., 2.9.1., 2.9.4. and 3.2.2.2., was assessed using *en face* preparation and immunofluorescent analysis of portions of the LSV. Supplementary video 2. shows a representative Z-stack from LSV immunofluorescence staining for MCP-1 (red), vWF (green) and TO-PRO3/nuclei (blue) from a portion of LSV which was exposed to 6 hours AHSS in section 3.2.2.2. Overlaid on the immunofluorescent images are the object maps from the segmentation of MCP-1 protein, obtained using FIJI. The segmentation of objects for the same image is also represented in 2D in section 2.9.4. The video pans from the top to bottom, showing first the ECs, marked by vWF co-staining (green), and then underlying VSMCs. Co-localised with the MCP-1 staining are the segmented objects in multiple colours.

**SUPPLEMENTARY VIDEO 3. Z-STACK OF NF-κB *EN FACE* IMMUNOFLUORESCENCE**

NF-κB protein immunofluorescence in the LSV endothelium, described in sections 2.7.2., 2.9.1. and 3.2.4.1., was assessed using *en face* preparation and analysis of portions of the LSV. Supplementary video 3. shows a representative Z-stack from LSV immunofluorescence staining for NF-κB (red), vWF (green) and TO-PRO3/nuclei (blue) from a portion of LSV which was exposed to 30 minutes AHSS in section 3.2.4.1. The video pans from the the top to bottom, showing first the ECs, marked by vWF co-staining (green), and then underlying VSMCs.

**SUPPLEMENTARY VIDEO 4. REAL-TIME MONOCYTE ADHESION TO vECs *IN VITRO***

THP-1 monocytic-like cell adhesion to the vEC monolayer, *in vitro*, was performed in real-time using the Fluxion Bioflux 200, as described in sections 2.6. and 3.2.7.4. Briefly, HUVECs were pre-treated using the NF-κB inhibitor, BAY11-7085 (upper red channel in video), or DMSO (lower channel in video). Following which, they were exposed to AHSS for 6 hours and then dynamically co-cultured with THP-1 monocytes under shear stress for 10 minutes using the Bioflux microfluidic channel system, during this time sequential images were acquired (33milliseconds apart) to assess adhesion in real-time. Supplementary video 4. shows 10 minutes (sped up to one minute in length) of dynamic co-culture of THP-1 monocytes with ECs and subsequent adhesion of Calcein-labelled THP-1 monocytes (green) to HUVECs (red).

# 7. REFERENCES

Abe, J. and Berk, B. C. (2014). "Novel Mechanisms of Endothelial Mechanotransduction." Arteriosclerosis Thrombosis and Vascular Biology **34**(11): 2378-2386

Ahmad, M., Theofanidis, P. and Medford, R. M. (1998). "Role of activating protein-1 in the regulation of the vascular cell adhesion molecule-1 gene expression by tumor necrosis factor-alpha." Journal of Biological Chemistry **273**(8): 4616-4621

Ahmed, S. M. U., Luo, L., Namani, A., Wang, X. J. and Tang, X. W. (2017). "Nrf2 signaling pathway: Pivotal roles in inflammation." Biochimica Et Biophysica Acta - Molecular Basis of Disease **1863**(2): 585-597

Aird, W. C. (2007). "Phenotypic heterogeneity of the endothelium I. Structure, function, and mechanisms." Circulation Research **100**(2): 158-173

Aird, W. C. (2007). "Phenotypic heterogeneity of the endothelium II. Representative vascular beds." Circulation Research **100**(2): 174-190

Aitsebaomo, J., Portbury, A. L., Schisler, J. C. and Patterson, C. (2008). "Brothers and Sisters Molecular Insights Into Arterial-Venous Heterogeneity." Circulation Research **103**(9): 929-939

Akowuah, E. F., Gray, C., Lawrie, A., Sheridan, P. J., Su, C. H., Bettinger, T., Brisken, A. F., Gunn, J., Crossman, D. C., Francis, S. E., Baker, A. H. and Newman, C. M. (2005). "Ultrasound-mediated delivery of TIMP-3 plasmid DNA into saphenous vein leads to increased lumen size in a porcine interposition graft model." Gene Therapy **12**(14): 1154-1157

Alam, J., Stewart, D., Touchard, C., Boinapally, S., Choi, A. M. K. and Cook, J. L. (1999). "Nrf2, a Cap'n'Collar transcription factor, regulates induction of the heme oxygenase-1 gene." Journal of Biological Chemistry **274**(37): 26071-26078

Alderman, E., Bourassa, M., Brooks, M. M., Califf, R., Chaitman, B., Detre, K., Faxon, D. P., Feit, F., Frye, R. L., Hardison, R. M., Holmes, D., Holubkov, R., Kouchoukos, N., Krone, R., Rogers, W., Rosen, A. D., Schaff, H., Schwartz, L., Siewers, A. S., Sopko, G., Suttontyrrell, K. and Whitlow, P. (1997). "Influence of diabetes on 5-year mortality and morbidity in a randomized trial comparing CABG and PTCA in patients with multivessel disease - The bypass angioplasty revascularization investigation (BARI)." Circulation **96**(6): 1761-1769

Alexander, J. H., Ferguson, T. B., Joseph, D. M., Mack, M. J., Wolf, R. K., Gibson, M., Gennevois, D., Lorenz, T. J., Harrington, R. A., Peterson, E. D., Lee, K. L., Califf, R. M., Kouchoukos, N. T. and Investigators, P. I. (2005). "The PRoject of ex-vivo vein graft ENgineering via Transfection IV

(PREVENT IV) trial: Study rationale, design, and baseline patient characteristics." American Heart Journal **150**(4): 643-649

Alexander, J. H., Hafley, G., Harrington, R., Peterson, E. D., Ferguson, T. B., Lorenz, T. J., Goyal, A., Gibson, M., Mack, M. J., Gennevois, D., Califf, R. M., Kouchoukos, N. T. and Investigators, P. I. (2005). "Efficacy and safety of edifoligide, an E2F transcription factor decoy, for prevention of vein graft failure following coronary artery bypass graft surgery - PREVENT IV: A randomized controlled trial." Jama-Journal of the American Medical Association **294**(19): 2446-2454

Ali, F., Zakkar, M., Karu, K., Lidington, E. A., Hamdulay, S. S., Boyle, J. J., Zloh, M., Bauer, A., Haskard, D. O., Evans, P. C. and Mason, J. C. (2009). "Induction of the Cytoprotective Enzyme Heme Oxygenase-1 by Statins Is Enhanced in Vascular Endothelium Exposed to Laminar Shear Stress and Impaired by Disturbed Flow." Journal of Biological Chemistry **284**(28): 18882-18892

Amano, J., Suzuki, A., Sunamori, M., Tsukada, T. and Numano, F. (1991). "CYTOKINETIC STUDY OF AORTOCORONARY BYPASS VEIN GRAFTS IN PLACE FOR LESS THAN 6 MONTHS." American Journal of Cardiology **67**(15): 1234-1236

Anderson, R. D., Haskell, R. E., Xia, H., Roessler, B. J. and Davidson, B. L. (2000). "A simple method for the rapid generation of recombinant adenovirus vectors." Gene Therapy **7**(12): 1034-1038

Angelini, G. D., Bryan, A. J., Williams, H. M. J., Morgan, R. and Newby, A. C. (1990). "DISTENSION PROMOTES PLATELET AND LEUKOCYTE ADHESION AND REDUCES SHORT-TERM PATENCY IN PIG ARTERIOVENOUS BYPASS GRAFTS." Journal of Thoracic and Cardiovascular Surgery **99**(3): 433-439

Angelini, G. D., Izzat, M. B., Bryan, A. J. and Newby, A. C. (1996). "External stenting reduces early medial and neointimal thickening in a pig model of arteriovenous bypass grafting." Journal of Thoracic and Cardiovascular Surgery **112**(1): 79-84

Antoniades, C., Bakogiannis, C., Leeson, P., Guzik, T. J., Zhang, M. H., Tousoulis, D., Antonopoulos, A. S., Demosthenous, M., Marinou, K., Hale, A., Paschalis, A., Psarros, C., Triantafyllou, C., Bendall, J., Casadei, B., Stefanadis, C. and Channon, K. M. (2011). "Rapid, Direct Effects of Statin Treatment on Arterial Redox State and Nitric Oxide Bioavailability in Human Atherosclerosis via Tetrahydrobiopterin-Mediated Endothelial Nitric Oxide Synthase Coupling." Circulation **124**(3): 335-U176

Antoniades, C., Bakogiannis, C., Tousoulis, D., Reilly, S., Zhang, M. H., Paschalis, A., Antonopoulos, A. S., Demosthenous, M., Miliou, A., Psarros, C., Marinou, K., Sfyras, N., Economopoulos, G., Casadei, B., Channon, K. M. and Stefanadis, C. (2010). "Preoperative

Atorvastatin Treatment in CABG Patients Rapidly Improves Vein Graft Redox State by Inhibition of Rae1 and NADPH-Oxidase Activity." Circulation **122**(11): S66-S73

Antoniades, C., Tousoulis, D., Tentolouris, C., Toutouzas, P. and Stefanadis, C. (2003). "Oxidative stress, antioxidant vitamins, and atherosclerosis - From basic research to clinical practice." Herz **28**(7): 628-638

Arruebo, M., Fernandez-Pacheco, R., Ibarra, M. R. and Santamaria, J. (2007). "Magnetic nanoparticles for drug delivery." Nano Today **2**(3): 22-32

Ascione, R., Lloyd, C. T., Underwood, M. J., Lotto, A. A., Pitsis, A. A. and Angelini, G. D. (2000). "Inflammatory response after coronary revascularization with or without cardiopulmonary bypass." Annals of Thoracic Surgery **69**(4): 1198-1204

Baeuerle, P. A. and Henkel, T. (1994). "Function amd activation of NF-kappa-B in the immune-system." Annual Review of Immunology **12**(1):141-179

Baird, L. and Dinkova-Kostova, A. T. (2011). "The cytoprotective role of the Keap1-Nrf2 pathway." Archives of Toxicology **85**(4): 241-272

Barter, P., Gotto, A. M., Larosa, J. C., Maroni, J., Szarek, M., Grundy, S. M., Kastelein, J. J. P., Bittner, V., Fruchart, J. C. and Treating New Targets, I. (2007). "HDL cholesterol, very low levels of LDL cholesterol, and cardiovascular events." New England Journal of Medicine **357**(13): 1301-1310

Bazzoni, G. and Dejana, E. (2004). "Endothelial cell-to-cell junctions: Molecular organization and role in vascular homeostasis." Physiological Reviews **84**(3): 869-901

Berk, B. C. (2008). "Atheroprotective signaling mechanisms activated by steady laminar flow in endothelial cells." Circulation **117**(8): 1082-1089

Berk, B. C., Abe, J., Min, W., Surapisitchat, J. and Yan, C. (2001). "Endothelial atheroprotective and anti-inflammatory mechanisms." Atherosclerosis Vi **947**:93-111

Berk, B. C., Corson, M. A., Peterson, T. E. and Tseng, H. (1995). "Protein kinases as mediators of fluid shear stress stimulated signal transduction in endothelial cells: A hypothesis for calcium-dependent and calcium-independent events activated by flow." Journal of Biomechanics **28**(12): 1439-1450

Bhullar, I. S., Li, Y. S., Miao, H., Zandi, E., Kim, M., Shyy, J. Y. J. and Chien, S. (1998). "Fluid shear stress activation of I kappa B kinase is integrin-dependent." Journal of Biological Chemistry **273**(46): 30544-30549

Birch, K. A., Ewenstein, B. M., Golan, D. E. and Pober, J. S. (1994). "Prolonged peak elevations in cytoplasmic free calcium-ions, derived from intracellular stores, correlate with the extent of thrombin-stimulated exocytosis in single human umbilical vein endothelial-cells." Journal of Cellular Physiology **160**(3): 545-554

Biswas, C., Shah, N., Muthu, M., La, P., Fernando, A. P., Sengupta, S., Yang, G. and Dennery, P. A. (2014). "Nuclear Heme Oxygenase-1 (HO-1) Modulates Subcellular Distribution and Activation of Nrf2, Impacting Metabolic and Anti-oxidant Defenses." Journal of Biological Chemistry **289**(39): 26882-26894

Bloom, D. A. and Jaiswal, A. K. (2003). "Phosphorylation of Nrf2 at Ser(40) by protein kinase C in response to antioxidants leads to the release of Nrf2 from INrf2, but is not required for Nrf2 stabilization/accumulation in the nucleus and transcriptional activation of antioxidant response element-mediated NAD(P)H : quinone oxidoreductase-1 gene expression." Journal of Biological Chemistry **278**(45): 44675-44682

Bocci, V. and Valacchi, G. (2015). "Nrf2 activation as target to implement therapeutic treatments." Front. Chem. **3**(4): 1-6

Bolte, S. and Cordelieres, F. P. (2006). "A guided tour into subcellular colocalization analysis in light microscopy." Journal of Microscopy-Oxford **224**(3): 213-232

Bonetti, P. O., Lerman, L. O. and Lerman, A. (2003). "Endothelial dysfunction - A marker of atherosclerotic risk." Arteriosclerosis Thrombosis and Vascular Biology **23**(2): 168-175

Boon, R. A. and Horrevoets, A. J. G. (2009). "Key transcriptional regulators of the vasoprotective effects of shear stress." Hamostaseologie **29**(1): 39-43

Boon, R. A., Leyen, T. A., Fontijn, R. D., Fledderus, J. O., Baggen, J. M. C., Volger, O. L., Amerongen, G. P. V. and Horrevoets, A. J. G. (2010). "KLF2-induced actin shear fibers control both alignment to flow and JNK signaling in vascular endothelium." Blood **115**(12): 2533-2542

Bradley, J. (2008). "TNF-mediated inflammatory disease." The Journal of pathology **214**(2): 149-160

Brigelius-Flohe, R. and Flohe, L. (2011). "Basic Principles and Emerging Concepts in the Redox Control of Transcription Factors." Antioxidants & Redox Signaling **15**(8): 2335-2381

Bryan, A. J. and Angelini, G. D. (1994). "The biology of saphenous-vein graft occlusion - etiology and strategies for prevention." Current Opinion in Cardiology **9**(6): 641-649

Cadenas, E. (1997). "Basic mechanisms of antioxidant activity." Biofactors **6**(4): 391-397

Cai, H. and Harrison, D. G. (2000). "Endothelial dysfunction in cardiovascular diseases - The role of oxidant stress." Circulation Research **87**(10): 840-844

Cameron, A. A., Green, G. E., Brogno, D. A. and Thornton, J. (1995). "Internal thoracic artery grafts: 20-year clinical follow-up." Journal of the American College of Cardiology **25**(1): 188-192

Canham, P. B., Finlay, H. M. and Boughner, D. R. (1997). "Contrasting structure of the saphenous vein and internal mammary artery used as coronary bypass vessels." Cardiovascular Research **34**(3): 557-567

Cannon, C. P., Braunwald, E., Mccabe, C. H., Rader, D. J., Rouleau, J. L., Belder, R., Joyal, S. V., Hill, K. A., Pfeffer, M. A., Skene, A. M. and Pravastatin Atorvastatin, E. (2004). "Intensive versus moderate lipid lowering with statins after acute coronary syndromes." New England Journal of Medicine **350**(15): 1495-1504

Carpenter, A. E., Jones, T. R., Lamprecht, M. R., Clarke, C., Kang, I. H., Friman, O., Guertin, D. A., Chang, J. H., Lindquist, R. A., Moffat, J., Golland, P. and Sabatini, D. M. (2006). "CellProfiler: image analysis software for identifying and quantifying cell phenotypes." Genome Biology **7**(10): r100

Castier, Y., Ramkhelawon, B., Riou, S., Tedgui, A. and Lehoux, S. (2009). "Role of NF-kappa B in Flow-Induced Vascular Remodeling." Antioxidants & Redox Signaling **11**(7): 1641-1649

Castier, Y., Ramkhelawon, B., Riou, S., Tedgui, A. and Lehoux, S. (2009). "Role of NF-κB in flow-induced vascular remodeling." Antioxidants & Redox Signaling **11**(7): 1641-1649

Charo, I. F. and Taubman, M. B. (2004). "Chemokines in the pathogenesis of vascular disease." Circulation Research **95**(9): 858-866

Chaudhury, H., Zakkar, M., Boyle, J., Cuhlmann, S., Van Der Heiden, K., Luong, L. A., Davis, J., Platt, A., Mason, J. C., Krams, R., Haskard, D. O., Clark, A. R. and Evans, P. C. (2010). "c-Jun N-Terminal Kinase Primes Endothelial Cells at Atheroprone Sites for Apoptosis." Arteriosclerosis Thrombosis and Vascular Biology **30**(3): 546-U393

Chen, B., Lu, Y. R., Chen, Y. N. and Cheng, J. Q. (2015). "The role of Nrf2 in oxidative stress-induced endothelial injuries." Journal of Endocrinology **225**(3): R83-R99

Chen, J., Green, J., Yurdagul, A., Albert, P., Mcinnis, M. C. and Orr, A. W. (2015). "Alpha v beta 3 Integrins Mediate Flow-Induced NF-kappa B Activation, Proinflammatory Gene Expression, and Early Atherogenic Inflammation." American Journal of Pathology **185**(9): 2575-2589

Chen, L. F. and Greene, W. C. (2004). "Shaping the nuclear action of NF-kappa B." Nature Reviews Molecular Cell Biology **5**(5): 392-401

Chen, X. L., Dodd, G., Thomas, S., Zhang, X. L., Wasserman, M. A., Rovin, B. H. and Kunsch, C. (2006). "Activation of Nrf2/ARE pathway protects endothelial cells from oxidant injury and inhibits inflammatory gene expression." American Journal of Physiology-Heart and Circulatory Physiology **290**(5): H1862-H1870

Chi, J. T., Chang, H. Y., Haraldsen, G., Jahnsen, F. L., Troyanskaya, O. G., Chang, D. S., Wang, Z., Rockson, S. G., Van De Rijn, M., Botstein, D. and Brown, P. O. (2003). "Endothelial cell diversity revealed by global expression profiling." Proceedings of the National Academy of Sciences of the United States of America **100**(19): 10623-10628

Chien, S. (2007). "Mechanotransduction and endothelial cell homeostasis: the wisdom of the cell." American Journal of Physiology-Heart and Circulatory Physiology **292**(3): H1209-H1224

Chistiakov, D. A., Orekhov, A. N. and Bobryshev, Y. V. (2017). "Effects of shear stress on endothelial cells: go with the flow." Acta Physiology **219**(2): 382-408

Chiu, J.-J., Wang, D., Chien, S., Skalak, R. and Usami, S. (1998). "Effects of disturbed flow on endothelial cells." Journal of Biomechanical Engineering **120**(1): 2-8

Chiu, J. J., Chang, S. F., Lee, P. L., Lee, C. I., Tsai, M. C., Lee, D. Y., Hsieh, H. P., Usami, S. and Chien, S. (2005). "Shear stress inhibits smooth muscle cell-induced inflammatory gene expression in endothelial cells - Role of NF-kappa B." Arteriosclerosis Thrombosis and Vascular Biology **25**(5): 963-969

Chiu, J. J. and Chien, S. (2011). "Effects of Disturbed Flow on Vascular Endothelium: Pathophysiological Basis and Clinical Perspectives." Physiological Reviews **91**(1): 327-387

Chiu, J. J., Lee, P. L., Chen, C. N., Lee, C. I., Chang, S. F., Chen, L. J., Lien, S. C., Ko, Y. C., Usami, S. and Chien, S. (2004). "Shear stress increases ICAM-1 and decreases VCAM-1 and E-selectin

expressions induced by tumor necrosis factor-alpha in endothelial cells." Arteriosclerosis Thrombosis and Vascular Biology **24**(1): 73-79

Christian, F., Smith, E. L. and Carmody, R. J. (2016). "The Regulation of NF-kappa B Subunits by Phosphorylation." Cells **5**(12): 1-19

Christiansen, J. F., Hartwig, D., Bechtel, J. F. M., Kluter, H., Sievers, H. H., Schonbeck, U. and Bartels, C. (2004). "Diseased vein grafts express elevated inflammatory cytokine levels compared with atherosclerotic coronary arteries." Annals of Thoracic Surgery **77**(5): 1575-1579

Collins, T. and Cybulsky, M. I. (2001). "NF-kappa B: pivotal mediator or innocent bystander in atherogenesis?" Journal of Clinical Investigation **107**(3): 255-264

Conway, D. E., Breckenridge, M. T., Hinde, E., Gratton, E., Chen, C. S. and Schwartz, M. A. (2013). "Fluid Shear Stress on Endothelial Cells Modulates Mechanical Tension across VE-Cadherin and PECAM-1." Current Biology **23**(11): 1024-1030

Cornelissen, J., Armstrong, J. and Holt, C. M. (2004). "Mechanical stretch induces phosphorylation of p38-MAPK and apoptosis in human saphenous vein." Arteriosclerosis Thrombosis and Vascular Biology **24**(3): 451-456

Cox, J. L., Chiasson, D. A. and Gotlieb, A. I. (1991). "Stranger in a strange land - the pathogenesis of saphenous-vein graft stenosis with emphasis on structural and functional differences between veins and arteries." Progress in Cardiovascular Diseases **34**(1): 45-68

Crook, M. F., Newby, A. C. and Southgate, K. M. (2000). "Expression of intercellular adhesion molecules in human saphenous veins: effects of inflammatory cytokines and neointima formation in culture." Atherosclerosis **150**(1): 33-41

Cuhlmann, S., Van Der Heiden, K., Saliba, D., Tremoleda, J. L., Khalil, M., Zakkar, M., Chaudhury, H., Le Anh, L., Mason, J. C., Udalova, I., Gsell, W., Jones, H., Haskard, D. O., Krams, R. and Evans, P. C. (2011). "Disturbed Blood Flow Induces RelA Expression via c-Jun N-Terminal Kinase 1 A Novel Mode of NF-kappa B Regulation That Promotes Arterial Inflammation." Circulation Research **108**(8): 950-959

Cunningham, K. S. and Gotlieb, A. I. (2005). "The role of shear stress in the pathogenesis of atherosclerosis." Laboratory Investigation **85**(1): 9-23

Curl, K., Lebude, B., Ruggiero, N., Fischman, D., Rose, A., Patel, S., Ogilby, D., Walinsky, P., Jasti, B. and Savage, M. (2016). "Frequency of Use of Statins and Aspirin in Patients With Previous Coronary Artery Bypass Grafting." American Journal of Cardiology **118**(1): 40-43

Dardik, A., Yamashita, A., Aziz, F., Asada, H. and Sumpio, B. E. (2005). "Shear stress-stimulated endothelial cells induce smooth muscle cell chemotaxis via platelet-derived growth factor-BB and interleukin-1 alpha." Journal of Vascular Surgery **41**(2): 321-331

Dashwood, M. R. and Tsui, J. C. (2013). "'No-touch' saphenous vein harvesting improves graft performance in patients undergoing coronary artery bypass surgery: A journey from bedside to bench." Vascular Pharmacology **58**(3): 240-250

Davies, P. F. (1997). "Temporal and spatial relationships in shear stress-mediated endothelial signalling - Overview." Journal of Vascular Research **34**(3): 208-211

Davignon, J., Gregg, R. E. and Sing, C. F. (1988). "Apolipoprotein-e polymorphism and atherosclerosis." Arteriosclerosis **8**(1): 1-21

De Souza, D. R., Dashwood, M. R. and Samano, N. (2017). "Saphenous vein graft harvesting and patency: no-touch harvesting is the answer." Journal of Thoracic and Cardiovascular Surgery **154**(4): 1300-1301

De Vries, M. R., Simons, K. H., Jukema, J. W., Braun, J. and Quax, P. H. A. (2016). "Vein graft failure: from pathophysiology to clinical outcomes." Nature Reviews Cardiology **13**(8): 451-470

Dejana, E. (2004). "Endothelial cell-cell junctions: Happy together." Nature Reviews Molecular Cell Biology **5**(4): 261-270

Dekker, R. J., Boon, R. A., Rondaij, M. G., Kragt, A., Volger, O. L., Elderkamp, Y. W., Meijers, J. C. M., Voorberg, J., Pannekoek, H. and Horrevoets, A. J. G. (2006). "KLF2 provokes a gene expression pattern that establishes functional quiescent differentiation of the endothelium." Blood **107**(11): 4354-4363

Dekker, R. J., Van Soest, S., Fontijn, R. D., Salamanca, S., De Groot, P. G., Vanbavel, E., Pannekoek, H. and Horrevoets, A. J. G. (2002). "Prolonged fluid shear stress induces a distinct set of endothelial cell genes, most specifically lung Kruppel-like factor (KLF2)." Blood **100**(5): 1689-1698

Dekker, R. J., Van Thienen, J. V., Rohlena, J., De Jager, S. C., Elderkamp, Y. W., Seppen, J., De Vries, C. J. M., Biessen, E. a. L., Van Berkel, T. J. C., Pannekoek, H. and Horrevoets, A. J. G. (2005).

"Endothelial KLF2 links local arterial shear stress levels to the expression of vascular tone-regulating genes." American Journal of Pathology **167**(2): 609-618

Deng, D. X. F., Tsalenko, A., Vailaya, A., Ben-Dor, A., Kundu, R., Estay, I., Tabibiazar, R., Kincaid, R., Yakhini, Z., Bruhn, L. and Quertermous, T. (2006). "Differences in vascular bed disease susceptibility reflect differences in gene expression response to atherogenic stimuli." Circulation Research **98**(2): 200-208

Deo, S. V., Dunlay, S. M., Shah, I. K., Altarabsheh, S. E., Erwin, P. J., Boilson, B. A., Park, S. J. and Joyce, L. D. (2013). "Dual Anti-platelet Therapy After Coronary Artery Bypass Grafting: Is There Any Benefit? A Systematic Review and Meta-Analysis." Journal of Cardiac Surgery **28**(2): 109-116

Deshmane, S. L., Kremlev, S., Amini, S. and Sawaya, B. E. (2009). "Monocyte Chemoattractant Protein-1 (MCP-1): An Overview." Journal of Interferon and Cytokine Research **29**(6): 313-326

Dewey, C. F., Bussolari, S. R., Gimbrone, M. A. and Davies, P. F. (1981). "The dynamic-response of vascular endothelial-cells to fluid shear-stress." Journal of Biomechanical Engineering-Transactions of the Asme **103**(3): 177-185

Dickinson, D. A., Levonen, A. L., Moellering, D. R., Arnold, E. K., Zhang, H. Q., Darley-Usmar, V. M. and Forman, H. J. (2004). "Human glutamate cysteine ligase gene regulation through the electrophile response element." Free Radical Biology and Medicine **37**(8): 1152-1159

Dinkova-Kostova, A. T., Holtzclaw, W. D. and Kensler, T. W. (2005). "The role of Keap1 in cellular protective responses." Chemical Research in Toxicology **18**(12): 1779-1791

Dixit, N. and Simon, S. I. (2012). "Chemokines, selectins and intracellular calcium flux: temporal and spatial cues for leukocyte arrest." Frontiers in Immunology **3**(188): 1-9

Dobrin, P. B., Golan, J., Fareed, J., Blakeman, B. and Littoy, F. N. (1992). "Preoperative vs postoperative pharmacological inhibition of platelets - effect on intimal hyperplasia in canine autogenous vein grafts." Journal of Cardiovascular Surgery **33**(6): 705-709

Dobrin, P. B., Littooy, F. N. and Endean, E. D. (1989). "Mechanical factors predisposing to intimal hyperplasia and medial thickening in autogenous vein grafts." Surgery **105**(3): 393-400

Dong, C., Davis, R. J. and Flavell, R. A. (2002). "MAP kinases in the immune response." Annual Review of Immunology **20**: 55-72

Dries, D., Mohammad, S. F., Woodward, S. C. and Nelson, R. M. (1992). "The influence of harvesting technique on endothelial preservation in saphenous veins." Journal of Surgical Research **52**(3): 219-225

Durante, W. (2010). "Targeting Heme Oxygenase-1 in Vascular Disease." Current Drug Targets **11**(12): 1504-1516

Eagle, K. A., Guyton, R. A., Davidoff, R., Edwards, F. H., Ewy, G. A., Gardner, T. J., Hart, J. C., Herrmann, H. C., Hillis, L. D., Hutter, A. M., Jr., Lytle, B. W., Marlow, R. A., Nugent, W. C., Orszulak, T. A., American College Of, C. and American Heart, A. (2004). "ACC/AHA 2004 guideline update for coronary artery bypass graft surgery: a report of the American College of Cardiology/American Heart Association Task Force on Practice Guidelines (Committee to Update the 1999 Guidelines for Coronary Artery Bypass Graft Surgery)." Circulation **110**(14): e340-437

Enesa, K., Zakkar, M., Chaudhury, H., Luong, L. A., Rawlinson, L., Mason, J. C., Haskard, D. O., Dean, J. L. E. and Evans, P. C. (2008). "NF-kappa B suppression by the deubiquitinating enzyme Cezanne - A novel negative feedback loop in pro-inflammatory signaling." Journal of Biological Chemistry **283**(11): 7036-7045

Fernandez-Alfonso, M. S., Gil-Ortega, M., Aranguez, I., Souza, D., Dreifaldt, M., Somoza, B. and Dashwood, M. R. (2017). "Role of PVAT in coronary atherosclerosis and vein graft patency: friend or foe?" British Journal of Pharmacology **174**(20): 3561-3572

Flaherty, J. T., Ferrans, V. J., Tucker, W. K., Fry, D. L., Patel, D. J. and Pierce, J. E. (1972). "Endothelial nuclear patterns in canine arterial tree with particular reference to hemodynamic events." Circulation Research **30**(1): 23-28

Fledderus, J. O., Boon, R. A., Volger, O. L., Hurttila, H., Yla-Herttuala, S., Pannekoek, H., Levonen, A. L. and Horrevoets, A. J. G. (2008). "KLF2 primes the antioxidant transcription factor Nrf2 for activation in endothelial cells." Arteriosclerosis Thrombosis and Vascular Biology **28**(7): 1339-1346

Fledderus, J. O., Van Thienen, J. V., Boon, R. A., Dekker, R. J., Rohlena, J., Volger, O. L., Bijnens, A., Daemen, M., Kuiper, J., Van Berkel, T. J. C., Pannekoek, H. and Horrevoets, A. J. G. (2007). "Prolonged shear stress and KLF2 suppress constitutive proinflarnmatory transcription through inhibition of ATF2." Blood **109**(10): 4249-4257

Flohe, L., Brigeliusflohe, R., Saliou, C., Traber, M. G. and Packer, L. (1997). "Redox regulation of NF-kappa B activation." Free Radical Biology and Medicine **22**(6): 1115-1126

Florey, L. (1966). "The endothelial cell." British Medical Journal **2**(5512): 487-90

Forstermann, U. (2008). "Oxidative stress in vascular disease: causes, defense mechanisms and potential therapies." Nature Clinical Practice Cardiovascular Medicine **5**(6): 338-349

Frangos, J. A., Eskin, S. G., Mcintire, L. V. and Ives, C. L. (1985). "Flow effects on prostacyclin production by cultured human-endothelial cells." Science **227**(4693): 1477-1479

Franklin, C. C., Backos, D. S., Mohar, I., White, C. C., Forman, H. J. and Kavanagh, T. J. (2009). "Structure, function, and post-translational regulation of the catalytic and modifier subunits of glutamate cysteine ligase." Molecular Aspects of Medicine **30**(1-2): 86-98

Fraser, C. C. (2006). "Exploring the positive and negative consequences of NF-kappa B inhibition for the treatment of human disease." Cell Cycle **5**(11): 1160-1163

Fu, C. H., Yu, P., Tao, M., Gupta, T., Moldawer, L. L., Berceli, S. A. and Jiang, Z. H. (2012). "Monocyte Chemoattractant Protein-1/CCR2 Axis Promotes Vein Graft Neointimal Hyperplasia Through Its Signaling in Graft-Extrinsic Cell Populations." Arteriosclerosis Thrombosis and Vascular Biology **32**(10): 2418-2432

Gainetdinov, R. R., Premont, R. T., Bohn, L. M., Lefkowitz, R. J. and Caron, M. G. (2004). "Desensitization of G protein-coupled receptors and neuronal functions." Annual Review of Neuroscience **27**: 107-144

Garatti, A., Castelvecchio, S., Canziani, A., Corain, L., Generali, T., Mossuto, E., Gagliardotto, P., Anastasia, L., Salmaso, L., Giacomazzi, F. and Menicanti, L. (2014). "Long-term results of sequential vein coronary artery bypass grafting compared with totally arterial myocardial revascularization: a propensity score-matched follow-up study." European Journal of Cardio-Thoracic Surgery **46**(6): 1006-1013

Gareus, R., Kotsaki, E., Xanthoulea, S., Van Der Made, I., Gijbels, M. J., Kardakaris, R., Polykratis, A., Kollias, G., De Winther, M. P. and Pasparakis, M. (2008). "Endothelial cell-specific NF-κB inhibition protects mice from atherosclerosis." Cell metabolism **8**(5): 372-383

Garstkiewicz, M., Strittmatter, G. E., Grossi, S., Sand, J., Fenini, G., Werner, S., French, L. E. and Beer, H. D. (2017). "Opposing effects of Nrf2 and Nrf2-activating compounds on the NLRP3 inflammasome independent of Nrf2-mediated gene expression." European Journal of Immunology **47**(5): 806-817

Gaudino, M., Antoniades, C., Benedetto, U., Deb, S., Di Franco, A., Di Giammarco, G., Fremes, S., Glineur, D., Grau, J., He, G. W., Marinelli, D., Ohmes, L. B., Patrono, C., Puskas, J., Tranbaugh, R., Girardi, L. N., Taggart, D. P. and Atlantic Arterial Grafting, I. (2017). "Mechanisms, Consequences, and Prevention of Coronary Graft Failure." Circulation **136**(18): 1749-1764

Gaziano, T. A., Bitton, A., Anand, S., Abrahams-Gessel, S. and Murphy, A. (2010). "Growing Epidemic of Coronary Heart Disease in Low- and Middle-Income Countries." Current Problems in Cardiology **35**(2): 72-115

George, S. J., Baker, A. H., Angelini, G. D. and Newby, A. C. (1998). "Gene transfer of tissue inhibitor of metalloproteinase-2 inhibits metalloproteinase activity and neointima formation in human saphenous veins." Gene Therapy **5**(11): 1552-1560

George, S. J., Lloyd, C. T., Angelini, G. D., Newby, A. C. and Baker, A. H. (2000). "Inhibition of late vein graft neointima formation in human and porcine models by adenovirus-mediated overexpression of tissue inhibitor of metalloproteinase-3." Circulation **101**(3): 296-304

George, S. J., Wan, S., Hu, J., Macdonald, R., Johnson, J. L. and Baker, A. H. (2011). "Sustained Reduction of Vein Graft Neointima Formation by Ex Vivo TIMP-3 Gene Therapy." Circulation **124**(11): S135-S142

Gerschman, R., Gilbert, D. L., Nye, S. W., Dwyer, P. and Fenn, W. O. (1954). "Oxygen poisoning and x-irradiation - a mechanism in common." Science **119**(3097): 623-626

Gerszten, R. E., Garcia-Zepeda, E. A., Lim, Y. C., Yoshida, M., Ding, H. A., Gimbrone, M. A., Luster, A. D., Luscinskas, F. W. and Rosenzweig, A. (1999). "MCP-1 and IL-8 trigger firm adhesion of monocytes to vascular endothelium under flow conditions." Nature **398**(6729): 718-723

Ghista, D. N. and Kabinejadian, F. (2013). "Coronary artery bypass grafting hemodynamics and anastomosis design: a biomedical engineering review." Biomedical Engineering Online **12**(28):1-28

Ghosh, S., May, M. J. and Kopp, E. B. (1998). "NF-kappa B and rel proteins: Evolutionarily conserved mediators of immune responses." Annual Review of Immunology **16**: 225-260

Giangrande, P. H., Zhang, J. X., Tanner, A., Eckhart, A. D., Rempel, R. E., Andrechek, E. R., Layzer, J. M., Keys, J. R., Hagen, P. O., Nevins, J. R., Koch, W. J. and Sullenger, B. A. (2007). "Distinct roles of E2F proteins in vascular smooth muscle cell proliferation and intimal hyperplasia." Proceedings of the National Academy of Sciences of the United States of America **104**(32): 12988-12993

Gilmore, T. and Herscovitch, M. (2006). "Inhibitors of NF-κB signaling: 785 and counting." Oncogene **25**(51): 6887-6899

Gimbrone, M. A. and Garcia-Cardena, G. (2016). "Endothelial Cell Dysfunction and the Pathobiology of Atherosclerosis." Circulation Research **118**(4): 620-636

Gimbrone, M. A., Nagel, T. and Topper, J. N. (1997). "Biomechanical activation: An emerging paradigm in endothelial adhesion biology." Journal of Clinical Investigation **99**(8): 1809-1813

Goldman, S., Sethi, G. K., Holman, W., Thai, H., Mcfalls, E., Ward, H. B., Kelly, R. F., Rhenman, B., Tobler, G. H., Bakaeen, F. G., Huh, J., Soltero, E., Moursi, M., Haime, M., Crittenden, M., Kasirajan, V., Ratliff, M., Pett, S., Irimpen, A., Gunnar, W., Thomas, D., Fremes, S., Moritz, T., Reda, D., Harrison, L., Wagner, T. H., Wang, Y. J., Planting, L., Miller, M., Rodriguez, Y., Juneman, E., Morrison, D., Pierce, M. K., Kreamer, S., Shih, M. C. and Lee, K. (2011). "Radial Artery Grafts vs Saphenous Vein Grafts in Coronary Artery Bypass Surgery A Randomized Trial." Jama-Journal of the American Medical Association **305**(2): 167-174

Golledge, J. (1997). "Vein grafts: Haemodynamic forces on the endothelium - A review." European Journal of Vascular and Endovascular Surgery **14**(5): 333-343

Golledge, J., Gosling, M., Turner, R. J., Standfield, N. J. and Powell, J. T. (2000). "Arterial flow induces changes in saphenous vein endothelium proteins transduced by cation channels." European Journal of Vascular and Endovascular Surgery **19**(5): 545-550

Golledge, J., Turner, R. J., Harley, S. L., Springall, D. R. and Powell, J. T. (1997). "Circumferential deformation and shear stress induce differential responses in saphenous vein endothelium exposed to arterial flow." Journal of Clinical Investigation **99**(11): 2719-2726

Gorrini, C., Harris, I. S. and Mak, T. W. (2013). "Modulation of oxidative stress as an anticancer strategy." Nature Reviews Drug Discovery **12**(12): 931-947

Gosling, M., Golledge, J., Turner, R. J. and Powell, J. T. (1999). "Arterial flow conditions downregulate thrombomodulin on saphenous vein endothelium." Circulation **99**(8): 1047-1053

Gregory, S. M., Nazir, S. A. and Metcalf, J. P. (2011). "Implications of the innate immune response to adenovirus and adenoviral vectors." Future Virology **6**(3): 357-374

Griendling, K. K., Sorescu, D. and Ushio-Fukai, M. (2000). "NAD(P)H oxidase - Role in cardiovascular biology and disease." Circulation Research **86**(5): 494-501

Guzik, T. J., Olszanecki, R., Sadowski, J., Kapelak, B., Rudzinski, P., Jopek, A., Kawczynska, A., Ryszawa, N., Loster, J., Jawien, J., Czesnikiewicz-Guzik, M., Channon, K. M. and Korbut, R. (2005). "Superoxide dismutase activity and expression in human venous and arterial bypass graft vessels." Journal of Physiology and Pharmacology **56**(2): 313-323

Hahn, C., Orr, A. W., Sanders, J. M., Jhaveri, K. A. and Schwartz, M. A. (2009). "The Subendothelial Extracellular Matrix Modulates JNK Activation by Flow." Circulation Research **104**(8): 995-U180

Hahn, C. and Schwartz, M. A. (2008). "The Role of Cellular Adaptation to Mechanical Forces in Atherosclerosis." Arteriosclerosis Thrombosis and Vascular Biology **28**(12): 2101-2107

Halliwell, B. (1996). "Antioxidants in human health and disease." Annu. Rev. Nutr. **16**: 33-50

Han, J., Zern, B. J., Shuvaev, V. V., Davies, P. F., Muro, S. and Muzykantov, V. (2012). "Acute and chronic shear stress differently regulate endothelial internalization of nanocarriers targeted to platelet-endothelial cell adhesion molecule-1." ACS nano **6**(10): 8824-8836

Hansson, G. K. (2005). "Mechanisms of disease - Inflammation, atherosclerosis, and coronary artery disease." New England Journal of Medicine **352**(16): 1685-1695

Harskamp, R. E., Lopes, R. D., Baisden, C. E., De Winter, R. J. and Alexander, J. H. (2013). "Saphenous Vein Graft Failure After Coronary Artery Bypass Surgery Pathophysiology, Management, and Future Directions." Ann. Surg. **257**(5): 824-833

Hay, D. C., Beers, C., Cameron, V., Thomson, L., Flitney, F. W. and Hay, R. T. (2003). "Activation of NF-kappa B nuclear transcription factor by flow in human endothelial cells." Biochimica Et Biophysica Acta-Molecular Cell Research **1642**(1-2): 33-44

Hayden, M. S. and Ghosh, S. (2008). "Shared principles in NF-kappa B signaling." Cell **132**(3): 344-362

Hennig, P., Garstkiewicz, M., Grossi, S., Di Filippo, M., French, L. E. and Beer, H. D. (2018). "The Crosstalk between Nrf2 and Inflammasomes." International Journal of Molecular Sciences **19**(2): 1-10

Hinokiyama, K., Valen, G., Tokuno, S., Vedin, J. B. and Vaage, J. (2006). "Vein graft harvesting induces inflammation and impairs vessel reactivity." Annals of Thoracic Surgery **82**(4): 1458-1464

Hoch, J. R., Stark, V. K., Hullett, D. A. and Turnipseed, W. D. (1994). "Vein graft intimal hyperplasia: leukocytes and cytokine gene expression." Surgery **116**(2): 463-70; discussion 470-1

Hoch, J. R., Stark, V. K., Van Rooijen, N., Kim, J. L., Nutt, M. P. and Warner, T. F. (1999). "Macrophage depletion alters vein graft intimal hyperplasia." Surgery **126**(2): 428-437

Hong, F., Freeman, M. L. and Liebler, D. C. (2005). "Identification of sensor cysteines in human Keap1 modified by the cancer chemopreventive agent sulforaphane." Chemical Research in Toxicology **18**(12): 1917-1926

Hsieh, C. Y., Hsiao, H. Y., Wu, W. Y., Liu, C. A., Tsai, Y. C., Chao, Y. J., Wang, D. L. and Hsieh, H. J. (2009). "Regulation of shear-induced nuclear translocation of the Nrf2 transcription factor in endothelial cells." Journal of Biomedical Science **16**(1): 1-14

Hsieh, H. J., Liu, C. A., Huang, B., Tseng, A. H. H. and Wang, D. L. (2014). "Shear-induced endothelial mechanotransduction: the interplay between reactive oxygen species (ROS) and nitric oxide (NO) and the pathophysiological implications." Journal of Biomedical Science **21**(3): 1- 15

Huang, H. C., Nguyen, T. and Pickett, C. B. (2002). "Phosphorylation of Nrf2 at Ser-40 by protein kinase C regulates antioxidant response element-mediated transcription." Journal of Biological Chemistry **277**(45): 42769-42774

Huang, Y., Li, W. J., Su, Z. Y. and Kong, A. N. T. (2015). "The complexity of the Nrf2 pathway: beyond the antioxidant response." Journal of Nutritional Biochemistry **26**(12): 1401-1413

Hwang, H. Y., Kim, M. A., Seo, J. W. and Kim, K. B. (2012). "Endothelial preservation of the minimally manipulated saphenous vein composite graft: Histologic and immunohistochemical study." Journal of Thoracic and Cardiovascular Surgery **144**(3): 690-696

Hybertson, B. M., Gao, B. F., Bose, S. K. and Mccord, J. M. (2011). "Oxidative stress in health and disease: The therapeutic potential of Nrf2 activation." Molecular Aspects of Medicine **32**(4-6): 234-246

Isaji, T., Hashimoto, T., Yamamoto, K., Santana, J. M., Yatsula, B., Hu, H. D., Bai, H. L., Guo, J. M., Kudze, T., Nishibe, T. and Dardik, A. (2017). "Improving the Outcome of Vein Grafts: Should Vascular Surgeons Turn Veins into Arteries?" Annals of Vascular Diseases **10**(1): 8-16

Ishida, T., Peterson, T. E., Kovach, N. L. and Berk, B. C. (1996). "MAP kinase activation by flow in endothelial cells - Role of beta 1 integrins and tyrosine kinases." Circulation Research **79**(2): 310-316

Itoh, K., Igarashi, K., Hayashi, N., Nishizawa, M. and Yamamoto, M. (1995). "Cloning and characterization of a novel erythroid cell-derived cnc family transcription factor heterodimerizing with the small maf family proteins." Molecular and Cellular Biology **15**(8): 4184-4193

Izzat, M. B., Mehta, D., Bryan, A. J., Reeves, B., Newby, A. C. and Angelini, G. D. (1996). "Influence of external stent size on early medial and neointimal thickening in a pig model of saphenous vein bypass grafting." Circulation **94**(7): 1741-1745

Jacot, J. G. and Wong, J. Y. (2008). "Endothelial injury induces vascular smooth muscle cell proliferation in highly localized regions of a direct contact co-culture system." Cell Biochemistry and Biophysics **52**(1): 37-46

Jaffe, E. A., Nachman, R. L., Becker, C. G. and Minick, C. R. (1973). "Culture of human endothelial cells derived from umbilical veins - identification by morphologic and immunological criteria." Journal of Clinical Investigation **52**(11): 2745-2756

Jaiswal, A. K. (2000). "Regulation of genes encoding NAD(P)H : quinone oxidoreductases." Free Radical Biology and Medicine **29**(3-4): 254-262

Jeremy, J. Y., Bulbulia, R., Johnson, J. L., Gadsdon, P., Vijayan, V., Shukla, N., Smith, F. C. T. and Angelini, G. D. (2004). "A bioabsorbable (polyglactin), nonrestrictive, external sheath inhibits porcine saphenous vein graft thickening." Journal of Thoracic and Cardiovascular Surgery **127**(6): 1766-1772

Jeremy, J. Y., Dashwood, M. R., Timm, M., Izzat, M. B., Mehta, D., Bryan, A. J. and Angelini, G. D. (1997). "Nitric oxide synthase and adenylyl and guanylyl cyclase activity in porcine interposition vein grafts." Annals of Thoracic Surgery **63**(2): 470-476

Jeremy, J. Y., Gadsdon, P., Shukla, N., Vijayan, V., Wyatt, M., Newby, A. C. and Angelim, G. D. (2007). "On the biology of saphenous vein grafts fitted with external synthetic sheaths and stents." Biomaterials **28**(6): 895-908

Jeremy, J. Y., Shukla, N., Muzaffar, S., Handley, A. and Angelini, G. D. (2004). "Reactive oxygen species, vascular disease and cardiovascular surgery." Current Vascular Pharmacology **2**(3): 229-236

Jiang, Z. H., Yu, P., Tao, M., Ifantides, C., Ozaki, C. K. and Berceli, S. A. (2009). "Interplay of CCR2 signaling and local shear force determines vein graft neointimal hyperplasia in vivo." Febs Letters **583**(21): 3536-3540

Jo, H., Dull, R. O., Hollis, T. M. and Tarbell, J. M. (1991). "Endothelial albumin permeability is shear dependent, time-dependent, and reversible." American Journal of Physiology **260**(6): H1992-H1996

Joddar, B., Firstenberg, M. S., Reen, R. K., Varadharaj, S., Khan, M., Childers, R. C., Zweier, J. L. and Gooch, K. J. (2015). "Arterial Levels of Oxygen Stimulate Intimal Hyperplasia in Human Saphenous Veins via a ROS-Dependent Mechanism." Plos One **10**(3): 1-16

Joddar, B., Reen, R. K., Firstenberg, M. S., Varadharaj, S., Mccord, J. M., Zweier, J. L. and Gooch, K. J. (2011). "Protandim attenuates intimal hyperplasia in human saphenous veins cultured ex vivo via a catalase-dependent pathway." Free Radical Biology and Medicine **50**(6): 700-709

Johnson, C., Van Antwerp, D. and Hope, T. J. (1999). "An N-terminal nuclear export signal is required for the nucleocytoplasmic shuttling of I kappa B alpha." Embo Journal **18**(23): 6682-6693

Kanner, J., Frankel, E., Granit, R., German, B. and Kinsella, J. E. (1994). "Natural antioxidants in grapes and wines." Journal of Agricultural and Food Chemistry **42**(1): 64-69

Karin, M. and Ben-Neriah, Y. (2000). "Phosphorylation meets ubiquitination: The control of NF-kappa B activity." Annual Review of Immunology **18**: 621-663

Katsumi, A., Orr, A. W., Tzima, E. and Schwartz, M. A. (2004). "Integrins in mechanotransduction." Journal of Biological Chemistry **279**(13): 12001-12004

Kawamura, K., Ishikawa, K., Wada, Y., Kimura, S., Matsumoto, H., Kohro, T., Itabe, H., Kodama, T. and Maruyama, Y. (2005). "Bilirubin from heme oxygenase-1 attenuates vascular endothelial activation and dysfunction." Arteriosclerosis Thrombosis and Vascular Biology **25**(1): 155-160

Kempfert, J., Anger, K., Rastan, A., Krabbes, S., Lehmann, S., Garbade, J., Sauer, M., Walther, T., Dhein, S. and Mohr, F. W. (2009). "Postoperative development of aspirin resistance following coronary artery bypass." European Journal of Clinical Investigation **39**(9): 769-774

Kensler, T. W., Wakabayash, N. and Biswal, S. (2007). "Cell survival responses to environmental stresses via the Keap1-Nrf2-ARE pathway." Annual Review of Pharmacology and Toxicology **47**: 89-116

Kensler, T. W. and Wakabayashi, N. (2010). "Nrf2: friend or foe for chemoprevention?" Carcinogenesis **31**(1): 90-99

Keynton, R. S., Evancho, M. M., Sims, R. L., Rodway, N. V., Gobin, A. and Rittgers, S. E. (2001). "Intimal hyperplasia and wall shear in arterial bypass graft distal anastomoses: An in vivo model study." Journal of Biomechanical Engineering-Transactions of the Asme **123**(5): 464-473

Khachigian, L. M., Resnick, N., Gimbrone, M. A. and Collins, T. (1995). "Nuclear factor-kappa-B interacts functionally with the platelet-derived growth-factor b-chain shear-stress response element in vascular endothelial-cells exposed to fluid shear-stress." Journal of Clinical Investigation **96**(2): 1169-1175

Kim, I., Moon, S. O., Kim, S. H., Kim, H. J., Koh, Y. S. and Koh, G. Y. (2001). "Vascular endothelial growth factor expression of intercellular adhesion molecule 1 (ICAM-1), vascular cell adhesion molecule 1 (VCAM-1), and E-selectin through nuclear factor-kappa B activation in endothelial cells." Journal of Biological Chemistry **276**(10): 7614-7620

Kim, J., Cha, Y. N. and Surh, Y. J. (2010). "A protective role of nuclear factor-erythroid 2-related factor-2 (Nrf2) in inflammatory disorders." Mutation Research -Fundamental Molecular Mechanisms of Mutagenesis **690**(1-2): 12-23

Kim, J. E., You, D. J., Lee., C., Seong., J. Y. and Hwang., J. I. (2010). "Suppression of NF kappa B signalling by Keap1 regulation of IKKbeta activity through autophagic degradation and inhibitionof phosphorylation." Cellular Signalling **22**(11): 1645-1654

Kobayashi, E. H., Suzuki, T., Funayama, R., Nagashima, T., Hayashi, M., Sekine, H., Tanaka, N., Moriguchi, T., Motohashi, H., Nakayama, K. and Yamamoto, M. (2016). "Nrf2 suppresses macrophage inflammatory response by blocking proinflammatory cytokine transcription." Nature Communications **7**(11624): 1-14

Kocarslan, A., Kocarslan, S., Aydin, M. S., Altiparmak, I. H., Demir, D., Sezen, H., Yuce, H. H. and Goz, M. (2016). "Relationship Between Echocardiographically Evaluated Aortic Stiffness and Prolidase Activity in Aortic Tissue of Patients with Critical Coronary Artery Disease." Archive of Medical Research **47**(3): 200-206

Komatsu, M., Kurokawa, H., Waguri, S., Taguchi, K., Kobayashi, A., Ichimura, Y., Sou, Y. S., Ueno, I., Sakamoto, A., Tong, K. I., Kim, M., Nishito, Y., Iemura, S., Natsume, T., Ueno, T., Kominami, E., Motohashi, H., Tanaka, K. and Yamamoto, M. (2010). "The selective autophagy substrate p62 activates the stress responsive transcription factor Nrf2 through inactivation of Keap1." Nature Cell Biology **12**(3): 213-U17

Komori, K., Inoguchi, H., Kume, M., Shoji, T. and Furuyama, T. (2002). "Differences in endothelial function and morphologic modulation between canine autogenous venous and arterial grafts: Endothelium and intimal thickening." Surgery **131**(1): S249-S255

Kovacic, P. and Jacintho, J. D. (2001). "Mechanisms of carcinogenesis: Focus on oxidative stress and electron transfer." Current Medicinal Chemistry **8**(7): 773-796

Kraft, A. D., Johnson, D. A. and Johnson, J. A. (2004). "Nuclear factor E2-related factor 2-dependent antioxidant response element activation by tert-butylhydroquinone and sulforaphane occurring preferentially in astrocytes conditions neurons against oxidative insult." Journal of Neuroscience. **24**(5): 1101-1112

Ku, D. N., Giddens, D. P., Zarins, C. K. and Glagov, S. (1985). "Pulsatile flow and atherosclerosis in the human carotid bifurcation - positive correlation between plaque location and low and oscillating shear-stress." Arteriosclerosis **5**(3): 293-302

Kulik, A., Brookhart, M. A., Levin, R., Ruel, M., Solomon, D. H. and Choudhry, N. K. (2008). "Impact of Statin Use on Outcomes After Coronary Artery Bypass Graft Surgery." Circulation **118**(18): 1785-1792

Kulik, A. and Ruel, M. (2009). "Statins and coronary artery bypass graft surgery: preoperative and postoperative efficacy and safety." Expert Opinion on Drug Safety **8**(5): 559-571

Kulik, A., Voisine, P., Mathieu, P., Masters, R. G., Mesana, T. G., Le May, M. R. and Ruel, M. (2011). "Statin Therapy and Saphenous Vein Graft Disease After Coronary Bypass Surgery: Analysis From the CASCADE Randomized Trial." Annals of Thoracic Surgery **92**(4): 1284-1290

Kwei, S., Stavrakis, G., Takahas, M., Taylor, G., Folkman, M. J., Gimbrone, M. A. and Garcia-Cardena, G. (2004). "Early adaptive responses of the vascular wall during venous arterialization in mice." American Journal of Pathology **164**(1): 81-89

Lacorre, D.-A., Baekkevold, E. S., Garrido, I., Brandtzaeg, P., Haraldsen, G., Amalric, F. and Girard, J.-P. (2004). "Plasticity of endothelial cells: rapid dedifferentiation of freshly isolated high

endothelial venule endothelial cells outside the lymphoid tissue microenvironment." Blood **103**(11): 4164-4172

Lan, Q. X., Mercurius, K. O. and Davies, P. F. (1994). "STIMULATION OF TRANSCRIPTION FACTORS NF-KAPPA-B AND AP1 IN ENDOTHELIAL-CELLS SUBJECTED TO SHEAR-STRESS." Biochemical and Biophysical Research Communications **201**(2): 950-956

Lassegue, B. and Griendling, K. K. (2010). "NADPH Oxidases: Functions and Pathologies in the Vasculature." Arteriosclerosis Thrombosis and Vascular Biology **30**(4): 653-661

Lau, A., Villeneuve, N. F., Sun, Z., Wong, P. K. and Zhang, D. D. (2008). "Dual roles of Nrf2 in cancer." Pharmacological Research **58**(5-6): 262-270

Lawrence, T. (2009). "The Nuclear Factor NF-kappa B Pathway in Inflammation." Cold Spring Harbor Perspectives in Biology **1**(6): 1-10

Lee, D. F., Kuo, H. P., Liu, M., Chou, C. K., Xia, W. Y., Du, Y., Shen, J., Chen, C. T., Huo, L., Hsu, M. C., Li, C. W., Ding, Q. Q., Liao, T. L., Lai, C. C., Lin, A. C., Chang, Y. H., Tsai, S. F., Li, L. Y. and Hung, M. C. (2009). "KEAP1 E3 Ligase-Mediated Downregulation of NF-kappa B Signaling by Targeting IKK beta." Molecular Cell **36**(1): 131-140

Lee, S., Choi, S. Y., Choo, Y. Y., Kim, O., Tran, P. T., Dao, C. T., Min, B. S. and Lee, J. H. (2015). "Sappanone A exhibits anti-inflammatory effects via modulation of Nrf2 and NF-kappa B." International Immunopharmacology **28**(1): 328-336

Lehoux, S., Castier, Y. and Tedgui, A. (2006). "Molecular mechanisms of the vascular responses to haemodynamic forces." Journal of Internal Medicine **259**(4): 381-392

Ley, K., Laudanna, C., Cybulsky, M. I. and Nourshargh, S. (2007). "Getting to the site of inflammation: the leukocyte adhesion cascade updated." Nature Reviews Immunology **7**(9): 678-689

Li, Q. T. and Verma, I. M. (2002). "NF-kappa B regulation in the immune system." Nature Reviews Immunology **2**(10): 725-734

Li, Y. S., Shyy, J. Y. J., Li, S., Lee, J. D., Su, B., Karin, M. and Chien, S. (1996). "The Ras-JNK pathway is involved in shear-induced gene expression." Molecular and Cellular Biology **16**(11): 5947-5954

Li, Y. S. J., Haga, J. H. and Chien, S. (2005). "Molecular basis of the effects of shear stress on vascular endothelial cells." Journal of Biomechanics **38**(10): 1949-1971

Liu, G. H., Qu, J. and Shen, X. (2008). "NF-kappa B/p65 antagonizes Nrf2-ARE pathway by depriving CBP from Nrf2 and facilitating recruitment of HDAC3 to MafK." Biochimica Et Biophysica Acta-Molecular Cell Research **1783**(5): 713-727

Liu, X. T., Zhang, X., Ding, Y., Zhou, W., Tao, L., Lu, P., Wang, Y. J. and Hu, R. (2017). "Nuclear Factor E2-Related Factor-2 Negatively Regulates NLRP3 Inflammasome Activity by Inhibiting Reactive Oxygen Species-Induced NLRP3 Priming." Antioxidants & Redox Signaling **26**(1): 28-43

Lu, J. M., Lin, P. H., Yao, Q. Z. and Chen, C. Y. (2010). "Chemical and molecular mechanisms of antioxidants: experimental approaches and model systems." Journal of Cellular and Molecular Medicine **14**(4): 840-860

Luo, S. Z., Truong, A. H. and Makino, A. (2016). "Isolation of Mouse Coronary Endothelial Cells." Jove-Journal of Visualized Experiments **113**: e53985

Lytle, B. W., Loop, F. D., Cosgrove, D. M., Ratliff, N. B., Easley, K. and Taylor, P. C. (1985). "Long-term (5 to 12 years) serial studies of internal mammary artery and saphenous-vein coronary-bypass grafts." Journal of Thoracic and Cardiovascular Surgery **89**(2): 248-258

Malek, A. M., Alper, S. L. and Izumo, S. (1999). "Hemodynamic shear stress and its role in atherosclerosis." Jama-Journal of the American Medical Association **282**(21): 2035-2042

Margaritis, M., Channon, K. M. and Antoniades, C. (2012). "Statins and vein graft failure in coronary bypass surgery." Current Opinion in Pharmacology **12**(2): 172-180

Margaritis, M., Channon, K. M. and Antoniades, C. (2014). "Statins as Regulators of Redox State in the Vascular Endothelium: Beyond Lipid Lowering." Antioxidants & Redox Signaling **20**(8): 1198-1215

Marin, T., Gongol, B., Chen, Z., Woo, B., Subramaniam, S., Chien, S. and Shyy, J. Y. J. (2013). "Mechanosensitive microRNAs-role in endothelial responses to shear stress and redox state." Free Radical Biology and Medicine **64**: 61-68

Masella, R., Di Benedetto, R., Vari, R., Filesi, C. and Giovannini, C. (2005). "Novel mechanisms of natural antioxidant compounds in biological systems: Involvement of glutathione and glutathione-related enzymes." Journal of Nutritional Biochemistry **16**(10): 577-586

Mason, J. C. (2016). "Cytoprotective pathways in the vascular endothelium. Do they represent a viable therapeutic target?" Vascular Pharmacology **86**: 41-52

Mayr, M., Hu, Y. H., Hainaut, P. and Xu, Q. B. (2002). "Mechanical stress-induced DNA damage and rac-p38MAPK signal pathways mediate p53-dependent apoptosis in vascular smooth muscle cells." Faseb Journal **16**(9): 1423-1425

Mcsweeney, S. R., Warabi, E. and Siow, R. C. M. (2016). "Nrf2 as an Endothelial Mechanosensitive Transcription Factor Going With the Flow." Hypertension **67**(1): 20-29

Menegon, S., Columbano, A. and Giordano, S. (2016). "The Dual Roles of NRF2 in Cancer." Trends in Molecular Medicine **22**(7): 578-593

Miller, S. C., Huang, R., Sakamuru, S., Shukla, S. J., Attene-Ramos, M. S., Shinn, P., Van Leer, D., Leister, W., Austin, C. P. and Xia, M. (2010). "Identification of known drugs that act as inhibitors of NF-κB signaling and their mechanism of action." Biochemical Pharmacology **79**(9): 1272-1280

Mitra, A. K., Gangahar, D. M. and Agrawal, D. K. (2006). "Cellular, molecular and immunological mechanisms in the pathophysiology of vein graft intimal hyperplasia." Immunology and Cell Biology **84**(2): 115-124

Miyake, T., Aoki, M., Makino, H. and Morishita, R. (2007). "Inhibition of anastomotic intimal hyperplasia using a chimeric decoy strategy against NF kappa B and E2F in a rabbit model." Circulation **116**(16): 110-110

Miyake, T., Aoki, M., Shiraya, S., Tanemoto, K., Ogihara, T., Kaneda, Y. and Morishita, R. (2006). "Inhibitory effects of NF kappa B decoy oligodeoxynucleotides on neointimal hyperplasia in a rabbit vein graft model." Journal of Molecular and Cellular Cardiology **41**(3): 431-440

Miyake, T., Ihara, S., Tsukada, Y., Watanabe, H., Matsuda, H., Kiguchi, H., Tsujimoto, H., Nakagami, H. and Morishita, R. (2014). "Prevention of Neointimal Formation After Angioplasty Using Nuclear Factor-kappa B Decoy Oligodeoxynucleotide-Coated Balloon Catheter in Rabbit Model." Circulation-Cardiovascular Interventions **7**(6): 787-796

Mohr, F. W., Morice, M. C., Kappetein, A. P., Feldman, T. E., Stahle, E., Colombo, A., Mack, M. J., Holmes, D. R., Morel, M. A., Van Dyck, N., Houle, V. M., Dawkins, K. D. and Serruys, P. W. (2013). "Coronary artery bypass graft surgery versus percutaneous coronary intervention in patients with three-vessel disease and left main coronary disease: 5-year follow-up of the randomised, clinical SYNTAX trial." Lancet **381**(9867): 629-638

Moi, P., Chan, K., Asunis, I., Cao, A. and Kan, Y. W. (1994). "Isolation of NF-E2-related factor-2 (Nrf2), a NF-E2-like basic leucine-zipper transcriptional activator that binds to the tandem nf-

e2/ap1 repeat of the beta-globin locus-control region." Proceedings of the National Academy of Sciences of the United States of America **91**(21): 9926-9930

Moore, M. M., Goldman, J., Patel, A. R., Chien, S. and Liu, S. Q. (2001). "Role of tensile stress and strain in the induction of cell death in experimental vein grafts." Journal of Biomechanics **34**(3): 289-297

Morgan, M. J. and Liu, Z. G. (2011). "Crosstalk of reactive oxygen species and NF-kappa B signaling." Cell Research **21**(1): 103-115

Motwani, J. G. and Topol, E. J. (1998). "Aortocoronary saphenous vein graft disease - Pathogenesis, predisposition, and prevention." Circulation **97**(9): 916-931

Mozaffarian, D., Benjamin, E. J., Go, A. S., Arnett, D. K., Blaha, M. J., Cushman, M., Das, S. R., De Ferranti, S., Després, J.-P. and Fullerton, H. J. (2015). "Heart Disease and Stroke Statistics—2016 Update A Report From the American Heart Association." Circulation **137**(24): e1-e852

Munro, J. M., Pober, J. S. and Cotran, R. S. (1989). "Tumor necrosis factor and interferon-gamma induce distinct patterns of endothelial activation and associated leukocyte accumulation in skin of papio-anubis." American Journal of Pathology **135**(1): 121-133

Murphy, G. J., Newby, A. C., Jeremy, J. Y., Baumbach, A. and Angelini, G. D. (2007). "A randomized trial of an external Dacron sheath for the prevention of vein graft disease: The Extent study." Journal of Thoracic and Cardiovascular Surgery **134**(2): 504-505

Mustafa, A. K., Gadalla, M. M. and Snyder, S. H. (2009). "Signaling by Gasotransmitters." Science Signaling **2**(68): 1-8

Muzaffar, S., Shukla, N. and Jeremy, J. Y. (2005). "Nicotinamide adenine dinucleotide phosphate oxidase: A promiscuous therapeutic target for cardiovascular drugs?" Trends in Cardiovascular Medicine **15**(8): 278-282

Nagel, T., Resnick, N., Atkinson, W. J., Dewey, C. F. and Gimbrone, M. A. (1994). "Shear stress selectively up-regulates intercellular-adhesion molecule-1 expression in cultured human vascular endothelial-cells." Journal of Clinical Investigation **94**(2): 885-891

Nam, D., Ni, C. W., Rezvan, A., Suo, J., Budzyn, K., Llanos, A., Harrison, D., Giddens, D. and Jo, H. (2009). "Partial carotid ligation is a model of acutely induced disturbed flow, leading to rapid endothelial dysfunction and atherosclerosis." American Journal of Physiology-Heart and Circulatory Physiology **297**(4): H1535-H1543

Navarro-Yepes, J., Burns, M., Anandhan, A., Khalimonchuk, O., Del Razo, L. M., Quintanilla-Vega, B., Pappa, A., Panayiotidis, M. I. and Franco, R. (2014). "Oxidative Stress, Redox Signaling, and Autophagy: Cell Death Versus Survival." Antioxidants & Redox Signaling **21**(1): 66-85

Newby, A. C. (2005). "Dual role of matrix metalloproteinases (matrixins) in intimal thickening and atherosclerotic plaque rupture." Physiological Reviews **85**(1): 1-31

Newby, A. C. (2008). "Metalloproteinase Expression in Monocytes and Macrophages and its Relationship to Atherosclerotic Plaque Instability." Arteriosclerosis Thrombosis and Vascular Biology **28**(12): 2108-U20

Newby, A. C. and Zaltsman, A. B. (2000). "Molecular mechanisms in intimal hyperplasia." Journal of Pathology **190**(3): 300-309

Nguyen, B. a. V., Fiorentino, F., Reeves, B. C., Baig, K., Athanasiou, T., Anderson, J. R., Haskard, D. O., Angelini, G. D. and Evans, P. C. (2016). "Mini Bypass and Proinflammatory Leukocyte Activation: A Randomized Controlled Trial." Annals of Thoracic Surgery **101**(4): 1454-1463

Nguyen, T., Nioi, P. and Pickett, C. B. (2009). "The Nrf2-Antioxidant Response Element Signaling Pathway and Its Activation by Oxidative Stress." Journal of Biological Chemistry **284**(20): 13291-13295

Nguyen, T., Sherratt, P. J., Nioi, P., Yang, C. S. and Pickett, C. B. (2005). "Nrf2 controls constitutive and inducible expression of ARE-driven genes through a dynamic pathway involving nucleocytoplasmic shuttling by Keap1." Journal of Biological Chemistry **280**(37): 32485-32492

Niture, S. K. and Jaiswal, A. K. (2009). "Prothymosin-alpha Mediates Nuclear Import of the INrf2/Cul3 center dot Rbx1 Complex to Degrade Nuclear Nrf2." Journal of Biological Chemistry **284**(20): 13856-13868

Niture, S. K., Khatri, R. and Jaiswal, A. K. (2014). "Regulation of Nrf2-an update." Free Radical Biology and Medicine **66**: 36-44

Noris, M., Morigi, M., Donadelli, R., Aiello, S., Foppolo, M., Todeschini, M., Orisio, S., Remuzzi, G. and Remuzzi, A. (1995). "Nitric-oxide synthesis by cultured endothelial-cells is modulated by flow conditions." Circulation Research **76**(4): 536-543

Oakley, F. D., Smith, R. L. and Engelhardt, J. F. (2009). "Lipid Rafts and Caveolin-1 Coordinate Interleukin-1 beta (IL-1 beta)-dependent Activation of NF kappa B by Controlling Endocytosis of

Nox2 and IL-1 beta Receptor 1 from the Plasma Membrane." Journal of Biological Chemistry **284**(48): 33255-33264

Oliveira-Marques, V., Marinho, H. S., Cyrne, L. and Antunes, F. (2009). "Role of Hydrogen Peroxide in NF-kappa B Activation: From Inducer to Modulator." Antioxidants & Redox Signaling **11**(9): 2223-2243

Orr, A. W., Hahn, C., Blackman, B. R. and Schwartz, M. A. (2008). "p21-activated kinase signaling regulates oxidant-dependent NF-kappa B activation by flow." Circulation Research **103**(6): 671-679

Orr, A. W., Sanders, J. M., Bevard, M., Coleman, E., Sarembock, I. J. and Schwartz, M. A. (2005). "The subendothelial extracellular matrix modulates NF-kappa B activation by flow: a potential role in atherosclerosis." Journal of Cell Biology **169**(1): 191-202

Osgood, M. J., Hocking, K. M., Voskresensky, I. V., Li, F. D., Komalavilas, P., Cheung-Flynn, J. and Brophy, C. M. (2014). "Surgical vein graft preparation promotes cellular dysfunction, oxidative stress, and intimal hyperplasia in human saphenous vein." Journal of Vascular Surgery **60**(1): 202-211

Owens, C. D. (2010). "Adaptive changes in autogenous vein grafts for arterial reconstruction: Clinical implications." Journal of Vascular Surgery **51**(3): 736-746

Owens, C. D., Gasper, W. J., Rahman, A. S. and Conte, M. S. (2015). "Vein graft failure." Journal of Vascular Surgery **61**(1): 203-216

Pahl, H. L. (1999). "Activators and target genes of Rel/NF-kappa B transcription factors." Oncogene **18**(49): 6853-6866

Papaharalambus, C. A. and Griendling, K. K. (2007). "Basic mechanisms of oxidative stress and reactive oxygen species in cardiovascular injury." Trends in Cardiovascular Medicine **17**(2): 48-54

Park, H. S., Jung, H. Y., Park, E. Y., Kim, J., Lee, W. J. and Bae, Y. S. (2004). "Cutting edge: Direct interaction of TLR4 with NAD(P)H oxidase 4 isozyme is essential for lipopolysaccharide-induced production of reactive oxygen species and activation of NF-kappa B." Journal of Immunology **173**(6): 3589-3593

Parsonnet, V., Lari, A. A. and Shah, I. H. (1963). "NEW STENT FOR SUPPORT OF VEINS IN ARTERIAL GRAFTS." Archives of Surgery **87**(4): 696-702

Partridge, J., Carlsen, H., Enesa, K., Chaudhury, H., Zakkar, M., Luong, L., Kinderlerer, A., Johns, M., Blomhoff, R., Mason, J. C., Haskard, D. O. and Evans, P. C. (2007). "Laminar shear stress acts as a switch to regulate divergent functions of NF-kappa B in endothelial cells." Faseb Journal **21**(13): 3553-3561

Pearce, J. E., Dujovny, M., Ho, K. L., Shrontz, C., Ausman, J. I., Berman, S. K. and Diaz, F. G. (1985). "ACUTE-INFLAMMATION AND ENDOTHELIAL INJURY IN VEIN GRAFTS." Neurosurgery **17**(4): 626-634

Pedrigi, R. M., Papadimitriou, K. I., Kondiboyina, A., Sidhu, S., Chau, J., Patel, M. B., Baeriswyl, D. C., Drakakis, E. M. and Krams, R. (2017). "Disturbed Cyclical Stretch of Endothelial Cells Promotes Nuclear Expression of the Pro-Atherogenic Transcription Factor NF-kappa B." Annals of Biomedical Engineering **45**(4): 898-909

Petzold, T., Orr, A. W., Hahn, C., Jhaveri, K. A., Parsons, J. T. and Schwartz, M. A. (2009). "Focal adhesion kinase modulates activation of NF-kappa B by flow in endothelial cells." American Journal of Physiology-Cell Physiology **297**(4): C814-C822

Pi, X. C., Yan, C. and Berk, B. C. (2004). "Big mitogen-activated protein kinase (BMK1)/ERK5 protects endothelial cells from apoptosis." Circulation Research **94**(3): 362-369

Pierce, J. W., Schoenleber, R., Jesmok, G., Best, J., Moore, S. A., Collins, T. and Gerritsen, M. E. (1997). "Novel inhibitors of cytokine-induced IκBα phosphorylation and endothelial cell adhesion molecule expression show anti-inflammatory effects in vivo." Journal of Biological Chemistry **272**(34): 21096-21103

Pisoschi, A. M. and Pop, A. (2015). "The role of antioxidants in the chemistry of oxidative stress: A review." European Journal of Medicinal Chemistry **97**: 55-74

Pober, J. S. and Sessa, W. C. (2007). "Evolving functions of endothelial cells in inflammation." Nature Reviews Immunology **7**(10): 803-815

Poljsak, B. and Milisav, I. (2012). "The Neglected Significance of "Antioxidative Stress"." Oxidative Medicine and Cellular Longevity **2012**(480895): 1-12

Poljsak, B., Suput, D. and Milisav, I. (2013). "Achieving the Balance between ROS and Antioxidants: When to Use the Synthetic Antioxidants." Oxidative Medicine and Cellular Longevity **2013**(956792): 1-11

Powell, J. T. and Gosling, M. (1998). "Molecular and cellular changes in vein grafts: influence of pulsatile stretch." Current Opinion in Cardiology **13**(6): 453-458

Prim, D. A., Zhou, B., Hartstone-Rose, A., Uline, M. J., Shazly, T. and Eberth, J. F. (2016). "A mechanical argument for the differential performance of coronary artery grafts." Journal of Mechanical Behaviour of Biomedical Materials **54**: 93-105

Ratliff, N. B. and Myles, J. L. (1989). "Rapidly progressive atherosclerosis in aortocoronary saphenous-vein grafts - possible immune-mediated disease." Archives of Pathology & Laboratory Medicine **113**(7): 772-776

Resnick, N. and Gimbrone, M. A. (1995). "Hemodynamic forces are complex regulators of endothelial gene-expression." Faseb Journal **9**(10): 874-882

Resnick, N., Yahav, H., Shay-Salit, A., Shushy, M., Schubert, S., Zilberman, L. C. M. and Wofovitz, E. (2003). "Fluid shear stress and the vascular endothelium: for better and for worse." Progress in Biophysics & Molecular Biology **81**(3): 177-199

Roque, M., Kim, W. J. H., Gazdoin, M., Malik, A., Reis, E. D., Fallon, J. T., Badimon, J. J., Charo, I. F. and Taubman, M. B. (2002). "CCR2 deficiency decreases intimal hyperplasia after arterial injury." Arteriosclerosis Thrombosis and Vascular Biology **22**(4): 554-559

Rotblat, B., Melino, G. and Knight, R. A. (2012). "NRF2 and p53: Januses in cancer?" Oncotarget **3**(11): 1272-1283

Rousou, L. J., Taylor, K. B., Lu, X. G., Healey, N., Crittenden, M. D., Khuri, S. F. and Thatte, H. S. (2009). "Saphenous Vein Conduits Harvested by Endoscopic Technique Exhibit Structural and Functional Damage." Annals of Thoracic Surgery **87**(1): 62-70

Rupec, R. A., Poujol, D., Grosgeorge, J., Carle, G. F., Livolsi, A., Peyron, J. F., Schmid, R. M., Baeuerle, P. A. and Messer, G. (1999). "Structural analysis, expression, and chromosomal localization of the mouse ikba gene." Immunogenetics **49**(5): 395-403

Rzucidlo, E. M., Martin, K. A. and Powell, R. J. (2007). "Regulation of vascular smooth muscle cell differentiation." Journal of Vascular Surgery **45**: 25A-32A

Sabik, J. F. (2011). "Understanding Saphenous Vein Graft Patency." Circulation **124**(3): 273-275

Sarjeant, J. M. and Rabinovitch, M. (2002). "Understanding and treating vein graft atherosclerosis." Cardiovascular Pathology **11**(5): 263-271

Satta, S., Mahmoud, A. M., Wilkinson, F. L., Alexander, M. Y. and White, S. J. (2017). "The Role of Nrf2 in Cardiovascular Function and Disease." Oxidative Medicine and Cellular Longevity **2017**(9237263): 1-18

Saunders, P. C., Pintucci, G., Bizekis, C. S., Sharony, R., Hyman, K. M., Saponara, F., Baumann, F. G., Grossi, E. A., Colvin, S. B., Mignatti, P. and Galloway, A. C. (2004). "Vein graft arterialization causes differential activation of mitogen-activated protein kinases." Journal of Thoracic and Cardiovascular Surgery **127**(5): 1276-1284

Schepers, A., Eefting, D., Bonta, P. I., Grimbergen, J. M., De Vries, M. R., Van Weel, V., De Vries, C. J., Egashira, K., Van Bockel, J. H. and Quax, P. H. A. (2006). "Anti-MCP-1 gene therapy inhibits vascular smooth muscle cells proliferation and attenuates vein graft thickening both in vitro and in vivo." Arteriosclerosis Thrombosis and Vascular Biology **26**(9): 2063-2069

Schieber, M. and Chandel, N. S. (2014). "ROS Function in Redox Signaling and Oxidative Stress." Current Biology **24**(10): R453-R462

Schober, A., Zernecke, A., Liehn, E. A., Von Hundelshausen, P., Knarren, S., Kuziel, W. A. and Weber, C. (2004). "Crucial role of the CCL2/CCR2 axis in neointimal hyperplasia after arterial injury in hyperlipidemic mice involves early monocyte recruitment and CCL2 presentation on platelets." Circulation Research **95**(11): 1125-1133

Sen, O., Gonca, S., Solakoglu, S., Dalcik, H., Dalcik, C. and Ozkara, A. (2013). "Comparison of Conventional and No-Touch Techniques in Harvesting Saphenous Vein for Coronary Artery Bypass Grafting in View of Endothelial Damage." Heart Surgery Forum **16**(4): E177-E183

Sen, R. and Baltimore, D. (1986). "Multiple nuclear factors interact with the immunoglobulin enhancer sequences." Cell **46**(5): 705-716

Serruys, P. W., Morice, M. C., Kappetein, A. P., Colombo, A., Holmes, D. R., Mack, M. J., Stahle, E., Feldman, T. E., Van Den Brand, M., Bass, E. J., Van Dyck, N., Leadley, K., Dawkins, K. D., Mohr, F. W. and Investigators, S. (2009). "Percutaneous Coronary Intervention versus Coronary-Artery Bypass Grafting for Severe Coronary Artery Disease." New England Journal of Medicine **360**(10): 961-972

Shintani, T., Sawa, Y., Takahashi, T., Matsumiya, G., Matsuura, N., Miyamoto, Y. and Matsuda, H. (2002). "Intraoperative transfection of vein grafts with the NF kappa B decoy in a canine

aortocoronary bypass model: A strategy to attenuate intimal hyperplasia." Annals of Thoracic Surgery **74**(4): 1132-1137

Shukla, N. and Jeremy, J. Y. (2012). "Pathophysiology of saphenous vein graft failure: a brief overview of interventions." Current Opinion in Pharmacology **12**(2): 114-120

Shyy, J. Y. J., Li, Y. S., Lin, M. C., Chen, W., Yuan, S. L., Usami, S. and Chien, S. (1995). "Multiple cis-elements mediate shear stress-induced gene expression." Journal of Biomechanics **28**(12): 1451-1457

Shyy, J. Y. J., Lin, M. C., Han, J. H., Lu, Y. J., Petrime, M. and Chien, S. (1995). "The cis-acting phorbol ester 12-o-tetradecanoylphorbol 13-acetate-responsive element is involved in shear stress-induced monocyte chemotactic protein-1 gene-expression." Proceedings of the National Academy of Sciences of the United States of America **92**(17): 8069-8073

Shyy, Y. J., Hsieh, H. J., Usami, S. and Chien, S. (1994). "Fluid shear-stress induces a biphasic response of human monocyte chemotactic protein-1 gene-expression in vascular endothelium." Proceedings of the National Academy of Sciences of the United States of America **91**(11): 4678-4682

Sies, H. (2015). "Oxidative stress: a concept in redox biology and medicine." Redox Biology. **4**: 180-183

Siragusa, M. and Fleming, I. (2016). "The eNOS signalosome and its link to endothelial dysfunction." Pflugers Archive. **468**(7): 1125-1137

Souza, D. S. R., Christofferson, R. H. B., Bomfim, V. and Filbey, D. (1999). ""No-touch" technique using saphenous vein harvested with its surrounding tissue for coronary artery bypass grafting maintains an intact endothelium." Scandinavian Cardiovascular Journal **33**(6): 323-329

Souza, D. S. R., Dashwood, M. R., Tsui, J. C. S., Filbey, D., Bodin, L., Johansson, B. and Borowiec, J. (2002). "Improved patency in vein grafts harvested with surrounding tissue: Results of a randomized study using three harvesting techniques." Annals of Thoracic Surgery **73**(4): 1189-1195

Spadaccio, C., De Marco, F., Di Domenico, F., Coccia, R., Lusini, M., Barbato, R., Covino, E. and Chello, M. (2014). "Simvastatin attenuates the endothelial pro-thrombotic shift in saphenous vein grafts induced by Advanced glycation endproducts." Thromb. Res. **133**(3): 418-425

Sporn, M. B. and Liby, K. T. (2012). "NRF2 and cancer: the good, the bad and the importance of context." Nature Reviews Cancer **12**(8): 564-571

Sprague, A. H. and Khalil, R. A. (2009). "Inflammatory cytokines in vascular dysfunction and vascular disease." Biochemical Pharmacology **78**(6): 539-552

Stark, V., Hoch, J., Warner, T. and Hullett, D. (1997). "Monocyte chemotactic protein-1 expression is associated with the development of vein graft intimal hyperplasia." Arteriosclerosis, Thrombosis, and Vascular Biology **17**(8): 1614-1621

Stein, P. D., Schunemann, H., Dalen, J. E. and Gutterman, D. (2004). "Antithrombotic therapy in patients with saphenous vein and internal mammary artery bypass grafts." Chest **126**(3): 600S-608S

Suleiman, M. S., Zacharowski, K. and Angelini, G. D. (2008). "Inflammatory response and cardioprotection during open-heart surgery: the importance of anaesthetics." British Journal of Pharmacology **153**(1): 21-33

Sun, S.-C. (2011). "Non-canonical NF-κB signaling pathway." Cell research **21**(1): 71-85

Sun, Z., Zhang, S., Chan, J. Y. and Zhang, D. D. (2007). "Keap1 controls postinduction repression of the Nrf2-mediated antioxidant response by escorting nuclear export of Nrf2." Molecular and Cellular Biology **27**(18): 6334-6349

Surapisitchat, J., Hoefen, R. J., Pi, X. C., Yoshizumi, M., Yan, C. and Berk, B. C. (2001). "Fluid shear stress inhibits TNF-alpha activation of JNK but not ERK1/2 or p38 in human umbilical vein endothelial cells: Inhibitory crosstalk among MAPK family members." Proceedings of the National Academy of Sciences of the United States of America **98**(11): 6476-6481

Suzuki, T. and Yamamoto, M. (2017). "Stress-sensing mechanisms and the physiological roles of the Keap1-Nrf2 system during cellular stress." Journal of Biological Chemistry **292**(41): 16817-16824

Sykiotis, G. P. and Bohmann, D. (2010). "Stress-Activated Cap'n'collar Transcription Factors in Aging and Human Disease." Science Signaling **3**(112): re3

Szasz, T. and Webb, R. C. (2012). "Perivascular adipose tissue: more than just structural support." Clinical Science **122**(1-2): 1-12

Szmitko, P. E., Wang, C. H., Weisel, R. D., De Almeida, J. R., Anderson, T. J. and Verma, S. (2003). "New markers of inflammation and endothelial cell activation - Part I." Circulation **108**(16): 1917-1923

Taggart, D. P., Altman, D. G., Gray, A. M., Lees, B., Gerry, S., Benedetto, U., Flather, M. and Investigators, A. R. T. (2016). "Randomized Trial of Bilateral versus Single Internal-Thoracic-Artery Grafts." New England Journal of Medicine **375**(26): 2540-2549

Taggart, D. P., Ben Gal, Y., Lees, B., Patel, N., Webb, C., Rehman, S. M., Desouza, A., Yadav, R., De Robertis, F., Dalby, M., Banning, A., Channon, K. M., Di Mario, C. and Orion, E. (2015). "A Randomized Trial of External Stenting for Saphenous Vein Grafts in Coronary Artery Bypass Grafting." Annals of Thoracic Surgery **99**(6): 2039-2045

Tak, P. P. and Firestein, G. S. (2001). "NF-kappa B: a key role in inflammatory diseases." Journal of Clinical Investigation **107**(1): 7-11

Takahashi, M., Ishida, T., Traub, O., Corson, M. A. and Berk, B. C. (1997). "Mechanotransduction in endothelial cells: Temporal signaling events in response to shear stress." Journal of Vascular Research **34**(3): 212-219

Tarbell, J. M. (2010). "Shear stress and the endothelial transport barrier." Cardiovascular Research **87**(2): 320-330

Tashiro, S., Muto, A., Tanimoto, K., Tsuchiya, H., Suzuki, H., Hoshino, H., Yoshida, M., Walter, J. and Igarashi, K. (2004). "Repression of PML nuclear body-associated transcription by oxidative stress-activated Bach2." Molecular and Cellular Biology **24**(8): 3473-3484

Thiene, G., Miazzi, P., Valsecchi, M., Valente, M., Bortolotti, U., Casarotto, D. and Gallucci, V. (1980). "Histological survey of the saphenous-vein before its use as autologous aortocoronary bypass graft." Thorax **35**(7): 519-522

Thimmulappa, R. K., Mai, K. H., Srisuma, S., Kensler, T. W., Yamamato, M. and Biswal, S. (2002). "Identification of Nrf2-regulated genes induced by the chemopreventive agent sulforaphane by oligonucleotide microarray." Cancer Research **62**(18): 5196-5203

Tong, K. I., Katoh, Y., Kusunoki, H., Itoh, K., Tanaka, T. and Yamamoto, M. (2006). "Keap1 recruits Neh2 through binding to ETGE and DLG motifs: Characterization of the two-site molecular recognition model." Molecular and Cellular Biology **26**(8): 2887-2900

Torsney, E., Mayr, U., Zou, Y. P., Thompson, W. D., Hu, Y. H. and Xu, Q. B. (2004). "Thrombosis and neointima formation in vein grafts are inhibited by locally applied aspirin through endothelial protection." Circulation Research **94**(11): 1466-1473

Traub, O. and Berk, B. C. (1998). "Laminar shear stress - Mechanisms by which endothelial cells transduce an atheroprotective force." Arteriosclerosis Thrombosis and Vascular Biology **18**(5): 677-685

Tsapenko, M. V., D'uscio, L. V., Grande, J. P., Croatt, A. J., Hernandez, M. C., Ackerman, A. W., Katusic, Z. S. and Nath, K. A. (2012). "Increased production of superoxide anion contributes to dysfunction of the arteriovenous fistula." American Journal of Physiology-Renal Physiology **303**(12): F1601-F1607

Turner, N. A., O'regan, D. J., Ball, S. G. and Porter, K. E. (2005). "Simvastatin inhibits MMP-9 secretion from human saphenous vein smooth muscle cells by inhibiting the RhoA/ROCK pathway and reducing MMP-9 mRNA levels." Faseb Journal **19**(2): 804-815

Tzima, E., Del Pozo, M. A., Kiosses, W. B., Mohamed, S. A., Li, S., Chien, S. and Schwartz, M. A. (2002). "Activation of Rac1 by shear stress in endothelial cells mediates both cytoskeletal reorganization and effects on gene expression." Embo Journal **21**(24): 6791-6800

Tzima, E., Irani-Tehrani, M., Kiosses, W. B., Dejana, E., Schultz, D. A., Engelhardt, B., Cao, G. Y., Delisser, H. and Schwartz, M. A. (2005). "A mechanosensory complex that mediates the endothelial cell response to fluid shear stress." Nature **437**(7057): 426-431

Uchida, K., Sasahara, M., Morigami, N., Hazama, F. and Kinoshita, M. (1996). "Expression of platelet-derived growth factor B-chain in neointimal smooth muscle cells of balloon injured rabbit femoral arteries." Atherosclerosis **124**(1): 9-23

Ueda, A., Ishigatsubo, Y., Okubo, T. and Yoshimura, T. (1997). "Transcriptional regulation of the human monocyte chemoattractant protein-1 gene - Cooperation of two NF-kappa B sites and NF-kappa B/Rel subunit specificity." Journal of Biological Chemistry **272**(49): 31092-31099

Ueda, A., Okuda, K., Ohno, S., Shirai, A., Igarashi, T., Matsunaga, K., Fukushima, J., Kawamoto, S., Ishigatsubo, Y. and Okubo, T. (1994). "NF-kappa-B and sp1 regulate transcription of the human monocyte chemoattractant protein-1 gene." Journal of Immunology **153**(5): 2052-2063

Valko, M., Leibfritz, D., Moncol, J., Cronin, M. T. D., Mazur, M. and Telser, J. (2007). "Free radicals and antioxidants in normal physiological functions and human disease." International Journal of Biochemistry & Cell Biology **39**(1): 44-84

Van Der Heiden, K., Cuhlmann, S., Luong, L. A., Zakkar, M. and Evans, P. C. (2010). "Role of nuclear factor kappa B in cardiovascular health and disease." Clinical Science **118**(9-10): 593-605

Vara, D. S., Punshon, G., Sales, K. M., Salacinski, H. J., Dijk, S., Brown, R. A., Hamilton, G. and Seifalian, A. M. (2005). "Development of an RNA isolation procedure for the characterisation of human endothelial cell interactions with polyurethane cardiovascular bypass grafts." Biomaterials **26**(18): 3987-3993

Velichkova, M. and Hasson, T. (2005). "Keap1 regulates the oxidation-sensitive shuttling of Nrf2 into and out of the nucleus via a Crm1-dependent nuclear export mechanism." Molecular and Cellular Biology **25**(11): 4501-4513

Venugopal, R. and Jaiswal, A. K. (1996). "Nrf1 and Nrf2 positively and c-Fos and Fra1 negatively regulate the human antioxidant response element-mediated expression of NAD(P)H:quinone oxidoreductase(1) gene." Proceedings of the National Academy of Sciences of the United States of America **93**(25): 14960-14965

Verma, I. M., Stevenson, J. K., Schwarz, E. M., Vanantwerp, D. and Miyamoto, S. (1995). "Rel/nf-kappa-b/i-kappa-b family - intimate tales of association and dissociation." Genes & Development **9**(22): 2723-2735

Verrier, E. D. and Boyle, E. M. (1996). "Endothelial cell injury in cardiovascular surgery." Annals of Thoracic Surgery **62**(3): 915-922

Vetrini, F. and Ng, P. (2010). "Gene Therapy with Helper-Dependent Adenoviral Vectors: Current Advances and Future Perspectives." Viruses-Basel **2**(9): 1886-1917

Vomund, S., Schafer, A., Parnham, M. J., Brune, B. and Von Knethen, A. (2017). "Nrf2, the Master Regulator of Anti-Oxidative Responses." International Journal of Molecular Sciences **18**(12):
Walts, A. E., Fishbein, M. C. and Matloff, J. M. (1987). "Thrombosed, ruptured atheromatous plaques in saphenous-vein coronary-artery bypass grafts - 10 years experience." American Heart Journal **114**(4): 718-723

Wakabayashi., N., Slocum., S. L., Skoko., J. J., Shin., S. and Kensler., T. W. (2010) "When Nrf2 talks, who's listening?" Antioxidant and Redox Signalling **13**(11): 1649-1663

Wan, S., George, S. J., Berry, C. and Baker, A. H. (2012). "Vein graft failure: current clinical practice and potential for gene therapeutics." Gene Therapy **19**(6): 630-636

Wan, S., Leclerc, J. L. and Vincent, J. L. (1997). "Cytokine responses to cardiopulmonary bypass: Lessons learned from cardiac transplantation." Annals of Thoracic Surgery **63**(1): 269-276

Wan, S., Shukla, N., Angelini, G. D., Yim, A. P. C., Johnson, J. L. and Jeremy, J. Y. (2007). "Nitric oxide-donating aspirin (NCX 4016) inhibits neointimal thickening in a pig model of saphenous veincarotid artery interposition grafting: A comparison with aspirin and morpholinosydnonimine (SIN-1)." Journal of Thoracic and Cardiovascular Surgery **134**(4): 1033-1039

Wang, Y. J., Wang, J. T., Fan, Q. X. and Geng, J. G. (2007). "Andrographolide inhibits NF-kappa B activation and attenuates neointimal hyperplasia in arterial restenosis." Cell Research **17**(11): 933-941

Warabi, E., Takabe, W., Minami, T., Inoue, K., Itoh, K., Yamamoto, M., Ishii, T., Kodama, T. and Noguchi, N. (2007). "Shear stress stabilizes NF-E2-related factor 2 and induces antioxidant genes in endothelial cells: Role of reactive oxygen/nitrogen species." Free Radical Biology and Medicine **42**(2): 260-269

Warboys, C. M., Berson, R. E., Mann, G. E., Pearson, J. D. and Weinberg, P. D. (2010). "Acute and chronic exposure to shear stress have opposite effects on endothelial permeability to macromolecules." American Journal of Physiology-Heart and Circulatory Physiology **298**(6): H1850-H1856

Ward, A. O., Caputo, M., Angelini, G. D., George, S. J. and Zakkar, M. (2017). "Activation and inflammation of the venous endothelium in vein graft disease." Atherosclerosis **265**: 266-274

Washington, K. S. and Bashur, C. A. (2017). "Delivery of Antioxidant and Anti-inflammatory Agents for Tissue Engineered Vascular Grafts." Front. Pharmacol. **8**(659): 1-18

Weaver, H., Shukla, N., Ellinsworth, D. and Jeremy, J. Y. (2012). "Oxidative stress and vein graft failure: a focus on NADH oxidase, nitric oxide and eicosanoids." Current Opinion in Pharmacology **12**(2): 160-165

Weber, K. S. C., Draude, G., Erl, W., De Martin, R. and Weber, C. (1999). "Monocyte arrest and transmigration on inflamed endothelium in shear flow is inhibited by adenovirus-mediated gene transfer of I kappa B-alpha." Blood **93**(11): 3685-3693

Weibel, E. R. and Palade, G. E. (1964). "New cytoplasmic components in arterial endothelia." The Journal of Cell Biology **23**(1): 101-112

Wenzel, P., Kossmann, S., Munzel, T. and Daiber, A. (2017). "Redox regulation of cardiovascular inflammation - Immunomodulatory function of mitochondrial and Nox-derived reactive oxygen and nitrogen species." Free Radical Biology and Medicine **109**: 48-60

Wertz, I. E., O'rourke, K. M., Zhou, H. L., Eby, M., Aravind, L., Seshagiri, S., Wu, P., Wiesmann, C., Baker, R., Boone, D. L., Ma, A., Koonin, E. V. and Dixit, V. M. (2004). "De-ubiquitination and ubiquitin ligase domains of A20 downregulate NF-kappa B signalling." Nature **430**(7000): 694-699

West, N. E. J., Qian, H. S., Guzik, T. J., Black, E., Cai, S. J., George, S. E. and Channon, K. M. (2001). "Nitric oxide synthase (nNOS) gene transfer modifies venous bypass graft remodeling - Effects on vascular smooth muscle cell differentiation and superoxide production." Circulation **104**(13): 1526-1532

White, S. J., Hayes, E. M., Lehoux, S., Jeremy, J. Y., Horrevoets, A. J. G. and Newby, A. C. (2011). "Characterization of the Differential Response of Endothelial Cells Exposed to Normal and Elevated Laminar Shear Stress." Journal of Cellular Physiology **226**(11): 2841-2848

Wise, E. S., Hocking, K. M., Luo, W. F., Feldman, D. L., Song, J., Komalavilas, P., Cheung-Flynn, J. and Brophy, C. M. (2016). "Traditional graft preparation decreases physiologic responses, diminishes viscoelasticity, and reduces cellular viability of the conduit: A porcine saphenous vein model." Vascular Medicine **21**(5): 413-421

Woodward, L. C., Antoniades, C. and Taggart, D. P. (2016). "Intraoperative Vein Graft Preservation: What Is the Solution?" Annals of Thoracic Surgery **102**(5): 1736-1746

Wrighton, C. J., Hoferwarbinek, R., Moll, T., Eytner, R., Bach, F. H. and Demartin, R. (1996). "Inhibition of endothelial cell activation by adenovirus-mediated expression of I kappa B alpha, an inhibitor of the transcription factor NF-kappa B." Journal of Experimental Medicine **183**(3): 1013-1022

Wruck, C. J., Streetz, K., Pavic, G., Gotz, M. E., Tohidnezhad, M., Brandenburg, L. O., Varoga, D., Eickelberg, O., Herdegen, T., Trautwein, C., Cha, K. M., Kan, Y. W. and Pufe, T. (2011). "Nrf2 Induces Interleukin-6 (IL-6) Expression via an Antioxidant Response Element within the IL-6 Promoter." Journal of Biological Chemistry **286**(6): 4493-4499

Xu, C. H., Tang, F. T., Lu, M. L., Yang, J., Han, R. H., Mei, M., Hu, J. and Wang, H. X. (2016). "Pretreatment with Astragaloside IV protects human umbilical vein endothelial cells from hydrogen peroxide induced oxidative stress and cell dysfunction via inhibiting eNOS uncoupling and NADPH oxidase - ROS - NF-kappa B pathway." Canadian Journal of Physiology and Pharmacology **94**(11): 1132-1140

Xu, Q. B. (2004). "Mouse models of arteriosclerosis - From arterial injuries to vascular grafts." American Journal of Pathology **165**(1): 1-10

Xu, Q. B., Zhang, Z. Y., Davison, F. and Hu, Y. H. (2003). "Circulating progenitor cells regenerate endothelium of vein graft atherosclerosis, which is diminished in ApoE-deficient mice." Circulation Research **93**(8): E76-E86

Yadav, A., Saini, V. and Arora, S. (2010). "MCP-1: Chemoattractant with a role beyond immunity: A review." Clin. Chim. Acta **411**(21-22): 1570-1579

Yahagi, K., Kolodgie, F. D., Otsuka, F., Finn, A. V., Davis, H. R., Joner, M. and Virmani, R. (2016). "Pathophysiology of native coronary, vein graft, and in-stent atherosclerosis." Nature Reviews Cardiology **13**(2): 79-98

Yan, C., Takahashi, M., Okuda, M., Lee, J. D. and Berk, B. C. (1999). "Fluid shear stress stimulates big mitogen-activated protein kinase 1 (BMK1) activity in endothelial cells - Dependence on tyrosine kinases and intracellular calcium." Journal of Biological Chemistry **274**(1): 143-150

Yang, H., Zhao, F. L., Li, Y., Xu, M. M., Li, L., Wu, C. H., Miyoshi, H. and Liu, Y. Y. (2013). "VCAM-1-targeted core/shell nanoparticles for selective adhesion and delivery to endothelial cells with lipopolysaccharide-induced inflammation under shear flow and cellular magnetic resonance imaging in vitro." International Journal of Nanomedicine **8**: 1897-1906

Yet, S. F., Layne, M. D., Liu, X. L., Chen, Y. H., Ith, B., Sibinga, N. E. S. and Perrella, M. A. (2003). "Absence of heme oxygenase-1 exacerbates atherosclerotic lesion formation and vascular remodeling." Faseb Journal **17**(10): 1759-1768

Yu., M., Li., H., Liu., Q., Liu., F., Tang., L., Li., C., Yuan., Y., Zhan., Y., Xu., W., Li., W., Chen., H., Ge., C., Wang., J. and Yang., X. (2011). "Nuclear factor p65 interacts with Keap1 to repress the Nrf2-ARE pathway." Cellular Signalling **23**(5): 883-892

Yuan, X., Du, J. L., Liu, Q. and Zhang, L. (2017). "Defining the role of perioperative statin treatment in patients after cardiac surgery: A meta-analysis and systematic review of 20 randomized controlled trials." International Journal of Cardiology **228**: 958-966

Zakkar, M., Angelini, G. and Emanueli, C. (2015). "Regulation of Vascular Endothelium Inflammatory Signalling by Shear Stress." Current Vascular Pharmacology **14**(2): 181-186

Zakkar, M., Chaudhury, H., Punjabi, P. P., Haskard, D. O. and Evans, P. C. (2008). "Acute high shear stress activates venous but not arterial endothelial cells by signalling through the p38 MAP kinase pathway." Heart **94**(9): 1-14

Zakkar, M., Chaudhury, H., Sandvik, G., Enesa, K., Luong, L. A., Cuhlmann, S., Mason, J. C., Krams, R., Clark, A. R., Haskard, D. O. and Evans, P. C. (2008). "Increased endothelial mitogen-activated protein kinase phosphatase-1 expression suppresses proinflammatory activation at sites that are resistant to atherosclerosis." Circulation Research **103**(7): 726-732

Zakkar, M., Luong, L. A., Chaudhury, H., Ruud, O., Punjabi, P. P., Anderson, J. R., Mullholand, J. W., Clements, A. T., Krams, R., Foin, N., Athanasiou, T., Leen, E. L. S., Mason, J. C., Haskard, D. O. and Evans, P. C. (2011). "Dexamethasone Arterializes Venous Endothelial Cells by Inducing Mitogen-Activated Protein Kinase Phosphatase-1 A Novel Antiinflammatory Treatment for Vein Grafts?" Circulation **123**(5): 524-U141

Zakkar, M., Van Der Heiden, K., Luong, L. A., Chaudhury, H., Cuhlmann, S., Hamdulay, S. S., Krams, R., Edirisinghe, I., Rahman, I., Carlsen, H., Haskard, D. O., Mason, J. C. and Evans, P. C. (2009). "Activation of Nrf2 in Endothelial Cells Protects Arteries From Exhibiting a Proinflammatory State." Arteriosclerosis Thrombosis and Vascular Biology **29**(11): 1851-U353

Zampetaki, A., Kirton, J. P. and Xu, Q. B. (2008). "Vascular repair by endothelial progenitor cells." Cardiovascular Research **78**(3): 413-421

Zhang, D. D., Lo, S. C., Sun, Z., Habib, G. M., Lieberman, M. W. and Hannink, M. (2005). "Ubiquitination of Keap1, a BTB-Kelch substrate adaptor protein for Cul3, targets Keap1 for degradation by a proteasome-independent pathway." Journal of Biological Chemistry **280**(34): 30091-30099

Zhang, L. S., Peppel, K., Brian, L., Chien, L. and Freedman, N. J. (2004). "Vein graft neointimal hyperplasia is exacerbated by tumor necrosis factor receptor-1 signaling in graft-intrinsic cells." Arteriosclerosis Thrombosis and Vascular Biology **24**(12): 2277-2283

Zhao, S. M., Suciu, A., Ziegler, T., Moore, J. E., Burki, E., Meister, J. J. and Brunner, H. R. (1995). "Synergistic effects of fluid shear-stress and cyclic circumferential stretch on vascular endothelial-cell morphology and cytoskeleton." Arteriosclerosis Thrombosis and Vascular Biology **15**(10): 1781-1786

Zou, Y., Hu, Y., Mayr, M., Dietrich, H., Wick, G. and Xu, Q. (2000). "Reduced neointima hyperplasia of vein bypass grafts in intercellular adhesion molecule-1–deficient mice." Circulation Research **86**(4): 434-440